Coupled Structural-Acoustic Analytical Models for the Prediction of Turbulent Boundary-Layer-Induced Noise in Aircraft Cabins

by

Joana Luíz Torres da Rocha
B.Sc., Portuguese Air Force Academy, 2002
M.A.Sc., University of Victoria, 2005

A Dissertation Submitted in Partial Fulfillment of the
Requirements for the Degree of

DOCTOR OF PHILOSOPHY

in the Department of Mechanical Engineering

Coupled Structural-Acoustic Analytical Models for the Prediction of Turbulent Boundary-Layer-Induced Noise in Aircraft Cabins

by

Joana Luíz Torres da Rocha
B.Sc., Portuguese Air Force Academy, 2002
M.A.Sc., University of Victoria, 2005

Supervisory Committee

Dr. Afzal Suleman, Co-Supervisor
(Department of Mechanical Engineering)

Dr. Fernando Lau, Co-Supervisor
(Instituto Superior Técnico, Technical University of Lisbon)

Dr. Peter Oshkai, Departmental Member
(Department of Mechanical Engineering)

Dr. Arif Babul, Outside Member
(Department of Physics and Astronomy, University of Victoria)

Supervisory Committee

Dr. Afzal Suleman, Co-Supervisor
(Department of Mechanical Engineering)

Dr. Fernando Lau, Co-Supervisor
(Instituto Superior Técnico, Technical University of Lisbon)

Dr. Peter Oshkai, Departmental Member
(Department of Mechanical Engineering)

Dr. Arif Babul, Outside Member
(Department of Physics and Astronomy, University of Victoria)

ABSTRACT

Significant interior noise and vibrations in aircraft cabins are generated by the turbulent flow over the fuselage. The turbulent boundary layer (TBL) excitation is the most important noise source for jet powered aircraft during cruise flight. Reduced levels of interior noise are desirable both for comfort and health reasons. However, to efficiently design noise control systems, and to design new and optimized structures that are more efficient in the noise reduction, a clearer understanding of the sound radiation and transmission mechanisms is crucial. This task is far from being straightforward, mainly due to the complexity of the system consisted by the aircraft fuselage, and all the sound transmission mechanisms involved in a such complex environment. The present work aims to give a contribution for the understanding of these mechanisms. For that, a coupled *aero-vibro-acoustic* analytical model for the prediction of the TBL-induced noise and vibration in aircraft is developed. Closed form analytical expressions are obtained to predict the structural vibration levels, noise radiated from the structure and interior sound pressure levels.

As well as the physical system under study, the mathematical model is composed by three distinct submodels: the aerodynamic model, which describe the TBL wall pressure fluctuations over the aircraft fuselage skin, the structural model, representing the aircraft panels structural vibration, and the acoustic model, which represents the acoustic pressure field in the aircraft cabin. These individual submodels are then mathematically coupled, such that the effect of the first submodel can be observed in the second and third submodels. As a random process, the TBL wall pressure is statistically described in terms of the power spectral density (PSD), by the use of empirical models. The structural response of the aircraft panels is defined using the linear plate and shell theories. The wave equation is used to define the cabin acoustic field. The displacement of the panels and the interior acoustic pressure are represented, respectively, through the panel and acoustic natural modes. The models were developed for the Cartesian and the cylindrical coordinates systems, respectively, for a rectangular and a cylindrical cabin. The flexible structure can be composed by one or several panels, which are considered to be simply supported. For both the structural and acoustic models, a damping factor was added in the equations of dynamics, in order to account for the structural and acoustic damping of the respective subsystems.

Results for the prediction of the vibration level of the aircraft panels, radiated sound power, and interior sound pressure levels in the aircraft cabin are obtained. The analytical models are validated through the successful comparison with several independent experimental studies. The TBL empirical models existent nowadays provide different predictions for the TBL wall pressure fluctuations PSD. For this reason, it is important to understand the range of conditions that different wall pressure fluctuations PSD produce in the noise radiation problem. To accomplish that, a sensitivity analysis on the sound radiated by the structural panels to the change of TBL parameters is undertaken. The models are able to predict localized and average values of interior noise level and structural vibration level. It is shown that average values and localized values can be very dissimilar from each other. Usually, the average values are assumed to be representative of the physical system response. This can be of particular importance, for instance, in the noise reduction systems design, where the accurate information about the system behavior is crucial. It is shown that the number of structural and acoustic modes considered in the analysis can greatly affect the accuracy of the predicted quantities.

Keywords:

- Aircraft Cabin Noise
- Aircraft Fuselage Panel
- Turbulent Boundary-Layer-Induced Noise
- Turbulent Flow Modeling
- Structural-Acoustic Coupling
- Analytical Modeling
- Structural Vibration Level
- Radiated Sound Power
- Sound Pressure Level
- Power Spectral Density.

Contents

List of Figures

ACKNOWLEDGEMENTS

I would like to thank:

Dr. Afzal Suleman, supervisor of the present research, for his mentoring, support, and encouragement during all the Ph.D. program. I am extremely thankful for his guidance in finding the best path to achieve the goals of this work. Thank you for offering me the great opportunity to perform this research, which allowed me to grow so much scientifically and personally.

Dr. Fernando Lau, for his co-supervision, for sharing his knowledge with me, for his help and guidance, especially in the stage of the work in which the mathematical modeling approach was defined. I want to thank his total availability. Even not being close by, Dr. Fernando Lau was always available to give his support.

Dan Palumbo, who supervised my research work during my stay at the Structural Acoustics Branch, NASA Langley Research Center, in the last phase of my Ph.D. program. I am profoundly thankful for his guidance, dedication, long discussions and advices on the research subject, and for sharing his talent, knowledge and experience with me.

Department of Mechanical Engineering, University of Victoria, I would like to thank my friends and colleagues at the University of Victoria, who, over the past few years, have accompanied me in this terrific and challenging journey, being a source of relaxation and insight from different perspectives. To *Michelle Fuller*, for her friendship and the great coffee times, allowing me to be more time in touch with the real world! To *Sandra* and *Art Makosinski*, for their continuous support, generosity and friendship, for organizing and hosting the amazing get together lunches and dinners for the research group. To my peers *Kerem Karakoc*, *André Carvalho*, *Ricardo Paiva*, *Ali Taleb*, *Baris Ulutas*, *Casey Keulen*, *Ahmad Kermani* and *Jenner Richards*, for sharing their time with me, for the lunches together, for the good humor, and for making my day a better day.

NASA Langley Research Center, Structural Acoustics Branch, I would like to thank the research group at NASA LaRC - StAB for the amazing opportunity they offered me to collaborate with their team during three months. A special

thank you to *Dr. Richard Silcox* for his time and consideration, and taking care of all the logistics and long process necessary to make my stay at NASA possible. To *Dr. Kevin Shepherd*, for inviting me to the Branch meetings and making me feel as part of the group. To *Alexandra Loubeau*, *Jonathan Rathsam*, *John Faller*, *Noah Schiller*, *Steve Miller*, *Chris Kilzer* and *Eric Greenwood*, for the lunch times together, for inviting me to join the group social events, and for making my stay at NASA even more amazing and enjoyable.

My family and friends, the final words of acknowledgment go to my family and friends. To my friends *Alannah Hanlen* and *Alan Bryant*, who were extraordinarily supportive, always believed in me and give me encouragement to keep in the road. Thank you for your friendship and love, and for being our family in Victoria, BC. To my *friends in Portugal*, who despite not being present were always with me. Thank you for your unconditional friendship and for always believing in me. Thank you to my mother-in-law, *Maria Odete Rocha*, for being my friend and for helping me so many times during the last few years. Thanks to my grandparents, *Madalena Martins* and *Fernando Rocha*, for giving me unconditional love and for believing in me for all my life. You both died years ago, but you still are and always will be present during all the phases of my life. Thank you to the most amazing sisters ever, *Inês Rocha* and *Libânia Rocha*. Thank you for your love, generosity, patience listening to me, encouragement, for believing in me and for always being there. To my parents, *Maria da Luz Torres* and *Luis Rocha*, how can I say thank you to you in few words? I owe everything I achieved in my life to my family's love, constant support and encouragement. Thank you for always believing in me, in the good and bad times. I owe you my life, my identity and who I am today. To my husband, *Bruno Rocha*, who was always supportive, for his love and friendship, for sharing his life with me. You have my eternal thank you. Finally, to the most important person in my life, my daughter, *Helena Rocha*, to whom I dedicate this work. *Helena*, the real thank you for you is well beyond words. Thank you, thank you, ..., thank you for always believing in me, for giving me your smile all days, for the happiness you give to all of us, for your sincere love, for your inner encouragement, for everything you are.

To all of you, *thank you*.

DEDICATION

Dedicated to my daughter, *Helena Rocha*.

Chapter 1

Introduction

1.1 Motivation

1.1.1 Significance of TBL as Noise Source in Aircraft Cabins

Aircraft interior noise is a result of several sources, namely: (i) discrete tones at the fundamental blade passage frequency of the engines and their harmonics, for propeller-driven aircraft; (ii) structure-borne noise caused by out-of-balance forces within the engines, inducing vibrations into the aircraft structure; (iii) aircraft systems, such as auxiliary power unit, pressurization and conditioning systems; (iv) aerodynamic noise, in which turbulent boundary layer induced noise is included. For all types of aircraft, the TBL over the fuselage surface is characterized by a fluctuating pressure which excites the fuselage skin. In fact, at cruise flight conditions, the TBL wall pressure fluctuations represent the major source of noise in jet aircraft cabins [1,5,6], and they become even more significant as the flight Mach number increases [2,7].

Figure 1.1 illustrates the importance of the several noise sources during the course of a flight of a jet transport aircraft [1]. Flight measurements show that while during takeoff and climb the engine noise is the dominant source of cabin noise, the TBL is the major contribution during cruise flight. When cruise flight condition is reached, the TBL becomes the dominant source of noise, resulting from the increase from climb to cruise speed; a reduction of engine noise is also observed, as the engine thrust is reduced to cruise setting. As referred in [8], TBL excitation is regarded as the most important noise source for jet powered aircraft at cruise speed, particularly, as quieter jet engines are being developed. Figure 1.2 shows the increase of TBL pressure levels on the exterior of the fuselage with the flight speed, for subsonic flight [2].

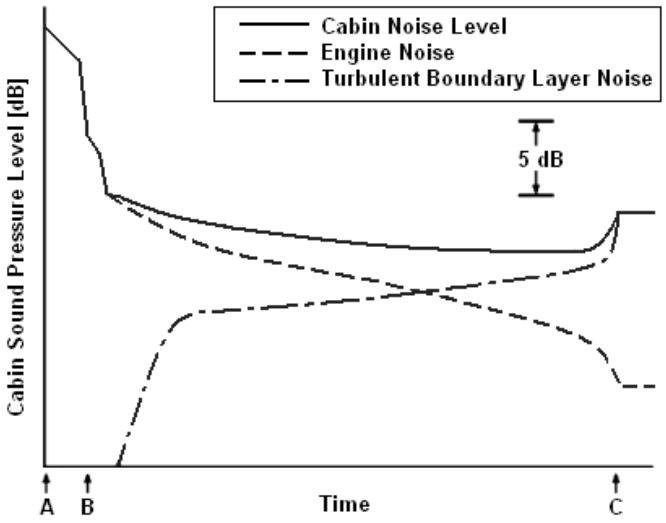

Figure 1.1: Typical variation of noise levels in a jet airplane cabin during takeoff and climb to cruising altitude: A, start of takeoff roll; B, liftoff from the runway; C, stabilized level flight at cruising altitude and air speed. Figure from [1].

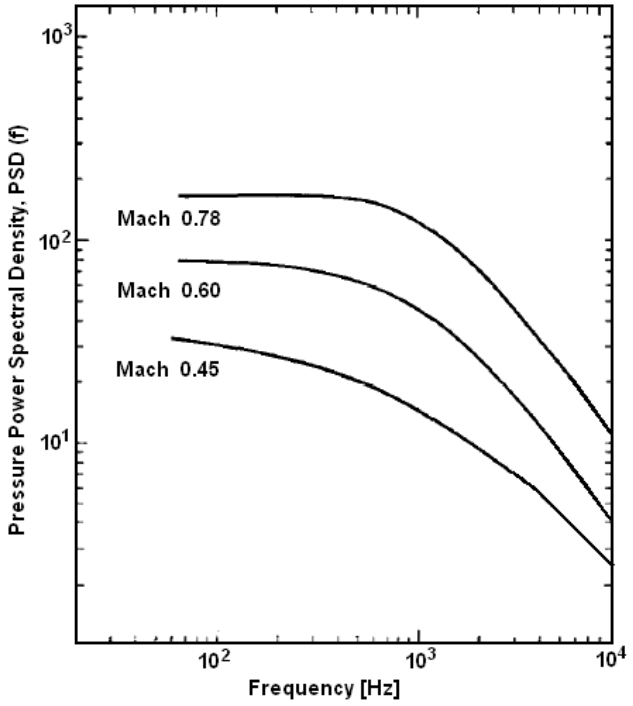

Figure 1.2: Boeing 737 aircraft forward turbulent boundary layer pressure power spectral density of the TBL. Figure from [2].

1.1.2 Noise Effects on Health and Comfort

High levels of cabin interior noise is a challenging problem in most aircraft and many other transport vehicles. Reduced levels of cabin noise are desirable both for comfort and health-related reasons. As shown in the recent study by [9], high levels of noise and vibration in aircraft cabins have a significant influence on the human response to various symptoms and health indices, particularly in long flights. High noise levels, specially low-frequency noise ($20-500Hz$), can be annoying and during long exposure periods it produces hearing loss, fatigue, loss of concentration, and reduced comfort. Moreover, reduced concentration may lead to increased risk for accidents.

The study of aircraft passenger's comfort is a subjective matter, since the sensation of comfort is influenced by a large variety of physical and psychological factors, such as air quality, pressure, temperature, humidity, odors, etc., and it is different from person to person. However, in [10] it is concluded that an increase in sound pressure level, in loudness, fluctuation strength or vibration magnitude causes a decrease in comfort sensation by aircraft passengers. Specifically, the study by [11] showed that low-frequency sound can lead to various negative symptoms, including general annoyance, deterioration of task performance, reduced wakefulness and sleep disturbance both reflecting a general slowdown of physiological and psychological states. In [12], it is shown that the prolonged exposure to a combination of high-intensity and low-frequency noise and vibration can influence the respiratory rate, heart functions, stomach and intestine functions, and function of central nervous system. The effect of low-frequency noise and vibrations on health is described in [13–17], as the "Vibroacoustic Disease" (VAD), characterized by the abnormal thickening of cardiac structures. VAD was observed on long-term low-frequency-exposed professionals, such as commercial aircraft pilots and cabin crews. In consequence, most aircraft manufacturers are interested in noise control techniques, both passive and active, and recently the application of the active techniques in passenger's cabins had an increased interest. This interest was mainly due to the advent of prop-fan powered aircraft, characterized by their high level of low-frequency internal noise. Additionally, the developments in electronics and computers allow the implementation of such systems. As shown in Figure 1.2 low frequency noise is the dominant form of noise in aircraft cabin during cruise flight.

1.1.3 Application of Noise Reduction Techniques

Noise can be defined as any undesirable sound. The definition of what is and what is not desirable differs between individuals. However, the suppression of aircraft interior noise can be appreciated by anyone who spends a long time in continuous flight. In consequence, most aircraft manufacturers are interested in noise control techniques. Noise control methods can be classified in two categories: passive control, and active control. The choice of the most appropriate technique is determined by the characteristics of the noise environment and the application. Both approaches can also be applied simultaneously in the same aircraft, since they are complementary.

Passive noise control (PNC) consists in the use of supplementary treatments or structural modification, and do not require a power source to reduce noise and/or vibration. Supplementary treatments include damping materials, stiffeners and additional mass. Typically, PNC approaches are inexpensive and easy to implement. However, their performance is limited to the mid- and high-frequency range [18]. Figure 1.3 illustrates the reduction in vibration of an aircraft skin panel when a structural damping treatment is applied. Acoustic damping materials, like insulating blankets and acoustic foam, are usually applied in the aircraft fuselage wall cavity, but they are ineffective for attenuating low-frequency noise. To be effective for low-frequency noise, an acoustic absorber would be very thick, involving a forbidden weight increase in aeronautics [19].

It may be possible to overcome these problems using active control techniques. Many noise problems exist as a result of structural vibrations and, consequently, two primary active control approaches have emerged: Active Noise Control (ANC) and Active Structural Acoustic Control (ASAC). Unlike passive treatments, active control methods require additional energy to be introduced into a system through a series of control inputs or secondary sources. These sources are used to create a secondary field that couples with the primary field, such that the total system response is minimized or altered in a desired way. ANC focuses in the reduction of the radiated sound pressure from a system. This control approach involves the generation of an "anti-sound" field [20], by exciting the acoustic medium with secondary noise sources, usually produced by loudspeakers. When the electronically produced inverse wave is added to original unwanted sound the result is zero sound at that location (the called destructive interference). However, noise cancellation in three-dimensional spaces is difficult or impossible to achieve [21]. The ASAC approach takes advantage of the

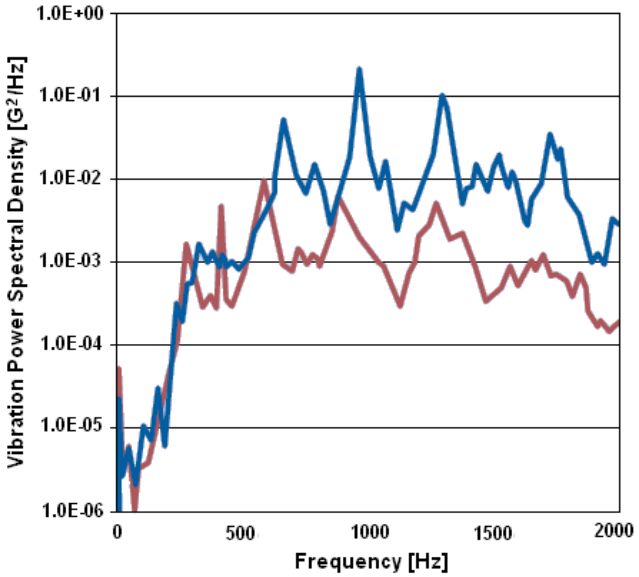

Figure 1.3: Vibration spectrum of a McDonnell Douglas MD-80 aircraft skin panel: blue, untreated skin panel; red, treated skin panel. Figure from [3].

close coupling between the structural vibration and the radiated sound field, and involves applying a mechanical input directly to the vibrating structure [22, 23], and thus reducing the noise caused by the reduced vibration. The secondary vibrational sources are normally produced by shakers or piezoelectric actuators, which are the control sources, having the same amplitude and opposite phase comparatively with the primary source (the vibration field to be controlled). The advantage of these techniques in aircraft applications is the ability to decrease sound levels without a big penalty in terms of weight, compared to the PNC alternatives. Current aircraft structures have poor acoustic transmission loss in the low frequency range (up to $500Hz$) and this problem can be even more significant in the future, with the composite fuselages.

However, the implementation of these techniques is far from being straightforward. One of the main reasons is the complexity of the coupled structural-acoustic system consisted of the fuselage structure together with the cabin acoustic field. Another difficulty is the fact that the airflow noise transmission is a random phenomena, from which is difficult to obtain a reasonable number of time-advanced reference signals. To design an efficient noise control system, a clear understanding of the mechanisms of sound transmission through the structure and noise radiation in the cavity is crucial.

1.1.4 Noise as a Variable in the Aircraft Conceptual Design

With the recent interest in environment friendliness and sustainable societies, noise pollution tends to be a global major concern. In aircraft and automotive industries the requirements linked to environmental issues, such as emissions and noise limits, are strongly gaining importance. This applies to the aircraft interior noise, as well to the external noise, related to the increasingly strict exterior noise regulations around airports. To achieve the noise reduction goal, it is expected that environmental requirements may become driving parameters for a given aircraft design, including these parameters within the conceptual design phase of aircraft development [24]. The aircraft cabin design can have a big impact on the noise levels during flight. With the early inclusion of the noise as variable in aircraft design, it is expected that any needed design change can be made prior to the initial prototype. If the design is right the first time, there is a reduction in engineering and prototyping expenses. However, to be able to predict the acoustic characteristics of a specific cabin design, an accurate predictive model is needed.

1.2 Statement of the Problem, Objectives and Approach

When an aircraft is in flight, the external turbulent boundary layer developed over the aircraft causes vibration of the aircraft skin, which in turn radiates noise in the aircraft cabin, as illustrated in part (a) of Figure 1.4. As previously discussed in this report, the turbulent flow can be a major source of aircraft interior noise, and increases with the flight speed. The increased interior noise levels due to the higher cruise speeds, the use of new materials in the structure, the development of advanced noise reduction techniques, and the inclusion of noise as a variable in the conceptual design of aircraft, generate a need for better understanding the noise radiation and transmission mechanisms into the aircraft cabin. Currently, there is a lack of accurate and fast models for the prediction of noise in aircraft cabins.

In this context, the aim of the present work is to develop an analytical framework for the prediction of flow-induced noise and vibration in aircraft cabins. As shown in Figure 1.4, the physical system can be divided in three subsystems, that are coupled among them. Similarly to what is physically observed, the mathematical model is developed as a *aero-vibro-acoustic* coupled model. Specifically, the analytical model

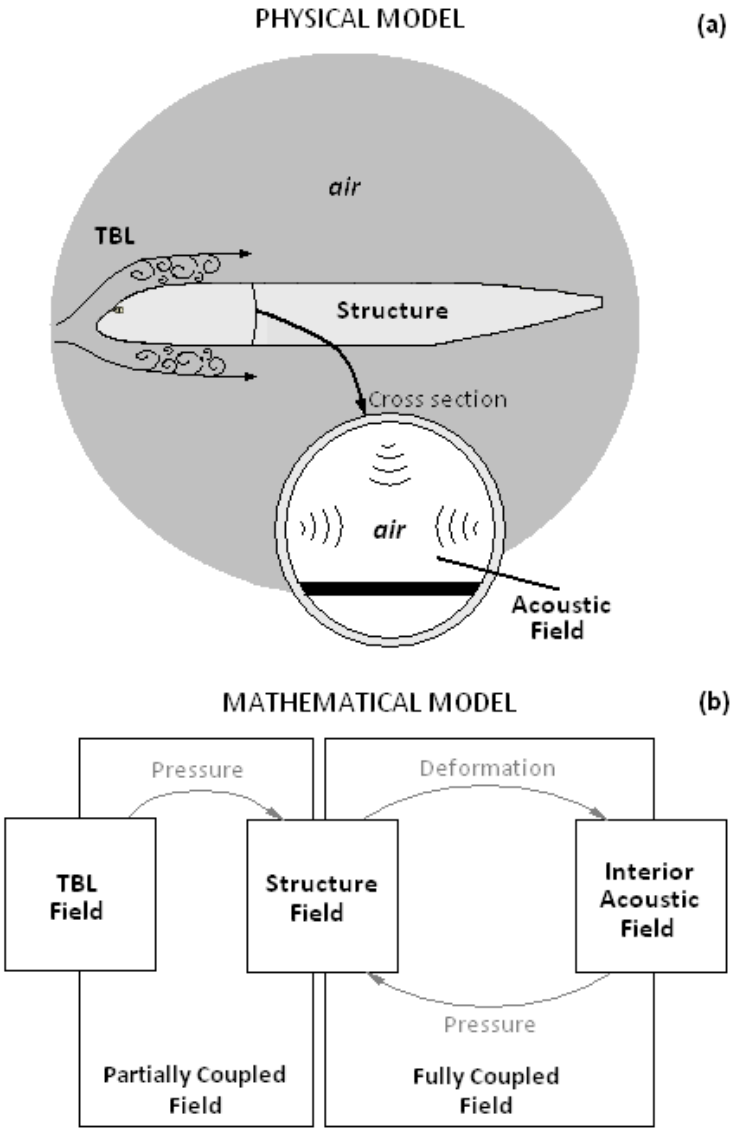

Figure 1.4: Schematic representation of the *aero-vibro-acoustic* coupled model: (a) physical system, (b) mathematical model.

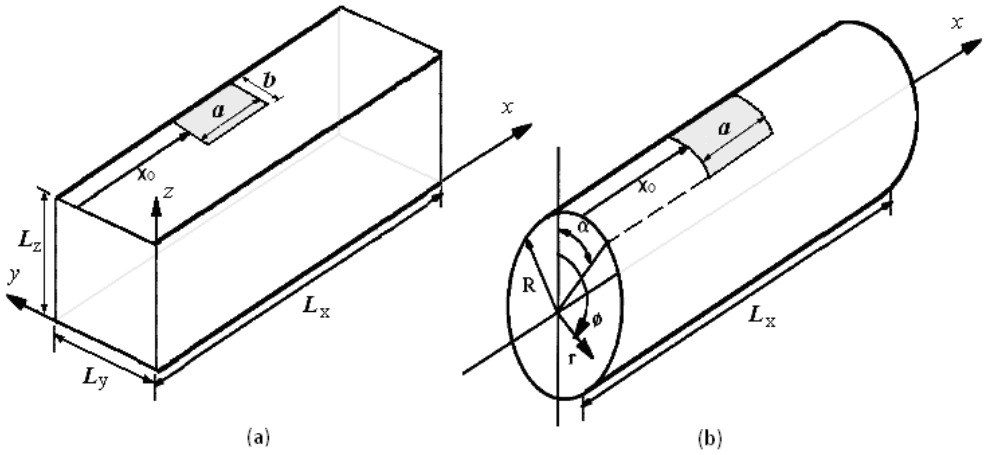

Figure 1.5: Schematic diagram for (a) a rectangular enclosure coupled with a flat plate, and (b) a cylindrical cabin coupled with a curved panel.

is divided in three submodels: (1) the aerodynamic model, in which the output is the wall pressure fluctuations induced by the TBL, developed over the aircraft fuselage skin; (2) the structural model, representing the aircraft fuselage skin vibration, in which the output is the vibration of the structure; and (3) the acoustic model, which represents the acoustic pressure field in the aircraft cabin section, and has the interior sound pressure as output. These individual submodels are then mathematically coupled, such that the effect of the first submodel can be observed in the second and third submodels. Closed form analytical expressions are obtained to predict the structural vibration levels, radiated sound power and interior sound pressure levels. All the mathematical computations were performed using Fortran.

As represented in Figure 1.5, the models are developed for two types of systems: (a) the rectangular system, defined in Cartesian coordinates, and (b) the cylindrical system, using the cylindrical coordinates. In the rectangular system the cabin is a rectangular enclosure, filled with air, and having one flexible flat wall excited by the TBL. The cylindrical system represents a cylindrical cabin, filled with air, and with a flexible cylindrical wall excited by the turbulent flow. The flexible wall can be composed by one or several panels or shells, respectively, for the Cartesian and cylindrical system, which are considered to be simply supported. For both the structural and acoustic models, a damping factor is added in the equations of dynamics, in order to account for the structural and acoustic damping of the respective subsystems.

As a random process, the TBL wall pressure is statistically described in terms of the power spectral density, by the use of empirical models. In the present work, the

TBL is described through these empirical models. The structural model represents the aircraft fuselage panels/shells vibration, and is described using the linear plate and shell theories. The wave equation is used to define the cabin acoustic field. The displacement of the plate/shell and the interior acoustic pressure are represented, respectively, through the plate/shell natural modes and acoustic modes.

The analytical models are validated through the successful comparison with several independent experimental studies. Results for the prediction of aircraft panels' vibration level, radiated sound power, and interior sound pressure levels in the aircraft cabin are obtained. The models are able to predict localized and average values of interior noise and structural vibration levels.

1.3 Dissertation Outline

This dissertation is organized as following:

Chapter 1 provides the Introduction, which contains the motivation of the work, the statement of the problem, overall objectives and approach. The bulk of the work presented in this thesis is contained in the Appendices. Each Appendix (A-E) includes a complete scientific journal publication. These five peer-reviewed journal articles are either published, in press, or currently under review. The fifth paper is currently under review at NASA Langley Research Center. All publications made by or in collaboration with NASA need to undergo an internal revision process prior to submission. After this revision, the paper will be submitted to the Journal of Sound and Vibration.

Chapter 2 includes and overview of the research and previous work done to date on the scientific problem.

Chapter 3 summarizes each one of the articles, explaining the contribution of each publication, and how they are connected in order to meet the objectives of this dissertation.

Chapter 4 contains a brief summary of the overall contributions, conclusions, and enumerates avenues of future work for further development.

Chapter 2

State of the Art Review

2.1 Turbulent Boundary Layer Modeling

2.1.1 Physical Phenomenon and Context

A boundary layer is typically a thin region of fluid immediately adjacent to a solid structure, along which a fluid is moving. Any interaction between the fluid and the surface of the solid takes place through that layer of fluid. Boundary layers can be laminar or turbulent, depending on the velocity, density and viscosity of the fluid, and on the characteristic length of the solid surface. A TBL is characterized by high Reynolds number. For flow over a flat plate, the transition from laminar to turbulent flow occurs at a Reynolds number around 10^5 to 10^6. The Reynolds number is the ratio between inertial forces and viscous forces, being defined as follows

$$Re = \frac{\rho U L}{\mu} = \frac{U L}{\nu} = \frac{Inertial\ Forces}{Viscous\ Forces} \tag{2.1}$$

where U is the mean fluid velocity, L is the characteristic length of the solid surface, ρ is the density of the fluid, μ is the (absolute) dynamic fluid viscosity, and $\nu = \frac{\mu}{\rho}$ is the kinematic fluid viscosity.

Since the TBL is characterized by turbulent eddies of many different sizes, wall pressure fluctuations induced by turbulent flow are a broadband phenomena, making it a very complex physical problem, difficult to calculate, predict and measure. This broadband nature of the TBL limits the calculation of pressure fluctuations using the direct numerical simulation of the governing equations. Using current techniques, it is not possible to directly measure the pressure fluctuations within the boundary layer

without altering the flow field. Therefore, pressure fluctuations can only be measured at the solid surface beneath the solid surface. However, the transducer used for these measurements should be very small (miniature), since turbulent eddies, which produce the pressure fluctuations, extend to very small sizes. In recent studies, such as in [25–27], an array of wall pressure sensors have also been used to obtain the field of wall pressure fluctuations. For the measurement of the wall pressure flcutuations, the pressure sensor is usually equipped inside of the wall so that the distance between the pinhole on the wall surface and the diaphragm of the pressure sensor can be minimized in order to obtain better frequency response.

A TBL developed around an aircraft fuselage generates a fluctuating pressure, which excites the fuselage skin, and gives rise to high noise levels inside the cabin. As well as aircraft, trains and cars suffer from the same problem since other sources of noise (due to engines, wheel-road contact, or on board equipment), have been dramatically reduced. This problem affects the comfort of the passengers, and is more significant at higher flow speeds. The flow-induced noise increases more rapidly with respect to the vehicle velocity than other noise sources [2, 19].

The basic mechanisms related with the production of the TBL wall pressure fluctuations in subsonic flow appear to be two-fold. First, there is a component associated with the eddies at the edge of the laminar sublayer, tentatively associated with the laminar sublayer "eruption" process. The second component is associated with the eddies in the outer intermittent parts of the TBL. The intensity of this component appears to be affected by upstream conditions such as roughness or protuberances, and is typically of low frequency [28]. A viscous sublayer with a less solenoidal perturbation velocity is below the fully turbulent zone of the turbulent boundary layer, and a buffer zone connects them. As referred in [29], the majority of the turbulence energy is produced in the viscous sublayer and the buffer zone, and most of the energy in the turbulent flow is contained in large eddies. The energy associated with smaller eddies is smaller and their life span is considerably shorter.

The nature of the TBL excitation is random both in frequency and spatial domains [5]. A large number of empirical and theoretical models have been developed to describe these random TBL wall-pressure fluctuations on a smooth wall [30]. In these models, the TBL excitation is usually described in terms of the statistic properties of the wall pressure fluctuations, and it is assumed that pressure fluctuations are not modified by the vibrations of the structure. This way, the pressure developed on the structure is the pressure that would be observed on a rigid structure, also called

the *blocked pressure* - and thus, as shown in Figure 1.4, the aerodynamic model is partially coupled with the structural model. In other words, it is assumed that the wall-pressure fluctuations are not affected by the vibrations of the plate. This assumption holds as long as the flow-induced displacements are much smaller than the characteristic length scales of the flow and as long as we are further downstream from the transitional boundary layer, so that the flow is robust to small perturbations due to the plate vibrations [19]. This approximation makes the problem more tractable, and suitable for the derivation of analytical expressions. An exact approach, based upon the Lighthill theory of aerodynamic sound generation [31, 32], would be to consider the plate excited by the acoustic pressure generated by moving acoustic sources and with an integral representation, which requires the solution of the entire flow field.

The bulk of research on the behavior of surface pressure fluctuations in TBL flows were made for zero pressure gradient, two-dimensional turbulent boundary layers. Even though studied extensively, the pressure fluctuations for this case still subject of current research. Current studies considering the effect of pressure gradient and boundary layer separation on surface pressure fluctuations are typically highly idealized laboratory flows. For the case of TBL developed on a rigid surface, with zero mean pressure gradient, the boundary layer increases slowly in thickness and its turbulent pressure field can be expressed as stationary and homogeneous random phenomena [33–36]. Measurements of the TBL wall pressure fluctuations in a wind tunnel can be performed under controlled conditions with specified pressure gradients and surface roughness. This is not the case of flight measurements, in which the boundary layer on the exterior of the fuselage is subjected to adverse and favorable pressure gradients. However, to a first approximation, the TBL wall pressure fluctuations can be estimated based on relationships for flow over a flat plate with zero pressure gradient [4]. Furthermore, currently there is not a widely accepted systematic approach/model available to provide information about the TBL pressure fluctuations, other than for zero pressure gradient conditions.

2.1.2 Mathematical Formulation and Models

As a random process, the wall pressure fluctuations due to the TBL is usually statistical described. The experimental work performed is, then, usually concentrated on measurements of mean square pressure, space-time correlations, wavenumber-

frequency spectral density and cross (space-frequency) spectral density [37]. If the pressure is a random process, its cross correlation function is defined as the ensemble average of the product of the pressure at one point in space and time with that at another point.

The TBL over a rigid flat surface and at zero pressure gradient can be modeled as a homogeneous and stationary random process. Assuming this, the TBL pressure space-time correlation function is independent of the choice of the time and spatial origins, respectively, and is only a function of the separation of the points in space and time. This way, for turbulent flow in the $x-$direction and over the (x, y) plane, as shown in Figure 2.1, the space-time correlation of the pressure field, $R(\xi_x, \xi_y, \tau)$, is a function of the two-dimensional spatial separations, $\xi_x = x - x'$ and $\xi_y = y - y'$, and the time delay, $\tau = t - t'$, being defined as follows

$$R(\xi_x, \xi_y, \tau) = < p(x, y, t)\, p(x + \xi_x, y + \xi_y, t + \tau) > \tag{2.2}$$

where $p(x, y, t)$ is the fluctuating component of the wall pressure at the surface point (x, y) at time t, and $<>$ denotes the expected value. The wavenumber-frequency spectral density of the wall pressure fluctuations, $S(k_x, k_y, \omega)$, the space-time correlation function, $R(\xi_x, \xi_y, \tau)$, the space-frequency spectral density of the wall pressure fluctuations, $S(\xi_x, \xi_y, \omega)$ (usually called cross power spectral density), are all related by inverse Fourier and Fourier transforms as following:

$$S(k_x, k_y, \omega) = \frac{1}{(2\,\pi)^3} \int_{-\infty}^{\infty} \int_{-\infty}^{\infty} \int_{-\infty}^{\infty} R(\xi_x, \xi_y, \tau)\, e^{-i(k_x\,\xi_x + k_y\,\xi_y + \omega\,\tau)} d\xi_x d\xi_y d\tau \tag{2.3a}$$

$$R(\xi_x, \xi_y, \tau) = \int_{-\infty}^{\infty} \int_{-\infty}^{\infty} \int_{-\infty}^{\infty} S(k_x, k_y, \omega)\, e^{i(k_x\,\xi_x + k_y\,\xi_y + \omega\,\tau)} dk_x dk_y d\omega \tag{2.3b}$$

$$S(\xi_x, \xi_y, \omega) = \frac{1}{2\,\pi} \int_{-\infty}^{\infty} R(\xi_x, \xi_y, \tau)\, e^{-i\,\omega\,\tau} d\tau \tag{2.3c}$$

$$R(\xi_x, \xi_y, \tau) = \int_{-\infty}^{\infty} S(\xi_x, \xi_y, \omega)\, e^{i\,\omega\,\tau} d\omega \tag{2.3d}$$

where (k_x, k_y) is the two-dimensional wave-vector and ω is the radian frequency.

Experimental measurements of either of these quantities are difficult to make. In general, measurements have been restricted to intermediate functions such as [37]:

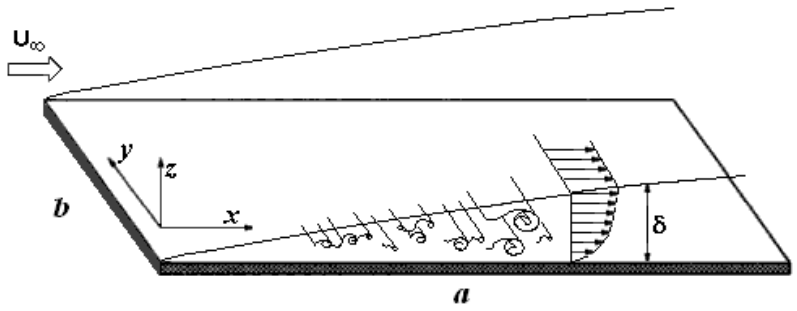

Figure 2.1: Sketch of the TBL over a flat surface.

the correlation function in the time domain $R(0,0,\tau)$; the correlation functions in the space-time domain, $R(\xi_x,0,\tau)$ and $R(0,\xi_y,\tau)$; and the singe-point spectrum in the frequency-domain, $S_{ref}(\omega)$. The single-point reference pressure spectrum is related to the space-time correlation function by

$$S_{ref}(\omega) \;=\; \frac{1}{2\,\pi}\int\limits_{-\infty}^{\infty} R(0,0,\tau)\,e^{-i\,\omega\,\tau}d\tau \tag{2.4}$$

The mean square pressure fluctuation in a specific point is defined as

$$<\,p^2\,>=\,R(0,0,0)\;=\;\int\limits_{-\infty}^{\infty} S_{ref}(\omega)d\omega \tag{2.5}$$

One of the first models for power spectral density of the TBL wall pressure fluctuations was introduced by Corcos [38, 39]. Corcos developed a TBL statistical model based on a large number of measurements of the pressure field at the wall of turbulent attached flow, and concluded that the cross-PSD of the wall pressure fluctuations can be expressed in a separable form along the spanwise and streamwise directions. The model assumes that knowing the pressure PSD at one point of the surface, it is possible to derive the PSD at another point, which is apart ξ_x in the streamwise direction and ξ_y in the spanwise direction from the reference point. Thus, the TBL wall pressure cross-PSD is usually expressed as the product of a reference-PSD function and a spatial correlation function.

Consider two points at positions $\vec{x} = (x,y)$ and $\vec{x}' = (x',y')$ in the flat panel excited by the TBL, as shown in Figure 2.1, separated by a distance of ξ_x in the $x-$direction and ξ_y in the $y-$direction. The convective velocity in the boundary layer

is denoted by U_c, so that the flow direction is $\vec{e_f} = \frac{\vec{U_c}}{|\vec{U_c}|}$. The model proposed by Corcos considers the cross power spectral density defined in a separable form in the streamwise, $x-$, and spanwise, $y-$directions, as follows

$$S(\xi_x, \xi_y, \omega) = S_{ref}(\omega)\, f_1\big(\frac{\omega\,\xi_x}{U_c}\big)\, f_2\big(\frac{\omega\,\xi_y}{U_c}\big)\, e^{\frac{-i\,\omega\,\xi_x}{U_c}} \tag{2.6}$$

in which $S_{ref}(\omega)$ is the reference point-power spectrum, $U_c \approx 0.7U_\infty$ [40] is the eddy convective speed, in which U_∞ is the free-stream velocity. Corcos found that measurements of the particular forms of the cross spectral density $S(\xi_x, 0, \omega)$ and $S(0, \xi_y, \omega)$ could be well represented as functions of the variables $(\frac{\omega\xi_x}{U_c})$ and $(\frac{\omega\xi_y}{U_c})$, respectively. In practice, functions $f_1\big(\frac{\omega\xi_x}{U_c}\big)$ and $f_2\big(\frac{\omega\xi_y}{U_c}\big)$ are frequently approximated by exponential decay functions, i.e.

$$S(\xi_x, \xi_y, \omega) = S_{ref}(\omega)\, e^{\frac{-\alpha_x\,\omega\,|\xi_x|}{U_c}}\, e^{\frac{-\alpha_y\,\omega\,|\xi_y|}{U_c}}\, e^{\frac{-i\,\omega\,\xi_x}{U_c}} \tag{2.7}$$

where α_x and α_y are empirical parameters, chosen to yield the best agreement with the reality, which denote the loss of coherence in the longitudinal and transverse directions. Usually, $\alpha_x \in [0.1; 0.12]$ and $\alpha_y \in [0.7; 1.2]$. Recommended values for aircraft boundary layers are $\alpha_x = 0.1$ and $\alpha_y = 0.77$ [30, 41]. The lengths defined by $L_x = \frac{U_c}{\alpha_x\,\omega}$ and $L_y = \frac{U_c}{\alpha_y\,\omega}$ are the called coherence lengths in the streamwise and spanwise directions, respectively.

The Corcos model is well suited to describe the statistics of TBL wall-pressure fluctuations induced by high speed subsonic flows such as in aeronautical applications [42]. Although developed in 1963, this model continues to be widely used in several recent researches involving TBL induced noise [40, 42–46]. Corcos model has the main advantage of being simple enough to enable extensive simulations without a considerable computational effort. Its main drawback is that it assumes that the coherence lengths are independent of the boundary layer thickness.

Subsequent improvements of the Corcos model were proposed, which are *Corcos-like* models since they follow the same formulation initially developed by Corcos. In 1982, Efimtsov [47] incorporated the boundary layer thickness as a variable into the coherence lengths. To do this, he derived a new set of correlation lengths, which were based on a large experimental data set, over a Mach number range *0.41-2.1.* Also in 1982, Ffowcs Williams [48] derived an expression for the coherence length functions, which are very similar with Corcos model, containing several unknown constants and

functions to be determined experimentally. To the date, these remain unknown, but Hwang and Geib [49] proposed a simplified version. Their final expression was adjusted to agree with the Corcos parameters. In 1980 and 1987, Chase [50,51] developed two models of similar form to fowcs Williams, containing a number of adjustable constants. However, the final model does not have measurements available to determine the constants. Smol'yakov and Tkachenko [52], in 1991, developed a model which follows the same approach of Efimtsov. However, they followed a combined correlation to compute the correlations lengths, instead of the direct exponential decomposition proposed by Efimtsov, containing several unknown constants and functions, to be determined experimentally.

In the comparison of these models [30], the model developed by Efimtsov is cited as a suitable candidate, being the only model derived from aircraft rather than laboratory measurements. More recently, flight tests in the Tupolev 144LL aircraft [53], demonstrated that Efimtsov model has the best agreement with the experimental data.

For further information please refer to Appendices.

2.2 Modeling the Structural-Acoustic Problem

2.2.1 Characteristics of the Physical System and Context

One of the main differences between the acoustic behavior of a fluid contained within physical boundaries (the case of air enclosed in an aircraft cabin) and an unconstrained fluid (free space), is that the first has natural modes, normally called *acoustic natural modes*. The interaction between a structure and an enclosed volume of fluid, and the calculation of this coupled response, is of great interest in many practical applications in the aerospace and automotive industries.

The typical aircraft structure incorporates aluminum ribs and stringers, which provide localized stiffness. The aircraft frame is usually covered with thin aluminum skin, which is composed by several panels. During flight, the combination of the frame covered with the thin skin results in a structure that behaves as an array of panels and shells, whose vibratory behavior couples with the interior acoustics [54]. As mentioned before in this report, the vibration of panels due to the TBL is one of the several noise transmission paths into the aircraft cabin, and represents a major source of interior noise in cruise conditions, increasing as the flight speed increases.

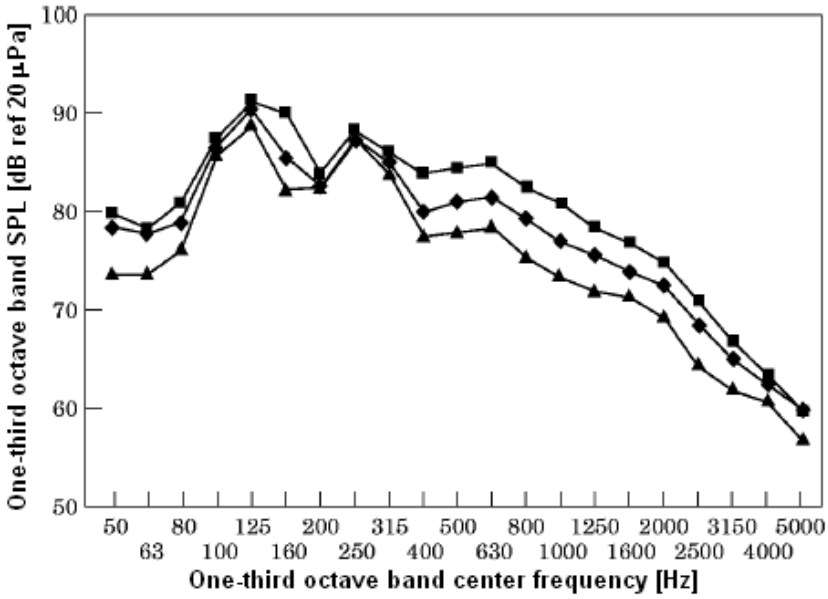

Figure 2.2: Airplane interior sound pressure levels for different flight Mach numbers: $\triangle$, M=0.55; $\diamond$, M=0.65; $\square$, M=0.8. Figure from [4].

Figure 2.2 shows interior sound pressure levels measured in a business jet airplane at three Mach numbers, in which the TBL dominates the SPL at frequencies above about $400Hz$. Furthermore, at certain cruise speeds, the *hydrodynamic coincidence* phenomenon can occur [5]. When hydrodynamic coincidence occurs, the TBL phase matches the phase of the bending wave vibration of the fuselage structure, and as a result, large vibration amplitudes of the fuselage skin and large sound pressure levels in the aircraft cabin are observed.

The sound transmission into the interior of aircraft and aerospace vehicles has received significant attention, since interior noise levels have in some cases exceeded acceptable criteria. The work performed in sound transmission has essentially captured the dominant mechanisms involved when the structure is subjected to harmonic sources. However, when the structural excitation is the turbulent boundary layer, much work still to be done to understand the mechanisms involved [55]. When a structure is subjected to a random excitation, the case of the TBL induced wall pressure fluctuations, the first challenge of the problem is that no deterministic solution can be obtained. There is a need to better understand the interaction between the random pressure fluctuations and its induced structural vibration field.

An important problem in modeling three-dimensional acoustic enclosures is to obtain a reliable and "low-order" model for the systems. This problem occurs since

the acoustic enclosure has a high modal density, and then a high model order. Despite this difficulty, analytical modeling of such systems is very important, in order to provide the essential basis for further analyzes, such as noise control and optimization applications. However, there is limited literature that addresses the modeling of structural-acoustic interaction. Most of the work in three-dimensional enclosures modeling deals with either "acoustic-only" or "structure-only" dynamic models [56]. Numerical methods can also be used to solve the structural-acoustic interaction. However, that is not the scope of the present research.

2.2.2 Mathematical Description and Modeling

Usually, to describe the structure response, the linear plate and shell theories (which assume that the plate/shell deflection is small compared to its thickness) are used. For the internal acoustic field, the wave equation is used. More details of the mathematical modeling of the structural and acoustic system are in the Appendices. The structural and acoustic damping effects may be included in the model by adding a damping term in the respective governing equations.

Probably, the most well known structural-acoustic coupling method, presented in [57], is the called *modal-interaction technique*, and was used in several other studies [58–62]. This technique assumes both structure and acoustic cavity responses expressed directly in terms of the uncoupled natural modes. It uses the *in vacuo* modal response of the structure, and the hard walled modal response of the cavity, combining the two responses into a coupled vibro-acoustic system. The normal surface displacement of the structure is the agent by which the structure influences the adjacent fluid, and the fluid pressure on the surface of the structure is the agent by which the fluid influences the structural displacement. Generally, the natural frequencies of a coupled system are different from those of the individual uncoupled systems. The advantage of this method is the considerably reduced computational time. The level of accuracy of this method depends on the number of modes considered.

Most of the models describing the vibro-acoustic response of aircraft structures excited by a TBL have considered the analysis of simply supported panels, vibrating individually and uncoupled with the interior acoustic field. Early analytical and experimental [35,63–65] investigations were performed for the TBL-induced vibration of isolated simply supported plates. For instance, in 1968, Strawderman and Brand [35] obtained an analytical solution for the plate-velocity statistics of a turbulent bound-

ary layer excited simply supported plate. Their results for plate-velocity spectral densities were in good agreement with experimental data. Similarly, in 1972, Chyu and Yang [66], investigated the response of a rectangular panel under the TBL excitation in subsonic flows, using the normal mode approach together with the spectral analysis. In their work they obtained a solution for the plate displacement PSD as a whole, and independent of the location of the panel.

More recently, additional studies were performed using the same approach of the flat plate driven by TBL excitation. In 1995, Thomas and Nelson [46] used a mathematical model of a simply supported plate excited by a TBL to investigate the use of ASAC to reduce the noise transmitted by the TBL. In 1996, Graham [41] presented results for a simply supported elastic plate (with parameters similar to those of a typical aircraft panel) forced by a pressure spectrum described by Efimtsov model, previously referred in this report. In 1999, Han et al. [67], obtained the structural vibration response and the radiated sound power of a plate excited by wall pressure fluctuations under turbulent boundary layers, and separated reattached flows. In 2005, Finnveden et al. [68], performed a comparative analysis of the plate response for different TBL wall pressure models.

Other studies have considered the coupling between structure and internal acoustic systems. Instead of evaluating the individual uncoupled structural and acoustic systems, and focusing the attention on the noise radiated by the uncoupled plate or shell, these studies also considered the coupling between the acoustic and the structural systems.

Between 1976 and 1985, Vaicaitis [69, 70] presented an analytical study to predict low frequency noise transmission through panels into rectangular enclosures, in order to predict the noise transmission through the sidewall of an aircraft, due to the turbulent boundary layer and propelled blade frequency. The acoustic pressure within the cavity was determined by solving the coupled system. However, the cavity pressure effects on the plate response was only retained for the fundamental panel mode. The external pressure was obtained applying a *100* dB random white noise on the panel. Good agreement between theory and experiments was obtained.

In 1978, Barton and Daniels [71] presented an experimental and analytical study on five panel locations coupled with a small acoustic cavity. Similarly to the work performed by Vaicaitis, a random source (white noise) of *120* dB was used as the excitation. Results indicated that both the location and material absorption characteristics had significant effects on the noise reduction. Increasing panel mass improved

the noise reduction at almost all frequencies, and increasing panel stiffness improved noise reduction below the fundamental resonance frequency. Different locations resulted in a *15* dB difference in noise reduction at a particular frequency.

Frampton and Clark [8] investigated the response of an elastic plate coupled with a rectangular acoustic enclosure and subjected to TBL excitation in 1997. In their work, the external force, the plate and acoustic responses are computed using a power balance of the entire system. The dimensions of the studied enclosure are $L_x = 3.0$ m, $L_y = 0.3$ m and $L_z = 0.3$ m, and of the plate are $a = 0.3$ m and $b = 0.3$ m, and flow Mach numbers between *0.1* and *2.0* were considered. The results show that the cavity power spectrum increases with the Mach number, and emphasize the importance of including the convected fluid loading.

A first point of concern in these studies is the fact that usually the cavity dimensions do not match those of a real aircraft cabin section. This results in different modal characteristics of the acoustic field compared with the real case, which in turn results in different structural-acoustic response, compromising the predicted levels of structural vibration and interior noise. A second point of concern is the reduced number of natural modes considered mainly to model the acoustic field. These simplifications are usually made to reduce the processing time to a manageable level. However, in order to obtain accurate predictions, the essential features of noise transmission should be retained. A third point is the geometry of the modeled system. The conventional aircraft has a cylindrical fuselage, and the effects of curvature should be considered. However, the influence of curvature still appears negligible when compared with the influence of in-plane stresses acting on the panels [41,72]. These in-plane tensions are due to the cabin pressurization and lead to an increase of the fundamental resonance frequency of each bay by a factor of up to about 7 [19].

Considering the analysis of aircraft cabin noise induced by the TBL excitation, some studies considered the curvature of the panels, as well as cylindrical enclosures. In 1996, Tang et al. [55] examined the sound transmission into two concentric cylindrical shells subjected to turbulent flow on the exterior part of the shell. The classical thin shell theory was used to model the structural shell. The analysis was performed for Mach numbers between *0.67* and *1.42*. In this study it was concluded that the change of convective speed of the flow does not lead to a significant difference in the overall structural response or the interior pressure.

In 2001, Henry and Clark [73] developed an analytical model of a single curved panel coupled to the interior acoustic field of a rigid-walled cylinder. They applied

a criteria for maximal structural acoustic coupling between the modes of the curved panel and the modes of the cylindrical enclosure. For panels with aspect ratios typical of those found in aircraft, results indicate that predominantly axial structural modes couple most efficiently to the acoustic modes of the enclosure. In this analysis, they concluded that the structural-acoustic coupling is not significantly affected by varying panel position. However, their analysis does not focus the TBL excitation. The curved panel was considered to be subjected to a static pressure load.

Regarding the aircraft cabin interior noise induced by the TBL, several studies were conducted providing measurements of the interior SPL and fuselage skin vibrations spectrum, made at various locations in the cabin and cockpit of commercial aircraft [74–77], for aluminum and composite fuselages. The effect of aircraft speed on boundary layer induced interior noise can be seen to be dramatic, with the SPL being higher for higher flight speeds (as expected, following the same tendency of the external TBL pressure levels). These results are a good database for comparison with theoretical predictions of interior noise levels induced by the TBL.

The vibro-acoustic problem for the TBL excitation can also be solved using numerical methods. In each instant, or time step, one individual system is solved independently, and its solution will then provide a boundary condition to solve the other individual system. The solution of this system is then used as a boundary condition for the first one, that will be solved again. Before advancing for the next time step, this iterative process will be repeated until convergence for the coupled system is achieved for all the domain. For the numerical analysis of the sound field, it is possible to use Finite Difference (FD) analysis. The fluid is divided in a line grid, and field values are assigned to the grid intersection points. In a Cartesian coordinates system the grid is square, while in Finite Element (FE) analysis can have various geometric forms. FE analysis consists in the subdivision of the materials space into a finite set of transmittable elements, which can be straight or curved. At the nodes of the grid, connecting the several elements, the field variables and their partial derivatives are selected as the nodal degrees of freedom. Some studies were performed for the turbulent boundary layer excitation of plates and shells coupled with acoustic enclosures using numerical methods, in which the Finite Element (FE) analysis is usually used, such as in [78, 79]. However, numerical methods are not in the scope of the present work.

Another method that can be used to solve structural-acoustic coupling is the called Statistical Energy Analysis (SEA). In this context, SEA is a method for predicting

vibration transmission in dynamic systems made of coupled acoustic cavities and structures. The method estimates the time-average energy flow between the fluid and the structure, and divides the system in coupled sub-systems. It is assumed that the total energy flow between a structure and a volume of fluid is given by the sum of energy flows attributable to coupling between isolated pair of modes of the uncoupled components. Then, it is necessary to identify pairs of modes that are well matched spatially and that have approximate natural frequencies. The accuracy of the results highly depends on the choice of those pairs of modes. The equations of the method involve energies and power flows which are averaged over time, and also over the modes of vibration having natural frequencies in a band of frequencies which is large enough to contain a statistical usable modal population. This method, however, is more reliable in applications to systems which have fairly close natural frequencies, as described in [80]. Since the vibrational behavior of the system is described in a time-averaged energy flow, this method is usually used to obtain global information about the overall system.

For further information please refer to Appendices.

Chapter 3

Summary of Contributions

The contributions in this dissertation are contained in the five journal articles provided in Appendices A through E. This chapter summarizes these contributions and explains how they are connected toward the aims of the present work.

3.1 Prediction of Flow-Induced Noise in Transport Vehicles: Development and Validation of a Coupled Structural-Acoustic Analytical Framework

In this part of the study, a complete analytical framework for the prediction of flow-induced noise and vibration in transport vehicle cabins is presented. The mathematical model here developed represents a coupled structural-acoustic system, consisted by a plate subjected to a random excitation or to flow-induced noise, and a rectangular acoustic enclosure representing the transport vehicle cabin. The panels are considered to be flat and simply supported in all four boundaries, and the acoustic cabin is filled with air, with five rigid walls and one wall completely or partially flexible. The flexible part of the enclosure wall is excited by the turbulent boundary layer or by normally impinging random noise.

The coupled analytical model is developed using the contribution of both structural and acoustic natural modes. It is shown that the analytical framework can be used for the prediction of flow-induced noise for different types of transport vehicles, by changing some of the parameters, as shown by the good agreement between the analytical results and several experimental studies. The results indicate that the analytical model is sensitive to the measurement location, with the change in position significantly affecting the predicted interior noise levels, as should be expected.

Different sizes for the acoustic enclosure, as well as different types of panels were investigated. This study demonstrates the importance of including the acoustic receiving room (i.e., the vehicle cabin) contribution in the analytical formulation, in order to accurately predict the noise transmission and interior noise levels.

The mathematical model representing the problem of TBL-induced noise and vibration in transport vehicles' cabins was developed through the coupling between three different submodels: (1) an aerodynamic model, representing the TBL pressure fluctuations on the cabin structure; (2) a structural model, which characterize the vibration of the cabin structure; and (3) an acoustic model that represents the cabin interior sound pressure level. Corcos model [38, 39] was used to provide the cross power spectral density of the TBL wall pressure field, described by Eq. (2.7), in Section 2.1.2 of this dissertation. For the TBL reference power spectrum all the chosen studies for the validation of the analytical framework provide information about its value. However, in case of the absence of an adequate reference power spectrum function or value, the model proposed by Efimtsov [47] provides the best agreement with experimental data for the case of an aircraft in cruise flight. The classical plate theory was used as the governing equation for the plate structural displacement, w, which for a given applied external pressure is defined by

$$D_p \nabla^4 w + \rho_p h_p \ddot{w} + \zeta_p \dot{w} = p_{ext}(x, y, t), \tag{3.1}$$

where where ρ_p is the density of the plate, h_p is the thickness, $D_p = \frac{E_p h_p^3}{12\left(1-\nu_p^2\right)}$ is the panel stiffness constant, ζ_p was added to account for the damping of the plate, and w is defined through the plate natural modes as follows

$$w(x, y, t) = \sum_{m_x=1}^{M_x} \sum_{m_y=1}^{M_y} \alpha_{m_x}(x) \beta_{m_y}(y) q_{m_x m_y}(t), \tag{3.2}$$

where $\alpha_{m_x}(x)$ and $\beta_{m_y}(y)$ are the spatial functions, defining the variation of $w(x, y, t)$ with x and y respectively, $q_{m_x m_y}(t)$ are the temporal functions, defining the variation of $w(x, y, t)$ with time, and $M = M_x \times M_y$ is the total number of plate modes (m_x, m_y) considered. For simply supported plates, the spatial functions were defined as [57,81]:

$$\alpha_{m_x}(x) = \sqrt{\frac{2}{a}} \sin\left(\frac{m_x \pi x}{a}\right), \tag{3.3a}$$

$$\beta_{m_y}(y) = \sqrt{\frac{2}{b}} \sin\left(\frac{m_y \pi y}{b}\right), \tag{3.3b}$$

where a and b are the dimensions of the plate in the $x-$ and $y-$directions. The wave equation was used as the cabin acoustic field governing equation, defined as follows

$$\nabla^2 p - \frac{1}{c_0^2}\ddot{p} - \zeta_{ac}\dot{p} = 0, \tag{3.4}$$

in which c_0 is the speed of sound inside the cabin, ζ_{ac} is added to account for the acoustic damping in the enclosure, and the pressure p is given through the cabin acoustic modes [57, 82] by

$$p(x,y,z,t) = \sum_{n_x=1}^{N_x} \sum_{n_y=1}^{N_y} \sum_{n_z=1}^{N_z} \psi_{n_x}(x)\phi_{n_y}(y)\Gamma_{n_z}(z) r_{n_x n_y n_z}(t), \tag{3.5}$$

where $\psi_{n_x}(x)$, $\phi_{n_y}(y)$ and $\Gamma_{n_z}(z)$ are the spatial functions, $r_{n_x n_y n_z}(t)$ are the temporal functions, and $N = N_x \times N_y \times N_z$ is the number of acoustic modes (n_x, n_y, n_z) considered. The individual spatial functions are assumed to be orthogonal between each other, and given by the rigid body enclosure modes [83, 84], as following:

$$\psi_{n_x}(x) = \frac{A_{n_x}}{\sqrt{L_x}} \cos\left(\frac{n_x \pi x}{L_x}\right), \tag{3.6a}$$

$$\phi_{n_y}(y) = \frac{A_{n_y}}{\sqrt{L_y}} \cos\left(\frac{n_y \pi y}{L_y}\right), \tag{3.6b}$$

$$\Gamma_{n_z}(z) = \frac{A_{n_z}}{\sqrt{L_z}} \cos\left(\frac{n_z \pi z}{L_z}\right), \tag{3.6c}$$

in which L_x, L_y and L_z are the dimensions of the enclosure in the $x-, y-$ and $z-$directions, respectively, and the constants A_n were chosen in order to satisfy normalization.

The equations of each subsystem are then coupled in order to obtain a system of equations which describes the behavior of the structural-acoustic system, excited by the turbulent flow. This system of equations is developed such that three system matrices are obtained: (1) mass matrix, $\mathbf{M}$, (2) damping matrix, $\mathbf{D}$, and (3) stiffness

matrix, $\mathbf{K}$, as following:

$$\begin{bmatrix} \mathbf{M}_{pp} & 0 \\ \mathbf{M}_{cp} & \mathbf{M}_{cc} \end{bmatrix} \begin{pmatrix} \ddot{\mathbf{q}}(t) \\ \ddot{\mathbf{r}}(t) \end{pmatrix} + \begin{bmatrix} \mathbf{D}_{pp} & 0 \\ 0 & \mathbf{D}_{cc} \end{bmatrix} \begin{pmatrix} \dot{\mathbf{q}}(t) \\ \dot{\mathbf{r}}(t) \end{pmatrix} + \begin{bmatrix} \mathbf{K}_{pp} & \mathbf{K}_{pc} \\ 0 & \mathbf{K}_{cc} \end{bmatrix} \begin{pmatrix} \mathbf{q}(t) \\ \mathbf{r}(t) \end{pmatrix} = \begin{pmatrix} \mathbf{p}_{tbl}(t) \\ 0 \end{pmatrix}, \tag{3.7}$$

where:

$$\mathbf{M}_{pp} = diag\left[\rho_p h_p\right], \tag{3.8a}$$

$$\mathbf{D}_{pp} = diag\left[2\rho_p h_p \omega_m \xi_p\right], \tag{3.8b}$$

$$\mathbf{K}_{pp} = diag\left[\omega_m^2 \rho_p h_p\right], \tag{3.8c}$$

$$\mathbf{M}_{cc} = diag\left[\frac{1}{c_0^2}\right], \tag{3.8d}$$

$$\mathbf{D}_{cc} = diag\left[2\frac{1}{c_0^2}\omega_n \xi_{ac}\right], \tag{3.8e}$$

$$\mathbf{K}_{cc} = diag\left[\omega_n^2 \frac{1}{c_0^2}\right], \tag{3.8f}$$

$$\mathbf{M}_{cp} = \rho_0 \left[\frac{(-1)^{n_z} A_{n_z}}{\sqrt{L_z}} \int_{x_{p_i}}^{x_{p_f}} \alpha_{m_x}(x)\psi_{n_x}(x)dx \int_{y_{p_i}}^{y_{p_f}} \beta_{m_y}(y)\phi_{n_y}(y)dy\right], \tag{3.8g}$$

$$\mathbf{K}_{pc} = -\left[\frac{(-1)^{n_z} A_{n_z}}{\sqrt{L_z}} \int_{x_{p_i}}^{x_{p_f}} \alpha_{m_x}(x)\psi_{n_x}(x)dx \int_{y_{p_i}}^{y_{p_f}} \beta_{m_y}(y)\phi_{n_y}(y)dy\right], \tag{3.8h}$$

$$\mathbf{p}_{tbl}(t) = -\left[\int_{y_{p_i}}^{y_{p_f}} \int_{x_{p_i}}^{x_{p_f}} \alpha_{m_x}(x)\beta_{m_y}(y)p_{tbl}(x,y,t)dxdy\right]. \tag{3.8i}$$

in which ω_m and ω_n are, respectively, the natural frequencies of the plate and acoustic enclosure, the subscripts p and c correspond respectively to plate and cavity, with $\mathbf{M}_{pp}, \mathbf{D}_{pp}$, and $\mathbf{K}_{pp} \in \Re^{M\times M}$, $\mathbf{M}_{cc}, \mathbf{D}_{cc}$ and $\mathbf{K}_{cc} \in \Re^{N\times N}, \mathbf{M}_{cp} \in \Re^{N\times M}, \mathbf{K}_{pc} \in \Re^{M\times N}, \mathbf{q}(t)$ and $\mathbf{p}_{tbl}(t) \in \Re^{M\times 1}$, and $\mathbf{r}(t) \in \Re^{N\times 1}$. All matrices and vectors expressions were obtained analytically, as shown in more detail in the Appendix A.

The equations are then written in the frequency domain and in terms of the power spectral density, in order to obtain the PSD matrix of the plate displacement and the

PSD matrix of the cabin pressure, respectively defined as following:

$$\mathbf{S}_{WW}(\omega) = \mathbf{H}_W^*(\omega)\mathbf{S}_{tbl}(\omega)\mathbf{H}_W^T(\omega), \tag{3.9a}$$

$$\mathbf{S}_{PP}(\omega) = \mathbf{H}_P^*(\omega)\mathbf{S}_{tbl}(\omega)\mathbf{H}_P^T(\omega), \tag{3.9b}$$

where the system response matrices $\mathbf{H}_W(\omega)$ and $\mathbf{H}_P(\omega)$ are defined, respectively, by

$$\mathbf{H}_W(\omega) = \left(\mathbf{A} - \mathbf{B}\mathbf{D}^{-1}\mathbf{C}\right)^{-1}, \tag{3.10a}$$

$$\mathbf{H}_P(\omega) = -\mathbf{D}^{-1}\mathbf{C}\mathbf{H}_W(\omega). \tag{3.10b}$$

The generalized PSD matrix of the turbulent boundary layer excitation, $\mathbf{S}_{tbl}(\omega) \in \Re^{M\times M}$, is defined by

$$\mathbf{S}_{tbl}(\omega) = \left[\int_{y_{p_i}}^{y_{p_f}}\int_{y_{p_i}}^{y_{p_f}}\int_{x_{p_i}}^{x_{p_f}}\int_{x_{p_i}}^{x_{p_f}} \alpha_{m_x}(x)\alpha_{m_{x'}}(x')\beta_{m_y}(y)\beta_{m_{y'}}(y')S(\xi_x,\xi_y,\omega)dxdx'dydy'\right], \tag{3.11}$$

The PSD functions of the plate displacement and interior pressure are obtained, respectively, as follows:

$$S_{ww}(x_1,y_1,x_2,y_2,\omega) = \sum_{m_{x_1},m_{x_2}=1}^{M_x^2}\sum_{m_{y_1},m_{y_2}=1}^{M_y^2} \alpha_{m_{x_1}}(x_1)\alpha_{m_{x_2}}(x_2)\beta_{m_{y_1}}(y_1)\beta_{m_{y_2}}(y_2)\mathbf{S}_{WW}(\omega)_{m_1,m_2} \tag{3.12a}$$

$$S_{pp}(x_1,y_1,z_1,x_2,y_2,z_2,\omega) = \sum_{n_{x_1},n_{x_2}=1}^{N_x^2}\sum_{n_{y_1},n_{y_2}=1}^{N_y^2}\sum_{n_{z_1},n_{z_2}=1}^{N_z^2} \psi_{n_{x_1}}(x_1)\psi_{n_{x_2}}(x_2)\phi_{n_{y_1}}(y_1)\phi_{n_{y_2}}(y_2)\Gamma_{n_{z_1}}(z_1)\Gamma_{n_{z_2}}(z_2)\mathbf{S}_{PP}(\omega)_{n_1,n_2} \tag{3.12b}$$

Finally, the overall displacement PSD and overall interior pressure PSD can be found by integrating the individual power spectral densities over the plate surface and the cavity volume, respectively, as:

$$S_{ww}(\omega) = \int_{y_{p_i}}^{y_{p_f}} \int_{y_{p_i}}^{y_{p_f}} \int_{x_{p_i}}^{x_{p_f}} \int_{x_{p_i}}^{x_{p_f}} S_{ww}(x_1, y_1, x_2, y_2, \omega) dx_1 dx_2 dy_1 dy_2, \tag{3.13a}$$

$$S_{pp}(\omega) = \int_{z_{p_i}}^{z_{p_f}} \int_{z_{p_i}}^{z_{p_f}} \int_{y_{p_i}}^{y_{p_f}} \int_{y_{p_i}}^{y_{p_f}} \int_{x_{p_i}}^{x_{p_f}} \int_{x_{p_i}}^{x_{p_f}} S_{pp}(x_1, y_1, z_1, x_2, y_2, z_2, \omega) dx_1 dx_2 dy_1 dy_2 dz_1 dz_2. \tag{3.13b}$$

Closed-form analytical expressions were obtained for the prediction of flow-induced noise and vibration, as shown in Appendix A. The analytical expressions are able to predict overall values of interior SPL, overall values of plate vibration levels, as well as the SPL at a chosen point in the interior of the enclosure, and the level of structural vibration at a given point of the structure. The spectral quantities were obtained for frequencies up to $1000Hz$. The predictions obtained with the analytical framework are validated through the good agreement with several experimental studies [8,71,85,86]. The analytical predictions showed an overall match with the data from the validation cases, indicating that the developed framework can be used for the accurate prediction of noise and vibration levels, for vehicles with rectangular shape. Furthermore, it is shown that the number of plate and acoustic natural modes used in the analysis play an important role in the model accurate prediction. There is a minimum number of natural modes which needs to be used in the analysis, in order to accurately predict the noise and vibration levels up to a maximum frequency.

The main contributions of this part of the research are:

- Closed-form analytical expressions were obtained, that can be used in order to predict the noise and vibration inside transport vehicles with rectangular enclosures coupled with flow-excited panels.

- Validation of the analytical framework through the successfully comparison between the analytical predictions and the several experimental studies.

- Results lead to conclude that the analytical model is sensitive to the position (x, y, z), with the change in position (i.e., point of interest) significantly affecting the predicted interior noise levels and structural vibration levels, as should be expected. This study demonstrates the importance of including the acoustic receiving room (i.e., the vehicle cabin) contribution in the analytical formula-

tion, in order to accurately predict the cabin interior noise levels. Additionally, to obtain accurate predictions for the vibration and noise levels up to a certain frequency, a minimum number of structural and acoustic modes should be used in the analysis.

- The analytical framework developed represents a fundamental basis for further analysis (such as optimization and noise reduction analyses) on the rectangular system. The availability of fast and accurate models for the prediction of vibration and interior noise is fundamental for the implementation of these techniques.

For further information, the reader is directed to Appendix A.

3.2 Turbulent Boundary Layer Induced Noise and Vibration of a Multi-Panel Walled Acoustic Enclosure

This part of the work investigated the analytical prediction of turbulent boundary layer induced noise and vibration of a multi-panel system. In this phase of the research, the objective was to investigate the coupling between individual panels, located in different positions, and the acoustic enclosure. Each panel is coupled with the acoustic enclosure, which consists of a large rectangular room, with five rigid walls and one partially flexible wall. Different locations of the panels are examined, and the respective contributions to the interior noise compared.

The characteristics of the physical system were selected to represent an aircraft cabin, and the external flow considered is representative of typical cruise conditions of a commercial aircraft. This way, the properties of the panels and acoustic enclosure represent a typical fuselage skin panel and a rectangular cabin section, respectively. The turbulent boundary layer wall pressure PSD is defined through the Corcos model, for each panel, as follows

$$S(x,\xi_x,\xi_y,\omega) = S_{ref}(x,\omega)e^{\frac{-\alpha_x\omega|\xi_x|}{U_c}}e^{\frac{-\alpha_y\omega|\xi_y|}{U_c}}e^{\frac{-i\omega\xi_x}{U_c}} \tag{3.14}$$

in which, comparatevely with Eq. (2.7), the x dependence was added to account for the variation of the panel position along the streamwise direction, and the TBL

reference PSD was provided by the Efimtsov model [47], defined by

$$S_{ref}(x,\omega) = \frac{\tau_w^2(x)\delta(x)}{U_\tau(x)} \frac{0.01\pi}{1+0.02Sh^{\frac{2}{3}}(x,\omega)}, \tag{3.15}$$

with

$$U_\tau(x) = U_\infty\sqrt{\frac{C_f(x)}{2}}, \quad \tau_w(x) = \frac{1}{2}\rho U_\infty^2 C_f(x), \quad \text{and} \quad Sh(x,\omega) = \frac{\omega\delta(x)}{U_\tau(x)}, \tag{3.16}$$

in which τ_w is the mean wall shear stress, δ is the boundary layer thickness, U_τ is the friction velocity, C_f is the friction coefficient, and Sh is the Strouhal number. The functions $C_f(x)$ [87] and $\delta(x)$ [88], needed in previous equations were computed using the following semi-empirical expressions for turbulent boundary layer:

$$C_f(x) = 0.37\left(Log_{10}Re_x\right)^{-2.584}, \tag{3.17a}$$

$$\delta(x) = 0.37xRe_x^{-\frac{1}{5}}\left[1+\left(\frac{Re_x}{6.9\times10^7}\right)^2\right]^{\frac{1}{10}}, \tag{3.17b}$$

in which $Re_x = Ux/\nu$ is the Reynolds number.

The panels are considered to be flat, simply supported in all four edges, and assumed to represent the distance between adjacent stringers and frames of a conventional aircraft skin-stringer-frame structure. Each panel is individually vibrating and coupled with the acoustic enclosure. The governing equation of the panels, for the unpressurized cabin, is the one previously presented in Eq. (3.1), and for the pressurized cabin, is defined by

$$D_p\nabla^4 w + \rho_p h_p\ddot{w} + \zeta_p\dot{w} - \left[T_x\left(\frac{m_x\pi}{a}\right)^2 + T_y\left(\frac{m_y\pi}{b}\right)^2\right]w = p_{ext}(x,y,t), \tag{3.18}$$

in which T_x and T_y are the plates' in-plane tensions in $x-$ and $y-$directions, respectively. The plates' displacement w was defined through the panels' natural modes, as defined by Eq. (3.2), but with the spatial functions described as follows:

$$\alpha_{m_x}(x) = \sqrt{\frac{2}{a}}\sin\left(\frac{m_x\pi(x-x_{p_i})}{a}\right), \tag{3.19a}$$

$$\beta_{m_y}(y) = \sqrt{\frac{2}{b}}\sin\left(\frac{m_y\pi(y-y_{p_i})}{b}\right), \tag{3.19b}$$

in which (x_{p_i}, y_{p_i}) is the position of the origin of the i^{th} plate coordinates system, written in the global coordinates system. The governing equation of the acoustic system is the wave equation, as previously defined in Eq. (3.4), and the interior pressure p was described through the acoustic modes, as shown in Eqs. (3.5) and (3.6). The solutions for local and average values of the plates' displacement PSD and acoustic enclosure pressure PSD were derived from Eqs. (3.12) and (3.13).

A convergence study was performed to determine the number of structural and acoustic modes required for the calculation of the spectral quantities, indicating that a large number of non-resonant modes need to be considered in the analysis. For the aircraft panel considered in the present study, and for $f_{max} = 1000Hz$, the number of structural modes required to accurately calculate the PSD of the panel response is $M_x = 11$ and $M_y = 4$ for the untensioned plate, and $M_x = 9$ and $M_y = 3$ for the tensioned panel. Additionally, an hydrodynamic coincidence analysis was undertaken, showing that the hydrodynamic coincidence lines match the plate natural modes over a large part of the frequency range, which confirms the importance of inefficient, but resonant and highly excited modes in the aircraft noise problem.

Analytical predictions were obtained for both the space-averaged interior sound pressure level and local interior sound pressure level, as well as space-averaged and localized plate displacement PSD, for the pressurized and unpressurized cabins, as shown in results of the Appendix B.

It is shown that panels located at different locations have similar average displacement PSD (ADPSD), with panels located at bigger x-coordinates having a slightly higher ADPSD at all frequencies. This can be explained since an increase in x-station results in a higher value for the reference PSD of the TBL excitation. The first 3 ADPSD peaks correspond to plate bending modes, for both untensioned and tensioned plates. Additionally, considering pressurization effects results in a decreased radiated ADPSD for lower frequencies compared with the unpressurized cabin, resulted by the shift in the plate natural frequencies.

Results for local values of panels' displacement PSD (DPSD) were obtained for three different locations in the surface of the plate (1,1). It is shown that the point located at the center of the panel follow the same line as the ADPSD, with the peaks located at the same frequencies. However, the same does not occur for the other points considered, in which additional peaks can be observed for the DPSD curves. This can be explained since the point at the center of the plate is not affected when the longitudinal mode number, m_x, or the lateral mode number, m_y, is even. Thus,

when evaluating the PSD of the plate response, it is important to know the position of interest in the plate, since its value is dependent on the position of measurement.

The acoustic enclosure average pressure PSD (APPSD), due to the individual contribution of the panels, located at two different positions in the flexible wall, was analyzed. It is concluded that some peaks correspond to plate natural frequencies and other to acoustic natural frequencies, which illustrates the importance of the structural-acoustic coupling for the accurate prediction of the pressure in the interior of an enclosure. The uncoupled study of the sound radiated by an individual plate, vibrating due to turbulent flow, does not give the total information when the main goal is to predict aircraft interior noise. Another conclusion is that plates located at different positions have dissimilar contributions to the enclosure interior pressure levels.

The localized pressure PSD (PPSD) was obtained for four points inside the enclosure, due to the individual radiation of plates, located at four different positions - specifically, plates (1,1), (3,1), (3,5), and (5,1) are analyzed. It can be observed that point located closer to the vibrating panels have higher PPSD at almost all frequencies, compared with the other points. As expected, decreasing z-coordinate (i.e., moving away from the plates) results in lower PPSD values. It is interesting to verify that the structural-acoustic coupling has an important role in the prediction of the interior SPL. Analyzing the results for the four different plates, and the same observing point (x_1, y_1, z_1), one can verify that the PPSD plot has some variations from plate to plate. Since point (x_1, y_1, z_1) is always at the same relative position at each plate, that difference can only be due to the enclosure acoustic modes. The fact that each plate is in a different position with relation to the enclosure global coordinate system, changes the way it couples with the acoustic enclosure. This way, and as concluded for the DPSD, when evaluating the PSD of the interior pressure is important to know which is the position of interest in the enclosure, since the SPL value is dependent on the position of measurement.

The main contributions of this part of the research are:

- The application of the analytical framework to the prediction the turbulent flow-induced noise and vibration in a real-scale rectangular cabin, in which the panels, cabin and flow have properties that are representative of a real aircraft.

- Analysis of the hydrodynamic coincidence and unpressurized/pressurized cabin

effects on the prediction of vibration and noise levels.

- Study of the variation of the panels position in the cabin flexible wall. The results lead to conclude that, for the accurate prediction of aircraft interior noise and vibration, the position of the panel as well as the structural-acoustic coupling need to be considered. The traditional approach of assuming a single panel vibrating to free air does not provide all the information necessary for the accurate prediction of cabin interior noise.

- It is shown that the space-averaged values are different from the localized values, both for the plate displacement and interior pressure. It is concluded that identical panels located at different positions have dissimilar contributions to the cabin interior noise, showing that the panel position is an important variable for the accurate prediction and suppression of cabin noise. In this context, considering the traditional approach of a single panel coupled with an acoustic enclosure may not be enough for an accurate prediction of the cabin noise levels.

For further information, the reader is directed to Appendix B.

3.3 Prediction of Turbulent Boundary Layer Induced Noise in the Cabin of a BWB Aircraft

While in the previous paper the contribution of individual panels to the cabin interior noise was considered, in this part of the study the objective was to investigate the simultaneous contribution of multiple turbulent flow-excited panels to the cabin interior noise. The analytical framework is further developed and advanced to account for several panels vibrating simultaneously. The structural-acoustic system analyzed aims to describe a Blended Wing Body (BWB) cabin bay, filled with air and pressurized. The cabin bay is considered to have five rigid walls and one flexible wall, composed with 50 structural panels. The dimensions and properties of the panels and cabin are similar to those of a typical aircraft structural panel and passenger cabin section, respectively. The TBL excitation is representative of typical cruise conditions of a commercial aircraft, in high subsonic cruise and stabilized flight conditions.

As in the previous analyses, the TBL wall pressure fluctuations was defined through the Corcos and Efimtsov models, and the modal approach was used to define the panels' displacement and cabin interior pressure. The plate governing equation

and the wave number equation were used to describe the structural and acoustic systems, respectively. The individual systems were coupled and the basic coupled model system, represented previously in Eq. (3.7), was modified to represent the system consisted by a single acoustic enclosure coupled with several vibrating panels, as follows

$$\begin{bmatrix} \mathbf{M}_{1_{pp}} & 0 & \dots & 0 & 0 & 0 \\ 0 & \mathbf{M}_{2_{pp}} & \dots & 0 & 0 & 0 \\ \vdots & \vdots & \ddots & \vdots & \vdots & \vdots \\ 0 & 0 & \dots & \mathbf{M}_{Np-1_{pp}} & 0 & 0 \\ 0 & 0 & \dots & 0 & \mathbf{M}_{Np_{pp}} & 0 \\ \mathbf{M}_{1_{cp}} & \mathbf{M}_{2_{cp}} & \dots & \mathbf{M}_{Np-1_{cp}} & \mathbf{M}_{Np_{cp}} & \mathbf{M}_{cc} \end{bmatrix} \begin{pmatrix} \ddot{\mathbf{q}}_1(t) \\ \ddot{\mathbf{q}}_2(t) \\ \vdots \\ \ddot{\mathbf{q}}_{Np-1}(t) \\ \ddot{\mathbf{q}}_{Np}(t) \\ \ddot{\mathbf{r}}(t) \end{pmatrix} +$$

$$+ \begin{bmatrix} \mathbf{D}_{1_{pp}} & 0 & \dots & 0 & 0 & 0 \\ 0 & \mathbf{D}_{2_{pp}} & \dots & 0 & 0 & 0 \\ \vdots & \vdots & \ddots & \vdots & \vdots & \vdots \\ 0 & 0 & \dots & \mathbf{D}_{Np-1_{pp}} & 0 & 0 \\ 0 & 0 & \dots & 0 & \mathbf{D}_{Np_{pp}} & 0 \\ 0 & 0 & \dots & 0 & 0 & \mathbf{D}_{cc} \end{bmatrix} \begin{pmatrix} \dot{\mathbf{q}}_1(t) \\ \dot{\mathbf{q}}_2(t) \\ \vdots \\ \dot{\mathbf{q}}_{Np-1}(t) \\ \dot{\mathbf{q}}_{Np}(t) \\ \dot{\mathbf{r}}(t) \end{pmatrix} +$$

$$+ \begin{bmatrix} \mathbf{K}_{1_{pp}} & 0 & \dots & 0 & 0 & \mathbf{K}_{1_{pc}} \\ 0 & \mathbf{K}_{2_{pp}} & \dots & 0 & 0 & \mathbf{K}_{2_{pc}} \\ \vdots & \vdots & \ddots & \vdots & \vdots & \vdots \\ 0 & 0 & \dots & \mathbf{K}_{Np-1_{pp}} & 0 & \mathbf{K}_{Np-1_{pc}} \\ 0 & 0 & \dots & 0 & \mathbf{K}_{Np_{pp}} & \mathbf{K}_{Np_{pc}} \\ 0 & 0 & \dots & 0 & 0 & \mathbf{K}_{cc} \end{bmatrix} \begin{pmatrix} \mathbf{q}_1(t) \\ \mathbf{q}_2(t) \\ \vdots \\ \mathbf{q}_{Np-1}(t) \\ \mathbf{q}_{Np}(t) \\ \mathbf{r}(t) \end{pmatrix} = \begin{pmatrix} \mathbf{p}_{1_{tbl}}(t) \\ \mathbf{p}_{2_{tbl}}(t) \\ \vdots \\ \mathbf{p}_{Np-1_{tbl}}(t) \\ \mathbf{p}_{Np_{tbl}}(t) \\ 0 \end{pmatrix} \tag{3.20}$$

where N_p is the number of vibrating panels, $\mathbf{M}_{i_{pp}}$ and $\mathbf{M}_{i_{cp}}$ are mass matrices of the i^{th} plate, $\mathbf{D}_{i_{pp}}$ is the damping matrix of the i^{th} plate, $\mathbf{K}_{i_{pp}}$ and $\mathbf{K}_{i_{pc}}$ are stiffness matrices of the i^{th} plate. The local and average values of displacement and interior pressure PSD were obtained by Eqs. (3.12) and (3.13), in which the TBL excitation PSD matrix was now defined by

$$\mathbf{S}_{tbl}(\omega) = \begin{bmatrix} \mathbf{S}_{1_{tbl}}(\omega) & 0 & \dots & 0 & 0 \\ 0 & \mathbf{S}_{2_{tbl}}(\omega) & \dots & \vdots & \vdots \\ \vdots & \vdots & \ddots & \vdots & \vdots \\ 0 & 0 & \dots & \mathbf{S}_{Np-1_{tbl}}(\omega) & 0 \\ 0 & 0 & \dots & 0 & \mathbf{S}_{Np_{tbl}}(\omega) \end{bmatrix}, \tag{3.21}$$

with each $\mathbf{S}_{i_{tbl}}(\omega)$ matrix representing the TBL wall pressure fluctuation for the i^{th} plate, obtained by previous Eq. (3.11).

As discussed in the Appendix C, analytical predictions are obtained for the average and local interior of sound pressure level inside the cabin. Results show that average SPL increases with the number of vibrating panels and that the SPL curve maintains a similar shape as all plates have the same properties and dimensions. As shown in previous works, the peaks on the cavity power spectrum curve correspond to both plate and acoustic natural modes. For the local values of SPL, it is shown that as the number of vibrating plates is increased, the SPL also increases in all locations. However, the SPL curve shape is different from location to location. When considering 50 panels vibrating, the SPL curves for the locations considered are similar for frequencies greater than 355.45 Hz, i.e., for frequencies above the first panels mode. For frequencies below 355.45 Hz, the same does not occur, with curves having dissimilar shapes in the several locations. In the frequency range]0; 355.45] Hz, the peaks in the SPL curve correspond to the acoustic natural modes. Even though the SPL values are smaller in this frequency range, compared with the level for the 355.45 Hz peak, some of the SPL peaks lying in this range correspond to almost 60 dB SPL in the 50 panels configuration. This can be of particular interest, since these peaks lie in the human audible range, creating tones and directly affecting the passengers comfort. It is also important to verify that, depending on the location, these peaks have different amplifications, with their importance shifting from point to point.

The main contributions of this part of the research are:

- The development of an analytical framework and derivation of closed-form expressions for the prediction of vibration and noise levels for the Cartesian system with the simultaneous vibration of panels, excited by the turbulent flow.
- Investigation of the effects on SPL and vibration levels of increased number of vibrating panels.

- It is concluded that average SPL values show an overall increase with the number of panels, with the SPL curve essentially maintaining the same shape when all the vibrating panels have the same properties. Local SPL values, in specific locations inside the cabin, are also affected by the number of vibrating panels, generally increasing with the number of vibrating panels. As the number of vibrating panels increases, the local SPL curves and values become more similar among the several locations, for frequencies above the first panel resonance. For frequencies below this resonance, where the acoustic modes are dominant, the SPL curves are different from point to point, showing dissimilar amplifications of the acoustic modes.

For further information, the reader is directed to Appendix C.

3.4 Flow-Induced Noise and Vibration in Aircraft Cylindrical Cabins: Closed-Form Analytical Model Validation

The main objective of this state of the research was to develop closed-form analytical models for the prediction of turbulent boundary-layer-induced noise in the interior of aircraft cylindrical cabins. The mathematical model represents the structural-acoustic coupled system, consisted by the aircraft cabin section coupled with the fuselage structure. The aircraft cabin section is modeled as a cylindrical acoustic enclosure, filled with air. The fuselage structure, excited by external random excitation or by turbulent flow, is represented through two different models: (1) as a whole circular cylindrical shell with simply supported end caps, and (2) as a set of individual simply supported open circular cylindrical shells. So, the model was also developed for the case in which several shells are simultaneously vibrating. The predictions obtained from the developed analytical framework are validated through the successful comparison with several experimental studies. Analytical predictions are obtained for the shell structural vibration and sound pressure levels, for the frequency range up to 10,000 Hz. Compared with the rectangular system, the cylindrical system presents additional challenges in the mathematical manipulations, mainly due to the introduction of the Bessel functions, needed to model the acoustic natural modes.

The Corcos model [38,39] was used to describe the TBL excitation. Assuming that in substitution of a flat panel, one has a shallow open circular shell, the Corcos model, previous defined in Eq.(3.14) was written in the cylindrical coordinates systems as

$$S(x,\xi_x,\xi_\theta,\omega) = S_{ref}(x,\omega)e^{-\frac{\alpha_x\omega|\xi_x|}{U_c}}e^{-\frac{\alpha_y\omega|\xi_\theta|}{U_c}}e^{-\frac{i\omega\xi_x}{U_c}}, \tag{3.22}$$

where $\xi_\theta = R(\theta - \theta')$, in which R is the radius of the cylindrical cabin, and the reference spectrum $S_{ref}(x,\omega)$ is given by the Efimtsov model [47], defined in Eq. (3.15). The shells' governing equation was defined by [89]

$$w + \nu_s R\frac{\partial u}{\partial x} + \frac{\partial v}{\partial \theta} + \frac{h_s^2}{12R^2}\nabla^4 w + \frac{\rho_s(1-\nu_s^2)R^2}{E_s}\ddot{w} + \zeta_s\dot{w} = \frac{(1-\nu_s^2)R^2}{E_s h_s}p_{ext}(x,\theta,t), \tag{3.23}$$

in which ν_s is the Poisson ratio of the shell, h_s is the shell thickness, E_s is the shell Young's modulus, $\zeta_s = 2\,\omega^s_{m_x m_\theta}\xi_s$ is the structural modal damping, ξ_s is the shell damping ratio, $\omega^s_{m_x m_\theta}$ is the shell natural frequency corresponding to the (m_x, m_θ) shell mode. The structural displacement was defined by the modal approach, as follows

$$w(x,\theta,t) = \sum_{m_x=1}^{M_x}\sum_{m_\theta=1}^{M_\theta}\alpha_{m_x}(x)\beta_{m_\theta}(\theta)q_{m_x m_\theta}(t), \tag{3.24}$$

where $\alpha_{m_x}(x)$ and $\beta_{m_\theta}(\theta)$ are the shell mode shape functions, $q_{m_x m_\theta}(t)$ is a function of time, and $M = M_x \times M_\theta$ is the total number of shell structural modes considered in the analysis. Considering a circular cylindrical shells with simply supported end caps, and without axial constraint at its ends, the mode shape functions were defined by

$$\alpha_{m_x}(x) = \sqrt{\frac{2}{L_x}}\sin\left(\frac{m_x\pi x}{L_x}\right), \tag{3.25a}$$

$$\beta_{m_\theta}(\theta) = \sqrt{\frac{1}{\pi}}\cos\left(m_\theta\theta\right), \tag{3.25b}$$

and considering a circular cylindrical cabin composed by several open cylindrical shells, with simply supported edges, the mode shape functions were defined as follows

$$\alpha_{m_x}(x) = \sqrt{\frac{2}{a}}\sin\left(\frac{m_x\pi(x-x_i)}{a}\right), \tag{3.26a}$$

$$\beta_{m_\theta}(\theta) = \sqrt{\frac{2}{\theta_0}}\cos\left(\frac{m_\theta\pi(\theta-\theta_i)}{\theta_0}\right), \tag{3.26b}$$

in which a is the shell length, θ_0 is its arc, and (x_i, θ_i) is the origin of the i^{th} shell with relation to the cabin global coordinates system. The governing equation of a cylindrical acoustic enclosure is the wave equation written in the cylindrical coordinates system, as following

$$\nabla^2 p - \frac{1}{c_0^2}\ddot{p} - \zeta_{ac}\dot{p} = 0, \tag{3.27}$$

where $\zeta_{ac} = 2\omega^{ac}_{n_x n_\theta n_r}\xi_{ac}$ is the acoustic modal damping, ξ_{ac} is the acoustic damping ratio, and $\omega^{ac}_{n_x n_\theta n_r}$ is the acoustic natural frequency corresponding to the (n_x, n_θ, n_r) acoustic mode. The pressure field inside the enclosure was defined by

$$p(x, \theta, r, t) = \sum_{n_x=0}^{N_x}\sum_{n_\theta=0}^{N_\theta}\sum_{n_r=0}^{N_r} \psi_{n_x}(x)\phi_{n_r}(\theta)\Gamma_{n_\theta}(r) r_{n_x n_\theta n_r}(t), \tag{3.28}$$

in which $\psi_{n_x}(x)$, $\phi_{n_r}(\theta)$ and $\Gamma_{n_\theta}(r)$ are the mode shape functions, $r_{n_x n_\theta n_r}(t)$ are functions of time, and $N = (N_x + 1) \times (N_\theta + 1) \times (N_r + 1)$ is the total number of acoustic modes considered. The mode shape functions are assumed to be orthogonal between each other, and were defined as follows [81]

$$\psi_{n_x}(x) = \frac{A_{n_x}}{\sqrt{L_x}} \cos\left(\frac{n_x \pi x}{L_x}\right), \tag{3.29a}$$

$$\phi_{n_r}(\theta) = \frac{1}{\sqrt{\pi}} \sin\left(n_r\theta + \gamma\frac{\pi}{2}\right), \tag{3.29b}$$

$$\Gamma_{n_\theta}(r) = \frac{A_{n_\theta}}{R J_{n_r}(\lambda_{n_r n_\theta})} J_{n_r}\left(\lambda_{n_r n_\theta}\frac{r}{R}\right), \tag{3.29c}$$

where J_{n_r} are Bessel functions of the 1^{st} kind of n_r^{th} order, $\lambda_{n_r n_\theta}$ factor represents the n_r^{th} root of the equation $dJ_{n_r}(\lambda_{n_r n_\theta} r/R)/\ d(r/R) = 0$ at $r = R$, and A_n are chosen to satisfy normalization.

Combining the equations of the individual uncoupled subsystems, the governing equations of the coupled system are defined by Eq. (3.7), for the closed cylindrical shell, and by Eq. (3.20), for the cylindrical cabin composed by a set of curved panels, but now with the system matrices and excitation defined by:

$$\mathbf{M}_{ss} = \text{diag}\left[\frac{\rho_s(1-\nu_s^2)R^2}{E_s}\right], \tag{3.30a}$$

$$\mathbf{D}_{ss} = \text{diag}\left[\frac{\rho_s(1-\nu_s^2)R^2}{E_s} 2\omega^s_{m_x m_\theta}\xi_s\right], \tag{3.30b}$$

$$\mathbf{K}_{ss} = \text{diag}\left[\frac{\rho_s(1-\nu_s^2)R^2}{E_s} (\omega^s_{m_x m_\theta})^2\right], \tag{3.30c}$$

$$\mathbf{M}_{cc} = \text{diag}\left[\frac{1}{c_0^2}\right], \tag{3.30d}$$

$$\mathbf{D}_{cc} = \text{diag}\left[\frac{1}{c_0^2} 2\,\omega^{ac}_{n_x n_\theta n_r}\xi_{ac}\right], \tag{3.30e}$$

$$\mathbf{K}_{cc} = \text{diag}\left[\frac{1}{c_0^2} (\omega^{ac}_{n_x n_\theta n_r})^2\right], \tag{3.30f}$$

$$\mathbf{M}_{cs} = \rho_0\left[A_{n_r}\int_{x_i}^{x_f}\alpha_{m_x}\psi_{n_x}dx\int_{\theta_i}^{\theta_f}\beta_{m_\theta}\phi_{n_r}d\theta\right], \tag{3.30g}$$

$$\mathbf{K}_{sc} = \frac{(\nu_s^2-1)R^2}{E_s h_s}\left[A_{n_r}\int_{x_i}^{x_f}\alpha_{m_x}\psi_{n_x}dx\int_{\theta_i}^{\theta_f}\beta_{m_\theta}\phi_{n_r}d\theta\right], \tag{3.30h}$$

$$\mathbf{p}_{tbl}(t) = \frac{(\nu_s^2-1)R^2}{E_s h_s}\left[\int_{\theta_i}^{\theta_f}\int_{x_i}^{x_f}\alpha_{m_x}(x)\beta_{m_\theta}(\theta)p_{tbl}(x,\theta,t)dxd\theta\right]. \tag{3.30i}$$

The closed-form analytical expressions obtained for matrices $\mathbf{M}_{cs}$ and $\mathbf{K}_{sc}$ are shown in Appendix D. Previous matrices are then used to compute the PSD matrix of TBL excitation, $\mathbf{S}_{TBL}(\omega)$, the PSD matrix of the coupled shells displacement, $\mathbf{S}_{WW}(\omega)$, and the PSD matrix of the coupled acoustic cabin pressure, $\mathbf{S}_{PP}(\omega)$. Finally, through the PSD matrices, one can obtain the PSD functions of the shells displacement, S_{ww}, and of the acoustic cabin pressure, S_{pp}, as following

$$S_{ww}(x_1,\theta_1,x_2,\theta_2,\omega) = \sum_{m_{x_1},m_{x_2}=1}^{M_x^2}\sum_{m_{\theta_1},m_{\theta_2}=1}^{M_\theta^2}\alpha_{m_{x_1}}(x_1)\alpha_{m_{x_2}}(x_2)\beta_{m_{\theta_1}}(\theta_1)\beta_{m_{\theta_2}}(\theta_2)\mathbf{S}_{WW}(\omega)_{m_1,m_2} \tag{3.31a}$$

$$S_{pp}(x_1,\theta_1,r_1,x_2,\theta_2,r_2,\omega) = \sum_{n_{x_1},n_{x_2}=0}^{N_x^2}\sum_{n_{\theta_1},n_{\theta_2}=0}^{N_\theta^2}\sum_{n_{r_1},n_{r_2}=0}^{N_r^2}\psi_{n_{x_1}}(x_1)\psi_{n_{x_2}}(x_2)\phi_{n_{r_1}}(\theta_1)\phi_{n_{r_2}}(\theta_2)\Gamma_{n_{\theta_1}}(r_1)\Gamma_{n_{\theta_2}}(r_2)\mathbf{S}_{PP}(\omega)_{n_1,n_2} \tag{3.31b}$$

Finally, the overall-average PSD functions, $S_{ww}(\omega)$ and $S_{pp}(\omega)$, are obtained by

integration of $S_{ww}(x_1, \theta_1, x_2, \theta_2, \omega)$ over the shell area and of $S_{pp}(x_1, \theta_1, r_1, x_2, \theta_2, r_2, \omega)$ over the cabin volume. Closed-form analytical expressions obtained for functions $S_{ww}(\omega)$ and $S_{pp}(\omega)$ are shown in Appendix D.

Predictions for the shell vibration and interior acoustic field are presented for frequencies up to $10,000Hz$. To validate the analytical framework, two independent studies were considered for comparison [90,91]. It is shown that the analytical framework provides a good prediction of the reality, and once again, that the full coupling between structural and acoustic systems is important to obtain accurate predictions. The study by [73,92], which investigates a single-shell system coupled with a cylindrical acoustic cabin, was used as the basis for analysis of the cylindrical cabin composed by a set of shells. In this study, the dimensions of the curved panel have been selected to approximate the Boeing 737 fuselage sub-panels, while the dimensions of the cylinder approximate the size of a Boeing 737 fuselage, and results for the shell vibration and interior acoustic field are presented. Using our analytical model, predictions were calculated for three different cases, as follows: (1) single shell, excited by random white noise, coupled with the cylindrical enclosure; (2) the same single shell, but now excited by the TBL, coupled with the same cylindrical enclosure; (3) twelve shells (of the same dimensions and properties as the previous ones, and all located along the same x-coordinate), excited by the TBL, and coupled with the same cylindrical enclosure.

As shown by the results in Appendix D, it is concluded, both for local and average values, that the shell response due to the TBL differs from the shell response due to the random excitation, mainly for frequencies above approximately $338Hz$, i.e., above the first shell natural mode. This result should be expected as the white random excitation has a flat power spectral density, exciting all the frequencies with the same power, while the TBL excitation power spectral density varies through the frequency spectrum, exciting the low frequencies with higher power than the high frequencies. It is shown that dissimilar shell vibration curves are found for different points of the shell. Furthermore, it is shown that predictions for average and local values of the shell velocity are different, demonstrating the significance of including the position as an important variable in the development of predictive models.

The SPL analytical predictions were obtained for the three different cases previously described. Similarly to what was observed for the shell vibration level, it is shown that the random excitation is responsible for a higher amplification in the frequency range above $338Hz$, than the observed for the TBL excitation. In fact,

it is observed that compared with the case of the 12 shells excited by the TBL (the bold curve), a single shell, excited by white noise, can be responsible for generating a higher SPL for frequencies above approximately $1000Hz$. Comparing the SPL from a single shell excited by the TBL, and the SPL from the 12 shells excited by the TBL, it is clear that increasing the number of shells causes an overall increase in SPL. It is noted that SPL has the tendency to increase in the range $100 - 338Hz$ (below the shell first mode), and then a general decrease is observed. However, the increase in the number of shells can be responsible for changing the shape of the SPL over the frequency. It is clear that peaks in the SPL curves correspond not only to structural but also to acoustic modes. Specifically, for frequencies below the first shell resonance, the observed peaks correspond to acoustic modes, showing the importance of including the acoustic field contribution in the development of the analytical model. Depending on the location being analyzed, each mode has a dissimilar amplification, with their importance shifting from point to point. Results show that not only SPL is dependent on the position, but also different from the average values. This leads again to the conclusion that the ability of the model to predict average and local values is essential to obtain an accurate prediction of the reality.

The main contributions of this part of the research are:

- Closed-form analytical expressions were obtained for the prediction of turbulent flow-induced noise and vibration in aircraft cylindrical cabins, for systems with a single vibrating shell and for multiple shells.

- Validation of the analytical cylindrical framework through the successful comparison with experimental studies.

- It is shown that the type of excitation (random and TBL) produce different interior noise results, and that the number of structural and acoustic modes considered is a very important aspect in the accuracy of the predicted values. The random excitation is responsible for a higher amplification of the SPL for frequencies above the first shell resonance, compared with the TBL excitation.

- It is concluded that the increase in the number of vibrating shells causes an overall increase in SPL, and it can be responsible for changing the shape of the SPL curve over the frequency spectrum. Results show that not only SPL is dependent on the position, but also different from the average values. This

leads to the conclusion that the ability of the model to predict average and local values is essential to obtain an accurate prediction of the reality.

- A basis was created for further analysis on the cylindrical system.

For further information, the reader is directed to Appendix D.

3.5 On the Sensitivity of Sound Power Radiated by Aircraft Panels to Turbulent Boundary Layer Parameters

This stage of the research aimed to investigate and quantify how sensitive the sound radiated by aircraft panels is to the change of TBL excitation parameters, and was performed in collaboration with NASA Langley Research Center, Structural Acoustics Branch. Several empirical models exist nowadays for the prediction of the TBL wall pressure cross spectrum. These wall pressure cross spectrum models are usually dependent on four parameters: the reference power spectrum, the Mach number (associated with the TBL convective velocity), and the coherence lengths in streamwise and spanwise directions. The existent empirical models provide different predictions for the TBL wall pressure cross spectrum. Furthermore, real flow conditions over aircraft do not conform to the ideal behavior of the TBL wall pressure predicted by these models. However, the accuracy of the empirical models is important to the prediction of aircraft cabin interior noise. In this context, the questions that this research aims to explore are "What is the impact of different wall pressure estimates in the radiated sound power?" and "What is the effect of the range of possible flow conditions on the radiated sound power?". For that objective, data from flight tests and estimates provided by the empirical models are used to predict radiated sound power, and the results are compared. The panel radiated sound power (RSP) was calculated through the analytical closed-form expressions obtained in the previous papers.

As described in the Appendix E, the flight tests measurements were acquired at 3 different flight conditions, which were identified as Cases 1, 2 and 3 throughout the paper. Measurements of the TBL wall pressure PSD, and coherence lengths in the streamwise and spanwise directions were undertaken for the 3 flight conditions [93]. The TBL reference PSD and the coherence lengths from flight measurements were compared with those predicted through Corcos and Efimtsov models. To obtain the

predicted values for the coherence lengths for Corcos model, the following equations were used [38]:

$$L_x = \frac{U_c}{\alpha_x \omega}, \tag{3.32a}$$

$$L_y = \frac{U_c}{\alpha_y \omega}, \tag{3.32b}$$

in which U_c is the TBL convective velocity, ω is the angular frequency, $\alpha_x = 0.1$ and $\alpha_y = 0.77$. The coherence lengths predicted by the Efimtsov model were defined as following [47]:

$$L_x = \delta \left[\left(\frac{a_1 Sh}{U_c/U_\tau} \right)^2 + \frac{a_2^2}{Sh^2 + (a_2/a_3)^2} \right]^{-\frac{1}{2}}, \tag{3.33a}$$

$$L_y = \begin{cases} \delta \left[\left(\frac{a_4 Sh}{U_c/U_\tau} \right)^2 + \frac{a_5^2}{Sh^2 + (a_5/a_6)^2} \right]^{-\frac{1}{2}}, & \text{for } M < 0.75 \\ \delta \left[\left(\frac{a_4 Sh}{U_c/U_\tau} \right)^2 + a_7^2 \right]^{-\frac{1}{2}}, & \text{for } M > 0.9 \end{cases}, \tag{3.33b}$$

where δ is the TBL thickness, $U_\tau = U\sqrt{C_f/2}$ is the friction velocity, C_f is the friction coefficient, $Sh = \omega\delta/U_\tau$ is the Strouhal number, M is the flight Mach number, and constants a_1-a_7 are, respectively, 0.1, 72.8, 1.54, 0.77, 548, 13.5, and 5.66. Predicted L_y values for $M = 0.8$ were obtained through interpolation. Values for C_f and δ were calculated using the Eqs. (3.17a) and (3.17b), respectively. To calculate the TBL pressure spectrum, the following Efimtsov equation was used [53]:

$$S_{ref}(\omega) = 2\,\pi\,\alpha\,U_\tau^3\,\rho^2\,\delta\,\frac{\beta}{(1 + 8\alpha^3 Sh^2)^{\frac{1}{3}} + \alpha\,\beta\,Re_\tau \left(\frac{Sh}{Re_\tau} \right)^{\frac{10}{3}}}, \tag{3.34}$$

where $\alpha = 0.01$ and

$$\beta = \left[1 + \left(\frac{Re_{\tau_0}}{Re_\tau} \right)^3 \right]^{\frac{1}{3}}. \tag{3.35}$$

The radiated sound power matrix, containing the several $\Pi_{m_x m_y}$ components, was defined by

$$\mathbf{\Pi}(\omega) = \mathbf{S}_{VV}\mathbf{M}(\omega), \tag{3.36}$$

in which the panel velocity PSD matrix is $\mathbf{S}_{VV} = \omega^2 \mathbf{S}_{WW}$, where $\mathbf{S}_{WW}$ is the panel

displacement PSD matrix - determined by previous Eq. (3.9a) - , and $\mathbf{M}(\omega)$ is the radiation matrix, given by

$$\mathbf{M}(\omega) = 8\frac{\rho_0}{c_0}\left(\frac{\omega ab}{\pi^3 m_x m_y}\right)^2 \int_0^{\frac{\pi}{2}} \int_0^{\frac{\pi}{2}} \left\{ \frac{\begin{matrix}\cos \left(\frac{\alpha}{2}\right) & \cos \left(\frac{\beta}{2}\right) \\ \sin \left(\frac{\alpha}{2}\right) & \sin \left(\frac{\beta}{2}\right)\end{matrix}}{\left[\left(\frac{\alpha}{m_x \pi}\right)^2 - 1\right]\left[\left(\frac{\beta}{m_y \pi}\right)^2 - 1\right]} \right\}^2 \sin\theta d\theta d\phi \tag{3.37}$$

Data from flight measurements were compared with the data provided by the Efimtsov model, and the RSP was obtained both for flight measurements data and for data predicted by the empirical model. The RSP for both conditions was then compared, to investigate the the effect of different flow conditions on the RSP. The numerical study was obtained assuming appropriate parameters for a typical aircraft panel [19, 40]. A total number of $M_x = 19$ and $M_y = 14$ panel modes were used to achieve convergence of the results up to $5KHz$. As in [19, 40], the quantities were calculated based on the panel displacement level predicted for the point $(x, y) = (0.3a; 0.2b)$. The predicted RSP is in good agreement with the results shown in [19]. Additionally, the average RSP, calculated based on the average panel displacement level, was also analyzed. It is observed that, mainly for the low frequency range, the RSP for measured data have higher values than the RSP for the predicted values from Efimtsov model.

To understand how each TBL parameter affects the panel RSP, an uncertainty and sensitivity analyses were performed. As shown in detail in Appendix E, the influence of the change of each TBL parameter on the variation of the RSP was individually investigated, through the derivation of mathematical functions which describe the change of RSP as function of each individual parameter. With relation to the TBL reference PSD parameter, its was concluded that increasing the TBL power spectrum has a direct effect on the RSP without regard to hydrodynamic coincidence and modal interaction, i.e., an increase of xdB in S_{ref} yields an increase of xdB in RSP, over the entire frequency spectrum. For the change in streamwise coherence length, a different behavior was observed for RSP variation for frequencies below or above the hydrodynamic frequency. In the absence of hydrodynamic coincidence, i.e., for frequencies above the coincidence frequency, shorter lengths produce higher RSP levels. Below this frequency, in the regions where the hydrodynamic coincidence occur, longer coherence lengths produce higher RSP levels. Considering the coherence

length in the spanwise direction, it is found that higher values of coherence length produce an increase in RSP. Finally, the increase in Mach number will also increase the hydrodynamic coincidence frequency, and this is reflected in the RSP predictions. An increase in the Mach number results in higher RSP levels for frequencies above the hydrodynamic coincidence frequency.

It is shown that different TBL parameters have different effect on the RSP. For the frequency range analyzed, it is shown that higher values of Mach number, TBL reference spectrum, and spanwise coherence length produce higher values of RSP, while higher values of streamwise coherence length produce lower RSP. It is concluded that the Mach number is the parameter that most affects the RSP, followed by TBL PSD, and then by coherence lengths. For instance, an uncertainty of 1% in the Mach number parameter (or in the convective velocity) is responsible for a 41% difference in RSP at $4000Hz$, while 1% uncertainty in TBL PSD causes a 9% difference in RSP at $4000Hz$. This leads to conclude that a better understanding of the TBL wall pressure in the aircraft sidewall is necessary to have more reliable RSP predictions, and to tighten uncertainty in RSP predictions.

The main contributions of this part of the research are:

- Comparison between TBL parameters obtained from flight measurements and predicted by empirical models. This allowed to understand the level of uncertainty of the TBL measured parameters related with the predicted parameters. The RSP for each TBL data set (measured and predicted) is obtained and compared.

- Determination of individual functions which describe the variation of RSP with relation to the variation of each TBL parameter.

- Quantitative answer on how much $x_1\%$ of variation in the TBL parameter Y will affect the panel RSP, given as $x_2\%$.

For further information, the reader is directed to Appendix E.

Chapter 4

Conclusions and Future Work

This dissertation is devoted to the development of analytical models for the prediction of flow-induced noise and vibration in aircraft cabins. The turbulent boundary layer is a major source of aircraft cabin interior noise, while in cruise flight, making it an important subject of research. Furthermore, there is an increased concern about the effect of high noise levels in our society, but at the same time a lack of understanding of the mechanisms of sound radiation and transmission involved in the aircraft cabin noise problem. This thesis main contribution is to provide an analytical framework in the direction of this understanding. Closed-form analytical expressions were derived. Predictions of noise and vibrations levels for several representative cases were obtained, and validated through the successful comparison with several independent experimental studies. The analytical models were developed for Cartesian and cylindrical coordinates, for systems with one or more vibrating panels/shells, providing a basis for the prediction of noise and vibration for future and conventional aircraft configurations.

Results indicate that the analytical model is sensitive to the change of position, i.e., the vibration level is different from point to point in the plate surface, and the SPL is different from point to point in the interior of the cabin. It is shown that the change in position can significantly affect the predicted values of interior noise and structural vibration. Furthermore, to an accurate prediction of aircraft interior noise and vibration, the position of the panel, with relation to the cabin, should also be considered. The traditional approach of assuming a single panel vibrating to free air does not provide all the information necessary for the accurate prediction of cabin interior noise prediction. Also, considering a single panel coupled with an acoustic enclosure may not be enough as well, since similar panels at different locations have

different contributions for the interior noise, as shown by this investigation.

It is concluded that an increase in the number of vibrating panels/shells causes an overall increase of the average SPL values, and that the average SPL curve essentially maintains the same shape over the entire frequency range, when all the panels are kept with the same properties. Local SPL values, in specific locations inside the cabin, are also affected by the number of vibrating panels/shells. When the number of panels increase, the local SPL curves and values become more similar among the several locations, for frequencies above the first panel resonance. For frequencies below this resonance, the SPL curves are different from point to point, showing dissimilar amplifications of the acoustic modes. Results show that not only the SPL is dependent on the position, but it can also be very different from the average values. This leads to the conclusion that the ability of the model to predict average and local values is essential to obtain accurate predictions. Additionally, the type of excitation (random and TBL) produce different predictions of interior SPL, with the random excitation being responsible for a higher amplification of the SPL for frequencies above the first shell resonance, compared with the TBL excitation.

The analysis of the panel RSP sensitivity to TBL parameters provides useful information, since the several empirical models existent nowadays provide dissimilar predictions for the TBL wall pressure spectrum. The sensitivity and uncertainty analyzes performed show that the change in the TBL parameters have dissimilar effects on the RSP. The effect of the variation of each TBL parameter is individually studied, and functions are obtained to describe these variations, providing a quantitative measure for the effect of each parameter. It is shown that an increase of xdB in TBL reference PSD produces an increase of xdB in RSP. For the change in streamwise coherence length, for frequencies above the coincidence frequency, shorter lengths produce higher RSP levels. Below this frequency, in the regions where the hydrodynamic coincidence occur, longer coherence lengths produce higher RSP levels. Considering the coherence length in the panels' spanwise direction, it is observed that higher values of coherence length yield an increase in RSP. The increase in Mach number will increase the hydrodynamic coincidence frequency, and this is reflected in the RSP predictions. An increase in the Mach number results in higher RSP levels for frequencies above the hydrodynamic coincidence frequency.

Finally, for the frequency range analyzed, it is shown that the Mach number is the parameter that most affects the RSP, followed by TBL PSD, and then by coherence lengths. For instance, an uncertainty of 1% in the Mach number parameter (or in

the convective velocity) is responsible for a 41% difference in RSP at $4000Hz$, while 1% uncertainty in TBL PSD causes a 9% difference in RSP at $4000Hz$. This leads to conclude that a better understanding of the TBL wall pressure in the aircraft sidewall is necessary to obtain more reliable RSP predictions, and to tighten uncertainty in RSP predictions.

As future work, the objective will be to investigate different configurations of aircraft panels to obtain reduced aircraft interior noise. The panel shape, size, material properties, boundary conditions, number of stringers, and panel location relative to the cabin are parameters that dictate how much noise is radiated into the cabin, for specific flight conditions. Currently, the typical aircraft panel is of rectangular shape. The aim will be to investigate several panel configurations, such that the radiated sound power can be evaluated and compared with the baseline rectangular panel, in order to find optimized panels.

Bibliography

[1] D. Bishop. Cruise flight noise levels in a turbojet transport airplane. *Noise Control*, 7:37–42, 1961.

[2] W. Bhat. Flight test measurement of measurement of exterior turbulent boundary layer pressure fluctuations on boeing model 737 airplane. *Journal of Sound and Vibration*, 14(4):439–457, 1971.

[3] J. Renninger. Aircraft interior acoustics, 2000. E-A-R Specialty Composites.

[4] J. F. Wilby. Aircraft interior noise. *Journal of Sound and Vibration*, 190(3):545–564, 1996.

[5] P. Gardonio. Review of active techniques for aerospace vibro-acoustic control. *Journal of Aircraft*, 39(2):206–214, 2002.

[6] W. Bhat and J. Wilby. Interior noise radiated by an airplane fuselage subjected to turbulent boundary layer excitation and evaluation of noise reduction treatments. *Journal of Sound and Vibration*, 18(4):449–464, 1971.

[7] G. P. Gibbs, R. H. Cabell, and J. Juang. Controller complexity for active control of turbulent boundary-layer noise from panels. *AIAA Journal*, 42(7):1314–1320, 2004.

[8] K. Frampton and R. Clark. Power flow in an aeroelastic plate backed by a reverberant cavity. *Journal of Acoustical Society of America*, 102(3):1620–1627, 1997.

[9] V. Mellert, I. Baumann, N. Freese, and R. Weber. Impact of sound and vibration on health, travel comfort and performance of flight attendants and pilots. *Aerospace Science and Technology*, 12:18–25, 2008.

[10] J. Quehl. *Comfort studies on aircraft interior sound and vibration.* PhD thesis, Universitat Oldenburg, 2001.

[11] K. Waye. On the effects on environmental low frequency noise. Technical report, Department of Environmental Medicine, Goteborg University Publication, 1995.

[12] C. Maschke. Editorial introduction to the special issue on low frequency noise. *Journal of Noise and Health*, 23:1–2, 2004.

[13] N. Castelo Branco. The clinical stages of vibroacoustic disease. *Aviation, Space and Environmental Medicine*, 70(3):32–39, 1999.

[14] N. Castelo Branco, A. guas, A. Pererira, E. Monteiro, J. Fragata, F. Tavares, and N. Grande. The human pericardium in vibroacoustic disease. *Aviation, Space and Environmental Medicine*, 70(3):54–62, 1999.

[15] A. Araujo, F. Pais, J. Lopo Tuna, M. Alves-Pereira, and N. Castelo Branco. Echocardiography in noise-exposed flight crew. In *Internoise 2001*, pages 1007–10, The Hague, Holland, 2001.

[16] N. Castelo Branco and M. Alves-Pereira. Vibroacoustic disease. *Journal of Noise and Health*, 6(23):3–20, 2004.

[17] N. Castelo Branco. The vibro-acoustic disease - a 25 year old saga. In *12th International Congress of Sound and Vibration*, 2005. Keynote Paper 560.

[18] J. Kim and J. Lee. Broadband transmission noise reduction of smart panels featuring piezoelectric shunt circuits and sound-absorbing material. *Journal of the Acoustical Society of America*, 112(3):990–998, 2002.

[19] C. Maury, P. Gardonio, and S. Elliott. Active control of the flow-induced noise transmitted through a panel. *AIAA Journal*, 39:1860–1867, 2001.

[20] J. E. Efowcs Williams. Anti-sound. In *Royal Society of London*, volume 395, pages 63–88, 1984.

[21] A. Campanella et al. Acoustical frequent asked questions. Technical report, Campanella Acoustics Consultants, May 2007.

[22] C. R. Fuller. Apparatus and method for global noise reduction. Technical report, U.S. Patent No. 4,715,599, 1987.

[23] C. R. Fuller. Active control of sound transmission/radiation from elastic plate by vibration inputs: I. analysis. *Journal of Sound and Vibration*, 136(1):1–15, 1990.

[24] C. Werner-Westphal, W. Heinze, and P. Horst. Structural sizing for an unconventional, environment-friendly aircraft configuration within integrated conceptual design. *Aerospace Science and Technology*, 12:184–194, 2008.

[25] I. Lee and H. Sung. Multiple-arrayed pressure measurement for investigation of the unsteady flow structure of a reattaching shear layer. *Journal of Fluid Mechanics*, 463:377–402, 2002.

[26] L. Hudy, A. Naguib, and W. Humphreys. Stochastic estimation of a separated-flow field using wall-pressure-array measurements. *Physics of Fluids*, 19(2), 2007.

[27] A. Aditjandra, B. Trosin, and A. Naguib. Array measurements of the surface pressure beneath a forced axi-symmetric separation bubble. *Experiments in Fluids*, 46:297–308, 2009.

[28] M. Lowson. Prediction of boundary layer pressure fluctuations. Technical report, AFFDL-TR-67-167, Air Force Flight Dynamics Laboratory, Ohio, 1968.

[29] K. Hoffmann and S. Chiang. *Computational fluid dynamics*. Engineering Education Systems, Wichita, Kansas, USA, 2000.

[30] W. Graham. A comparison of models for the wavenumber-frequency spectrum of turbulent boundary layer pressures. *Journal of Sound and Vibration*, 206(4):541–565, 1997.

[31] M. J. Lighthill. On sound generated aerodynamically. i. general theory. *Proceedings of the Royal Society of London*, 211(1107):564–587, 1952.

[32]

[33] M. Bull et al. Wall-pressure fluctuations in boundary layer flow and response of simple structures to random pressure field. Technical report, Univiversity of Southampton, 1963.

[34] W. Willmarth and C. Woohlridge. Measurements of the correlation between the fluctuating velocities and fluctuating wall pressure in a thick turbulent boundary layer. Technical report, Univiversity of Michigan Coll. Eng., 1962.

[35] W. Strawderman and R. Brand. Turbulent-flow-excited vibration of a simply supported, rectangular flat plate. *The Journal of the Acoustical Society of America*, 45(1):177–192, 1969.

[36] W. Strawderman. Turbulence-induced plate vibrations: an evaluation of finite- and infinite-plate models. *The Journal of the Acoustical Society of America*, 46(5):1294–1304, 1969.

[37] M. Bull. Wall-pressure fluctuations beneath turbulent boundary layers: some reflections on forty years of research. *Journal of Sound and Vibration*, 190(3):299–315, 1996.

[38] G. Corcos. The structure of the turbulent pressure field in boundary-layer flows. *Journal of Fluid Mechanics - Cambrigde Journal Online*, 18:353–378, 1964.

[39] G. Corcos. Resolution of pressure in turbulence. *Journal of the Acoustical Society of America*, 35(2):192–199, 1963.

[40] C. Maury, P. Gardonio, and S. Elliott. A wavenumber approach to the modelling the response of a randomly excited panel, part i: General theory. *Journal of Sound and Vibration*, 252(1):83–113, 2002.

[41] W. Graham. Boundary layer induced noise in aircraft, part i: The flat plate model. *Journal of Sound and Vibration*, 192(1):101–120, 1996.

[42] T. Bravo and C. Maury. The experimental synthesis of random pressure fields: Methodology. *Journal of the Acoustical Society of America*, 120(5):2702–2711, 2006.

[43] C. Maury and T. Bravo. The experimental synthesis of random pressure fields: Practical feasibility. *Journal of the Acoustical Society of America*, 120(5):2712–2723, 2006.

[44] C. Maury, P. Gardonio, and S. Elliott. A wavenumber approach to the modelling the response of a randomly excited panel, part ii: Application to aircarft panels excited by a turbulent boundary layer. *Journal of Sound and Vibration*, 252(1):115–139, 2002.

[45] S. Strumolo. Method and system for predicting sound pressure levels within a vehicle due to wind noise. *United States Paten Number 5,568,404*, 1996.

[46] D. Thomas and P. Nelson. Feedback control of sound radiation from a plate excited by a turbulent boundary layer. *Journal of the Acoustical Society of America*, 95(5):2651–2662, 1995.

[47] B. Efimtsov. Characteristics of the field of turbulent wall pressure fluctuations at large reynolds numbers. *Soviet Physics-Acoustics*, 28(4):289–292, 1982.

[48] J. Ffowcs Williams. Boundary-layer pressures and the corcos model: a development to incorporate low-wavenumber constraints. *Journal of Fluid Mechanics*, 125:9–25, 1982.

[49] Y. Hwang and F. Geib. Estimation of the wavevector-frequency spectrum of turbulent boundary layer wall pressure by multiple linear regression. *Journal of Vibration, Acoustics, Stress and Reliability in Design*, 106:334–342, 1984.

[50] D. Chase. Modelling the wavevector-frequency spectrum of turbulent boundary layer wall-pressure. *Journal of Sound and Vibration*, 70:29–67, 1980.

[51] D. Chase. The character of the turbulent wall pressure spectrum at subconvective wavenumbers and a suggested comprehensive model. *Journal of Sound and Vibration*, 112:125–147, 1987.

[52] A. Smol'yakov and V. Tkachenko. Model of a field of pseudonic turbulent wall pressures and experimental data. *Soviet Physics-Acoustics*, 37(6):627–631, 1991.

[53] R. Rackl and A. Weston. Modeling of turbulent boundary layer surface pressure fluctuation auto and cross spectra - verification and adjustments based on tu-144ll data. Technical report, NASA CR-213938, 2005.

[54] D. Sullivan. *Aircraft Interior Structural-Acoustic Control Design*. PhD thesis, Massachusetts Institute of Technology, 1998.

[55] Y. Tang, R. Silcox, and J. Robinson. Sound transmission through cylindrical shell structures excited by boundary layer pressure fluctuations. Technical report, NASA-AIAA-96-1760, 1996.

[56] B. Fang, A. Kelkar, S. Joshi, and H. Pota. Modelling, system identification, and control of acousticstructure dynamics in 3-d enclosures. *Control Engineering Practice*, 12:989–1004, 2004.

[57] F. Fahy. *Sound and Structural Vibration, Radiation, Transmission and Response*. Academic Press, 1985.

[58] F. Fahy. Vibration of containing structures by sound in the contained fluid. *Journal of Sound and Vibration*, 10(3):490–512, 1969.

[59] E. Dowell, G. Gorman, and D. Smith. Acoustoelasticity: General theory, acoustic natural modes and forced response to sinusoisal excitation, including comparisons with experiment. *Journal of Sound and Vibration*, 52(4):519–542, 1977.

[60] R. Vaicaitis, F. Grosveld, and J. Mixson. Noise transmission through aircraft panels. *Journal of Aircraft*, 22:303–310, 1985.

[61] A. Grewal, D. Zimcik, and R. Lapointe. Vibro-acoustic modeling in aircraft cabin noise transmission and control. In *38th AIAA/ASME/ASCE/AHS/ASC Structures, Structural Dynamics, and Materials Conference and Exhibit*, number 1101, 1997.

[62] A. Moustafa and B. Balachandran. Sound transmission through a flexible panel into an enclosure: structural-acoustic model. *Journal of Sound and Vibration*, 284:467–486, 2005.

[63] L. Maestrello. Measurement and analysis of the response field of turbulent boundary layer excited panels. *Journal of Sound and Vibration*, 2(3):270–292, 1965.

[64] L. Maestrello. Radiation from and panel response to a supersonic turbulent boundary layer. *Journal of Sound and Vibration*, 10(2):261–295, 1969.

[65] H. Davies. Sound from turbulent boundary layer excited panels. *The Journal of the Acoustical Society of America*, 55:213–219, 1971.

[66] W. Chyu and M. Yang. Random response of reacatngular plates to the pressure field beneath a turbulent boundary layer in subsonic flows. Technical report, NASA TN D-6970, 1972.

[67] F. Han, R. Bernhard, and L. Mongeau. Prediction of flow-induced structural vibration and sound radiation using energy analysis. *Journal of Sound and Vibration*, 227(4):685–709, 1999.

[68] S. Finnveden, F. Birgersson, U. Ross, and T. Kremer. A model of wall pressure correlation for prediction of turbulence-induced vibration. *Journal of Fluids and Structures*, 20:1127–1143, 2005.

[69] R. Vaicaitis and M. Slazak. Noise transmission through stiffned panels. *Journal of Sound and Vibration*, 70(3):413–426, 1980.

[70] R. Vaicaitis. Aircraft cabin noise prediction and optimization. Technical report, NASA CR 175982, 1985.

[71] C. Barton and E. Daniels. Noise transmission through flat rectangular panels into a closed cavity. Technical report, NASA TP 1321, 1978.

[72] J. K. Henry and R. Clark. A curved piezo-structure model: implications on active structural acoustic control. *Journal of the Acoustical Society of America*, 106(3):1400–1407, 1999.

[73] J. Henry and R. Clark. Noise transmission from a curved panel into a cylindrical enclosure: Analysis of structural acoustic coupling. *Journal of the Acoustical Society of America*, 109(4):1456–1463, 2001.

[74] A.Jackson, F. Balena, W. LaBarge, G. Pei, W. Pitman, and G. Wittlin. Transport composite fuselage technology - impact dynamics and acoustic transmission. Technical report, NASA CR-4035, 1986.

[75] D. Palumbo, R. Cabell, J. Cline, and B. Sullivan. Active structural interior noise on acoustic noise of raytheon 1900d. Technical report, NASA TM-209846, 2000.

[76] S. Rizzi, R. Rackl, and E. Andrianov. Flight test measurements from the tu-144ll structure/cabin noise experiment. Technical report, NASA TM-209858, 2000.

[77] T. Beier, W. Bhat, S. Rizzi, R. Silcox, and M. Simpson. High speed research program structural acoustics multi-year summary report. Technical report, NASA TM-213536, 2005.

[78] S. Engelstad. Computational modeling considerations for aircraft cockpit noise. In *15th AIAA Aeroacoustic Conference*, number 4378, 1993.

[79] F. Birgersson, N. Ferguson, and S. Finnveden. Application of the spectral finite element method to turbulent boundary layer induced vibration of plates. *Journal of of Sound and Vibration*, 259:873–891, 2003.

[80] F. Fahy. Statistical energy analysis - a critical review. *The Shock and Vibration Digest*, 6:14–33, 1974.

[81] J. Blevins. *Formulas for Natural Frequency and Mode Shape*. Krieger Publishing Company, Malabar, FL, 2001.

[82] A. Pierce. *Acoustics, An Introduction to its Physical Principles and Applications*. McGraw-Hill, 1981.

[83] H. Kuttruff. *Room Acoustics*. Applied Science, 1973.

[84] P. Nelson and S. Elliot. *Active Control of Sound*. Academic Press, 1992.

[85] C. M. Heatwole, R. J. Bernhard, and M. A. Francheck. Robust feedback control of flow induced structural radiation of sound. Technical report, NASA Report 0278-1, 1997.

[86] G. Smith and R. Clark. Optimal transducer placement for active control of sound transmission through aeroelastic plates. *Journal of Intelligent Materials Systems and Structures*, 9:975–987, 1998.

[87] R. Wahidi, W. Chakroun, and S. Al-Fahed. The behavior of the skin-friction coefficient of a turbulent boundary layer flow over a flat plate with differently configured transverse square grooves. *Experimental Thermal and Fluid Science*, 30:141–152, 2005.

[88] D. Bies. A review of flight and wind tunnel measurements of boundary layer pressure fluctuations and induced structural response. Technical report, NASA CR-626, 1966.

[89] A. Leissa. *Vibration of Shells*. National Aeronautics and Space Administration, Washigton, D.C., 1973.

[90] L. Pope, D. Rennison, C. Willis, and W. Mayes. Development and validation of preliminary analytical models for aircraft interior noise reduction. *Journal of Sound and Vibration*, 82(4):541–575, 1982.

[91] J. Missaoui and L. Cheng. Vibroacoustic analysis of a finite cylindrical shell with internal floor partition. *Journal of Sound and Vibration*, 226(1):101–123, 1999.

[92] J. Henry and R. Clark. Active control of sound transmission through a curved panel into a cylindrical enclosure. *Journal of Sound and Vibration*, 249(2):325–349, 2002.

[93] D. Palumbo. Determining correlation and coherence lengths in the wall pressure of the turbulent boundary layer. Technical report, NASA, 2010.

Appendix A

Prediction of Flow-Induced Noise in Transport Vehicles: Development and Validation of a Coupled Structural-Acoustic Analytical Framework

PREDICTION OF FLOW-INDUCED NOISE IN TRANSPORT VEHICLES: DEVELOPMENT AND VALIDATION OF A COUPLED STRUCTURAL-ACOUSTIC ANALYTICAL FRAMEWORK

Joana da Rocha[1], Afzal Suleman[1], and Fernando Lau[2]
[1]Dept. of Mechanical Engineering, University of Victoria, PO Box 3055, Stn. CSC, Victoria, BC, Canada, V8W 3P6
jdarocha@uvic.ca, suleman@uvic.ca
[2]Centro de Ciências e Tecnologias Aeronáuticas, Dept. de Engenharia Mecânica, Instituto Superior Técnico, Av. Rovisco Pais, Lisboa, Portugal, 1049-001 lau@ist.utl.pt

ABSTRACT

In this study, a complete analytical model framework able to accurately predict the flow-induced noise in the interior of a transport vehicle cabin is presented. The mathematical model framework presented represents a coupled structural-acoustic system, consisted by a plate subjected to a random excitation or to flow-induced noise, and an acoustic enclosure representing the transport vehicle cabin. The coupled analytical model is developed using the contribution of both structural and acoustic natural modes. It is shown that the analytical framework can be used for the prediction of flow-induced noise for different types of transport vehicles, by changing some of the parameters, as shown by the good agreement between the analytical results and several experimental studies. The results indicate that the analytical model is sensitive to the measurement location, with the change in position significantly affecting the predicted interior noise levels, as should be expected. Different sizes for the acoustic enclosure, as well as different types of panels were investigated. This study demonstrates the importance of including the acoustic receiving room (i.e., the vehicle cabin) contribution in the analytical formulation, in order to accurately predict the noise transmission and interior noise levels.

RESUME

Dans cette étude, un modèle analytique complet, capable de prédire avec précision le bruit à l'intérieur d'une cabine d'un véhicule de transport induite par l'écoulement externe, est présenté. Le modèle mathématique représente un système structurel-acoustique accouplé, qui consiste en une plaque avec une excitation aléatoire ou à l'excitation du écoulement turbulent, et une chambre acoustique qui représente la cabine du véhicule de transport. Le modèle analytique accouplé a été développé en considérant la contribution combinée des modes naturels de ces deux systèmes, structurel et acoustique. Il est démontré que le modèle analytique peut être utilisé pour prédire le bruit induit par l'écoulement externe dans différents types de véhicules de transport, en variant certains paramètres, tel que vérifié par la bonne concordance entre les resultants analytiques et les résultats des multiples études expérimentales. Les résultats indiquent que le modèle analytique est sensible à la variation du point de mesure, et que le changement de la position de mesure affecte significativement les niveaux de bruit intérieur prédit, comme cela était prévu. Différentes dimensions de chambres acoustiques, ainsi que différents types de panneaux ont été étudiés. Cette étude démontre l'importance d'inclure la contribution de la salle acoustique de reception (i.e., l'habitacle du véhicule) dans la formulation analytique, afin de prédire avec précision la transmission du bruit et les niveaux de bruit à l'intérieur.

INTRODUCTION

The interior noise and vibration in the cabin of an aircraft is mostly generated by the external flow excitation and engine noise. In opposition of what happens during takeoff, where the engine noise is the dominant cabin noise source, during cruise flight the airflow sources are the major contribution for the interior noise. Early measurements performed in jet transport aircraft by [1], have shown how the relative importance of engine and flow noise changes drastically during the course of a flight. This study concluded that, during takeoff and initial climb, the engine was the main source of cabin noise. However, during the climb to cruise flight altitude, the turbulent boundary layer (TBL) noise gradually increases and the engine noise decreases. Finally, when the cruise flight is reached, the TBL becomes the

dominant source of interior noise, resulting from the increase of flight speed, and there is a reduction of engine noise, as the engine thrust is reduced to cruise setting. Furthermore, as referred in [2], turbulent boundary layer excitation is regarded as the most important noise source for jet powered aircraft at cruise speed, particularly, as new quieter jet engines are being developed. Similarly, automotive industry is progressively more concerned with passengers comfort. Since major advances have been made to the reduction of sound transmitted to the interior from the engine, transmission, and tires, the reduction of flow-induced noise is becoming more important. Additionally, as concluded by several studies for subsonic flight, e.g. [3-5], turbulent boundary layer pressure levels on the exterior of the fuselage increases with the flight Mach number.

Nowadays, reduced cabin interior noise is an important factor when considering the design of aircraft and transport vehicles in general, and it will even become a more important issue in the future transport vehicles. Reduced levels of interior cabin noise are desirable for both comfort and health-related reasons, and they are balanced with the cost, complexity, and physical constraints of noise control systems. Passive noise control (PNC) techniques are not effective in the low-frequency noise (LFN) range, where the active noise control techniques (ANC and ASAC) have demonstrated better results, showing the ability to decrease sound levels without a big penalty in terms of weight, compared with the PNC solutions [6-9]. However, the successful implementation of noise control techniques is a challenging problem, and is far from being a straightforward task. The complexity of the physics of the structural-acoustic coupled system itself, consisting of the fuselage structure together with the cabin interior, is already a major difficulty for solving the problem. To efficiently design a noise control system, a clear understanding of the mechanisms of sound radiation and transmission of the coupled structural-acoustic system is crucial. Furthermore, when considering the TBL excitation, the noise reduction problem turns into even more complicated, since the turbulent boundary layer induced pressure has a random and broadband nature.

Early experimental tests have been conducted as an effort to characterize the radiation of sound from single panels excited by turbulent boundary layers [4, 10-15]. The results illustrate that the TBL is a major source of exterior pressure fluctuations and provide knowledge about the shape of the spectrum, convection velocity and space-time correlation of the turbulent boundary layer pressure fluctuations on aircraft panels, as well as displacement and acceleration spectra of the vibrating aircraft panels. In addition, theoretical studies have been performed for the vibration and sound radiated by isolated panels (i.e., not coupled with an acoustic enclosure) excited by turbulent flows [16-20], and for random vibration of a plate coupled with acoustic enclosures [2, 21, 22]. In these studies, when the TBL excitation is object of study, it is usually described in terms of the statistical properties of the wall pressure fluctuations based on the Corcos formulation [23, 24]. A number of new models were developed after Corcos model for the TBL statistical description [25-29]. The main limitation of the Corcos formulation is the assumption that spanwise and streamwise correlations lengths do not depend on the boundary layer thickness parameter, unlike other methods. Despite not being the most accurate, the Corcos model is widely used to describe the induced TBL pressure field, since it captures the fundamental pressure tendency along the frequency and requires significantly reduced computational effort to employ. In the other hand, the Corcos-like formulation provides a good estimation for the TBL wall-pressure fluctuations levels at and near the convective peak, which is of fundamental importance for aircraft boundary layers (for high subsonic Mach numbers) [30]. Finally, with the Corcos model it is possible to obtain analytical expressions for the response of simply supported panel, which is fundamental in the present study. For all these reasons, the Corcos formulation is still being used in recent studies to describe the TBL wall-pressure fluctuations, e.g., [2, 30-36].

As a physical problem, the TBL-induced noise into a cabin can be simply explained as follows: (1) the turbulent boundary layer pressure fluctuations induce vibrations on the cabin structure, and (2) the vibrating structure radiates noise into the cabin. Mathematically, this physical problem can be simulated by the interaction of three different models: (1) an aerodynamic model, representing the TBL pressure fluctuations on the cabin structure; (2) a structural model, which characterize the vibration of the cabin structure; and (3) an acoustic model that represents the cabin interior sound pressure level.

The mains goal of the current investigation is the development of an accurate analytical framework for the prediction TBL-induced noise into transport vehicles cabins, and its validation. The knowledge of the characteristics of the turbulent boundary layer excitation, its induced vibration on the structure, and the noise radiated into the cabin space is essential for the accurate prediction of the interior noise levels. The effect of the receiving room space, i.e. the cabin space, is an important factor for the accurate interior noise prediction, as shown by the results shown in this study.

For the validation of the analytical framework, four studies were considered for comparison, more specifically the investigations by [2, 8, 22, 37]. The acoustic enclosure is of rectangular shape, filled with air, with five rigid walls and one wall completely or partially flexible. The flexible part of the enclosure wall is backed by the turbulent boundary layer or by normally impinging random noise. The analytical expressions obtained in this study, shown in the Appendices section, are able to predict overall values of interior SPL, overall values of plate vibration levels, as well as the SPL at a chosen point in the interior of the enclosure, and the level of structural vibration at a given point of the structure. The spectral quantities were obtained for frequencies up to 1000 Hz. The analytical framework here

validated can be used to predict cabin noise for more complex cases, as the case shown [38].

The present article is organized as follows. First, the concepts and models used in the study are formally described. Section 2 presents the turbulent boundary layer wall pressure fluctuations model, Section 3 the structural model, Section 4 the acoustic model, and Section 5 the coupled structural-acoustic model. The method of solution for the prediction the spectral quantities is discussed in Section 6. Section 7 provides a discussion of the results obtained using the developed analytical framework, and their validation with the results from the literature. Finally, a summary of the results and concluding remarks are presented.

2. TURBULENT BOUNDARY LAYER WALL PRESSURE FIELD MODEL

The prediction of the vibration and sound of a flow-excited structure is dependent on a good description of the wall pressure field. Since numerical predictions are limited to low Reynolds number simple flow, one has to rely on semi-empirical models fitted to experimental data. Modeling the turbulent boundary layer wall pressure has been a subject of study for many years. As previously referred in this report, a large number of empirical models have been developed to describe the wall pressure fluctuations on a flat plate wall due to the TBL. The turbulent boundary layer wall pressure, p(x, y, t), is usually statistically described in terms of the pressure power spectral density, $S(s_1, s_2, \omega)$, where s_1 is the current position along the plate, and s_2 the separation vector between two measurement points.

In general, for a fully developed TBL, and for zero mean pressure gradient, the turbulent flow can be regarded as stationary and homogeneous in space, so that the s_1 dependence disappears in the $S(s_1, s_2, \omega)$ function. This way, for turbulent flow in the x-direction, the cross power spectral density (PSD) of the wall pressure over the (x, y) plane, can be defined as

$$S(\xi_x,\xi_y,\omega) = \langle\, p^*(x, y, \omega), p(x - \xi_x, y - \xi_y, \omega) \,\rangle\,, \tag{1}$$

in which $\xi_x = x - x'$ and $\xi_y = y - y'$ are the spatial separations in the streamwise and spanwise directions of the plate, respectively. Also, the cross PSD of a stationary random process can be expressed as the product of a reference PSD function, $S_{ref}(\omega)$, and a spatial correlation function, $\bar{S}(\xi_x,\xi_y,\omega)$, as

$$S(\xi_x,\xi_y,\omega) = S_{ref}(\omega)\, \bar{S}(\xi_x,\xi_y,\omega)\,. \tag{2}$$

Corcos [23, 24], proposed a model which considers the cross power spectral density of the stationary and homogeneous TBL wall pressure field in a separate form in the streamwise, x-, and spanwise, y-direction, as

$$S(\xi_x,\xi_y,\omega) = S_{ref}(\omega)\, f_1\left(\frac{\omega\,\xi_x}{U_c}\right) f_2\left(\frac{\omega\,\xi_y}{U_c}\right) e^{\frac{-i\,\omega\,\xi_x}{U_c}}, \tag{3}$$

where U_c is the TBL convective speed. Corcos found that measurements of particular forms of the cross PSD $S(\xi_x,0,\omega)$ and $S(0,\xi_y,\omega)$ could be well represented as functions of the variables $(\omega\xi_x/U_c)$ and $(\omega\xi_y/U_c)$, respectively. In practice, the functions $f_1(\omega\xi_x/U_c)$ and $f_2(\omega\xi_y/U_c)$ are frequently approximated by exponential decay functions, i.e.

$$S(\xi_x,\xi_y,\omega) = S_{ref}(\omega)\, e^{-\frac{\alpha_x\,\omega\,|\xi_x|}{U_c}}\, e^{-\frac{\alpha_y\,\omega\,|\xi_y|}{U_c}}\, e^{-\frac{i\,\omega\,\xi_x}{U_c}}, \tag{4}$$

where α_x and α_y are empirical parameters, chosen to yield the best agreement with the reality, which denote the loss of coherence in the longitudinal and transverse directions. Usually, $\alpha_x \in [0.1; 0.12]$ and $\alpha_y \in [0.7; 1.2]$. Recommended empirical values for aircraft boundary layers are $\alpha_x = 0.1$ and $\alpha_y = 0.77$ [39]. For the reference power spectrum, $S_{ref}(\omega)$, all the chosen studies for the validation of our model provide information about its value. However, in case of the absence of an adequate reference power spectrum function or value, the authors anticipate that the model proposed by Efimtsov [25] provides a good agreement with experimental data for the case of an aircraft in cruise flight [39, 40].

3. STRUCTURAL MODEL

Generally, an aircraft fuselage is a conventional skin-stringer-frame structure, with several panels connected between adjacent stringers and frames. Each individual panel can be assumed to vibrate independently of each other. As concluded in [13, 14], while jet noise induced vibration in aircraft is highly correlated over several aircraft panels, in both longitudinal and circumferential directions, the TBL induced vibration (in which the vibration correlation decays rapidly especially in the circumferential direction) is confined to one or two adjacent panels in the longitudinal direction.

The panels are considered to be flat and simply supported in all four boundaries. With these conditions, the vibration of an individual panel can be defined as [41, 42]

$$w(x,y,t) = \sum_{m_x=1}^{M_x} \sum_{m_y=1}^{M_y} \alpha_{m_x}(x)\, \beta_{m_y}(y)\, q_{m_x m_y}(t)\,, \tag{5}$$

in which $\alpha_{m_x}(x)$ and $\beta_{m_y}(y)$ are the spatial functions, defining the variation of w(x,y,t) with the variables x and y respectively, $q_{m_x m_y}(t)$ functions define the variation of w(x,y,t) with time, and $M = M_x \times M_y$ is the total number of plate modes (m_x, m_y) considered for the analysis. For simply supported plates, the spatial functions can be defined as:

$$\alpha_{m_x}(x) = \sqrt{\frac{2}{a}} \sin\left(\frac{m_x \pi x}{a}\right), \quad (6a)$$

$$\beta_{m_y}(y) = \sqrt{\frac{2}{b}} \sin\left(\frac{m_y \pi y}{b}\right), \quad (6b)$$

where a and b are the length and width of the plate, respectively. The natural frequencies of the simply supported panel are given by

$$\omega^p_{m_x m_y} = \sqrt{\frac{D_p}{\rho_p h_p}} \left[\left(\frac{m_x \pi}{a}\right)^2 + \left(\frac{m_y \pi}{b}\right)^2\right], \quad (7)$$

in which ρ_p is the density of the panel, h_p is its thickness, and $D_p = \frac{E_p h_p^3}{12(1-\nu_p^2)}$ is the panel stiffness constant, with E_p being the panel Elasticity modulus and ν_p the Poisson ratio. The plate governing equation, for a given applied external pressure, is defined as

$$D_p \nabla^4 w + \rho_p h_p \ddot{w} + \zeta_p \dot{w} = p_{ext}(x,y,t), \quad (8)$$

in which the term ζ_p was added to account for the damping of the plate.

4. ACOUSTIC MODEL

The acoustical physical system consists of a three-dimensional rectangular enclosure, with five fixed walls, and one totally or partially flexible wall. Similarly to the description of plate vibration in the structural model, the pressure field inside the acoustic enclosure can be defined through the acoustic modes, as following [43, 44]

$$p(x,y,z,t) = \sum_{n_x=1}^{N_x} \sum_{n_y=1}^{N_y} \sum_{n_z=1}^{N_z} \psi_{n_x}(x)\, \phi_{n_y}(y)\, \Gamma_{n_z}(z)\, r_{n_x n_y n_z}(t), \quad (9)$$

in which $\psi_{n_x}(x)$, $\phi_{n_y}(y)$ and $\Gamma_{n_z}(z)$ are the spatial functions, defining the variation of p(x,y,z,t) with the variables x, y and z respectively, $r_{n_x n_y n_z}(t)$ functions define the variation of p(x,y,z,t) with time, and $N = N_x \times N_y \times N_z$ is the total number of plate modes (n_x, n_y, n_z) considered. The spatial functions are assumed to be orthogonal between each other, and are given by the rigid body enclosure modes [45, 46], i.e.:

$$\psi_{n_x}(x) = \frac{A_{n_x}}{\sqrt{L_x}} \cos\left(\frac{n_x \pi x}{L_x}\right), \quad (10a)$$

$$\phi_{n_y}(y) = \frac{A_{n_y}}{\sqrt{L_y}} \cos\left(\frac{n_y \pi y}{L_y}\right), \quad (10b)$$

$$\Gamma_{n_z}(z) = \frac{A_{n_z}}{\sqrt{L_z}} \cos\left(\frac{n_z \pi z}{L_z}\right), \quad (10c)$$

where L_x, L_y and L_z are the dimensions of the acoustic enclosure in the x-, y- and z- direction, respectively, and constants A_n were chosen in order to satisfy normalization. It can be shown that:

$$A_n = \begin{cases} \sqrt{2}, & \text{for } n \neq 0 \\ 1, & \text{for } n = 0. \end{cases} \quad (11)$$

The natural frequencies of a rectangular cavity can be determined using the following equation [45]

$$\omega^{ac}_{n_x n_y n_z} = c_0 \sqrt{\left(\frac{n_x \pi}{L_x}\right)^2 + \left(\frac{n_y \pi}{L_y}\right)^2 + \left(\frac{n_z \pi}{L_z}\right)^2}, \quad (12)$$

in which c_0 is the speed of sound inside the acoustic enclosure. The governing equation of this subsystem is the wave equation, defined by

$$\nabla^2 p - \frac{1}{c_0^2} \ddot{p} - \zeta_{ac} \dot{p} = 0, \quad (13)$$

where the damping term ζ_{ac} was added to account for the acoustic damping in the enclosure.

5. STRUCTURAL-ACOUSTIC MODEL

The governing equations for the coupled structural acoustic system are obtained from the combination of the previously described governing equations for the individual uncoupled systems. To perform that combination, some mathematical manipulation is needed.

First, considering the plate governing equation, the right-hand side of Eq.(8) may be divided in two different contributions: (1) the external TBL excitation, $p_{tbl}(x, y, t)$, applied in the upper part of the panel, and (2) the pressure field, $p(x,y,z=L_z,t)$, applied in the panel due to the acoustic enclosure contribution. Considering this, Eq.(8) can be re-written as

$$D_p \nabla^4 w + \rho_p h_p \ddot{w} + \zeta_p \dot{w} = p(x,y,z=L_z,t) - p_{tbl}(x,y,t). \quad (14)$$

Substituting w(x,y,t) in Eq.(14) by the expression defined in Eq.(5), expressing $p(x,y,z=L_z,t)$ in terms of Eqs.(9) and (10), making use of the orthogonality of the plate modes, and integrating the entire equation over the plate area, Eq.(14) becomes

$$\rho_p h_p \left\{\ddot{q}_m(t) + 2\,\omega_m\,\xi_p\,\dot{q}_m(t) + \omega_m^2\,q_m(t)\right\} = \sum_{n=1}^{N} \frac{(-1)^{n_z} A_{n_z}}{\sqrt{L_z}} \int_{x_{p_i}}^{x_{p_f}} \alpha_{m_x}(x)\,\psi_{n_x}(x)dx \int_{y_{p_i}}^{y_{p_f}} \beta_{m_y}(y)\,\phi_{n_y}(y)dy\; r_n(t) - \int_{y_{p_i}}^{y_{p_f}} \int_{x_{p_i}}^{x_{p_f}} \alpha_{m_x}(x)\,\beta_{m_y}(y)\,p_{tbl}(x,y,z=L_z,t)\,dx\,dy, \quad (15)$$

where $\zeta_p = 2\ \omega_m\ \xi_p$ is the structural modal damping; x_{p_i} and x_{p_f} are, respectively, the initial and last x-coordinates of the plate (corresponding to the plate length); y_{p_i} and y_{p_f} are, respectively, the initial and last y-coordinates of the plate (plate width); and $\omega^p_{m_x m_y}$, $q_{m_x m_y}(t)$, and $r_{n_x n_y n_z}(t)$ were substituted, respectively, by ω_m , $q_m(t)$ and $r_n(t)$, for notation simplicity.

Second, considering the rectangular acoustic enclosure governing equation, Eq.(13), the boundary conditions may be defined as follows: (1) normal component of the air particle velocity equal to zero at the enclosure rigid walls, and (2) equal to normal velocity of the panel, at the flexible wall, i.e.,

$$\frac{\partial p}{\partial u} = \begin{cases} -\rho_0\ \ddot{w}, & \text{at } z = L_z \\ 0, & \text{at rigid boundaries}, \end{cases} \tag{16}$$

in which u represents the direction normal to the boundary, and ρ_0 is the air density into the acoustic enclosure.

Substituting Eqs.(10) and (11) into Eq.(9), and then into Eq.(13), making use of the orthogonality condition of the acoustic modes, integrating over the volume of the rectangular enclosure, and, finally, applying the boundary conditions given by Eq.(16), the rectangular enclosure governing equation Eq.(13) becomes

$$\frac{1}{c_0^2}\left\{\ddot{r}_n(t) + 2\ \omega_n\ \xi_{ac}\ \dot{r}_n(t) + \omega_n^2\ r_n(t)\right\} = -\rho_0\ \frac{(-1)^{n_z} A_{n_z}}{\sqrt{L_z}} \sum_{m=1}^{M} \int_{x_{p_i}}^{x_{p_f}} \alpha_{m_x}(x)\psi_{n_x}(x)dx \int_{y_{p_i}}^{y_{p_f}} \beta_{m_y}(y)\phi_{n_y}(y)dy\ \ddot{q}_m(t) \tag{17}$$

where $\zeta_{ac} = 2\ \omega_n\ \xi_{ac}$ is the acoustic modal damping, and $\omega^{ac}_{n_x n_y n_z}$, $r_{n_x n_y n_z}(t)$, and $q_{m_x m_y}(t)$ were substituted, respectively, by ω_n , $r_n(t)$ and $q_m(t)$, for notation simplicity. Note that the term on the right-hand side of Eq.(17) and the first term on the right-hand side of Eq.(15) represent the coupling between the structural vibration and the enclosure acoustic pressure.

Third, it is convenient to write the couple system governing equations, Eqs.(15) and (17), together into the following matrix form:

$$\begin{bmatrix} \mathbf{M}_{pp} & \mathbf{0} \\ \mathbf{M}_{cp} & \mathbf{M}_{cc} \end{bmatrix} \begin{Bmatrix} \ddot{\mathbf{q}}(t) \\ \ddot{\mathbf{r}}(t) \end{Bmatrix} + \begin{bmatrix} \mathbf{D}_{pp} & \mathbf{0} \\ \mathbf{0} & \mathbf{D}_{cc} \end{bmatrix} \begin{Bmatrix} \dot{\mathbf{q}}(t) \\ \dot{\mathbf{r}}(t) \end{Bmatrix} + \begin{bmatrix} \mathbf{K}_{pp} & \mathbf{K}_{pc} \\ \mathbf{0} & \mathbf{K}_{cc} \end{bmatrix} \begin{Bmatrix} \mathbf{q}(t) \\ \mathbf{r}(t) \end{Bmatrix} = \begin{Bmatrix} \mathbf{p}_{tbl}(t) \\ \mathbf{0} \end{Bmatrix}, \tag{18}$$

in which:

$$\mathbf{M}_{pp} = \text{diag}\left[\rho_p\ h_p\right] \quad \text{and} \quad \mathbf{M}_{cc} = \text{diag}\left[\frac{1}{c_0^2}\right], \tag{19a}$$

$$\mathbf{M}_{cp} = \rho_0 \left[\frac{(-1)^{n_z} A_{n_z}}{\sqrt{L_z}} \int_{x_{p_i}}^{x_{p_f}} \alpha_{m_x}(x)\psi_{n_x}(x)dx \int_{y_{p_i}}^{y_{p_f}} \beta_{m_y}(y)\phi_{n_y}(y)dy \right], \tag{19b}$$

$$\mathbf{D}_{pp} = \text{diag}\left[2\rho_p h_p \omega_m \xi_p\right] \quad \text{and} \quad \mathbf{D}_{cc} = \text{diag}\left[2\frac{1}{c_0^2}\omega_n \xi_{ac}\right], \tag{19c}$$

$$\mathbf{K}_{pp} = \text{diag}\left[\omega_m^2\ \rho_p\ h_p\right] \quad \text{and} \quad \mathbf{K}_{cc} = \text{diag}\left[\omega_n^2\ \frac{1}{c_0^2}\right], \tag{19d}$$

$$\mathbf{K}_{pc} = -\left[\frac{(-1)^{n_z} A_{n_z}}{\sqrt{L_z}} \int_{x_{p_i}}^{x_{p_f}} \alpha_{m_x}(x)\psi_{n_x}(x)dx \int_{y_{p_i}}^{y_{p_f}} \beta_{m_y}(y)\phi_{n_y}(y)dy \right], \tag{19e}$$

$$\mathbf{p}_{tbl}(t) = -\left[\int_{y_{p_i}}^{y_{p_f}} \int_{x_{p_i}}^{x_{p_f}} \alpha_{m_x}(x)\ \beta_{m_y}(y)\ p_{tbl}(x,y,z=L_z,t)\ dx\ dy \right]. \tag{19f}$$

In these equations, **M** corresponds to mass matrices, **D** to damping matrices, **K** to stiffness matrices, and subscripts *p* and *c* represent respectively *plate* and *cavity*, with: $\mathbf{M}_{pp}$, $\mathbf{D}_{pp}$, and $\mathbf{K}_{pp} \in \Re^{M\times M}$; $\mathbf{M}_{cc}$, $\mathbf{D}_{cc}$ and $\mathbf{K}_{cc} \in \Re^{N\times N}$; $\mathbf{M}_{cp} \in \Re^{N\times M}$; $\mathbf{K}_{pc} \in \Re^{M\times N}$; $\mathbf{q}(t)$ and $\mathbf{p}_{tbl}(t) \in \Re^{M\times 1}$; and $\mathbf{r}(t) \in \Re^{N\times 1}$. All matrices and vectors expressions were obtained analytically. Appendix A contains final analytical expressions derived for $\mathbf{M}_{cp}$ and $\mathbf{K}_{pc}$ matrices.

Since the TBL wall pressure field model, described in section 2 of this article, is expressed in the frequency domain, it is opportune to transform Eq.(18) from the time domain to the frequency domain. For this purpose, one may assume the components of the time functions defined as $q_m = Q_m\ e^{i\omega t}$ and $r_n = R_n\ e^{i\omega t}$. Using this form of the time function, Eq.(18) can be written in frequency domain as

$$\mathbf{Y}(\omega) = \mathbf{H}(\omega)\ \mathbf{X}(\omega)\ , \tag{19}$$

in which the $\mathbf{Y}(\omega)$ is the response of the system to the excitation $\mathbf{X}(\omega)$, and $\mathbf{H}(\omega)$ is the frequency response matrix of the system, and are defined, respectively, by:

$$\mathbf{Y}(\omega) = \begin{Bmatrix} \mathbf{W}(\omega) \\ \mathbf{P}(\omega) \end{Bmatrix} \quad \text{and} \quad \mathbf{X}(\omega) = \begin{Bmatrix} \mathbf{P_{tbl}}(\omega) \\ \mathbf{0} \end{Bmatrix}, \tag{20a}$$

$$\mathbf{H}(\omega) = \begin{bmatrix} -\omega^2\mathbf{M}_{pp} + i\omega\mathbf{D}_{pp} + \mathbf{K}_{pp} & \mathbf{K}_{pc} \\ -\omega^2\mathbf{M}_{cp} & -\omega^2\mathbf{M}_{cc} + i\omega\mathbf{D}_{cc} + \mathbf{K}_{cc} \end{bmatrix}^{-1}. \tag{20b}$$

In these equations, vectors $\mathbf{W}(\omega)$, $\mathbf{P}(\omega)$ and $\mathbf{P}_{tbl}(\omega)$ correspond to the frequency domain vectors of the previously defined time domain vectors $\mathbf{w}(t)$, $\mathbf{p}(t)$ and $\mathbf{p}_{tbl}(t)$, respectively.

6. METHOD FOR SOLUTION

One last step, needed to obtain a solution for the problem, is to transform the coupled system equations to PSD domain, as the TBL wall pressure model available is written in terms of the power spectral density of the wall pressure. This way, considering the TBL random excitation as a stationary and homogeneous function, the spectral density of the system response, $\mathbf{S_{YY}}(\omega)$, is defined by [47, 48]

$$\mathbf{S_{YY}}(\omega) = \mathbf{H}^*(\omega)\, \mathbf{S_{XX}}(\omega)\, \mathbf{H}^T(\omega)\,, \tag{21}$$

where $\mathbf{S_{XX}}(\omega)$ is the PSD matrix of the random excitation, $\mathbf{X}(\omega)$, $\mathbf{S_{YY}}(\omega)$ is the PSD matrix of the random response, $\mathbf{Y}(\omega)$, and superscripts * and T denote Hermitian conjugate and matrix transpose, respectively. It is convenient to write the system response matrix, $\mathbf{H}(\omega)$, defined by Eq.(20b), in the following form

$$\mathbf{H}(\omega) = \begin{bmatrix} \mathbf{A} & \mathbf{B} \\ \mathbf{C} & \mathbf{D} \end{bmatrix}^{-1}, \tag{22}$$

with:

$$\mathbf{A} = -\omega^2 \mathbf{M}_{pp} + i\,\omega\, \mathbf{D}_{pp} + \mathbf{K}_{pp}\,, \tag{23a}$$
$$\mathbf{B} = \mathbf{K}_{pc}\,, \tag{23b}$$
$$\mathbf{C} = -\omega^2 \mathbf{M}_{cp}\,, \tag{23c}$$
$$\mathbf{D} = -\omega^2 \mathbf{M}_{cc} + i\,\omega\, \mathbf{D}_{cc} + \mathbf{K}_{cc}\,. \tag{23d}$$

Also, for mathematical calculations, it is opportune to divide the matrix $\mathbf{S_{YY}}(\omega)$ into two matrices: (1) the PSD matrix of the coupled plate displacement, $\mathbf{S_{WW}}(\omega)$, and (2) the PSD matrix of the coupled acoustic pressure, $\mathbf{S_{PP}}(\omega)$. Similarly, the matrix $\mathbf{S_{XX}}(\omega)$ may be divided in two: (1) the PSD matrix of the TBL pressure, and (2) a null matrix. With this manipulation, Eq.(21) can be written in a separate form, defining matrices $\mathbf{S_{WW}}(\omega)$ and $\mathbf{S_{PP}}(\omega)$, independently, as functions of the PSD matrix of the TBL excitation, Stblω, respectively, as follows:

$$\mathbf{S_{WW}}(\omega) = \mathbf{H_W}^*(\omega)\, \mathbf{S_{tbl}}(\omega)\, \mathbf{H_W}^T(\omega)\,, \tag{24}$$

and

$$\mathbf{S_{PP}}(\omega) = \mathbf{H_P}^*(\omega)\, \mathbf{S_{tbl}}(\omega)\, \mathbf{H_P}^T(\omega)\,, \tag{25}$$

in which matrices the $\mathbf{H_W}(\omega)$ and $\mathbf{H_P}(\omega)$ are defined, respectively, by:

$$\mathbf{H_W}(\omega) = (\mathbf{A} - \mathbf{B}\,\mathbf{D}^{-1}\,\mathbf{C})^{-1}, \tag{26}$$

and

$$\mathbf{H_P}(\omega) = -\,\mathbf{D}^{-1}\,\mathbf{C}\,\mathbf{H_W}(\omega)\,. \tag{27}$$

The generalized PSD matrix of the TBL excitation, $\mathbf{S_{tbl}}(\omega) \in \Re^{M\times M}$, is defined as follows

$$\mathbf{S_{tbl}}(\omega) = \left[\int_{y_{p_i}}^{y_{p_f}} \int_{x_{p_i}}^{x_{p_f}} \alpha_{m_x}(x)\alpha_{m_{x'}}(x')\beta_{m_y}(y)\beta_{m_{y'}}(y')S(\xi_x,\xi_y,\omega)\,dx\,dx'\,dy\,dy' \right], \tag{28}$$

in which $S(\xi_x,\xi_y,\omega)$ is defined by Eq.(4). The analytically expression obtained for the matrix $\mathbf{S_{tbl}}(\omega)$ can be seen in Appendix B. Finally, the PSD functions of the plate displacement and acoustic enclosure pressure can be defined using the previously defined PSD matrices, respectively as:

$$S_{ww}(x_1, y_1, x_2, y_2, \omega) = \sum_{m_{x_1}, m_{x_2}=1}^{M_x^2} \sum_{m_{y_1}, m_{y_2}=1}^{M_y^2} \alpha_{m_{x_1}}(x_1)\alpha_{m_{x_2}}(x_2)\beta_{m_{y_1}}(y_1)\beta_{m_{y_2}}(y_2)\mathbf{S_{WW}}(\omega)_{m_1,m_2} \tag{29}$$

and

$$S_{pp}(x_1, y_1, z_1, x_2, y_2, z_2, \omega) = \sum_{n_{x_1}, n_{x_2}=1}^{N_x^2} \sum_{n_{y_1}, n_{y_2}=1}^{N_y^2} \sum_{n_{z_1}, n_{z_2}=1}^{N_z^2} \psi_{n_{x_1}}(x_1)\psi_{n_{x_2}}(x_2)\phi_{n_{y_1}}(y_1)\phi_{n_{y_2}}(y_2)\Gamma_{n_{z_1}}(z_1)\Gamma_{n_{z_2}}(z_2)\, \mathbf{S_{PP}}(\omega)_{n_1,n_2} \tag{30}$$

Eqs.(29) and (30) can be used, respectively, to calculate the displacement PSD at a certain point in the plate, and the pressure PSD at any given location of the acoustic enclosure. If one desires to predict the auto-spectral density solutions, for instance, at the location 1, it can be calculated by replacing x_2 by x_1, y_2 by y_1, and z_2 by z_1 in Eqs.(29) and (30). The overall PSD functions are calculated by integrating the individual PSD functions over the plate area and the cavity volume, respectively, as following:

$$S_{ww}(\omega) = \int_{y_{p_i}}^{y_{p_f}} \int_{x_{p_i}}^{x_{p_f}} S_{ww}(x_1, y_1, x_2, y_2, \omega)\, dx_1 dx_2 dy_1 dy_2\,, \tag{31}$$

and

$$S_{pp}(\omega) = \int_{z_{c_i}}^{z_{c_f}} \int_{y_{c_i}}^{y_{c_f}} \int_{x_{c_i}}^{x_{c_f}} S_{pp}(x_1,y_1,z_1,x_2,y_2,z_2,\omega)\, dx_1 dx_2 dy_1 dy_2 dz_1 dz_2. \tag{32}$$

in which x_{c_i} and x_{c_f} are, respectively, the initial and last x-coordinates of the acoustic enclosure (corresponding to the enclosure length); y_{c_i} and y_{c_f} are, respectively, the initial and last y-coordinates of the enclosure (enclosure width); and z_{c_i} and z_{c_f} are, respectively, the initial and last z-coordinates of the enclosure (enclosure height). The final analytical

expressions derived for $S_{ww}(\omega)$ and $S_{pp}(\omega)$ are shown in Appendix C.

7. VALIDATION OF THE MODEL

7.1 Validation Case 1

The study documented in [22] performed by NASA, presents an experimental and theoretical study with different panels in order to determine the noise transmission in a coupled panel-cavity system. The analytical model presented is a simple, one-dimensional model, providing a good fitting with the experimental results trend line. The noise sources considered were normally impinging sine waves (with an amplitude of 110 dB) and normally incident random noise (a white noise source providing 120 dB sound pressure level).

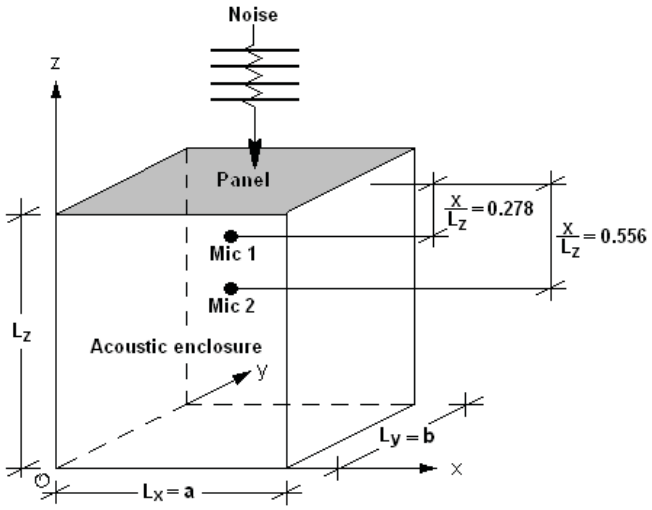

Figure 1. Details of the physical system of validation case 1.

Table 1. Parameters of the physical system for validation case 1.

Plate Properties (PVC)		
Variable	Description	Value
ρ_p	Density	1562.5 Kg m^{-3}
E_p	Elasticity Modulus	3.2×10^9 Pa^2
ν	Poisson's ratio	0.41
ξ_p	Damping ratio	0.02
h_p	Thickness	0.0016 m
a	Length	0.305 m
b	Width	0.381 m
Acoustic Enclosure Properties (Air)		
Variable	Description	Value
c_0	Speed of sound	348 m s^{-1}
ξ_{ac}	Damping ratio	0.001
L_x	Length	0.305 m
L_y	Width	0.381 m
L_z	Height	0.454 m

This study was considered as the validation case 1, and the system is composed by a PVC (Lead impregnated polyvinylchloride) panel coupled with a hard walled acoustic cavity, as shown in Fig. 1. The main properties of the system are displayed in Table 1. Two measurement microphones were located inside the cavity, directly behind the flexible panel, as shown in Fig. 1, in order to provide measurements of the interior sound pressure level. The noise reduction, NR, was obtained as following

$$NR = -10 \log_{10}\left(\frac{S_{pp}}{S_{ext}}\right), \quad (33)$$

in which, S_{pp} is the pressure PSD at the location of the interior microphone and S_{ext} is the external pressure PSD. Using our analytical framework, S_{pp} can be calculated from Eq.(30), while S_{ext} corresponds to S_{ref} expressed in Eqs. (2) to (4).

Figs. 2 and 3 show the noise reduction results obtained with our analytical model (part (a)), and the measured and theoretical results from [22] (part (b)), respectively, for the interior microphone locations 1 and 2, as shown in Fig. 1. Comparing these two figures, it is clear that changing the location of measurement also changes the noise reduction results, as should be expected. To obtain our analytical results, a total number of $M_x = 10$ and $M_y = 12$ plate modes, and $N_x = 3$, $N_y = 4$ and $N_z = 4$ acoustic modes, was necessary to achieve convergence of the results, for the maximum frequency of interest, i.e., 1000 Hz. It was found that, for the frequency range of interest, [0; 1000] Hz, it is necessary to include some non-resonant modes. A detailed explanation of criterion followed to determine the number of structural modes and acoustic modes required for convergence can be found in [38].

By comparison of parts (a) and (b) of Figs. 2 and 3, it can be concluded that our analytical model provides a good approximation to the experimental data from [22]. Comparing the analytical results in parts (a) and (b), it is clear that results from our framework confirm the existence of a more complex trend line, compared with the analytical results in [22]. This is explained by the fact that, in the present study, a much larger number of plate and acoustic modes were considered, compared with the number of modes used in [22]. An important conclusion from these results is that the number of modes, considered to obtain the analytical results, plays a crucial role in achieving an accurate prediction of the interior noise. However, some differences exist between our analytical results and the experimental results from [22]. As explained in [22], some acoustic leakage through the enclosure sides was observed during experiments, and those differences may be explained due to this factor.

7.2 Validation Case 2

The second case chosen for validation of our analytical model is based on the study described in [8]. It consists of a rectangular simply supported aluminum panel, which was flush mounted in the floor of a wind tunnel test section. An acoustically treated enclosure was mounted below the panel.

The sound pressure level, due to the noise radiated from the panel, was measured at various microphone locations inside the acoustic enclosure. Additionally, an accelerometer was located in the centre of the plate to evaluate the vibration levels. A schematic of the physical system is shown in Fig. 4.

The reference power spectral density of the external pressure field is approximately constant, as follows:

$$S_{ref} = 7.5 \times 10^{-5} \lambda^2 \rho^2 U_\infty^3 \delta^*, \quad (34)$$

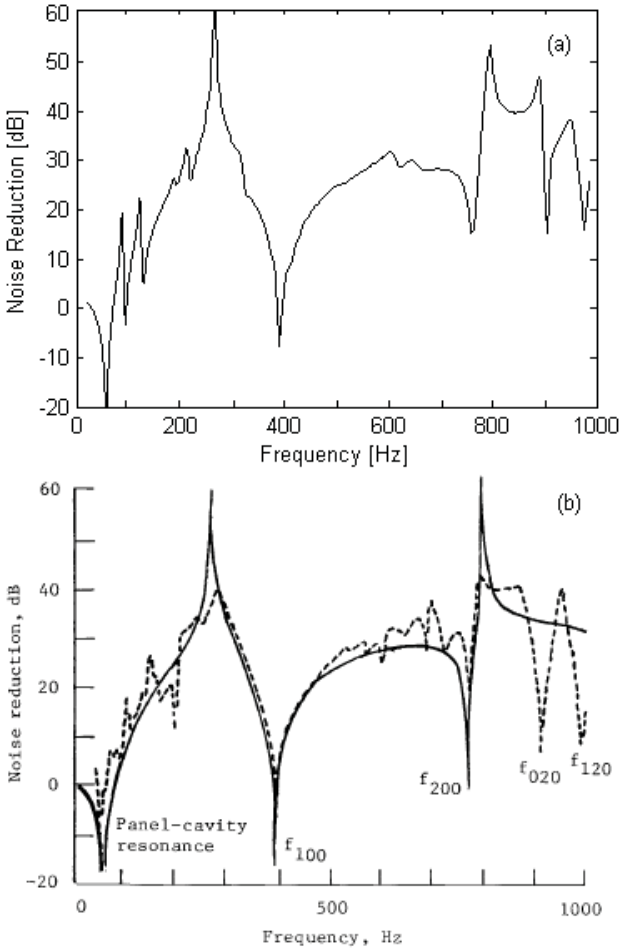

Figure 2. Noise reduction results for validation case 1, obtained for microphone location 1. (a) Obtained using our analytical model. (b) From [22]: ——, analytical results; – – –, experimental data.

in which $\lambda = 3$, ρ is the external air density, and δ^* is the boundary layer displacement thickness. As explained in [8], a displacement thickness of 12.8 cm gives a correct value for the pressure power spectra, and was used for the calculation of the turbulent excitation. The dimensions and characteristics of the panel and acoustic enclosure, and the properties of the external fluid are displayed in Table 2.

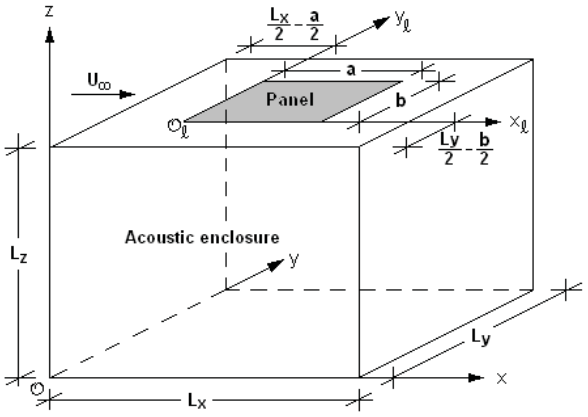

Figure 3. Schematic of physical system of validation case 2.

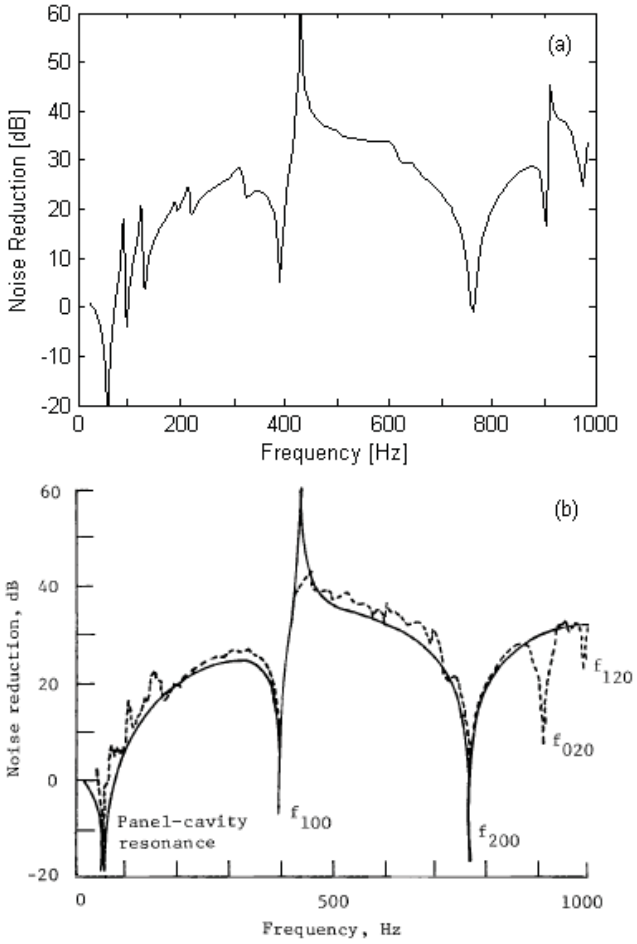

Figure 4. Noise reduction results for validation case 1, obtained for microphone location 2. (a) Obtained using our analytical model. (b) From [22]: ——, analytical results; – – –, experimental data.

The analytical results obtained using our framework are compared with the results from [8], as shown in Figs. 5 and 6. In Fig. 5, the response at higher frequencies is not accurately predicted by calculations in [8]. Both analytical results in parts (a) and (b) of Fig. 5 overpredict the acceleration level in the region from 900 Hz to 1000 Hz. However, our model is able to accurately predict the acceleration magnitude across the 700-900 Hz region. As

stated in the validation case 1 section, this may be related with the number of structural and acoustic modes considered in the analysis. To accomplish convergence of the spectral quantities, a total number of $M_x = 5$ and $M_y = 4$ plate modes, and $N_x = 8$, $N_y = 6$ and $N_z = 5$ acoustic modes were used in our model. Again, not only resonant modes were considered in the analyses - a considerable number of non-resonant modes were necessary to achieve convergence of the results. The predicted SPL from our model is shown in Fig. 6 (a). The model accurately predicts the sound pressure levels obtained experimentally in [8], with the main differences observed for low frequencies.

Table 2. Parameters of the physical system for validation case 2.

External Flow Properties (Air)		
Variable	Description	Value
ρ	Density	1..225 Kg m^{-3}
U_∞	Free stream velocity	35.8 m s^{-1}
U_c	Convective velocity	0.65 U_∞
α_x / α_y	Empirical parameters	0.115/0.7
Plate Properties (Aluminum)		
Variable		
ρ_p	Density	2800 Kg m^{-3}
E_p	Elasticity Modulus	6.5×10^{10} Pa^2
ν	Poisson's ratio	0.3
ξ_p	Damping ratio	0.01
h_p	Thickness	0.0048 m
a / b	Length / Width	0.46 m/0.33 m
Acoustic Enclosure Properties (Air)		
Variable	Description	Value
c_0	Speed of sound	340 m s^{-1}
ξ_{ac}	Damping ratio	0.03
L_x	Length	1.05 m
L_y	Width	0.857 m
L_z	Height	0.635 m

7.3 Validation Case 3

The study chosen as the validation case 3, [2], investigates the modeling of an elastic panel coupled with an acoustic enclosure, with the plate occupying a portion of the cavity and subjected to a convected flow, as shown in Fig. 7. The system parameters can be seen in Table 3.

In this study, the model consists of four parts: (1) the external aerodynamic model, (2) the TBL model, (3) the plate model, and (4) the acoustic cavity model. Their model is based on the power balance equation, written in the frequency domain, with the transfer functions of the system of equations computed using MATLAB, and using 4 plate modes and 17 cavity modes (i.e., resonant modes for frequencies up to 1000 Hz). For this frequency range, the TBL point pressure power spectrum was taken to be constant, as follows

$$S_{ref}(\omega_{max}) = 3.84 \times 10^{-5} \frac{\left(\rho\, U_\infty^2\right)^2}{4\,\omega_{max}} , \qquad (35)$$

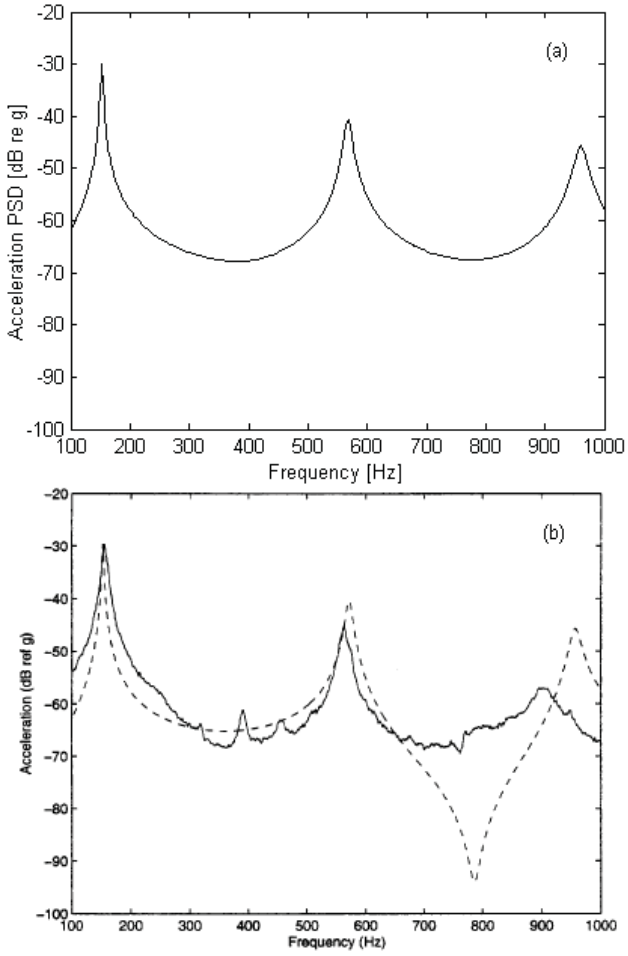

Figure 5. Validation case 2: acceleration power spectral density. (a) Analytical results obtained using our model. (b) From [8]: – – –, calculated; ——, measured.

in which ω_{max} is the maximum frequency of interest. Assuming 4 plate modes and 17 cavity modes, the results for the cavity power spectrum are shown in Fig. 8. The cavity power spectrum was calculated through the acoustic pressure PSD, $S_{pp}(\omega)$, defined in Eq.(30), as following

$$E_{pp}(\omega) = \frac{L_x\, L_y\, L_z}{4\,\rho_0\, c_0^2}\, \omega\, S_{pp}(\omega) , \qquad (36)$$

Comparing results in parts (a) and (b) of Fig. 8, one can conclude that they in very good agreement, taking into account the entire frequency spectrum. One might now consider a more accurate result as a larger number of plate and cavity modes should be needed in the model. Again, aiming for convergence of calculated spectral quantities, one must consider a total number of $M_x = 5$ and $M_y = 5$ plate modes, and $N_x = 21$, $N_y = 3$ and $N_z = 3$ acoustic modes in the series expansion. With this number of system natural modes, the results become different, as shown in Fig. 9. As can be concluded by comparison of Figs. 8 and 9, a larger number of modes results in higher cavity power spectrum amplitudes, mainly for frequencies above 300 Hz. The

bigger amount of spectral peaks above 300 Hz displayed in the more accurate results, shown in Fig. 9, is associated with the additional resonant modes considered. Results for lower frequencies remain essentially unaltered from Fig. 8 to Fig. 9.

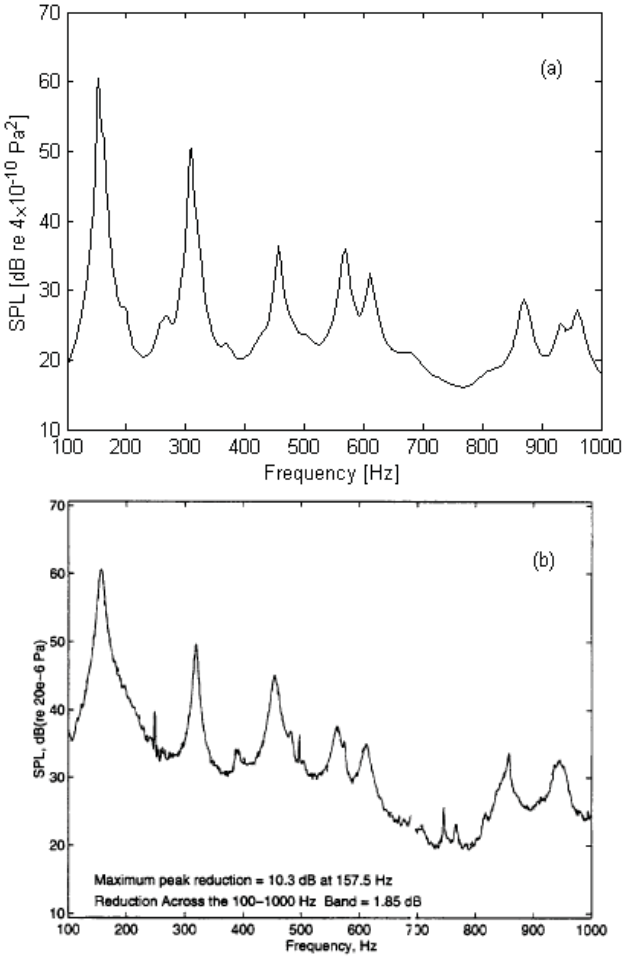

Figure 6. Validation case 2: Sound pressure level: (a) obtained using our analytical model; (b) experimental data from [8].

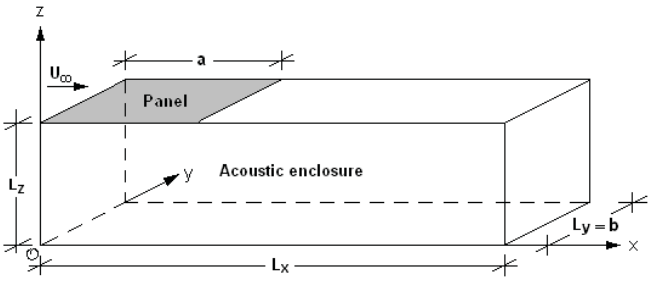

Figure 7. Schematic of the validation case 3 physical system.

Table 3. Properties of the system for the validation case 3.

External Flow Properties (Air)		
Variable	Description	Value
c_0	Speed of sound	310 m s $^{-1}$
ρ	Density	0.42 Kg m^{-3}
$U_{\infty 1}$	Free stream velocity 1	0.1 c_0
$U_{\infty 2}$	Free stream velocity 2	0.5 c_0
$U_{\infty 3}$	Free stream velocity 3	0.8 c_0
U_c	Convective velocity	0.6 U_∞
α_x	Empirical parameter	0.1
α_y	Empirical parameter	0.5
Plate Properties (Aluminum)		
Variable		
ρ_p	Density	2800 Kg m^{-3}
E_p	Elasticity Modulus	7.0×10^{10} Pa^2
ν	Poisson's ratio	0.3
ξ_{p1}	Damping ratio 1	0.01
ξ_{p2}	Damping ratio 2	0.02
ξ_{p3}	Damping ratio 3	0.03
h_p	Thickness	0.0018 m
a	Length	0.3 m
b	Width	0.3 m
Acoustic Enclosure Properties (Air)		
Variable	Description	Value
c_0	Speed of sound	310 m s $^{-1}$
ρ_0	Density	0.42 Kg m^{-3}
ξ_{ac}	Damping ratio	0.05
L_x	Length	3.0 m
L_y	Width	0.3 m
L_z	Height	0.3 m

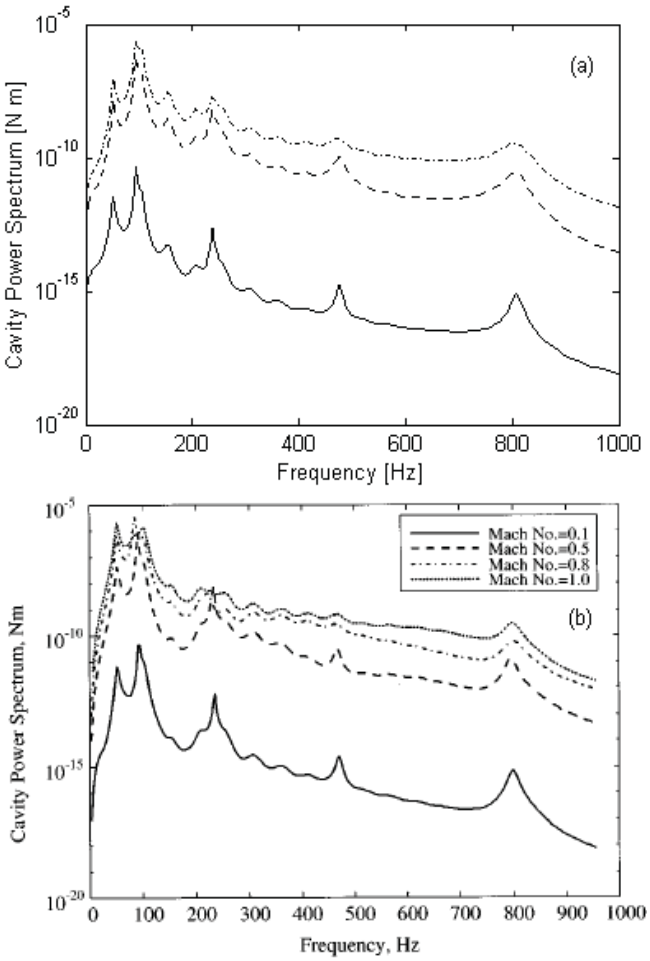

Figure 8. Validation case 3: cavity power spectrum results (using 4 plate modes and 17 cavity modes):——— , M=0.1; – – – , M=0.5; – · – · , M=0.8.
(a) From our analytical framework. (b) From [2].

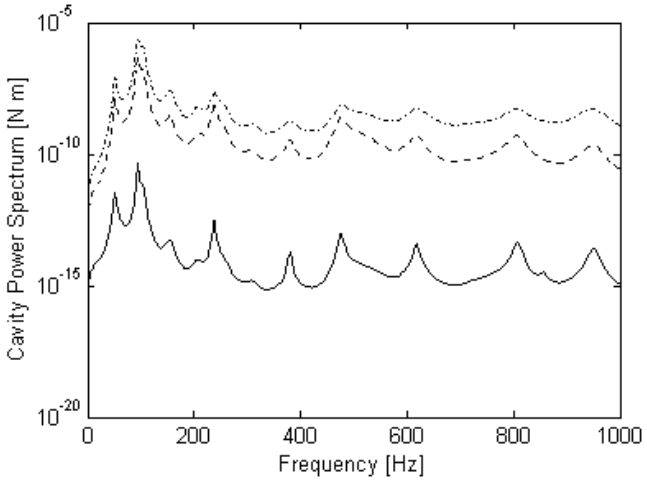

Figure 9. Validation case 3: cavity power spectrum results from our analytical framework (using a larger number of plate and cavity modes): ——, M=0.1; – – –, M=0.5; – · – · , M=0.8.

7.4 Validation Case 4

The validation case 4 is the study by [37]. As in the previous validation case, this study investigates the model of a convected fluid loaded plate coupled with an acoustic enclosure. However, the dimensions are different from the previous case, and were chosen to reproduce a small commercial aircraft. The physical system schematic is shown in Fig. 10 and the main parameters of the system are displayed in Table 4.

Table 4. System parameter of validation case 4.

External Flow Properties (Air)		
Variable	Description	Value
c_0	Speed of sound	310 m s $^{-1}$
ρ	Density	0.42 Kg m^{-3}
U_∞	Free stream velocity	0.1 c_0
U_c	Convective velocity	0.6 U_∞
α_x	Empirical parameter	0.1
α_y	Empirical parameter	0.5
Plate Properties (Aluminum)		
Variable		
ρ_p	Density	2700 Kg m^{-3}
E_p	Elasticity Modulus	7.1×10^{10} Pa^2
ν	Poisson's ratio	0.3
ξ_p	Damping ratio	0.01
h_p	Thickness	0.0022 m
a	Length	0.6 m
b	Width	0.525 m
x_p	Plate x-coordinate	0.6 m
y_p	Plate y-coordinate	0.6 m
Acoustic Enclosure Properties (Air)		
Variable	Description	Value
c_0	Speed of sound	310 m s $^{-1}$
ρ_0	Density	0.42 Kg m^{-3}
ξ_{ac}	Damping ratio	0.05
L_x	Length	6.0 m
L_y	Width	1.8 m
L_z	Height	1.8 m

In [37], a total number of 50 acoustic modes and 20 plate modes were used to obtain the numerical results. For this number of natural modes, the results for the cavity acoustic potential energy are shown in Fig. 11. Fig. 12 shows the

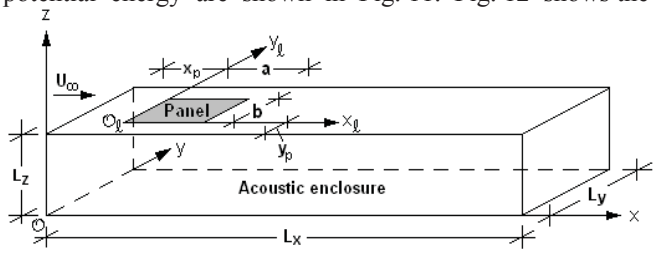

Figure 10. Physical system of validation case 4.

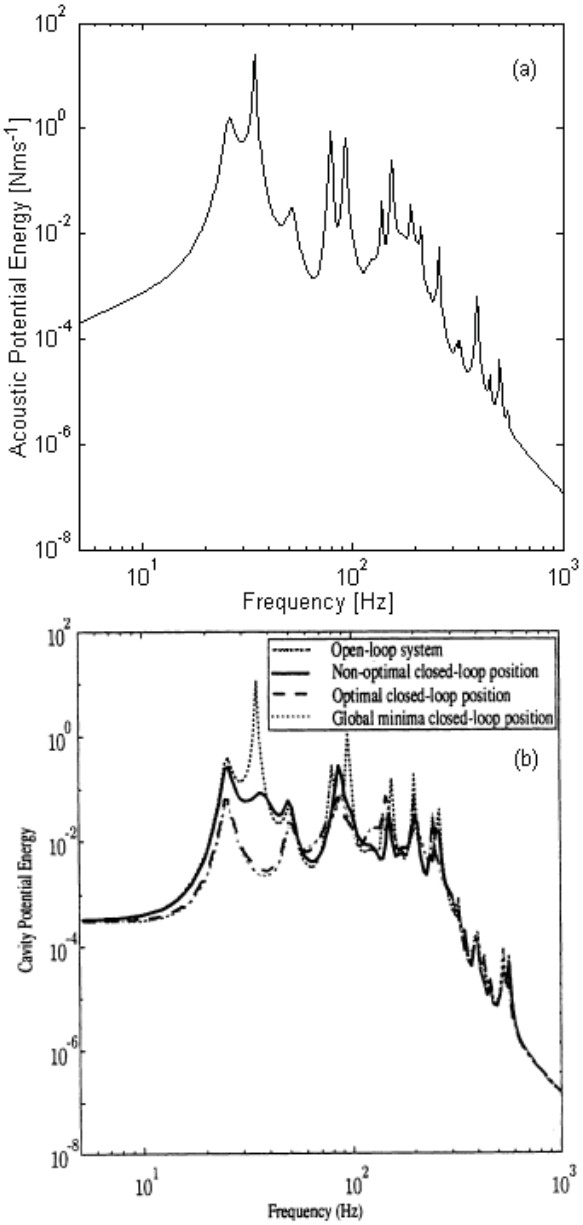

Figure 11. Validation case 4: acoustic potential energy results (using 20 plate modes and 50 cavity modes): (a) obtained using our analytical framework; (b) from [37].

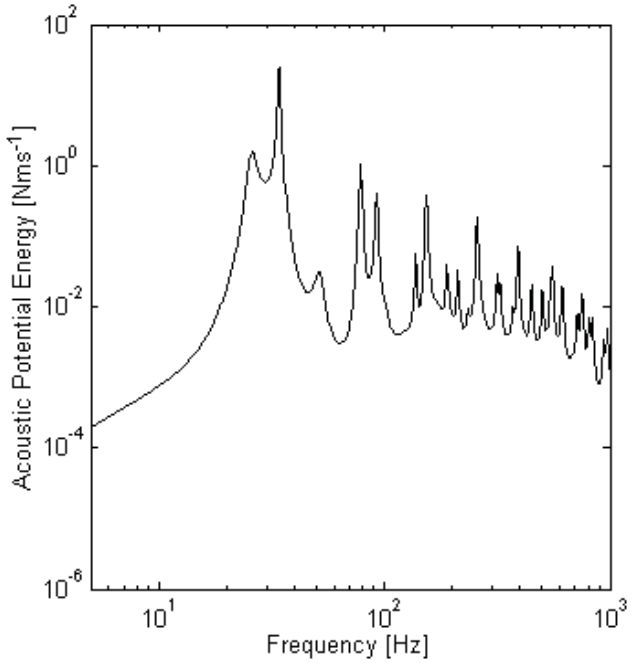

Figure 12. Validation case 4: acoustic potential energy results from our analytical framework (using a larger number of plate and acoustic modes).

results obtained with analytical results, but using a total number of $M_x = 9$ and $M_y = 7$ plate modes, and $N_x = 40$, $N_y = 7$ and $N_z = 7$ acoustic modes, in order to obtain accurate results in the bandwidth of interest. To calculate the cavity potential energy, in Figs. 11 and 12, the following equation was used

$$E_{pp}(\omega) = \frac{L_x L_y L_z}{4 \rho_0 c_0^2} \omega^2 S_{pp}(\omega) , \qquad (37)$$

in which $S_{pp}(\omega)$ is defined by Eq.(30). Comparing parts (a) and open-loop plot in part (b) of Fig. 11, one can conclude that results are in good agreement. However, when considering a larger number of natural modes, the results are very different, mainly for higher frequencies, as shown in Fig. 12. The consideration of the larger number of system modes results in an increase of acoustic energy for frequencies above 200 Hz.

8. CONCLUSIONS

The model validation is an essential part of the model development process in order to the models to be accepted and used as a predictive tool. Several independent experimental and numerical studies, with different physical properties and environment, were used for conducting the validation of our model. The analytical results from our model show an overall match with the data from the validation cases. This indicates that our model can be used for the prediction of noise levels, and applicable for different practical cases.

The analytical model has applied for the prediction of noise levels to 4 different cases. The analytical predictions of the plate vibration PSD and the enclosure pressure PSD were calculated in order to perform the comparative analysis with the experimental and numerical data from the validation cases. In all 4 analyses, the predicted values are in good agreement with the data from the validation chosen studies. Additionally, it was found that the number of plate and acoustic natural modes used in the analysis play an important role in the model accurate prediction. In fact, there is a minimum number of natural modes which needs to be used in the analysis, in order to accurately predict the noise and vibration levels up to a maximum frequency.

The analytical framework developed and here validated can be used for the noise and vibration levels prediction for physical systems with a rectangular shaped enclosure with one flexible wall. This framework presents a solid basis for further analyses, opening the doors for its use in the design and implementation of noise reduction techniques. As demonstrated, accurate analytical models can be used to solve the problem of cabin TBL-induced interior noise prediction. Moreover, being the cabin an acoustic enclosure, it is important to consider not only the structural natural modes associated with the structural panels, but also the cabin acoustic modes, as well. Even though the structural-acoustic coupling turns the analytical framework more complex, it can be a first alternative to the much more time consuming numerical solutions. Future work of the present research will aim for the prediction of TBL-induced noise into an acoustic enclosure with several flexible panels, and also the development of additional analytical frameworks for cylindrical and spherical acoustic enclosures.

REFERENCES

[1] D. E. Bishop, Cruise flight noise levels in a turbojet transport airplane. *Noise Control* (1961), 7, pp. 37-42.

[2] K. D. Frampton and R. L. Clark, Power flow in an aeroelastic plate backed by a reverberant cavity. *Journal of the Acoustical Society of America* (1997), 102(3), pp. 1620-1627.

[3] W. V. Bhat, Flight test measurement of measurement of exterior turbulent boundary layer pressure fluctuations on Boeing Model 737 airplane. *Journal of Sound and Vibration* (1971), 14 (4), pp. 439-457.

[4] W. V. Bhat and J. F. Wilby, Interior noise radiated by an airplane fuselage subjected to turbulent boundary layer excitation and evaluation of noise reduction treatments. *Journal of Sound and Vibration* (1971), 18 (4), pp. 449-464.

[5] G. P. Gibbs, R. H. Cabell and J. Juang, Controller Complexity for Active Control of Turbulent Boundary-Layer Noise from Panels. *AIAA Journal* (2004), 42(7), pp. 1314-1320.

[6] A. Bullmore, P. Nelson, and S. Elliot. Theoretical studies of the active control of propeller-induced cabin noise. *Journal of Sound and Vibration* (1990), 140(2), pp. 191-217.

[7] D. MacMartin. Collocated structural control for reduction of aircraft cabin noise. *Journal of Sound and Vibration* (1996), 190(1), pp. 105-119.

[8] C. M. Heatwole, R. J. Bernhard and M. A. Francheck, Robust feedback control of flow induced structural radiation of sound. *NASA Report 0278-1* (1997).

[9] J. Henry and R. Clark. Active control of sound transmission through a curved panel into a cylindrical enclosure. *Journal of Sound and Vibration* (2002), 249(2), pp. 325-349.

[10] D. A. Bies, A review of flight and wind tunnel measurements of boundary layer pressure fluctuations and induced structural response, *NASA CR-626* (1966).

[11] L. Maestrello, Measurement of noise radiated by turbulent boundary layer excited panels. *Journal of Sound and Vibration* (1965), 2(2), pp. 100-115.

[12] L. Maestrello, Radiation from and panel response to a supersonic turbulent boundary layer. *Journal of Sound and Vibration* (1969), 10(2), pp. 261-295.

[13] J. F. Wilby and F. L. Gloyna, Vibration measurements of an airplane fuselage structure I. Turbulent boundary layer excitation. *Journal of Sound and Vibration* (1972), 23, pp. 443-466.

[14] J. F. Wilby and F. L. Gloyna, Vibration measurements of an airplane fuselage structure II. Jet noise excitation. *Journal of Sound and Vibration* (1972), 23 (4), pp. 467-486.

[15] J. F. Wilby, Aircraft interior noise. *Journal of Sound and Vibration* (1996), 190 (3), pp. 545-564.

[16] W. A. Strawderman, Turbulent-flow-excited vibration of a simply supported, rectangular flat plate. *The Journal of the Acoustical Society of America* (1969), 45(1), pp. 177-192.

[17] H. G. Davies, Sound from turbulent boundary layer excited panels. *The Journal of the Acoustical Society of America* (1971), 55, pp. 213-219.

[18] R. L. Clark and K. Frampton, Aeroelastic structural acoustic coupling: implications on the control of turbulent boundary-layer noise transmission. *Journal of the Acoustical Society of America* (1997), 102(3), pp. 1639-1647.

[19] C. Maury, P. Gardonio and S.J. Elliot, A wavenumber approach to the modeling the response of a random excited panel, Part II: application to aircraft panels excited by a turbulent boundary layer. *Journal of Sound and Vibration* (2002), 252(1), pp. 115-139.

[20] J. Park, T. Siegmund and L. Mongeau, Analysis of the flow-induced vibration of viscoelastically supported rectangular plates. *Journal of Sound and Vibration* (2003), 261, pp. 225-245.

[21] R. Vaicaitis and M. Slazak, Noise transmission through stiffened panels. *Journal of Sound and Vibration* (1980), 70(3), pp. 413-426.

[22] C. K. Barton and E. F. Daniels, Noise transmission through flat rectangular panels into a closed cavity, *NASA TP-1321* (1978).

[23] G. Corcos, The structure of the turbulent pressure field in boundary layer flows. *Journal of Fluid Mechanics - Cambridge Journal Online* (1964), 18, pp. 353-378.

[24] G. Corcos, Resolution of pressure in turbulence. *Journal of the Acoustical Society of America* (1963), 35(2), pp. 192-199.

[25] B. M. Efimtsov, Characteristics of the field of turbulent wall pressure fluctuations at large Reynolds numbers. *Soviet Physics-Acoustics* (1982), 28 (4), pp. 289-292.

[26] D. M. Chase, Modelling the wavevector-frequency spectrum of turbulent boundary layer wall-pressure. *Journal of Sound and Vibration* (1980), 70, pp. 29-67.

[27] D. M. Chase, The character of the turbulent wall pressure spectrum at subconvective wavenumbers and a suggested comprehensive model. *Journal of Sound and Vibration* (1987), 112, pp. 125-147.

[28] J. E. Ffowcs Williams, Boundary-layer pressures and the Corcos model: a development to incorporate lowwavenumber constraints. *Journal of Fluid Mechanics* (1982), 125, pp. 9-25.

[29] A. V. Smol'yakov and V. M. Tkachenko, Model of a field of pseudonic turbulent wall pressures and experimental data. *Soviet Physics-Acoustics* (1991), 37 (6), pp. 627-631.

[30] C. Maury, P. Gardonio and S. J. Elliot, Active control of the flow-induced noise transmitted through a panel. *AIAA Journal* (2001), 39(10), pp. 1860-1867.

[31] D. R. Thomas and P. A. Nelson, Feedback control of sound radiation from a plate excited by a turbulent boundary layer. *Journal of the Acoustical Society of America* (1995), 98(5), pp. 2651-2662.

[32] F. Han, L. G. Mongeau and R. J. Bernhard, A model for the vibro-acoustic response of plates excited by complex flows. *Journal of Sound and Vibration* (2001), 246(5), pp. 901-926.

[33] C. Maury, P. Gardonio and S. J. Elliot, Model for the active control of flow-induced noise transmitted through double partitions. *AIAA Journal* (2002), 40(6), pp. 1113-1121.

[34] C. Maury, P. Gardonio and S. J. Elliot, A wavenumber approach to modeling the response of a randomly excited panel, part I: general theory. *Journal of Sound and Vibration* (2002), 252(1), pp. 83-113.

[35] S. J. Elliot, C. Maury and P. Gardonio, The synthesis of spatially correlated random pressure fields. *Journal of the Acoustical Society of America* (2005), 117(3), pp. 1186-1201.

[36] J. Rohlfing and P. Gardonio, Active Control of Sound Transmission through Panels with Flexible Boundaries under Deterministic and Stochastic Excitation, *Institute of Sound and Vibration Research (ISVR) Technical Memorandum 977* (2007), University of Southampton, England.

[37] G. C. Smith, R. L. Clark and K. D. Frampton. Optimal Tranducer Placement for Active Control of Sound Transmission through Aeroelastic Plates. *Journal of the Intelligent Material Systems and Structures* (1998), 9, pp. 975-987.

[38] J. da Rocha, A. Suleman and F. Lau. Structural-acoustic coupling of a multi-panel walled enclosure excited by turbulent flow: contribution of each panel, *Journal of the Acoustical Society of America (submitted 2009).*

[39] W. R. Graham, A comparison of models for the wavenumber frequency spectrum of turbulent boundary layer pressures. *Journal of Sound and Vibration* (1997), 206(4), pp. 541-565.

[40] R. Rackl and A. Weston, Modeling of turbulent boundary layer surface pressure fluctuation auto and cross spectra - verification and adjustments based on TU-144LL data, *NASA CR-213938* (2005).

[41] F. Fahy, Sound *and Structural Vibration, Radiation, Transmission and Response*, Academic Press Ltd., London, 1985.

[42] J. Blevins, *Formulas for Natural Frequency and Mode Shape*, Krieger Publishing Company, Malabar, Florida, 2001.

[43] F. Fahy, *Sound and Structural Vibration, Radiation, Transmission and Response*, Academic Press Ltd., London, 1985.

[44] J. Blevins, *Formulas for Natural Frequency and Mode Shape*, Krieger Publishing Company, Malabar, Florida, 2001.

[45] H. Kuttruff, *Room Acoustics*, Applied Science Publishers Ltd., London, 1973.

[46] P. A. Nelson and S. J. Elliot, *Active Control of Sound*, Academic Press Ltd., London, 1992.

[47] D. E. Newland, *An introduction to Random Vibration and Spectral Analysis*, Longman, New York, 1984.

[48] Y. K. Lin, *Probabilistic Theory of Structural Dynamics*, McGraw-Hill Book Company, New York, 1967.

ACKNOWLEDGEMENTS

The authors would like to thank Zonta International for the financial support to this research, through the Amelia Earhart Fellowship Program.

APPENDICES

A. Analytical expressions for $\mathbf{M}_{cp}$ and $\mathbf{K}_{pc}$ matrices

Matrices $\mathbf{M}_{cp}$ and $\mathbf{K}_{pc}$ are defined, respectively, by Eqs.(19b) and (19e). To derive the final analytical expressions for these matrices, the integrals over x_p and y_p on the equations need to be analytically obtained.
Starting by the derivation of the mass matrix, $\mathbf{M}_{cp}$, by substituting Eqs. (6) and (10) into Eq.(19b), it becomes

$$\mathbf{M}_{cp}=\frac{2\,\rho_0}{\sqrt{a\,b\,L_x\,L_y\,L_z}}\left[(-1)^{n_z}A_{n_x}A_{n_y}A_{n_z}\int_{x_{p_i}}^{x_{p_f}}\sin\left(\frac{m_x\pi\,(x-x_{p_i})}{a}\right)\cos\left(\frac{n_x\pi\,x}{L_x}\right)dx\int_{y_{p_i}}^{y_{p_f}}\sin\left(\frac{m_y\pi\,(y-y_{p_i})}{b}\right)\cos\left(\frac{n_y\pi\,y}{L_y}\right)dy\right], \quad (A.1)$$

where x and y correspond to the acoustic enclosure (global) coordinate system, and terms inside [ ] are developed to obtain a matrix, according with the n and m indexes. Note that, in Eq. (A.1), the plate spatial functions, defined in Eqs. (6a) and (6b), were modified in order to be expressed in the enclosure coordinate system. For convenience, one may consider Eq.(A.1) written as the an alternative form as

$$\mathbf{M}_{cp}=\frac{2\,\rho_0}{\sqrt{a\,b\,L_x\,L_y\,L_z}}\left[(-1)^{n_z}A_{n_x}A_{n_y}A_{n_z}B_{nm}(x)B_{nm}(y)\right], \quad (A.2)$$

with:

$$B_{nm}(x)=\int_{x_{p_i}}^{x_{p_f}}\sin\left(\frac{m_x\pi\,(x-x_{p_i})}{a}\right)\cos\left(\frac{n_x\pi\,x}{L_x}\right)dx\,, \quad (A.3a)$$

$$B_{nm}(y)=\int_{y_{p_i}}^{y_{p_f}}\sin\left(\frac{m_y\pi\,(y-y_{p_i})}{b}\right)\cos\left(\frac{n_y\pi\,y}{L_y}\right)dy\,. \quad (A.3b)$$

The analytical development of the functions $B_{nm}(x)$ and $B_{nm}(y)$ results in the following final expressions:

$$B_{nm}(x)=\begin{cases}f(x_{p_f})-f(x_{p_i}), & \left(\frac{m_x}{a}\neq\frac{n_x}{L_x}\right)\wedge\left(\frac{x_{p_i}}{a}\ \text{even}\right)\\ f(x_{p_f})-f(x_{p_i}), & \left(\frac{m_x}{a}\neq\frac{n_x}{L_x}\right)\wedge\left(\frac{x_{p_i}}{a}\ \text{odd}\right)\wedge(m_x\ \text{even})\\ f(x_{p_i})-f(x_{p_f}), & \left(\frac{m_x}{a}\neq\frac{n_x}{L_x}\right)\wedge\left(\frac{x_{p_i}}{a}\ \text{odd}\right)\wedge(m_x\ \text{odd})\\ 0, & \left(\frac{m_x}{a}=\frac{n_x}{L_x}\right)\end{cases} \quad (A.4a)$$

and

$$B_{nm}(y)=\begin{cases}g(y_{p_f})-g(y_{p_i}), & \left(\frac{m_y}{b}\neq\frac{n_y}{L_y}\right)\wedge\left(\frac{y_{p_i}}{b}\ \text{even}\right)\\ g(y_{p_f})-g(y_{p_i}), & \left(\frac{m_y}{b}\neq\frac{n_y}{L_y}\right)\wedge\left(\frac{y_{p_i}}{b}\ \text{odd}\right)\wedge(m_y\ \text{even})\\ g(y_{p_i})-g(y_{p_f}), & \left(\frac{m_y}{b}\neq\frac{n_y}{L_y}\right)\wedge\left(\frac{y_{p_i}}{b}\ \text{odd}\right)\wedge(m_y\ \text{odd})\\ 0, & \left(\frac{m_y}{b}=\frac{n_y}{L_y}\right)\end{cases} \quad (A.4b)$$

in which:

$$f(x)=\frac{\cos\left[\left(\frac{m_x}{a}+\frac{n_x}{L_x}\right)\pi x\right]}{2\left(\frac{m_x}{a}+\frac{n_x}{L_x}\right)\pi}+\frac{\cos\left[\left(\frac{m_x}{a}-\frac{n_x}{L_x}\right)\pi x\right]}{2\left(\frac{m_x}{a}-\frac{n_x}{L_x}\right)\pi}\,, \quad (A.5a)$$

and

$$g(y) = \frac{\cos\left[\left(\frac{m_y}{b}+\frac{n_y}{L_y}\right)\pi y\right]}{2\left(\frac{m_y}{b}+\frac{n_y}{L_y}\right)\pi} + \frac{\cos\left[\left(\frac{m_y}{b}-\frac{n_y}{L_y}\right)\pi y\right]}{2\left(\frac{m_y}{b}-\frac{n_y}{L_y}\right)\pi}, \qquad (A.5b)$$

Similarly to mass matrix, the stiffness matrix, $\mathbf{K}_{pc}$, may be written in the following form

$$\mathbf{K}_{cp} = -\frac{2}{\sqrt{a\,b\,L_x L_y L_z}}\left[(-1)^{n_z} A_{n_x} A_{n_y} A_{n_z} B_{mn}(x) B_{mn}(y)\right], \quad (A.6)$$

with functions $B_{mn}(x)$ and $B_{mn}(y)$ defined by Eqs.(A.4a) and (A.4b), respectively.

B. Analytical expression derived for $\mathbf{S}_{tbl}(\omega)$ matrix

Substituting Eqs.(4) and (6) into Eq.(28), $\mathbf{S}_{tbl}(\omega)$ matrix becomes defined as follows

$$\mathbf{S}_{tbl}(\omega) = \frac{4\,S_{ref}(\omega)}{a\,b}\left[\int_{x_{p_i}}^{x_{p_f}}\int \sin\left(\frac{m_x\pi\,x}{a}\right)\sin\left(\frac{m'_x\pi\,x'}{a}\right)e^{-\frac{\alpha_x\,\omega\,|\,x-x'|}{U_c}} e^{-\frac{i\,\omega\,(x-x')}{U_c}}dx\,dx' \int_{y_{p_i}}^{y_{p_f}}\sin\left(\frac{m_y\pi\,y}{b}\right)\sin\left(\frac{m'_y\pi\,y'}{b}\right)e^{-\frac{\alpha_y\,\omega\,|\,y-y'|}{U_c}}dy\,dy'\right] \qquad (B.1)$$

in which terms inside [ ] are developed to obtain a matrix, according with the m and m' indexes, and x and y correspond to plate (local) coordinate system. After some mathematical manipulation, Eq. (B.1) can be written as

$$\mathbf{S}_{tbl}(\omega) = \frac{4\,S_{ref}(\omega)}{a\,b}\left[\int_{x_{p_i}}^{x_{p_f}}\sin\left(\frac{m'_x\pi x'}{a}\right)\left\{e^{\frac{x'(-\alpha_x+i)\omega}{U_c}}\int_{x_{p_i}}^{x'}\sin\left(\frac{m_x\pi x}{a}\right)e^{\frac{x\,(\alpha_x-i)\,\omega}{U_c}}dx + e^{\frac{x'\,(\alpha_x+i)\,\omega}{U_c}}\int_{x'}^{x_{p_f}}\sin\left(\frac{m_x\pi\,x}{a}\right)e^{\frac{x\,(-\alpha_x-i)\,\omega}{U_c}}dx\right\}dx' \int_{y_{p_i}}^{y_{p_f}}\sin\left(\frac{m_{y'}\pi\,y'}{b}\right)\left\{e^{-\frac{y'\,\alpha_y\,\omega}{U_c}}\int_{y_{p_i}}^{y'}\sin\left(\frac{m_y\,\pi\,y}{b}\right)e^{\frac{y\,\alpha_y\,\omega}{U_c}}dy + e^{\frac{y'\,\alpha_y\,\omega}{U_c}}\int_{y'}^{y_{p_f}}\sin\left(\frac{m_y\,\pi\,y}{b}\right)e^{-\frac{y\,\alpha_y\,\omega}{U_c}}dy\right\}dy'\right], \qquad (B.2)$$

Developing Eq.(B.2) analytically, one obtains the final analytical expression for the $\mathbf{S}_{tbl}(\omega)$ matrix components, which become defined as follows:

$$S_{tbl}(\omega)_{m,m'} = \frac{4\,S_{ref}(\omega)}{a\,b}\{\left[C_{x_1}(\omega,m)\,C_{x_5}(m,m') + C_{x_2}(\omega,m)\,C_{x_6}(m,m') + C_{x_3}(\omega,m)\,C_{x_7}(\omega,m') + C_{x_4}(\omega,m)\,C_{x_8}(\omega,m')\right]$$
$$\left[C_{y_1}(\omega,m)\,C_{y_5}(m,m') + C_{y_3}(\omega,m)\,C_{y_7}(\omega,m') + C_{y_4}(\omega,m)\,C_{y_8}(\omega,m')\right], \qquad (B.3)$$

in which functions C's are defined by the following analytical expressions:

$$C_{x_1}(\omega,m) = \frac{2\alpha_x\omega}{U_c}\,\frac{\left(\frac{\omega}{U_c}\right)^2(\alpha_x^2+1)+\left(\frac{m_x\pi}{a}\right)^2}{\left[\left(\frac{\omega}{U_c}\right)^2(\alpha_x^2-1)+\left(\frac{m_x\pi}{a}\right)^2\right]^2+\left[2\alpha_x\left(\frac{\omega}{U_c}\right)^2\right]^2}, \qquad (B.4)$$

$$C_{x_2}(\omega,m) = -\frac{\left(\frac{m_x\pi}{a}\right)\left(\frac{4\alpha_x\omega^2}{U_c^2}\right)i}{\left[\left(\frac{\omega}{U_c}\right)^2(\alpha_x^2-1)+\left(\frac{m_x\pi}{a}\right)^2\right]^2+\left[2\alpha_x\left(\frac{\omega}{U_c}\right)^2\right]^2}, \qquad (B.5)$$

$$C_{x_3}(\omega,m) = -\frac{e^{\frac{x_{p_i}\,(\alpha_x-i)\,\omega}{U_c}}}{\left[\left(\frac{\omega}{U_c}\right)^2(\alpha_x^2-1)+\left(\frac{m_x\pi}{a}\right)^2\right]^2+\left[2\alpha_x\left(\frac{\omega}{U_c}\right)^2\right]^2} \left\{\left[\left(\frac{\omega}{U_c}\right)^2(\alpha_x^2-1)+\left(\frac{m_x\pi}{a}\right)^2\right]+2\alpha_x\left(\frac{\omega}{U_c}\right)^2 i\right\}\left[\frac{(\alpha_x-i)\omega}{U_c}\sin\left(\frac{m_x\pi x_{p_i}}{a}\right) - \frac{m_x\pi}{a}\cos\left(\frac{m_x\pi\,x_{p_i}}{a}\right)\right], \qquad (B.6)$$

$$C_{x_4}(\omega,m) = -\frac{e^{-\frac{(x_{p_i}+a)(\alpha_x+i)\,\omega}{U_c}}\cos(m_x\pi)}{\left[\left(\frac{\omega}{U_c}\right)^2(\alpha_x^2-1)+\left(\frac{m_x\pi}{a}\right)^2\right]^2+\left[2\alpha_x\left(\frac{\omega}{U_c}\right)^2\right]^2} \left\{\left[\left(\frac{\omega}{U_c}\right)^2(\alpha_x^2-1)+\left(\frac{m_x\pi}{a}\right)^2\right]-2\alpha_x\left(\frac{\omega}{U_c}\right)^2 i\right\}\left[\frac{(\alpha_x+i)\omega}{U_c}\sin\left(\frac{m_x\pi x_{p_i}}{a}\right) + \frac{m_x\pi}{a}\cos\left(\frac{m_x\pi\,x_{p_i}}{a}\right)\right], \qquad (B.7)$$

$$C_{x_5}(m,m') = \begin{cases}\frac{a}{2}, & \text{for } m_x = m'_x\\ \text{Const.}_{x_5}, & \text{for } m_x \neq m'_x\end{cases} \qquad (B.8a)$$

with:

$$\text{Const.}_{x_5} = \frac{-\sin\left[(m'_x+m_x)\frac{\pi}{a}(x_{p_i}+a)\right]+\sin\left[(m'_x+m_x)\frac{\pi}{a}x_{p_i}\right]}{2(m'_x+m_x)\frac{\pi}{a}} + \frac{\sin\left[(m'_x-m_x)\frac{\pi}{a}(x_{p_i}+a)\right]-\sin\left[(m'_x-m_x)\frac{\pi}{a}x_{p_i}\right]}{2(m'_x-m_x)\frac{\pi}{a}}, \qquad (B.8b)$$

$$C_{x_6}(m,m') = \begin{cases}0, & \text{for } m_x = m'_x\\ \text{Const.}_{x_6}, & \text{for } m_x \neq m'_x\end{cases} \qquad (B.9a)$$

$$\text{Const.}_{x_6}= \frac{-\cos\left[(m'_x+ m_x)\frac{\pi}{a}(x_{p_i}+ a)\right]+\cos\left[(m'_x+ m_x)\frac{\pi}{a}x_{p_i}\right]}{2(m'_x+m_x)\frac{\pi}{a}} + \frac{-\cos\left[(m'_x- m_x)\frac{\pi}{a}(x_{p_i}+ a)\right]+\cos\left[(m'_x- m_x)\frac{\pi}{a}x_{p_i}\right]}{2(m'_x- m_x)\frac{\pi}{a}}, \quad \text{(B.9b)}$$

$$C_{x_7}(\omega,m')= \frac{e^{\frac{(x_{p_i}+ a)(-\alpha_x+ i)\,\omega}{U_c}}}{\left[\frac{(-\alpha_x+i)\omega}{U_c}\right]^2+\left(\frac{m'_x\pi}{a}\right)^2}\left\{\frac{(-\alpha_x+i)\omega}{U_c}\sin\left[\frac{m'_x\pi(x_{p_i}+a)}{a}\right] - \frac{m'_x\pi}{a}\cos\left[\frac{m'_x\pi(x_{p_i}+a)}{a}\right]\right\} - \frac{e^{\frac{x_{p_i}(-\alpha_x+ i)\,\omega}{U_c}}}{\left[\frac{(-\alpha_x+i)\omega}{U_c}\right]^2+\left(\frac{m'_x\pi}{a}\right)^2}\left[\frac{(-\alpha_x+i)\omega}{U_c} \sin\left(\frac{m'_x\pi x_{p_i}}{a}\right) - \frac{m'_x\pi}{a}\cos\left(\frac{m'_x\pi x_{p_i}}{a}\right)\right], \quad \text{(B.10)}$$

$$C_{x_8}(\omega,m')= \frac{e^{\frac{(x_{p_i}+ a)(\alpha_x+ i)\,\omega}{U_c}}}{\left[\frac{(\alpha_x+i)\omega}{U_c}\right]^2+\left(\frac{m'_x\pi}{a}\right)^2}\left\{\frac{(\alpha_x+i)\omega}{U_c}\sin\left[\frac{m'_x\pi(x_{p_i}+a)}{a}\right] - \frac{m'_x\pi}{a}\cos\left[\frac{m'_x\pi(x_{p_i}+a)}{a}\right]\right\} - \frac{e^{\frac{x_{p_i}(\alpha_x+ i)\,\omega}{U_c}}}{\left[\frac{(\alpha_x+i)\omega}{U_c}\right]^2+\left(\frac{m'_x\pi}{a}\right)^2}\left[\frac{(\alpha_x+i)\omega}{U_c} \sin\left(\frac{m'_x\pi x_{p_i}}{a}\right) - \frac{m'_x\pi}{a}\cos\left(\frac{m'_x\pi x_{p_i}}{a}\right)\right], \quad \text{(B.11)}$$

and

$$C_{y_1}(\omega,m) = \frac{\frac{2\alpha_y\omega}{U_c}}{\left(\frac{\alpha_y\omega}{U_c}\right)^2+\left(\frac{m_y\pi}{b}\right)^2}, \quad \text{(B.12)}$$

$$C_{y_3}(\omega,m) = -\frac{e^{\frac{y_{p_i}\alpha_y\,\omega}{U_c}}}{\left(\frac{\alpha_y\omega}{U_c}\right)^2+\left(\frac{m_y\pi}{b}\right)^2}\left[\frac{\alpha_y\omega}{U_c}\sin\left(\frac{m_y\pi y_{p_i}}{b}\right) - \frac{m_y\pi}{b}\cos\left(\frac{m_y\pi y_{p_i}}{b}\right)\right], \quad \text{(B.13)}$$

$$C_{y_4}(\omega,m) = -\frac{e^{-\frac{(y_{p_i}+ b)\,\alpha_y\,\omega}{U_c}}}{\left(\frac{\alpha_y\omega}{U_c}\right)^2+\left(\frac{m_y\pi}{b}\right)^2}\left[\frac{\alpha_y\omega}{U_c}\sin\left(\frac{m_y\pi(y_{p_i}+ b)}{b}\right) + \frac{m_y\pi}{b}\cos\left(\frac{m_y\pi(y_{p_i}+ b)}{b}\right)\right], \quad \text{(B.14)}$$

$$C_{y_5}(m, m') = \begin{cases} \frac{b}{2}, & \text{for } m_y = m'_y \\ \text{Const.}_{y_5}, & \text{for } m_y \neq m'_y \end{cases} \quad \text{(B.15a)}$$

with:

$$\text{Const.}_{y_5}= \frac{-\sin\left[(m'_y+ m_y)\frac{\pi}{b}(y_{p_i}+ b)\right]+\sin\left[(m'_y+ m_y)\frac{\pi}{b}y_{p_i}\right]}{2(m'_y+ m_y)\frac{\pi}{b}} + \frac{\sin\left[(m'_y- m_y)\frac{\pi}{b}(y_{p_i}+ b)\right]-\sin\left[(m'_y- m_y)\frac{\pi}{b}y_{p_i}\right]}{2(m'_y- m_y)\frac{\pi}{b}}, \quad \text{(B.15b)}$$

$$C_{y_7}(\omega,m') = \frac{e^{-\frac{(y_{p_i}+ b)\,\alpha_y\,\omega}{U_c}}}{\left(\frac{\alpha_y\omega}{U_c}\right)^2+\left(\frac{m'_y\pi}{b}\right)^2}\left\{-\frac{\alpha_y\omega}{U_c}\sin\left[\frac{m'_y\pi(y_{p_i}+ b)}{b}\right] - \frac{m'_y\pi}{b}\cos\left[\frac{m'_y\pi(y_{p_i}+ b)}{b}\right]\right\} + \frac{e^{-\frac{y_{p_i}\,\alpha_y\,\omega}{U_c}}}{\left(\frac{\alpha_y\omega}{U_c}\right)^2+\left(\frac{m'_y\pi}{b}\right)^2}\left[\frac{\alpha_y\omega}{U_c} \sin\left(\frac{m'_y\pi y_{p_i}}{b}\right) + \frac{m'_y\pi}{b}\cos\left(\frac{m'_y\pi y_{p_i}}{b}\right)\right], \quad \text{(B.16)}$$

$$C_{y_8}(\omega,m') = \frac{e^{\frac{(y_{p_i}+ b)\,\alpha_y\,\omega}{U_c}}}{\left(\frac{\alpha_y\omega}{U_c}\right)^2+\left(\frac{m'_y\pi}{b}\right)^2}\left\{\frac{\alpha_y\omega}{U_c}\sin\left[\frac{m'_y\pi(y_{p_i}+ b)}{b}\right] - \frac{m'_y\pi}{b}\cos\left[\frac{m'_y\pi(y_{p_i}+ b)}{b}\right]\right\} - \frac{e^{\frac{y_{p_i}\,\alpha_y\,\omega}{U_c}}}{\left(\frac{\alpha_y\omega}{U_c}\right)^2+\left(\frac{m'_y\pi}{b}\right)^2}\left[\frac{\alpha_y\omega}{U_c} \sin\left(\frac{m'_y\pi y_{p_i}}{b}\right) - \frac{m'_y\pi}{b}\cos\left(\frac{m'_y\pi y_{p_i}}{b}\right)\right]. \quad \text{(B.17)}$$

For random incident white noise, the external PSD excitation may be defined as

$$\mathbf{S}_{ext} = \frac{4\,S_{ref}}{a\,b}\left[\iint_{x_{p_i}}^{x_{p_f}} \sin\left(\frac{m_x\pi\,x}{a}\right)\sin\left(\frac{m'_x\pi\,x'}{a}\right)dx\,dx' \iint_{y_{p_i}}^{y_{p_f}} \sin\left(\frac{m_y\pi\,y}{b}\right)\sin\left(\frac{m'_y\pi\,y'}{b}\right)dy\,dy'\right], \quad \text{(B.18)}$$

which analytically developed results in the following expression

$$\mathbf{S}_{ext}= \left[\frac{4\,a\,b\,S_{ref}}{m_x\,m'_x\,m_y\,m'_y\,\pi^4}\left\{\cos\left(\frac{m_x\pi(x_{p_i}+a)}{a}\right)-\cos\left(\frac{m_x\pi\,x_{p_i}}{a}\right)\right\} \left\{\cos\left(\frac{m'_x\pi\,(x_{p_i}+a)}{a}\right)-\cos\left(\frac{m'_x\pi\,x_{p_i}}{a}\right)\right\}\left\{\cos\left(\frac{m_y\pi\,(y_{p_i}+b)}{b}\right) - \cos\left(\frac{m_y\pi\,y_{p_i}}{b}\right)\right\}\left\{\cos\left(\frac{m'_y\pi\,(y_{p_i}+b)}{b}\right)-\cos\left(\frac{m'_y\pi\,y_{p_i}}{b}\right)\right\}\right], \quad \text{(B.19)}$$

where S_{ref} is the constant PSD amplitude of the normally impinging noise on the plate.

C. Analytical expressions for $S_{ww}(\omega)$ and $S_{pp}(\omega)$ functions

The plate overall displacement PSD function, $S_{ww}(\omega)$, was previously defined by Eq. (31). In order to obtain the final analytical expression for this function, one must substitute Eqs. (6) into Eq. (29), and then integrate over the plate area, as shown in Eq. (31). Doing this, the final expression for $S_{ww}(\omega)$ is

$$S_{ww}(\omega)=\frac{4ab}{\pi^4}\sum_{m_{x_1},m_{x_2}=1}^{M_x^2}\sum_{m_{y_1},m_{y_2}=1}^{M_y^2}\frac{\mathbf{S_{WW}}(\omega)_{m_1,m_2}}{m_{x_1}m_{x_2}m_{y_1}m_{y_2}}\cos\left(\frac{m_{x_1}\pi x_{p_i}}{a}\right)\cos\left(\frac{m_{x_2}\pi x_{p_i}}{a}\right)\cos\left(\frac{m_{y_1}\pi y_{p_i}}{b}\right)\cos\left(\frac{m_{y_1}\pi y_{p_i}}{b}\right)\left[\cos(m_{x_1}\pi)-1\right]\left[\cos(m_{x_2}\pi)-1\right]\left[\cos(m_{y_1}\pi)-1\right]\left[\cos(m_{y_2}\pi)-1\right]. \quad (C.1)$$

with each matrix component $\mathbf{S_{WW}}(\omega)_{m_1,m_2}$ corresponding to the respective element of the matrix previously defined in Eq. (24).

Similarly, the analytical expression for the enclosure overall pressure PSD function, $S_{pp}(\omega)$, may be obtained by replacing Eqs. (10) into Eq. (30), and then integrating over the enclosure volume, as shown in Eq. (32). It can be shown that the final analytical expression for $S_{pp}(\omega)$ is

$$S_{pp}(\omega)=\frac{L_xL_yL_z}{8}\sum_{n_{x_1},n_{x_1}=1}^{N_x^2}\sum_{n_{y_1},n_{y_1}=1}^{N_y^2}\sum_{n_{z_1},n_{z_1}=1}^{N_z^2}A_{n_{x_1}}^2A_{n_{y_1}}^2A_{n_{z_1}}^2\mathbf{S_{PP}}(\omega)_{n_1,n_2} \quad (C.2)$$

with each matrix component $\mathbf{S_{PP}}(\omega)_{n_1,n_2}$ corresponding to the respective element of the matrix previously defined in Eq. (25).

Appendix B

Turbulent Boundary Layer Induced Noise and Vibration of a Multi-Panel Walled Acoustic Enclosure

TURBULENT BOUNDARY LAYER INDUCED NOISE AND VIBRATION OF A MULTI-PANEL WALLED ACOUSTIC ENCLOSURE

Joana da Rocha[1], Afzal Suleman[1], and Fernando Lau[2]
[1]Dept. of Mechanical Engineering, University of Victoria, PO Box 3055, Stn. CSC, Victoria, BC, Canada, V8W 3P6
jdarocha@uvic.ca, suleman@uvic.ca
[2]Centro de Ciências e Tecnologias Aeronáuticas, Dept. de Engenharia Mecânica, Instituto Superior Técnico, Av. Rovisco Pais, Lisboa, Portugal, 1049-001 lau@ist.utl.pt

ABSTRACT

Flow-induced noise in aircraft cabins can be predicted through analytical models or numerical methods. To date, analytical methods have been used for simple structures and cabins, where usually a single panel is vibrating due to the flow excitation, and coupled with an acoustic enclosure. The present work investigates the analytical prediction of turbulent boundary layer induced noise and vibration of a multi-panel system. The objective is to investigate the coupling between individual panels and the acoustic enclosure. Each panel is coupled with the acoustic enclosure, which consists of a large rectangular room, with five rigid walls and one flexible wall. The properties of the panels and acoustic enclosure represent a typical fuselage skin panel and a cabin section, respectively. It is shown that identical panels located at different positions have dissimilar contributions to the cabin interior noise, showing that the panel position is an important variable for the accurate prediction and suppression of cabin noise. Analytical predictions were obtained for both the space-averaged interior sound pressure level and local interior sound pressure level. The space-averaged sound pressure level is usually accepted to provide the necessary information for the noise prediction; however, in some real life applications, the local sound pressure may also be desirable.

RESUME

Le bruit à l'intérieur d'es cabines d´es avions induite par écoulement externe peut être prédit par modèles analytiques ou méthodes numériques. À ce jour, les méthodes analytiques ont été utilisés pour structures et chambre simples, où, normalement, un seul panneau est considéré à vibrer en raison de l'écoulement externe, et couplé avec la chambre acoustique. Cet article étudie la prévision analytique des vibrations et du bruit dans un système avec plusieurs panneaux. L'objectif est d´examiner le couplage entre panneaux individuels et la chambre acoustique, en considérant de l'emplacement du panneau comme une variable. La cabine acoustique est une grande chambre rectangulaire et les panneaux rectangulaires sont considérés simplement appuyés. Les propriétés des matériaux et les dimensions des panneaux et de chambre acoustique sont représentatives d'un panneau de fuselage typique d'un avion et un compartiment de la cabine, respectivement. Il est conclu que panneaux similaires situés dans des positions différentes de la cabine ont contributions différentes du bruit intérieur, montrant que la position du panneau est une variable importante pour une prévision précise de bruit et de suppression de bruit dans la cabine. Ont été obtenu des prévisions analytiques des valeurs localisées du niveau de pression sonore à l'intérieur, et la moyenne de ces valeurs en l'espace. Le niveau moyen de pression acoustique à l'intérieur est habituellement utilisé pour obtenir information de la prévision du bruit; cependant, dans certaines situations et applications réelles, la valeur du niveau de pression acoustique d'un point précis dans l'espace peut être souhaitable.

1. INTRODUCTION

The turbulent boundary layer (TBL) induced vibration in transport vehicles, particularly in aircraft, is a major source of interior noise, and thus an important topic of investigation. As confirmed by flight measurements in [1], the interior noise in the cabin of a jet transport aircraft, during cruise flight, is mostly generated by the external TBL excitation. While during takeoff the engine noise is the dominant source of cabin noise, the airflow sources become the major contribution for the interior noise during cruise flight. For subsonic flight, the TBL pressure levels on the exterior of the fuselage increase with the flight speed [2–4], representing a major source of aircraft interior noise for frequencies below 1000 Hz [1, 5]. Specifically, in [6], flight test measurements in an aircraft cockpit indicated that

interior noise was dominated by low-frequency noise (<500 Hz), and that the main noise source was the external turbulent flow. As referred in [7], TBL excitation is regarded as the most important noise source for jet powered aircraft at cruise speed, particularly, as new quieter jet engines are being developed.

The main objective of the present work is the development of accurate analytical models for the prediction of TBL-induced noise in the interior of a real scale rectangular cabin. The physical system considered corresponds to a rectangular shaped acoustic enclosure, filled with air, with one flexible wall and five rigid walls. The flexible wall is composed of 50 identical simply supported panels. The dimensions and properties of the plates are similar to those of typical aircraft fuselage skin panels. A larger acoustic enclosure, compared with the plate's dimensions, was studied in order to simulate a more realistic approach of an aircraft fuselage section. Both the unpressurized and pressurized cabin are explored. The external flow excitation is representative of typical cruise conditions of a commercial aircraft, i.e., of the TBL wall pressure fluctuations in the aircraft fuselage, while in cruise and stabilized flight conditions. The TBL is assumed to be attached and completely developed over the aircraft structure. The amplitude of the wall pressure fluctuations is dependent on the TBL thickness, thus depends on the longitudinal position of the plate.

Previous work performed by the authors has validated the analytical models for single panel coupled with an acoustic enclosure, as in [8]. The analytical framework was successfully validated through comparison with several independent experimental studies. The present work adds a step forward compared to previous studies - it considers the TBL as the panel's excitation, while considering each panel (located at different positions in the flexible wall) coupled with a real scaled acoustic enclosure. The aim is to investigate the coupling between individual panels and the acoustic enclosure. It is shown that the position of the plate relative to the enclosure plays a crucial role in the accurate prediction of the interior pressure field. The difference between predicted space-averaged sound pressure level (SASPL) and predicted local sound pressure level (LSPL) is also explored.

The analytical formulation was developed from the fundamental equations and intrinsically derived as a structural-acoustic coupled model, i.e., it accounts for the natural modes of the plate and the acoustic modes of the enclosure. A convergence study was performed to calculate the minimum number of plate and acoustic modes needed for convergence of the predicted spectral quantities. Results were obtained for the prediction of vibration and sound pressure levels in the power spectral density (PSD) domain, up to a frequency of 1000 Hz. The model is able to predict the space-average plate displacement level, the space-average interior SPL, local plate displacement level (at a specified location on the panel surface), and local SPL. The occurrence of the hydrodynamic coincidence phenomenon is also investigated.

1.1 Turbulent Boundary Layer Excited Panels

Previous investigations on flow-induced noise and vibration have been reported, although, it is important to recognize how different these studies are, and how their nature can affect the development of a predictive mathematical model. Specifically, the study of the noise radiation by a isolated panel into free air, involves a different analysis compared with the study of cabin interior noise prediction due to the vibration of a panel. The later involves the coupling between the structural vibration and the cabin acoustic field. When the purpose is to develop analytical models for the prediction of cabin noise levels, one needs to consider the properties of: (1) the excitation, (2) the vibrating structure, and (3) the sound receiving room.

Several early experimental studies were performed to investigate the vibration and radiation of sound from structural panels, excited by the TBL, e.g. [9–12]. These studies provide knowledge about the shape of the spectrum, convection velocity and space-time correlation of the exterior TBL pressure fluctuations on aircraft panels, as well as displacement and acceleration spectra of the vibrating aircraft panels. Additionally, theoretical studies have also been performed to study the vibration and sound radiated by isolated panels (i.e., not coupled with an acoustic enclosure) excited by turbulent flows [13–17], and for random vibration of a single panel coupled with a small acoustic enclosure [7, 18, 19]. In these studies, the TBL excitation is usually described in terms of the statistical properties of the wall pressure fluctuations based on the Corcos formulation [20, 21]. Even though a number of new models were developed after the Corcos model for the TBL description, e.g. [22–25], the Corcos formulation is widely used in recent studies to describe the TBL pressure field [26–30], since it captures the fundamental pressure tendency along the frequency and requires significantly reduced computational effort to employ. Furthermore, Corcos formulation provides a good estimation for the TBL wall-pressure fluctuations levels at and near the convective peak, which is of fundamental importance for aircraft boundary layers (for high subsonic Mach numbers) [26], the case of the present study. In order to account with the streamwize variation of the boundary layer thickness, in the present study the Efimtsov model [22] is used to provide the point power spectrum. In the comparison of the several models available to describe the turbulent boundary layer wall pressure in [31], the model developed by Efimtsov is cited as a suitable candidate, being the only model derived from aircraft flight tests rather than laboratory measurements. More recently, flight tests performed in the Tupolev 144LL aircraft [32], demonstrated that the Efimtsov model shows the best agreement with the experimental data.

In the present study, the panels are considered to be simply supported in all four edges. Each panel represents the

distance between adjacent stringers and frames (no additional stiffeners are considered), and is individually vibrating and coupled with the acoustic enclosure. As concluded in [11, 33], while jet noise induced vibration is highly correlated over several panels in both longitudinal and circumferential directions, the TBL induced vibration (in which the vibration correlation decays rapidly especially in the circumferential direction) is confined to one or two adjacent panels in the longitudinal direction. For the TBL excitation, the vibration of an isolated panel can be considered with the limitation that it is not necessarily valid at frequencies below the lowest natural frequency of a single bay of the fuselage structure (which in the present study is 61.44 Hz for the unpressurized cabin, and 355.45 Hz for the pressurized cabin).

1.2 Aircraft Cabin Noise Induced by Turbulent Flow

Several experimental studies were conducted to investigate the aircraft cabin interior noise induced by the TBL [34–37], providing measurements of the interior SPL and fuselage skin vibrations spectrum, at various locations in the cabin and cockpit of commercial aircraft, for aluminum and composite fuselages. These studies are a good database for comparison with theoretical predictions of interior noise levels induced by the TBL. The effect of aircraft speed on boundary layer induced interior noise can be seen to be dramatic, with the interior sound pressure levels being generally higher for higher flight speeds. The TBL wall pressure levels increase with the flight Mach number, as concluded in [2, 4, 33]. In the absence of hydrodynamic coincidence phenomenon, the interior noise level usually follows the same tendency, i.e., it increases with the flight Mach number [7, 16, 38]. In the presence of hydrodynamic coincidence, the tendency of increased interior noise with higher flight speeds is generally valid for frequencies below and above the neighborhood of frequency at which hydrodynamic coincidence occurs, as shown in [11].

Interior cabin noise is a challenging problem in most aircraft and many other transport vehicles. The reduction of cabin noise levels is desirable for both comfort and health-related reasons, and they are balanced with the cost, complexity, and physical constraints of noise control systems. As well known, passive noise control techniques are not effective in the low-frequency noise range, where the active noise control techniques have demonstrated better results, showing the ability to decrease sound levels without a big penalty in terms of weight. However, because of the complexity of the coupled structural-acoustic system, the implementation of these techniques is far from being straightforward. To efficiently design a noise control system, a clear understanding of the mechanisms of sound radiation and transmission of the coupled structural-acoustic system is crucial. In this context, the objective of the present study is to contribute for the understanding of the sound transmission phenomenon involved in the multi-panel structural-acoustic system.

2. MATHEMATICAL MODELS

In this section, the mathematical models developed are presented. Three models need to be defined: (1) the TBL model, which represents the external force applied to each panel, (2) the structural model, representing each individual plate coupled with the acoustic enclosure, and (3) the acoustic model, consisting of a rectangular acoustic cabin. In the following subsections, the mathematical models involved in the analysis are presented. Since previous work was performed in order to validate the analytical model, for simple systems, in this work the new developments on the model are emphasized. If the reader wishes to see more details of the mathematical manipulations involved in the analysis, please refer to [8].

2.1 Turbulent Flow Model

As previously referred, modeling the TBL wall pressure has been a subject of study for many years. Since the TBL is a random process, the resultant wall pressure, p(x, y, t), is usually statistically described in terms of the pressure power spectral density (PSD). These models were developed for turbulent flow over a flat plate, assuming fully developed flow and zero mean pressure gradient. For these conditions, the turbulent flow can be regarded as stationary in time and homogeneous in space. The cross-spectral density of the wall pressure over the (x, y) plane, for flow in the x-direction, can be defined through the Corcos formulation [20, 21], as follows

$$S(x,\xi_x,\xi_y,\omega) = S_{ref}(x,\omega)\, e^{-\frac{\alpha_x \omega |\xi_x|}{U_c}}\, e^{-\frac{\alpha_y \omega |\xi_y|}{U_c}}\, e^{-\frac{i \omega \xi_x}{U_c}}, \quad (1)$$

in which ξ_x and ξ_y are the spatial separations in the streamwise and spanwise directions of the plate, respectively, ω is the angular frequency, U_c is the convective speed of the TBL, and α_x and α_y are empirical parameters that denote the lost of coherence in the longitudinal and transverse directions, and are chosen to yield the best agreement with the reality. Recommended empirical values for aircraft boundary layers are $\alpha_x = 0.1$ and $\alpha_y = 0.77$ [31]. Note that, with relation to previous study [8], x was added as a variable for the $S(x,\xi_x,\xi_y,\omega)$ and S_{ref} (x,ω) terms. This variable needs to be added since the TBL pressure cross-spectral density dependents on the position of each panel; i.e., panels positioned at different x-coordinates have different S_{ref} values. Efimtsov model, defined in [22], is in good agreement with experimental data for the flow speed of interest in the present work, and provide the reference PSD as follows:

$$S_{ref}(x,\omega) = \frac{\tau_w^2(x)\,\delta(x)}{U_\tau(x)}\,\frac{0.01\,\pi}{1+0.02\,Sh^{2/3}(x,\omega)}, \quad (2)$$

with:

$$U_\tau(x) = U_\infty \sqrt{\frac{C_f(x)}{2}},\ \tau_w(x) = \frac{1}{2}\rho U_\infty^2 C_f(x),\ \ Sh(x,\omega) = \frac{\omega\,\delta(x)}{U_\tau(x)}, \quad (3)$$

where U_τ is the friction velocity, τ_w is the mean wall shear stress, C_f is the friction coefficient, δ is the boundary layer thickness, Sh is the Strouhal number, and U_∞ is the free-stream velocity. Functions $C_f(x)$ and $\delta(x)$ were computed using the following semi-empirical expressions for turbulent boundary layers, respectively from [39] and [9]:

$$C_f(x) = 0.37(\mathrm{Log}_{10}\mathrm{Re}_x)^{-2.584}, \quad (4a)$$

$$\delta(x) = 0.37\ x\ \mathrm{Re}_x^{-\frac{1}{5}}\left[1+\left(\frac{\mathrm{Re}_x}{6.9\times10^7}\right)^2\right]^{\frac{1}{10}}. \quad (4b)$$

Values of C_f and δ for each plate are shown in Fig. 1. Plates located at the same x-coordinate have same values of C_f and δ. In these figures, points x_1 through x_5 correspond to the panel center locations from the first to the fifth rows of panels along x-direction. Points x_i and x_f correspond, respectively, to the x-coordinate in which the first row of panels starts (i.e., to x = 9.14 m) and to the x coordinate in which the last row of panels ends (i.e., x = 11.64 m) - refer to Fig. 3 for more details about the physical system under study. Fig. 2 shows $S_{ref}(x,\omega)$ for different flight speeds and altitudes, given by Eq.(2), for the fifth row of panels. For this row of panels, the curve corresponding to the present study is the one with solid line and bold circle – refer to Table 2 for more information about external fluid parameters. As concluded in [32], the predictions provided by the Efimtsov model, using Eq.(2), show a weaker decay than the measured data at high frequencies (above 1000 Hz), over predicting the spectral quantities above this frequency. Since the present study considers only frequencies up to 1 KHz, this problem does not significantly affect the results.

2.2 Panels Displacement Model

All plates are considered to be flat panels, simply supported in all four boundaries (as in Fig. 3b) and are assumed to represent the distance between adjacent stringers and frames of a conventional aircraft skin-stringer-frame structure. The displacement of each panel is defined in terms of its natural modes, as follows

$$w(x,y,t) = \sum_{m_x=1}^{M_x}\sum_{m_y=1}^{M_y} \alpha_{m_x}(x)\,\beta_{m_y}(y)\,q_{m_x m_y}(t)\,, \quad (5)$$

where $\alpha_{m_x}(x)$ and $\beta_{m_y}(y)$ functions define the variation of w with the x and y, respectively, $q_{m_x m_y}(t)$ define the variation of w with t, and $M = M_x \times M_y$ is the total number of plate modes considered in the analysis. As shown in Fig. 3a, the direction of the plate displacement, w, was chosen to be the

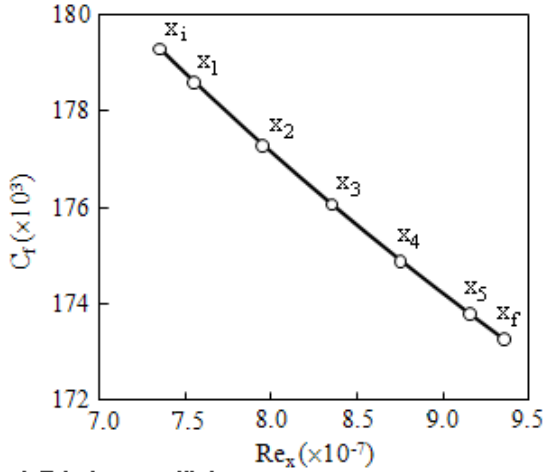

a) Friction coefficient

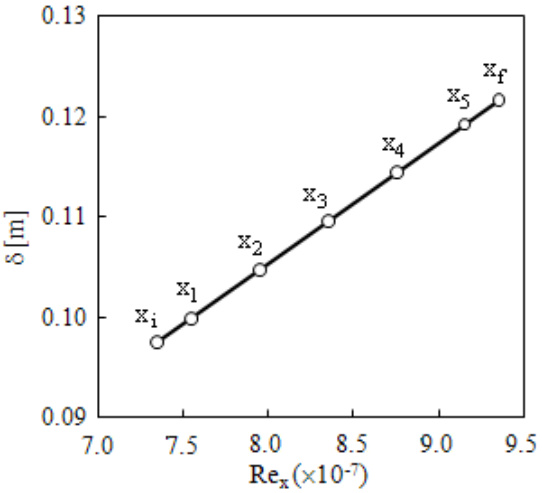

b) Boundary layer thickness

Figure 1. Comparison of the C_f and δ values along the several x panel rows.

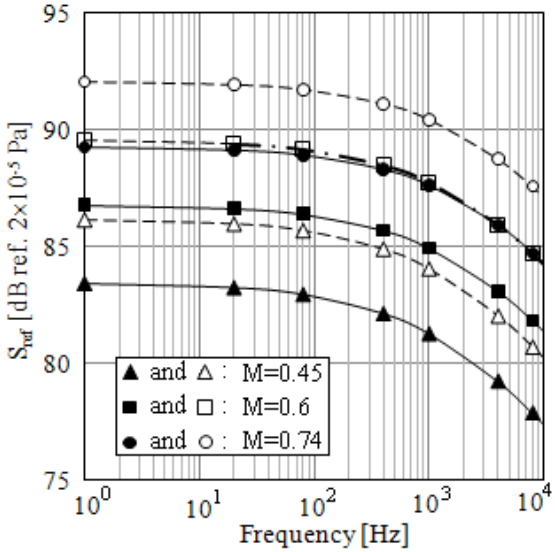

Figure 2. Reference PSD obtained from Efimtsov model, for altitudes 25000 ft (solid lines) and 16400 ft (dashed lines).

positive z-direction. Since the panels are simply supported plates, the spatial functions may be defined, in the plate (local) coordinates system, as:

$$\alpha_{m_x}(x_1) = \sqrt{\frac{2}{a}} \sin\left(\frac{m_x \pi x_1}{a}\right), \quad (6a)$$

$$\beta_{m_y}(y_1) = \sqrt{\frac{2}{b}} \sin\left(\frac{m_y \pi y_1}{b}\right), \quad (6b)$$

in which a and b are the dimensions of the plate in the x- and y-directions. However, in order to compute the structural-acoustic coupling, it is convenient to work in the enclosure (global) coordinates system. To accomplish that, Eqs.(6) can be written in the global coordinates system, for each individual plate, as follows:

$$\alpha_{m_x}(x) = \sqrt{\frac{2}{a}} \sin\left(\frac{m_x \pi (x-x_{p_i})}{a}\right), \quad (7a)$$

$$\beta_{m_y}(y) = \sqrt{\frac{2}{b}} \sin\left(\frac{m_y \pi (y-y_{p_i})}{b}\right), \quad (7b)$$

where (x_{pi}, y_{pi}) is the position of the origin of the i^{th} plate coordinates system, written in the global coordinates system. The natural frequencies for the simply supported untensioned plate (unpressurized cabin) and tensioned plate (pressurized cabin), are given respectively by:

$$\omega^p_{m_x m_y} = \sqrt{\frac{D_p}{\rho_p h_p}} \left[\left(\frac{m_x \pi}{a}\right)^2 + \left(\frac{m_y \pi}{b}\right)^2\right], \quad (8a)$$

$$\omega^p_{m_x m_y} = \sqrt{\frac{1}{\rho_p h_p}\left[D_p(f_x{}^2 + g_y{}^2)^2 + T_x f_x{}^2 + T_y g_y{}^2\right]}, \quad (8b)$$

in which ρ_p is the density of the panel, h_p is its thickness, $D_p = \frac{E_p h_p^3}{12(1-\nu_p^2)}$ is the panel stiffness constant, T_x and T_y are the in-plane tensions in x- and y-directions, respectively, and $f_x = \frac{m_x \pi}{a}$ and $g_y = \frac{m_y \pi}{b}$. The plate governing equations for a given applied external pressure, for the unpressurized and pressurized cabins, are respectively:

$$D_p \nabla^4 w + \rho_p h_p \ddot{w} + \zeta_p \dot{w} = p_{ext}(x,y,t), \quad (9a)$$

$$D_p \nabla^4 w + \rho_p h_p \ddot{w} + \zeta_p \dot{w} - (T_x f_x{}^2 + T_y g_y{}^2) w = p_{ext}(x,y,t), \quad (9b)$$

where ζ_p was added to account for the damping of the plate, and w is given by Eq.(5).

2.3 Acoustic Cabin Pressure Model

Following the same approach as for the plate's displacement models, the pressure inside the enclosure is defined in terms of the acoustic modes, as follows:

$$p(x,y,z,t) = \sum_{n_x=1}^{N_x} \sum_{n_y=1}^{N_y} \sum_{n_z=1}^{N_z} \psi_{n_x}(x)\, \phi_{n_y}(y)\, \Gamma_{n_z}(z)\, r_{n_x n_y n_z}(t), \quad (10)$$

where $\psi_{n_x}(x)$, $\phi_{n_y}(y)$ and $\Gamma_{n_z}(z)$ are spatial functions, $r_{n_x n_y n_z}(t)$ are functions of t, and $N = (N_x+1)\times(N_y+1)\times(N_z+1)$ is the number of acoustics modes considered. As shown in Fig. 3a, the direction of the interior pressure, p, was chosen to be the positive z-direction. The individual spatial functions are assumed to be orthogonal between each other, and given by the rigid body enclosure modes, as follows:

$$\psi_{n_x}(x) = \frac{A_{n_x}}{\sqrt{L_x}} \cos\left(\frac{n_x \pi x}{L_x}\right), \quad (11a)$$

$$\phi_{n_y}(y) = \frac{A_{n_y}}{\sqrt{L_y}} \cos\left(\frac{n_y \pi y}{L_y}\right), \quad (11b)$$

$$\Gamma_{n_z}(z) = \frac{A_{n_z}}{\sqrt{L_z}} \cos\left(\frac{n_z \pi z}{L_z}\right), \quad (11c)$$

where L_x, L_y and L_z are the dimensions of the enclosure in the x-, y- and z-directions, respectively, and the constants A_n were chosen to satisfy normalization. For a rectangular cavity, the natural frequencies are determined as follows:

$$\omega^{ac}_{n_x n_y n_z} = c_0 \sqrt{\left(\frac{n_x \pi}{L_x}\right)^2 + \left(\frac{n_y \pi}{L_y}\right)^2 + \left(\frac{n_z \pi}{L_z}\right)^2}, \quad (12)$$

where c_0 is the speed of sound inside the acoustic enclosure. The governing equation is the wave equation, defined by

$$\nabla^2 p - \frac{1}{c_0^2} \ddot{p} - \zeta_{ac} \dot{p} = 0, \quad (13)$$

in which ζ_{ac} was added to account for the acoustic damping in the enclosure.

2.4 Coupled System Model

To obtain the governing equations of the coupled structural-acoustic system, the equations of the individual uncoupled subsystems should be combined (please refer to [8] for the coupling details). The equations of the coupled plate-enclosure system can be written together in the matrix form, as follows:

$$\begin{bmatrix}\mathbf{M}_{pp} & \mathbf{0}\\ \mathbf{M}_{cp} & \mathbf{M}_{cc}\end{bmatrix}\begin{Bmatrix}\ddot{\mathbf{q}}(t)\\ \ddot{\mathbf{r}}(t)\end{Bmatrix}+\begin{bmatrix}\mathbf{D}_{pp} & \mathbf{0}\\ \mathbf{0} & \mathbf{D}_{cc}\end{bmatrix}\begin{Bmatrix}\dot{\mathbf{q}}(t)\\ \dot{\mathbf{r}}(t)\end{Bmatrix}+\begin{bmatrix}\mathbf{K}_{pp} & \mathbf{K}_{pc}\\ \mathbf{0} & \mathbf{K}_{cc}\end{bmatrix}\begin{Bmatrix}\mathbf{q}(t)\\ \mathbf{r}(t)\end{Bmatrix} = \begin{Bmatrix}\mathbf{p}_{tbl}(t)\\ \mathbf{0}\end{Bmatrix}, \quad (14)$$

with:

$$\mathbf{M}_{pp}= \text{diag}\left[\rho_p\, h_p\right] \quad \text{and} \quad \mathbf{M}_{cc}= \text{diag}\left[\frac{1}{c_0^2}\right], \quad (15a)$$

$$\mathbf{M}_{cp}= \rho_0\left[\frac{(-1)^{n_z}A_{n_z}}{\sqrt{L_z}}\int_{x_{p_i}}^{x_{p_f}}\alpha_{m_x}(x)\psi_{n_x}(x)dx\int_{y_{p_i}}^{y_{p_f}}\beta_{m_y}(y)\phi_{n_y}(y)dy\right], \quad (15b)$$

$$\mathbf{D}_{pp}= \text{diag}\left[2\rho_p h_p\omega_m\xi_p\right] \quad \text{and} \quad \mathbf{D}_{cc}= \text{diag}\left[2\frac{1}{c_0^2}\omega_n\xi_{ac}\right], \quad (15c)$$

$$\mathbf{K}_{pp}= \text{diag}\left[\omega_m^2\,\rho_p\, h_p\right] \quad \text{and} \quad \mathbf{K}_{cc}= \text{diag}\left[\omega_n^2\,\frac{1}{c_0^2}\right], \quad (15d)$$

$$\mathbf{K}_{pc}= -\left[\frac{(-1)^{n_z}A_{n_z}}{\sqrt{L_z}}\int_{x_{p_i}}^{x_{p_f}}\alpha_{m_x}(x)\psi_{n_x}(x)dx\int_{y_{p_i}}^{y_{p_f}}\beta_{m_y}(y)\phi_{n_y}(y)dy\right], \quad (15e)$$

$$\mathbf{p}_{tbl}(t) = -\left[\int_{y_{p_i}}^{y_{p_f}}\int_{x_{p_i}}^{x_{p_f}}\alpha_{m_x}(x)\,\beta_{m_y}(y)\,p_{tbl}(x,y,t)\,dx\,dy\right]. \quad (15f)$$

In the previous equations, **M** represents mass matrices, **D** damping matrices, **K** stiffness matrices, subscripts *p* and *c* correspond respectively to *plate* and *cavity*. All matrices and vectors expressions were obtained analytically as shown in [8]. Additionally, $\zeta_p= 2\omega_m\xi_p$ is the structural modal damping and $\zeta_{ac}=2\omega_n\xi_{ac}$ is the acoustic modal damping. For notation simplicity, $\omega^p_{m_xm_y}$, $\omega^{ac}_{n_xn_yn_z}$, $q_{m_xm_y}(t)$, and $r_{n_xn_yn_z}(t)$ were substituted, respectively, by ω_m , ω_n, $q_m(t)$ and $r_n(t)$. Note that ω_m, in Eqs.(15), is given by Eq.(8a) for the unpressurized cabin and by Eq.(8b) for the pressurized cabin. The cross terms, i.e., matrices $\mathbf{M_{cp}}$ and $\mathbf{K_{pc}}$, are responsible for the coupling between each panel displacement and the enclosure pressure. Note that Eq.(14) accounts for the coupling of only one plate with the enclosure, i.e., the contribution of each panel for the interior sound pressure level is individually analyzed.

3. SOLUTION IN THE SPECTRAL DOMAIN

Since the TBL wall pressure field model is expressed in the frequency domain, one needs to transform the equation of the coupled system, Eq.(14), from the time domain to the frequency domain. As introduced in [8], this can be performed by assuming $q_m = Q_m\, e^{i\omega t}$ and $r_n = R_n\, e^{i\omega t}$. The spectral density of the system response is then given by:

$$\mathbf{S_{YY}}(\omega) = \mathbf{H}^*(\omega)\,\mathbf{S_{XX}}(\omega)\,\mathbf{H}^T(\omega)\,, \quad (16)$$

in which superscripts * and T denote, respectively, Hermitian conjugate and matrix transpose, $\mathbf{S_{XX}}(\omega)$ is the spectral density matrix of the excitation, and $\mathbf{S_{YY}}(\omega)$ is the spectral density of the system response. For mathematical convenience, matrix $\mathbf{S_{YY}}(\omega)$ can be divided in two matrices: (1) the PSD matrix of the coupled plate displacement, $\mathbf{S_{WW}}(\omega)$, and (2) the PSD matrix of the coupled acoustic enclosure pressure, $\mathbf{S_{PP}}(\omega)$. Similarly, matrix $\mathbf{S_{XX}}(\omega)$ can be divided in: (1) the PSD matrix of the turbulent boundary layer excitation, $\mathbf{S_{tbl}}(\omega)$, and (2) a null matrix. Considering this, Eq.(16) can be written in the following separate form:

$$\mathbf{S_{WW}}(\omega) = \mathbf{H_W}^*(\omega)\,\mathbf{S_{tbl}}(\omega)\,\mathbf{H_W}^T(\omega)\,, \quad (17a)$$

$$\mathbf{S_{PP}}(\omega) = \mathbf{H_P}^*(\omega)\,\mathbf{S_{tbl}}(\omega)\,\mathbf{H_P}^T(\omega)\,, \quad (17b)$$

where matrices $\mathbf{H_W}(\omega)$ and $\mathbf{H_P}(\omega)$ are defined by:

$$\mathbf{H_W}(\omega) = (\mathbf{A} - \mathbf{B}\,\mathbf{D}^{-1}\,\mathbf{C})^{-1}, \quad (18a)$$

$$\mathbf{H_P}(\omega) = -\,\mathbf{D}^{-1}\,\mathbf{C}\,\mathbf{H_W}(\omega)\,, \quad (18b)$$

and

$$\mathbf{A} = -\,\omega^2\,\mathbf{M}_{pp} + i\,\omega\,\mathbf{D}_{pp} + \mathbf{K}_{pp}\,, \quad (19a)$$

$$\mathbf{B} = \mathbf{K}_{pc}\,, \quad (19b)$$

$$\mathbf{C} = -\,\omega^2\,\mathbf{M}_{cp}\,, \quad (19c)$$

$$\mathbf{D} = -\,\omega^2\,\mathbf{M}_{cc} + i\,\omega\,\mathbf{D}_{cc} + \mathbf{K}_{cc}\,. \quad (19d)$$

The generalized PSD matrix of the TBL excitation, $\mathbf{S_{tbl}}(\omega)$, the PSD function of the plate´s displacement, and the PSD function of the enclosure interior pressure are defined, respectively, as follows:

$$\mathbf{S_{tbl}}(\omega) = \left[\int_{S_p}\int_{S_p}\alpha_{m_x}(x)\alpha_{m_{x'}}(x')\beta_{m_y}(y)\beta_{m_{y'}}(y')S(x,\xi_x,\xi_y,\omega)dSdS'\right], \quad (20)$$

$$S_{ww}(x_1, y_1, x_2, y_2, \omega) = \sum_{m_{x_1},\,m_{x_2}=1}^{M_x^2}\sum_{m_{y_1},\,m_{y_2}=1}^{M_y^2}\alpha_{m_{x_1}}(x_1)\alpha_{m_{x_2}}(x_2)\beta_{m_{y_1}}(y_1)\beta_{m_{y_2}}(y_2)\mathbf{S_{WW}}(\omega)_{m_1,m_2} \quad (21)$$

$$S_{pp}(x_1, y_1, z_1, x_2, y_2, z_2, \omega) = \sum_{n_{x_1}, n_{x_2}=1}^{N_x^2} \sum_{n_{y_1}, n_{y_2}=1}^{N_y^2} \sum_{n_{z_1}, n_{z_2}=1}^{N_z^2}$$

$$\psi_{n_{x_1}}(x_1)\psi_{n_{x_2}}(x_2)\phi_{n_{y_1}}(y_1)\phi_{n_{y_2}}(y_2)\Gamma_{n_{z_1}}(z_1)\Gamma_{n_{z_2}}(z_2)\, \mathbf{S_{PP}}(\omega)_{n_1,n_2} \quad (22)$$

in which $S_p = a \times b$ is the plate surface area. Eqs.(21) and (22) can be used to predict the displacement PSD at a chosen point in the plate, and the pressure PSD at any given location of the acoustic enclosure, respectively. Finally, the space-averaged PSD functions can be found by integrating the individual power spectral densities over the plate area and the cavity volume, respectively, as:

$$S_{ww}(\omega) = \int_{S_p}\int_{S_p} S_{ww}(x_1, y_1, x_2, y_2, \omega)\, dS_1 dS_2, \quad (23)$$

$$S_{pp}(\omega) = \int_{V_c}\int_{V_c} S_{pp}(x_1,y_1,z_1,x_2,y_2,z_2,\omega)\, dV_1 dV_2, \quad (24)$$

in which $V_c = L_x \times L_y \times L_z$ is the enclosure volume. The analytical expressions derived for $\mathbf{S_{tbl}}(\omega)$, $S_{ww}(\omega)$ and $S_{pp}(\omega)$ are shown [8].

4. PHYSICAL SYSTEM

The geometry of the complete system is shown in Fig. 3. The turbulent flow is developed across the plates, at $z = L_z$, in the positive x-direction. The dimensions of the system are given in Table 1 and the physical parameters, including the external fluid, the plate, and the acoustic enclosure are listed in Table 2. The properties of the plates are for aluminum, and the parameters of the external fluid correspond to a cruise flight altitude of 25000 ft (i.e., 7628 m). Damping ratios for the structure and for the acoustic field of 1% were chosen to be representative of those in an aircraft [2, 26]. A large acoustic enclosure compared with the plates was chosen in order to simulate a more realistic approach of an aircraft cabin section. The flexible wall of the enclosure is composed by 50 simply supported identical plates (same dimensions and properties), with 5 panel rows along x-direction and 10 panel rows along y-direction. The panels have dimensions and properties similar to that of a typical commercial aircraft fuselage panel, representing the distance between adjacent frames and stringers. The fuselage cabin section is considered to start at x = 9.14 m from the nose of the aircraft, in order to consider a more realistic case of an aircraft fuselage section - as shown in [2], this is the start point of the forward section of a Boeing 727-200 airplane fuselage.

Table 1. Dimensions of the system.

Description	Symbol	Value, m
Plate length	a	0.5
Plate width	b	0.22
Plate thickness	h_p	0.00102
Enclosure length	L_x	2.5
Enclosure width	L_y	2.2
Enclosure height	L_z	2.1

Table 2. Properties of the physical system.

External Fluid:		
Description	Symbol	Value
Air density	ρ	0.54 Kg m^{-3}
Air kinematic viscosity	ν	2.85×10^{-5} m^2 s^{-1}
Speed of sound	c	309.6 m s^{-1}
Free stream velocity	U_∞	229.104 m s^{-1}
Convective velocity	U_c	0.7 U_∞
Empirical parameter	α_x	0.1
Empirical parameter	α_y	0.77
Panels:		
Description	Symbol	Value
Density	ρ_p	2800 Kg m^{-3}
Elasticity Modulus	E_p	7.24×10^{10} Pa^2
Poisson's ratio	ν	0.33
Damping ratio	ξ_p	0.01
Longitudinal tension	T_x	29300 N m^{-1}
Lateral tension	T_y	62100 N m^{-1}
Number of modes	M	
- unpressurized cabin: 44 (M_x=11, M_y=4)		
- pressurized cabin: 27 (M_x=9, M_y=3)		
Acoustic Enclosure:		
Description	Symbol	Value
Air density	ρ_0	1.2 Kg m^{-3}
Speed of sound	c_0	340 m s^{-1}
Damping ratio	ξ_{ac}	0.01
Number of modes	N	2912 (N_x=16, N_y=14, N_z=13)

5. RESULTS

5.1 Convergence

A convergence study was performed to determine the number of structural and acoustic modes required for the calculation of the spectral quantities. It was found that, for the frequency range of interest, [0; 1000] Hz, some non-resonant modes need to be considered. A simple criterion to determine the number of structural modes required for convergence of the modal series up to a frequency f_{max} is the following: convergence is reached when the distance between two nodes of the structural mode shape is less than or equal to the half-wavelength of the bending wave on the plate, $\lambda_b/2$, at the analysis frequency, i.e.,

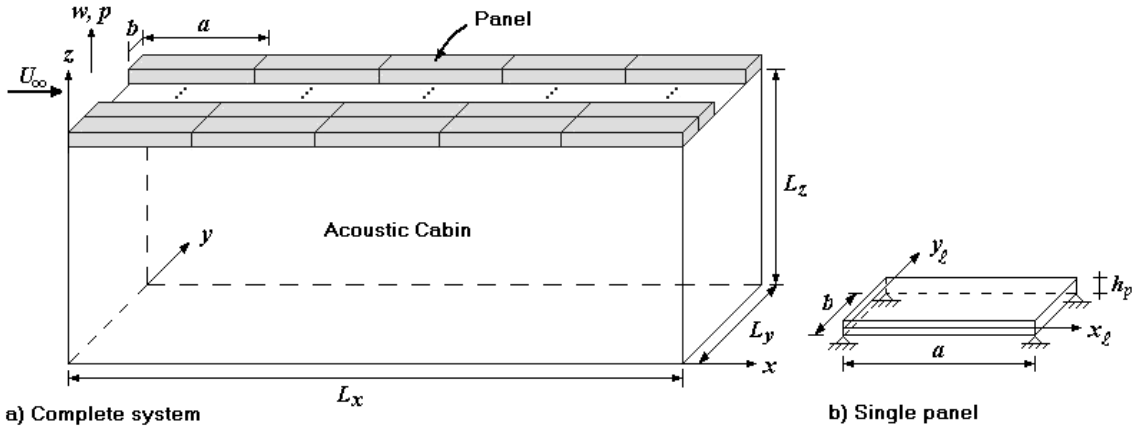

Figure 3. Geometry of the physical system.

$$\frac{a}{M_x} \leq \frac{\lambda_b(\omega)}{2}, \tag{25}$$

$$\lambda_b(\omega) = 2\,\pi\,\omega^{-\frac{1}{2}} \left(\frac{D_p}{\rho_p h_p}\right). \tag{26}$$

Thus, for f_{max}=1000 Hz, from Eq.(25) one obtains $M_x \geq 11$. Another convergence criterion is presented in [16] - for a given upper frequency f_{max}, the number of modes (M_x,M_y) required for the calculation of the spectral quantities, for a tensioned panel, can be calculated by

$$\left\{\left[\left(\frac{M_x}{a}\right)^2 + \left(\frac{M_y}{b}\right)^2\right]^2 + \frac{T_x}{D_p}\left(\frac{M_x}{a}\right)^2 + \frac{T_y}{D_p}\left(\frac{M_y}{b}\right)^2\right\}^{1/4} \geq \left(\frac{\rho_p h_p}{D_p}\right)^{1/4} \sqrt{\frac{2\,f_{max}}{\pi}}. \tag{27}$$

For the untensioned plate case, the convergence criterion is obtained from Eq.(27) with in-plane tensions equal to zero. For the aircraft panel considered in the present study (for f_{max}=1000 Hz), the number of structural modes required to accurately calculate the PSD of the panel response is M_x=11 and M_y=4 for the untensioned plate, and M_x=9 and M_y=3 for the tensioned plate. Table 3 displays the first 20 natural frequencies of the untensioned panel, and the corresponding frequencies for the in-tension panel. The number of enclosure acoustic modes required for the accurate calculation of the spectral quantities was also determined. Similarly to the plate, convergence is reached when the distance between two nodes of the acoustic mode shape is less or equal than half-wavelength of the acoustic wave in the interior of the enclosure, i.e.,

$$\frac{L_x}{N_x} \leq \frac{c_0}{2\,f_{max}}. \tag{28}$$

Thus, from Eq.(28) one obtains Nx ≥ 15. For the aircraft cabin considered and f_{max}=1000 Hz, the number of acoustic modes required to accurately calculate the PSD of the acoustic response is N_x=16, N_y=14 and N_y=13. The 2912 acoustic modes considered are plotted in Fig. 4, as well as the plate's mode lines for the untensioned and in-tension cases. As can be seen, several non-resonant modes need to be considered.

Table 3. Panels first 20 natural frequencies [Hz].

(m_x,m_y)	Untensioned panel	In-tension panel
(1,1)	61.44	355.45
(2,1)	91.34	402.11
(3,1)	141.17	473.89
(4,1)	210.93	566.52
(1,2)	215.87	711.41
(2,2)	245.77	742.08
(3,2)	295.60	793.07
(5,1)	300.62	677.62
(4,2)	365.36	864.22
(6,1)	410.25	806.19
(5,2)	455.05	955.41
(1,3)	473.26	1115.82
(2,3)	503.15	1142.37
(7,1)	539.81	952.05
(3,3)	552.98	1186.99
(6,2)	564.68	1066.51
(4,3)	622.75	1250.11
(8,1)	689.29	1115.36
(7,2)	694.24	1197.46
(5,3)	712.44	1332.24

5.2 Hydrodynamic Coincidence

To study the effect of hydrodynamic coincidence, it is important to first identify the degree of matching between the boundary layer and the plate modes. Figure 5 shows the plate natural frequencies plotted against longitudinal mode number, m_x, for modes with m_y=1,...,4. Also plotted in this figure are the hydrodynamic coincidence lines (representing $f = m_x U_c/2a$) for three cases: $U_c = 0.7\ U_\infty$ (reference case), $U_c = 0.75\ U_\infty$ and $U_c = 0.8\ U_\infty$.

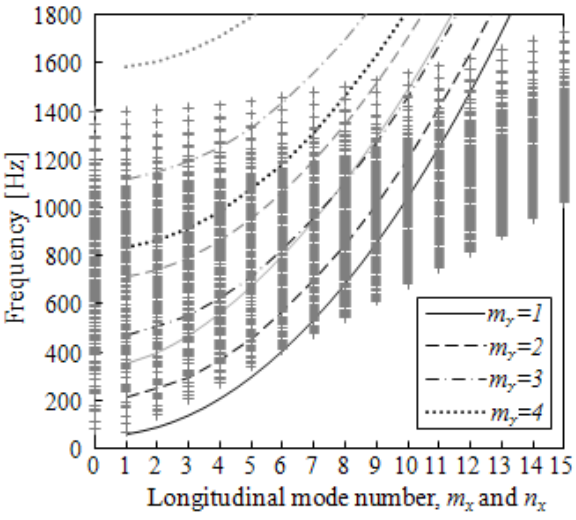

Figure 4. Matching between acoustic modes (+) and plates modes: untensioned (black lines), tensioned (grey lines).

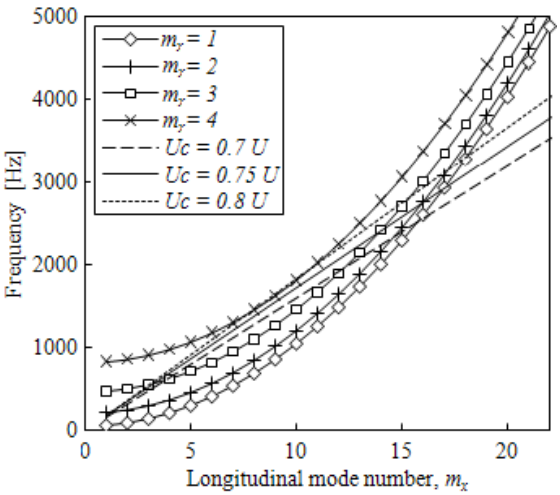

a) Untensioned Panel

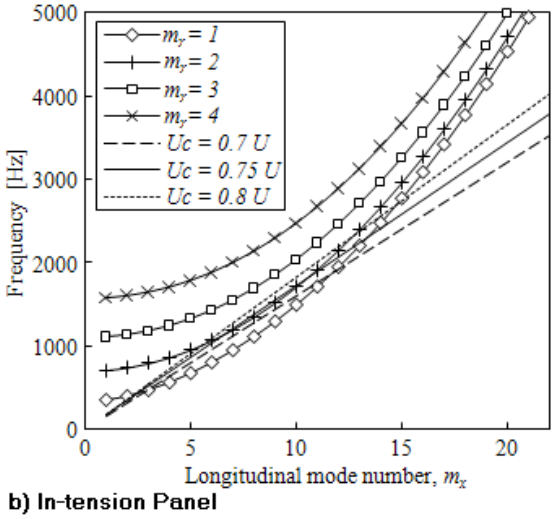

b) In-tension Panel

Figure 5. Matching between hydrodynamic coincidence lines and plate natural frequencies lines.

From Fig. 5 one can confirm that hydrodynamic coincidence lines 'match' the plate modes over a large part of the frequency range, mainly for the untensioned plate case. As explained in [40], this confirms the importance of inefficient, but resonant and highly excited modes in the aircraft noise problem. In the reference case, for the untensioned case, the plate modes (4,3), (12,3), (15,2) and (16,1) provide the best matching with the turbulent convecting scales ($m_x U_c/a\omega \approx 1$), and are thus highly excited modes. Of these 4 modes only (4,3) has a resonant frequency in the range of study, [0; 1000] Hz. For the tensioned case, the plate mode (3,1) provides the best matching with the hydrodynamic coincidence line. In the reference case, the hydrodynamic coincidence frequency, $f_c = \frac{U_c^2}{2\pi}\sqrt{\frac{\rho_p h_p}{D_p}}$, is 2580.74 Hz. Thus, in the frequency range under study all resonant and nonresonant modes considered are inefficient radiators.

5.3 Frequency Resolution

All spectral quantities were obtained for the frequency range [0; 1000] Hz. The frequency resolution for the PSD calculations was obtained through an adaptive algorithm to meet the damping coefficient constraint, both for the untensioned and tensioned plates. This algorithm was developed to guarantee enough frequency resolution to resolve all resonance peaks within the frequency range covered (maximum frequency was determined based on the convergence study), for both structural and acoustic modes.

5.4 Predicted Structural Vibration Levels

The space-averaged plates displacement power spectral density (ADPSD), expressed by Eq.(23), and the plate displacement power spectral density (DPSD) in several points on the plates, given by Eq.(21), were obtained.

Figure 6 shows the ADPSD for the panel (1,1), i.e., panel located at first row of panels and first row of columns. Panels in other locations have similar ADPSD, with panels located at bigger x-coordinates having a slightly higher ADPSD at all frequencies. This can be explained since an increase in x-station results in a higher value for the reference PSD of the TBL excitation. The first 3 ADPSD peaks correspond to the bending modes (1,1), (3,1) and (5,1), for both untensioned and tensioned plates. Additionally, considering pressurization effects results in a decreased radiated ADPSD for lower frequencies compared with the unpressurized cabin. For the untensioned panel, a large response due to resonant amplification of (4,3) plate mode does not occur. This can be explained because, in the present case of study, hydrodynamic coincidence is not well tuned at frequencies where the hydrodynamic matching line broadly coincides with the resonant modes. For the tensioned plate, the mode (3,1), which provides the best matching with the hydrodynamic coincidence line,

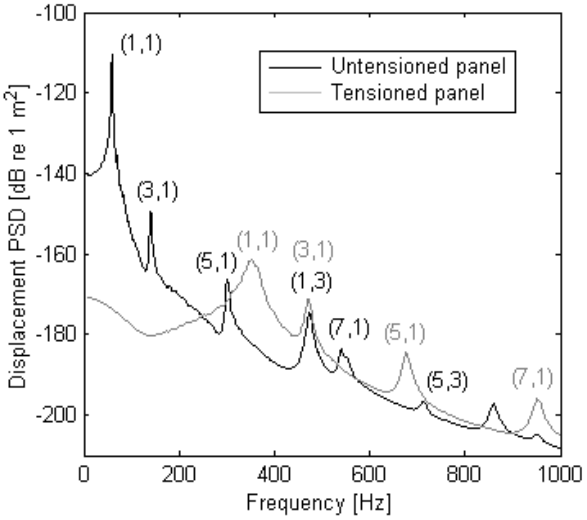

Figure 6. Space-averaged displacement PSD for plate (1,1).

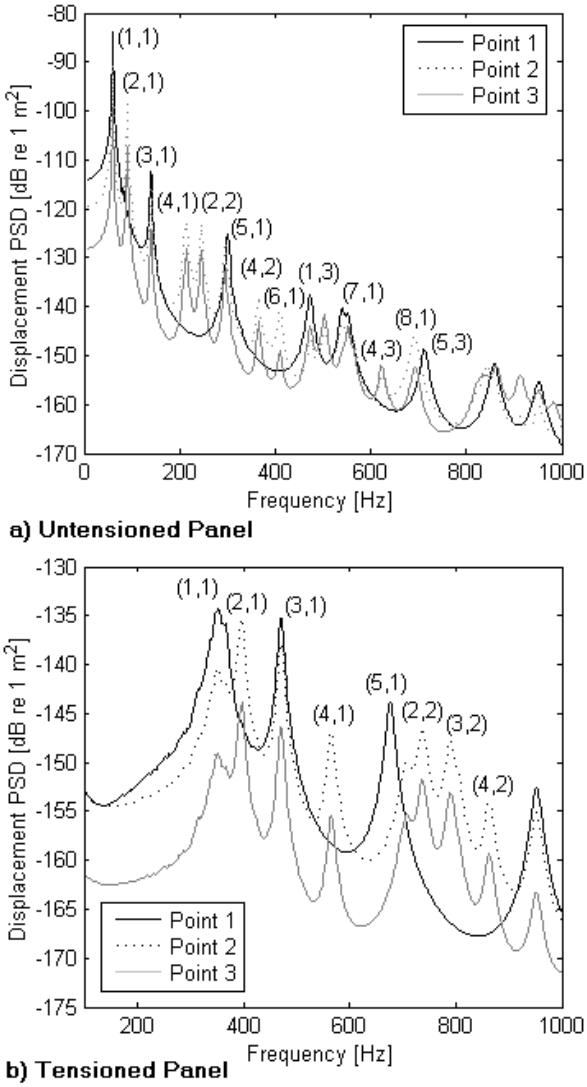

Figure 7. Displacement PSD at 3 points located at the surface of panel (1,1).

corresponds to the second ADPSD peak. This may be explained because (3,1) is the only plate mode which provides 'matching' with the hydrodynamic coincidence line, while for the untensioned plate a larger number of modes provide this matching.

The results for the DPSD are shown in Fig. 7, for three different locations in the surface of the plate (1,1), specifically at: (x_1, y_1)=(0.25,0.11)m, (x_2, y_2)=(0.1,0.06)m, and (x_3, y_3)=(0.4,0.06)m. DPSD plots for the other plates show similar results and, as for the ADPSD, it shows a slight overall increase with the increase of the x-coordinate. As shown in this figure, point 1, located at the center of the panel, follow the same line as the ADPSD, with the peaks located at the same frequencies. However, the same does not occur for the other points considered, in which additional peaks can be observed for the DPSD curves. This can be explained since the point at the center of the plate is not affected when the longitudinal mode number, m_x, or the lateral mode number, my, is even. Thus, when evaluating the PSD of the plate response, it is important to know the position of interest in the plate, since its value is dependent on the position of measurement. Comparing points 2 and 3 (both located at y = 0.06 m), one can conclude that points at higher x have generally bigger DPSD.

5.5 Predicted Cabin Sound Pressure Levels

The acoustic enclosure space-averaged pressure power spectral density (APPSD) and the acoustic pressure power spectral density (PPSD) at specific point in the enclosure, were obtained through Eqs.(24) and (22), respectively.

The acoustic enclosure APPSD, due to the individual contribution of the panels, located at two different positions in the flexible wall, is shown in Fig. 8. An important conclusion to draw from this figure is that some peaks correspond to plate natural frequencies and other to acoustic natural frequencies. This illustrates the importance of the structural-acoustic coupling for accurate prediction of the internal pressure in the interior of an enclosure, such as for example an aircraft cabin. The uncoupled study of the sound radiated by an individual plate, vibrating due to turbulent flow, does not give the total information when the main goal is to predict aircraft interior noise. Another conclusion is that plates located at different positions have dissimilar contributions to the enclosure interior pressure levels. For instance, plate (3,7) has a negligible contribution in the amplification of the acoustic mode (1,0,0) compared with plate (1,1). Since plates in row 3 are located in the centre of the enclosure in the x-direction, they do not add significant contribution to the frequency associated to this mode, which has a node at centre of the enclosure in this direction. For the same reason, plates in row 3 have a decreased contribution for the amplification of all other modes with longitudinal mode number, n_x, equal to 1, compared with the other plates. All other modes (i.e., with longitudinal

mode number equal to 0 or to 2) have similar mode amplification, since for modes with $n_x = 2$ the middle point correspond to an antinode, while for modes with $n_x = 0$ the pressure is constant along x-direction. For untensioned plates the interior SPL is bigger for lower frequencies, while for tensioned panels the maximum SPL is observed at higher frequencies. This occurs since the first plate mode increases from 61.44 Hz, in the unpressurized case, to 355.45 Hz in the pressurized case. However, for the pressurized case, frequencies below 355.45 Hz cannot be ignored, since several acoustic modes are amplified below this frequency.

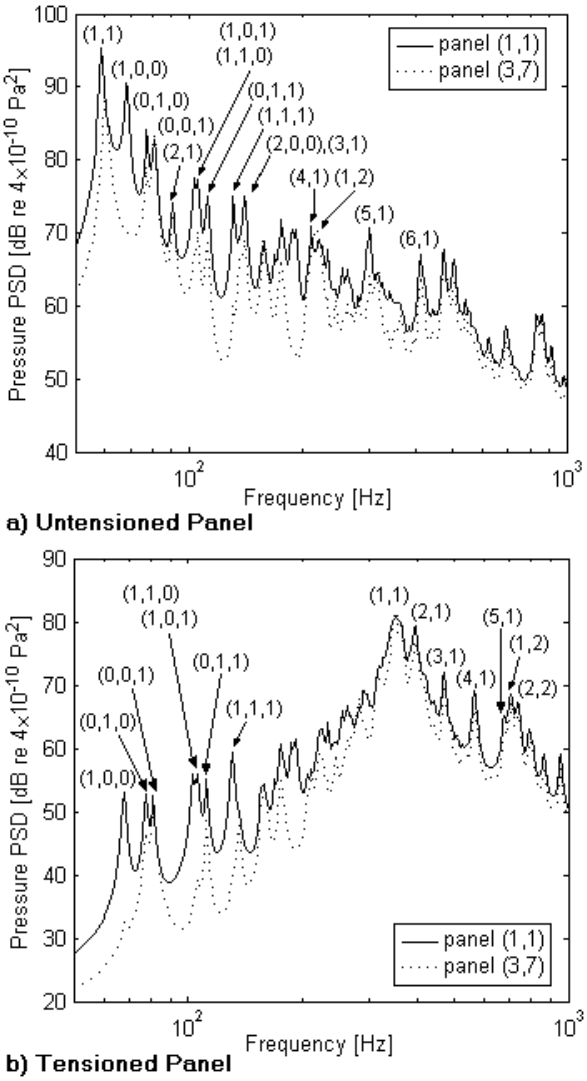

Figure 8. Space-averaged pressure PSD, for the contribution of panels (1,1) and (3,7).

Figure 9 shows the results for the interior pressure power spectral density (PPSD), at four chosen points inside the enclosure, due to the individual radiation of plates, located at four different positions - specifically, plates (1,1), (3,1), (3,5), and (5,1) are analyzed. The points inside the enclosure under study are the following (defined in the global coordinates system): $(x_1, y_1, z_1)=(x_{pi}+a/2, y_{pi}+b/2, 2)$ and $(x_2, y_2, z_2)=(x_{pi}+a/2, y_{pi}+b/2, 1)$, $(x_3, y_3, z_3)=(1,1,2)$, and $(x_4, y_4, z_4)=(1,1,1)$. Note that points 1 and 2 are different for each plate, with x_{pi} and y_{pi} corresponding to the initial x and y coordinates of each plate. It can be observed that point (x_1, y_1, z_1) has higher PPSD at almost all frequencies, compared with the other points. As expected, decreasing z-coordinate (i.e., moving away from the plates) results in lower PPSD values. It is interesting to verify that the structural-acoustic coupling has an important role in the prediction of the interior SPL. Analyzing the results for the four different plates, and the same observing point (x_1, y_1, z_1), one can verify that the PPSD plot has some variations from plate to plate. Since point (x_1, y_1, z_1) is always at the same relative position at each plate, that difference can only be due to the enclosure acoustic modes. If only the plate modes were considered, one would obtain the similar curves for all plates in point (x_1, y_1, z_1), and as well in point (x_2, y_2, z_2), which is not what is observed. The fact that each plate is in a different position with relation to the enclosure global coordinate system, changes the way it couples with the acoustic enclosure. This explains why plates (1,1) and (5,1) have similar curves for points (x_1, y_1, z_1) and (x_2, y_2, z_2). As concluded for the DPSD, when evaluating the PSD of the interior pressure is important to know which is the position of interest in the enclosure, since the SPL value is dependent on the position of measurement.

6. CONCLUSIONS

An analytical study to predict the turbulent boundary layer-induced noise in the interior of a rectangular enclosure with one flexible wall, consisting of several panels, is presented. Predictions of the space-averaged PSD and localized PSD were obtained for the displacement of the plates and interior acoustic pressure in the enclosure. The characteristics of the physical system were selected to represent an aircraft cabin, and the external flow considered is representative of typical cruise conditions of a commercial aircraft. The analytical model is based on modal analysis, and it considers the structural-acoustic coupling for frequencies up to 1000 Hz. A convergence study was performed to determine the number of structural and acoustic modes required for the calculation of the spectral quantities, indicating that a large number of non-resonant modes need to be considered in the analysis. Also, it was found that hydrodynamic coincidence lines 'match' the plate modes over a large part of the frequency range, confirming the importance of inefficient, but resonant and highly excited modes in the aircraft noise problem.

This study leads to conclude that, for the accurate prediction of aircraft interior noise, the position of the panel as well as the structural-acoustic coupling effects are important factors to consider. Thus, the traditional approach of assuming a single panel vibrating to free air or coupled with an acoustic enclosure needs to consider these two factors. Additionally,

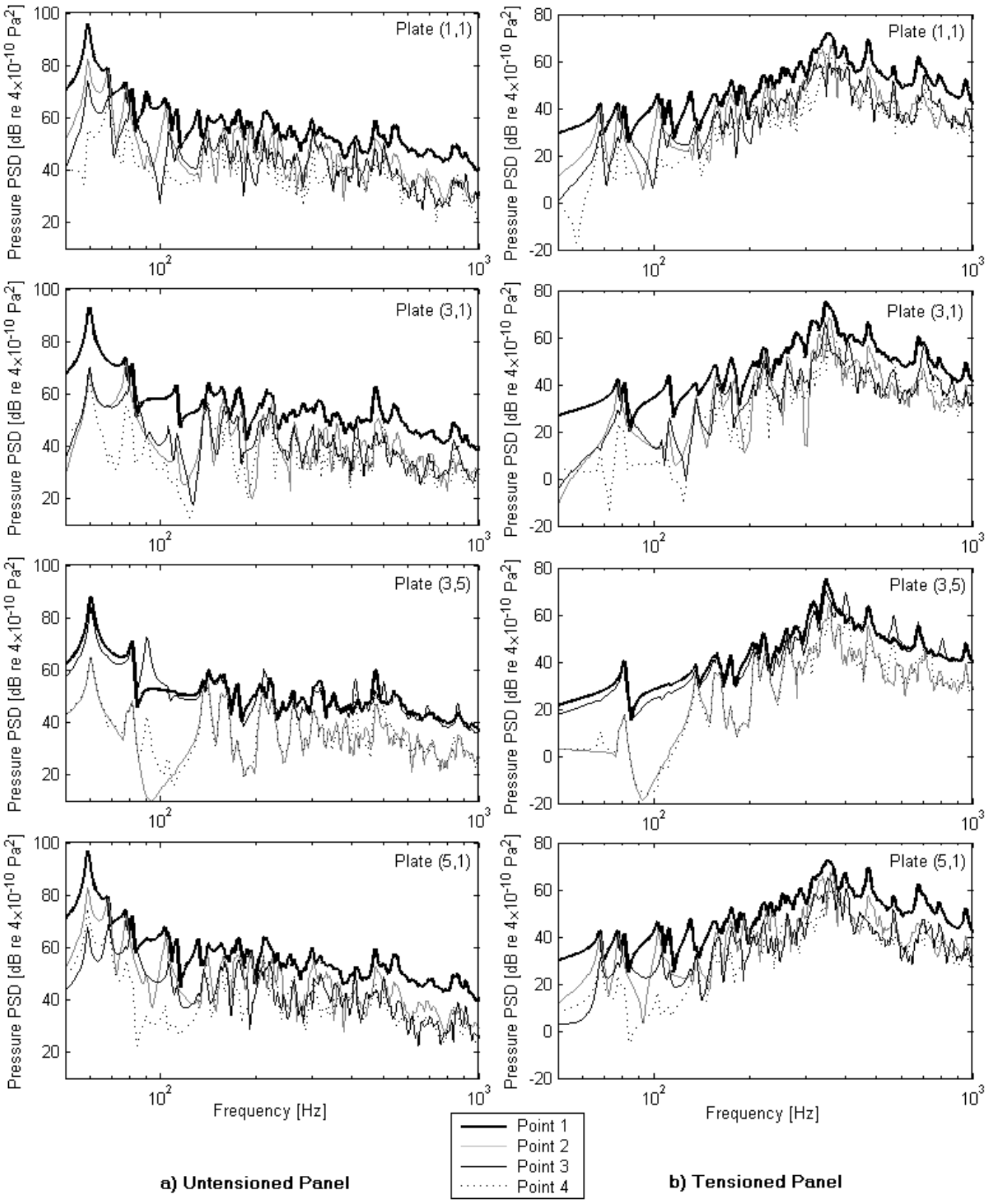

Figure 9. Pressure PSD at 4 points inside the enclosure, for the individual contribution of panels (1,1), (3,1), (3,5), and (5,1).

the space-averaged PSD values only give information about the mean value. If one desires to determine the localized PSD values (for the plate vibration or for the interior pressure level), then the space-averaged values may not sufficiently accurate, since predicted averaged and localized values are dissimilar. For instance, one might want to predict the interior SPL at the passenger's head height, while in flight.

The analytical model presents also a solid basis for further analyzes, such as multidisciplinary design optimization analysis, and design and implementation of noise reduction techniques, as for instance: the use of added masses in the structure as passive noise control methods; the use of structural actuators embedded in the plates as active structural acoustic control methods; or loudspeakers installed at the interior of the cabin as active control noise methods.

ACKNOWLEDGMENTS

The authors are grateful for the financial support of the Foundation for Science and Technology, through a post-graduate scholarship program.

REFERENCES

[1] D. E. Bishop, Cruise flight noise levels in a turbojet transport airplane. *Noise Control* (1961), 7, pp. 37-42.

[2] W. V. Bhat, Flight test measurement of measurement of exterior turbulent boundary layer pressure fluctuations on Boeing Model 737 airplane. *Journal of Sound and Vibration* (1971), 14 (4), pp. 439-457.

[3] W. V. Bhat and J. F. Wilby, Interior noise radiated by an airplane fuselage subjected to turbulent boundary layer excitation and evaluation of noise reduction treatments. *Journal of Sound and Vibration* (1971), 18 (4), pp. 449-464.

[4] G. P. Gibbs, R. H. Cabell and J. Juang, Controller Complexity for Active Control of Turbulent Boundary-Layer Noise from Panels. *AIAA Journal* (2004), 42(7), pp. 1314-1320.

[5] R. E. Hayden, B. S. Murray, and M. A. Theobald, A Study of Interior Noise Levels, Noise Sources and Transmission Paths in Light Aircraft, *NASA CR-172152* (1983).

[6] S. P. Engelstad, Computational modeling considerations for aircraft cockpit noise, *15th AIAA Aeroacoustic Conference*, Long Beach, CA, (1993), pp. 25–37.

[7] K. D. Frampton and R. L. Clark, Power flow in an aeroelastic plate backed by a reverberant cavity. *Journal of the Acoustical Society of America* (1997), 102(3), pp. 1620-1627.

[8] J. da Rocha, A. Suleman and F. Lau. Prediction of flow-induced noise in transport vehicles: development and validation of a coupled structural-acoustic analytical framework, *Canadian Acoustics* (2009), 37(4), pp. 13-29.

[9] D. A. Bies, A review of flight and wind tunnel measurements of boundary layer pressure fluctuations and induced structural response, *NASA CR-626* (1966).

[10] L. Maestrello, Measurement of noise radiated by turbulent boundary layer excited panels. *Journal of Sound and Vibration* (1965), 2(2), pp. 100-115.

[11] J. F. Wilby and F. L. Gloyna, Vibration measurements of an airplane fuselage structure I. Turbulent boundary layer excitation. *Journal of Sound and Vibration* (1972), 23(4), pp. 443-466.

[12] J. F. Wilby, Aircraft interior noise. *Journal of Sound and Vibration* (1996), 190 (3), pp. 545-564.

[13] W. A. Strawderman, Turbulent-flow-excited vibration of a simply supported, rectangular flat plate. *The Journal of the Acoustical Society of America* (1969), 45(1), pp. 177-192.

[14] H. G. Davies, Sound from turbulent boundary-layer-excited panels. *The Journal of the Acoustical Society of America* (1971), 49(3), pp. 879-889.

[15] R. L. Clark and K. Frampton, Aeroelastic structural acoustic coupling: implications on the control of turbulent boundary-layer noise transmission. *Journal of the Acoustical Society of America* (1997), 102(3), pp. 1639-1647.

[16] C. Maury, P. Gardonio and S.J. Elliot, A wavenumber approach to the modeling the response of a random excited panel, Part II: application to aircraft panels excited by a turbulent boundary layer. *Journal of Sound and Vibration* (2002), 252(1), pp. 115-139.

[17] J. Park, T. Siegmund and L. Mongeau, Analysis of the flow-induced vibration of viscoelastically supported rectangular plates. *Journal of Sound and Vibration* (2003), 261(2), pp. 225-245.

[18] C. K. Barton and E. F. Daniels, Noise transmission through flat rectangular panels into a closed cavity, *NASA TP-1321* (1978).

[19] R. Vaicaitis and M. Slazak, Noise transmission through stiffened panels. *Journal of Sound and Vibration* (1980), 70(3), pp. 413-426.

[20] G. Corcos, Resolution of pressure in turbulence. *Journal of the Acoustical Society of America* (1963), 35(2), pp. 192-199.

[21] G. Corcos, The structure of the turbulent pressure field in boundary layer flows. *Journal of Fluid Mechanics - Cambridge Journal Online* (1964), 18, pp. 353-378.

[22] B. M. Efimtsov, Characteristics of the field of turbulent wall pressure fluctuations at large Reynolds numbers. *Soviet Physics-Acoustics* (1982), 28 (4), pp. 289-292.

[23] D. M. Chase, The character of the turbulent wall pressure spectrum at subconvective wavenumbers and a suggested comprehensive model. *Journal of Sound and Vibration* (1987), 112, pp. 125-147.

[24] J. E. Ffowcs Williams, Boundary-layer pressures and the Corcos model: a development to incorporate low wavenumber constraints. *Journal of Fluid Mechanics* (1982), 125, pp. 9-25.

[25] A. V. Smol'yakov and V. M. Tkachenko, Model of a field of pseudonic turbulent wall pressures and experimental data. *Soviet Physics-Acoustics* (1991), 37 (6), pp. 627-631.

[26] C. Maury, P. Gardonio and S. J. Elliot, Active control of the flow-induced noise transmitted through a panel. *AIAA Journal* (2001), 39(10), pp. 1860-1867.

[27] F. Han, L. G. Mongeau and R. J. Bernhard, A model for the vibro-acoustic response of plates excited by complex flows. *Journal of Sound and Vibration* (2001), 246(5), pp. 901-926.

[28] C. Maury, P. Gardonio and S. J. Elliot, Model for the active control of flow-induced noise transmitted through double partitions. *AIAA Journal* (2002), 40(6), pp. 1113-1121.

[29] S. J. Elliot, C. Maury and P. Gardonio, The synthesis of spatially correlated random pressure fields. *Journal of the Acoustical Society of America* (2005), 117(3), pp. 1186-1201.

[30] J. Rohlfing and P. Gardonio, Active Control of Sound Transmission through Panels with Flexible Boundaries under Deterministic and Stochastic Excitation, *Institute of Sound and Vibration Research (ISVR) Technical Memorandum 977* (2007).

[31] W. R. Graham, A comparison of models for the wavenumber frequency spectrum of turbulent boundary layer pressures. *Journal of Sound and Vibration* (1997), 206(4), pp. 541-565.

[32] R. Rackl and A. Weston, Modeling of turbulent boundary layer surface pressure fluctuation auto and cross spectra - verification and adjustments based on TU-144LL data, *NASA CR-213938* (2005).

[33] J. F. Wilby and F. L. Gloyna, Vibration measurements of an airplane fuselage structure II. Jet noise excitation. *Journal of Sound and Vibration* (1972), 23 (4), pp. 467-486.

[34] A. C. Jackson et al, Transport composite fuselage technology - impact dynamics and acoustic transmission, *NASA CR-4035* (1986).

[35] D. Palumbo, R. Cabell, J. Cline, and B. Sullivan, Active structural interior noise on acoustic noise of Raytheon 1900D, *NASA TM-209846* (2000).

[36] S. A. Rizzi, R. G. Rackl, J. Cline and E. V. Andrianov, Flight test measurements from the Tu-144LL structure/cabin noise experiment, *NASA TM-209858* (2000).

[37] T. H. Beier, W. V. Bhat, S. A. Rizzi, R. J. Silcox and M. A. Simpson, High speed research program structural acoustics multi-year summary report, *NASA TM-213536* (2005).

[38] C. Maury, P. Gardonio and S. J. Elliot, A wavenumber approach to modeling the response of a randomly excited panel, part I: general theory. *Journal of Sound and Vibration* (2002), 252(1), pp. 83-113.

[39] R. Wahidi, W. Chakroun and S. Al-Fahed, The behavior of the skin friction coefficient of a turbulent boundary layer flow over a flat plate with differently configured transverse square grooves, *Experimental Thermal and Fluid Science* (2005), 30(2), pp. 141–152.

[40] W. R. Graham, Boundary layer induced noise in aircraft, Part I: the flat plate model, *Journal of Sound and Vibration* (1996), 192(1), pp. 101–120.

Appendix C

Prediction of Turbulent Boundary Layer Induced Noise in the Cabin of a BWB Aircraft

Prediction of turbulent boundary layer induced noise in the cabin of a BWB aircraft

Joana da Rocha*, Afzal Suleman* and Fernando Lau†

**Department of Mechanical Engineering, University of Victoria, Victoria, British Columbia, V8W 3P6 Canada, jdarocha@uvic.ca, suleman@uvic.ca*

†Departamento de Engenharia Mecânica (Aeroespacial), Instituto Superior Técnico, 1049-001 Lisboa, Portugal, lau@ist.utl.pt

ABSTRACT

This paper discusses the development of analytical models for the prediction of aircraft cabin noise induced by the external turbulent boundary layer (TBL). While, in previous works, the contribution of an individual panel to the cabin interior noise was considered, here, the simultaneous contribution of multiple flow-excited panels is analyzed. Analytical predictions are presented for the interior sound pressure level (SPL) at different locations inside the cabin of a Blended Wing Body (BWB) aircraft, for the frequency range 0-1000 Hz. The results show that the number of vibrating panels significantly affects the interior noise levels. It is shown that the average SPL, over the cabin volume, increases with the number of vibrating panels. Additionally, the model is able to predict local SPL values, at specific locations in the cabin, which are also affected with by number of vibrating panels, and are different from the average values.

1. INTRODUCTION

The structural response to turbulent flow excitation and the radiation of sound by vibrating structures have been a topic of investigation by many authors. These problems are of considerable interest, especially in aircraft, where the structural parts are subjected to fatigue, and the structural vibration being a significant cause of interior cabin noise levels. Even though these topics have been investigated for many years, there is still space for new developments in understanding the mechanisms of sound transmission and radiation involved in these problems. In particular, the TBL has been identified as the major source of interior noise in jet powered aircraft, while in cruise flight [1, 2]. Understanding the turbulent boundary layer phenomenon, the induced wall pressure fluctuations, consequent vibration and radiated noise is an ongoing subject of investigation.

Several theoretical, numerical and experimental studies were performed to explore the vibration and radiation of sound from isolated panels (i.e., not coupled with an acoustic cabin), excited by the turbulent flows [3-9]. These investigations provide knowledge about the shape of the power spectrum and space-time correlation of the TBL pressure fluctuations on aircraft panels, as well as displacement and acceleration spectra of the vibrating panels.

Additionally, a number of studies were conducted to investigate structural-acoustic coupled systems excited by random noise or by turbulent flow, consisted by a single panel coupled with a small acoustic enclosure [10-13]. These studies provide a good basis, and were utilized as validation examples in [14], to confirm the analytical predictions obtained for the structural vibration levels and interior noise levels. Several experimental studies were performed by NASA taking into consideration the aircraft interior noise induced by the TBL [15-17]. These studies make experimental data available for the interior SPL and fuselage skin vibrations spectrums, at various locations in the cabin and cockpit of commercial aircraft, for aluminum and composite fuselages. These measurements are a good validation database for future and more advanced models, capable of predicting interior noise levels for such complex systems.

The TBL has been shown to be a major source of interior noise in jet powered aircraft. Specifically, in [15], interior SPL measurements show that increasing the aircraft speed has a dramatic effect on the TBL-induced noise, as the interior sound levels increase with the flight

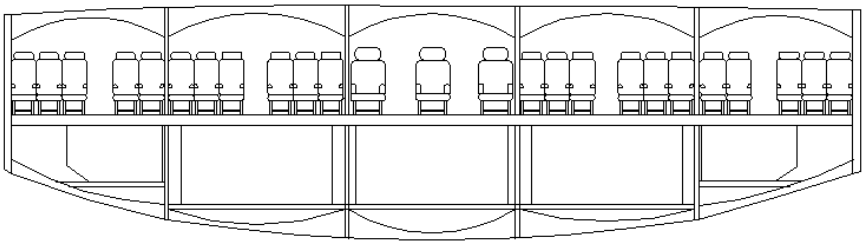

Figure 1: Cabin section layout of a 5 bay BWB aircraft.

speed. Additionally, as concluded in [18, 19], the TBL wall pressure levels increase with the flight Mach number, and in the absence of hydrodynamic coincidence, the interior SPL usually follow the same tendency [12, 20, 21]. In the presence of hydrodynamic coincidence, the increased interior SPL with the flight speed is generally valid for frequencies below and above the neighbourhood of the frequency at which hydrodynamic coincidence occurs, as verified in [6].

Nowadays, the TBL wall pressure fluctuations power spectral density is commonly defined using empirical models. The Corcos formulation [22, 23] has been widely used for this purpose. Although a number of other models were developed after Corcos model, the Corcos formulation is widely used in recent studies to describe the TBL pressure field, as in [24–27]. Corcos model captures the fundamental pressure tendency along the frequency, requires significantly reduced computational effort to employ, and provides a good estimation for the TBL wall-pressure fluctuations levels at and near the convective peak – which is of fundamental importance for aircraft boundary layers [24]. The main disadvantages of Corcos model is the fact that it does not account with the variation of the boundary layer thickness in the flow direction. In order to overcome this drawback, in the present study the Efimtsov model [28] is used to provide the TBL reference pressure power spectral density (PSD), which considers the boundary layer thickness as a variable. Comparing the several models available to describe the TBL wall pressure PSD [29], the Efimtsov model is a suitable candidate, which provides a good agreement with the experimental data [30].

Motivated by the previous studies, and by the significance of understanding the physics involved in the flow-induced noise problem in real transport vehicle cabins, with rectangular cross section, a three-dimensional analytical model is developed to investigate the coupling between the vibration of a multi-panel wall and a box acoustic cabin. A good example of a rectangular-shaped aircraft cabin section is a 5 bay cabin BWB (Blended-Wing-Body) aircraft, which configuration is shown in Figure 1 [31].

In the present study, a BWB cabin bay, filled with air and pressurized, is analyzed. The cabin bay is considered to have five rigid walls and one flexible wall, composed with 50 structural panels. The dimensions and properties of the panels and cabin are similar to those of a typical aircraft structural panel and passenger cabin section, respectively. The TBL excitation is representative of typical cruise conditions of a commercial aircraft, in high subsonic cruise and stabilized flight conditions, and the flow is assumed to be attached and completely developed over the aircraft structure. The amplitude of the wall pressure fluctuations is dependent on the turbulent boundary layer thickness, thus depends on the longitudinal position of the plate.

Previous works were performed by the authors that led to the present investigation. In [14], the base analytical model was validated, considering a single panel coupled with an acoustic enclosure. The analytical framework was successfully validated through the comparison with several independent experimental and numerical studies. Additionally, considering a system with a multi-panel wall vibrating and coupled with a large acoustic cabin, studies were conducted in order to investigate the individual contribution of each plate, located at different positions, to the interior SPL. It was shown that plates located at different positions have dissimilar contributions to the cabin interior SPL. In contrast with previous works, the present study investigates the structural-acoustic systems in which several plates are vibrating simultaneously. Several cases, varying the number of vibrating panels, are examined and compared.

2. MATHEMATICAL APPROACH

2.1 Turbulent boundary layer empirical model equations

The TBL wall pressure field is usually statistically described in terms of the pressure power spectral density. More specifically, the previously referred models, [22-27], were obtained for fully developed turbulent flow over a flat plate, for zero mean pressure gradient. For these conditions, the turbulent flow can be regarded as stationary in time and homogeneous in space. In this case, the cross-spectral density of the wall pressure over the (x, y) plane, for flow in the x-direction, is defined through the Corcos formulation [20, 21], as

$$S(x,\xi_x,\xi_y,\omega) = S_{ref}(x,\omega)\, e^{-\frac{\alpha_x\, \omega\, |\xi_x|}{U_c}}\, e^{-\frac{\alpha_y\, \omega\, |\xi_y|}{U_c}}\, e^{-\frac{i\, \omega\, \xi_x}{U_c}}, \tag{1}$$

where $S_{ref}(x,\omega)$ is defined through the Efimtsov model [28] as follows

$$S_{ref}(x,\omega) = \frac{\tau_w^2(x)\, \delta(x)}{U_\tau(x)}\, \frac{0.01\, \pi}{1+0.02\, Sh^{2/3}(x,\omega)}, \tag{2}$$

with:

$$U_\tau(x) = U_\infty \sqrt{\frac{C_f(x)}{2}}, \quad \tau_w(x) = \frac{1}{2}\rho\, U_\infty^2\, C_f(x), \quad \text{and} \quad Sh(x,\omega) = \frac{\omega\, \delta(x)}{U_\tau(x)}. \tag{3}$$

In the above equations, ξ_x and ξ_y are the spatial separations from the reference point in the x- and y-directions, ω is the angular frequency, α_x and α_y are the empirical parameters which denote the loss of coherence in the x- and y-directions (in [29], the recommended values for aircraft boundary layers are $\alpha_x = 0.1$ and $\alpha_y = 0.77$), $U_c \approx 0.7\, U_\infty$ is the TBL convective velocity, U_∞ is the free-stream velocity, $U_\tau(x)$ is the friction velocity, $\tau_w(x)$ is the mean wall shear stress, $C_f(x)$ is the friction coefficient, and $\delta(x)$ is the TBL thickness. For turbulent boundary layers, $C_f(x)$ and $\delta(x)$ may be defined, respectively from [32, 4], by

$$C_f(x) = 0.37(Log_{10}Re_x)^{-2.584}, \quad \text{and} \quad \delta(x) = 0.37\, x\, Re_x^{-\frac{1}{5}} \left[1+\left(\frac{Re_x}{6.9\times 10^7}\right)^2\right]^{\frac{1}{10}}. \tag{4}$$

The external flow parameters used in the present study are shown in Table 1, corresponding to a normal cruise flight conditions, at 25000 ft altitude.

Table 1: External flow properties (air).

Description	Variable	Value
Speed of sound	c	309.6 m s^{-1}
Air density	ρ	0.54 Kg m^{-3}
Air kinematic viscosity	ν	2.85×10^{-5} m^2 s^{-1}
Free stream velocity	U_∞	229.104 m s^{-1}
TBL convective velocity	U_c	0.7 U_∞
Empirical parameter (x-direction)	α_x	0.1
Empirical parameter (y-direction)	α_y	0.77

2.2 Structural-acoustic coupled system equations

2.2.1 The single-panel coupled with an acoustic cabin

The structural panel displacement and acoustic enclosure pressure may be defined, through the panels and enclosure natural modes, respectively as follows

$$w(x,y,t) = \sum_{m_x=1}^{M_x} \sum_{m_y=1}^{M_y} \alpha_{m_x}(x)\, \beta_{m_y}(y)\, q_{m_x m_y}(t)\,, \tag{5a}$$

And

$$p(x,y,z,t) = \sum_{n_x=1}^{N_x} \sum_{n_y=1}^{N_y} \sum_{n_z=1}^{N_z} \psi_{n_x}(x)\, \phi_{n_y}(y)\, \Gamma_{n_z}(z)\, r_{n_x n_y n_z}(t)\,, \tag{5b}$$

where $\alpha_{m_x}(x)$ and $\beta_{m_y}(y)$ are the w(x,y,t) spatial functions, $q_{m_x m_y}(t)$ are the w(x,y,t) time functions, $\psi_{n_x}(x)$, $\phi_{n_y}(y)$ and $\Gamma_{n_z}(z)$ are the p(x,y,z,t) spatial functions, $r_{n_x n_y n_z}(t)$ are the p(x,y,z,t) spatial time functions, $M = M_x \times M_y$ is the total number of plate modes (m_x, m_y), and $N = N_x \times N_y \times N_z$ is the total number of acoustics modes (n_x, n_y, n_z). For the simply supported panel and rigid body enclosure, the spatial functions can be defined, respectively, as

$$\alpha_{m_x}(x) = \sqrt{\frac{2}{a}}\, \sin\left(\frac{m_x \pi\, x}{a}\right), \quad \text{and} \quad \beta_{m_y}(y) = \sqrt{\frac{2}{b}}\, \sin\left(\frac{m_y \pi\, y}{b}\right), \tag{6a}$$

$$\psi_{n_x}(x) = \frac{A_{n_x}}{\sqrt{L_x}} \cos\left(\frac{n_x \pi\, x}{L_x}\right), \quad \phi_{n_y}(y) = \frac{A_{n_y}}{\sqrt{L_y}} \cos\left(\frac{n_y \pi\, y}{L_y}\right), \text{ and } \Gamma_{n_z}(z) = \frac{A_{n_z}}{\sqrt{L_z}} \cos\left(\frac{n_z \pi\, z}{L_z}\right), \tag{6b}$$

in which a is the panel length, b is the panel width, L_x, L_y and L_z are acoustic enclosure length, width and height, respectively, and A_n is $\sqrt{2}$ when $n \neq 0$ and equal to 1 when n=0. As described in more detail in [14], the governing equations on the coupled structural-acoustic system, consisting of a single panel-single acoustic enclosure, results in the following system of equations written in the matrix form:

$$\begin{bmatrix} \mathbf{M}_{pp} & \mathbf{0} \\ \mathbf{M}_{cp} & \mathbf{M}_{cc} \end{bmatrix} \begin{Bmatrix} \ddot{\mathbf{q}}(t) \\ \ddot{\mathbf{r}}(t) \end{Bmatrix} + \begin{bmatrix} \mathbf{D}_{pp} & \mathbf{0} \\ \mathbf{0} & \mathbf{D}_{cc} \end{bmatrix} \begin{Bmatrix} \dot{\mathbf{q}}(t) \\ \dot{\mathbf{r}}(t) \end{Bmatrix} + \begin{bmatrix} \mathbf{K}_{pp} & \mathbf{K}_{pc} \\ \mathbf{0} & \mathbf{K}_{cc} \end{bmatrix} \begin{Bmatrix} \mathbf{q}(t) \\ \mathbf{r}(t) \end{Bmatrix} = \begin{Bmatrix} \mathbf{p}_{tbl}(t) \\ \mathbf{0} \end{Bmatrix} \tag{7}$$

where subscripts *p* an *c* stand for *plate* and *cavity*, $\mathbf{q}(t)$ and $\mathbf{r}(t)$ are the vectors of the considered time functions $q_{m_x m_y}(t)$ and $r_{n_x n_y n_z}(t)$, respectively, $\mathbf{p}_{tbl}(t)$ express the TBL excitation, and **M**, **D**, and **K** are the mass, damping and stiffness matrices, defined as follows

$$\mathbf{M}_{pp} = \mathrm{diag}\left[\rho_p h_p\right], \mathbf{M}_{cc} = \mathrm{diag}\left[\frac{1}{c_0^2}\right], \mathbf{M}_{cp} = \rho_0 \left[\frac{(-1)^{n_z} A_{n_z}}{\sqrt{L_z}} \int_{x_{p_i}}^{x_{p_f}} \alpha_{m_x}(x)\psi_{n_x}(x)dx \int_{y_{p_i}}^{y_{p_f}} \beta_{m_y}(y)\phi_{n_y}(y)dy\right], \tag{8a}$$

$$\mathbf{D}_{pp} = \mathrm{diag}\left[2\rho_p h_p \omega_m \xi_p\right], \quad \mathbf{D}_{cc} = \mathrm{diag}\left[2\frac{1}{c_0^2}\omega_n \xi_{ac}\right], \tag{8b}$$

$$\mathbf{K}_{pp}=\text{diag}\left[\omega_m^2\rho_p h_p\right],\ \mathbf{K}_{cc}=\text{diag}\left[\frac{\omega_n^2}{c_0^2}\right],\ \mathbf{K}_{pc}=\left[\frac{-(-1)^{n_z}A_{n_z}}{\sqrt{L_z}}\int_{x_{p_i}}^{x_{p_f}}\alpha_{m_x}(x)\psi_{n_x}(x)dx\int_{y_{p_i}}^{y_{p_f}}\beta_{m_y}(y)\phi_{n_y}(y)dy\right], \quad (8c)$$

$$\mathbf{p}_{tbl}(t) = -\left[\int_{y_{p_i}}^{y_{p_f}}\int_{x_{p_i}}^{x_{p_f}}\alpha_{m_x}(x)\,\beta_{m_y}(y)\,p_{tbl}(x,y,z=L_z,t)\,dx\,dy\right]. \quad (8d)$$

In the above equations, ρ_p and h_p are the density and thickness of the panel, ω_m and ω_n are the natural frequencies of the panel and acoustic enclosure, ξ_p is the plate structural damping ratio, ξ_{ac} is the enclosure acoustic damping ratio, x_{p_i} and x_{p_f} are the initial and last x-coordinates of the plate, y_{p_i} and y_{p_f} are the initial and last y-coordinates of the plate, and c_0 is the speed of sound inside the enclosure. In the frequency domain, ω, eqn(7) can be written as follows

$$\mathbf{Y}(\omega) = \mathbf{H}(\omega)\,\mathbf{X}(\omega), \quad (9a)$$

with:

$$\mathbf{Y}(\omega)=\begin{Bmatrix}\mathbf{Q}(\omega)\\ \mathbf{R}(\omega)\end{Bmatrix},\ \mathbf{X}(\omega)=\begin{Bmatrix}\mathbf{P}_{tbl}(\omega)\\ \mathbf{0}\end{Bmatrix},\ \mathbf{H}(\omega) = \begin{bmatrix}\mathbf{A} & \mathbf{B}\\ \mathbf{C} & \mathbf{D}\end{bmatrix}^{-1}, \quad (9b)$$

and

$$\mathbf{A} = -\omega^2\,\mathbf{M}_{pp} + i\,\omega\,\mathbf{D}_{pp} + \mathbf{K}_{pp}, \quad (9c)$$

$$\mathbf{B} = \mathbf{K}_{pc}, \quad (9d)$$

$$\mathbf{C} = -\omega^2\,\mathbf{M}_{cp}, \quad (9e)$$

$$\mathbf{D} = -\omega^2\,\mathbf{M}_{cc} + i\,\omega\,\mathbf{D}_{cc} + \mathbf{K}_{cc}, \quad (9f)$$

in which $\mathbf{Q}(\omega)$, $\mathbf{R}(\omega)$ and $\mathbf{P}_{tbl}(\omega)$ are the frequency domain vectors of the $\mathbf{q}(t)$, $\mathbf{r}(t)$ and $\mathbf{p}_{tbl}(t)$ vectors defined in the time domain. In the spectral domain, eqn(9a) can be written as

$$\mathbf{S_{WW}}(\omega) = \mathbf{H_W}^*(\omega)\,\mathbf{S_{tbl}}(\omega)\,\mathbf{H_W}^T(\omega), \quad (10a)$$

and

$$\mathbf{S_{PP}}(\omega) = \mathbf{H_P}^*(\omega)\,\mathbf{S_{tbl}}(\omega)\,\mathbf{H_P}^T(\omega), \quad (10b)$$

where $\mathbf{S_{WW}}(\omega)$ is the PSD matrix of the plate displacement, $\mathbf{S_{PP}}(\omega)$, is the PSD matrix of the acoustic pressure, $\mathbf{S_{tbl}}(\omega)$ is the PSD matrix of the TBL pressure, and superscripts * and T denote Hermitian conjugate and matrix transpose, respectively. Finally, the system response matrices $\mathbf{H_W}(\omega)$ and $\mathbf{H_P}(\omega)$, and generalized PSD matrix, $\mathbf{S_{tbl}}(\omega)$, are defined as follows

$$\mathbf{H_W}(\omega) = (\mathbf{A} - \mathbf{B}\,\mathbf{D}^{-1}\,\mathbf{C})^{-1}, \quad (11a)$$

$$\mathbf{H_P}(\omega) = -\mathbf{D}^{-1}\,\mathbf{C}\,\mathbf{H_W}(\omega), \quad (11b)$$

$$\mathbf{S_{tbl}}(\omega) = \left[\int_{y_{p_i}}^{y_{p_f}} \int_{x_{p_i}}^{x_{p_f}} \alpha_{m_x}(x)\alpha_{m_{x'}}(x')\beta_{m_y}(y)\beta_{m_{y'}}(y')S(x,\xi_x,\xi_y,\omega)dxdx'dydy' \right], \tag{11b}$$

in which the term $S(x,\xi_x,\xi_y,\omega)$ is known from eqn(1). It is through the $\mathbf{S_{PP}}(\omega)$ matrix that is possible to determine the PSD of the acoustic enclosure pressure, in a specific point inside the enclosure as

$$S_{pp}(x_1,y_1,z_1,x_2,y_2,z_2,\omega) = \sum_{n_{x_1},\, n_{x_2}=1}^{N_x^2} \sum_{n_{y_1},\, n_{y_2}=1}^{N_y^2} \sum_{n_{z_1},\, n_{z_2}=1}^{N_z^2} \psi_{n_{x_1}}(x_1)\psi_{n_{x_2}}(x_2)\phi_{n_{y_1}}(y_1)\phi_{n_{y_2}}(y_2)\Gamma_{n_{z_1}}(z_1)\Gamma_{n_{z_2}}(z_2)\, \mathbf{S_{PP}}(\omega)_{n_1,n_2} \tag{12}$$

or space-averaged in the acoustic enclosure volume as

$$S_{pp}(\omega) = \int_0^{L_z} \int_0^{L_y} \int_0^{L_x} S_{pp}(x_1,y_1,z_1,x_2,y_2,z_2,\omega)\, dx_1 dx_2 dy_1 dy_2 dz_1 dz_2. \tag{13}$$

2.2.2 The multi-panel wall coupled with an acoustic cabin

Regarding the system consisted by a single acoustic enclosure coupled with several vibrating panels, the basic model presented previously needs to be modified. Shall one consider N_p plates, part of the same enclosure flexible, and all vibrating due to the TBL excitation, it can be shown that the system governing equations, defined in eqn(7) for one panel, becomes:

$$\underbrace{\begin{bmatrix} \mathbf{M_1}_{pp} & 0 & \dots & 0 & 0 & 0 \\ 0 & \mathbf{M_2}_{pp} & \dots & 0 & 0 & 0 \\ \vdots & \vdots & \ddots & \vdots & \vdots & \vdots \\ 0 & 0 & \dots & \mathbf{M_{N_p-1}}_{pp} & 0 & 0 \\ 0 & 0 & \dots & 0 & \mathbf{M_{N_p}}_{pp} & 0 \\ \mathbf{M_1}_{cp} & \mathbf{M_2}_{cp} & \dots & \mathbf{M_{N_p-1}}_{cp} & \mathbf{M_{N_p}}_{cp} & \mathbf{M}_{cc} \end{bmatrix}}_{\boldsymbol{M}} \begin{Bmatrix} \ddot{\mathbf{q}}_1(t) \\ \ddot{\mathbf{q}}_2(t) \\ \vdots \\ \ddot{\mathbf{q}}_{N_p-1}(t) \\ \ddot{\mathbf{q}}_{N_p}(t) \\ \ddot{\mathbf{r}}(t) \end{Bmatrix} + \underbrace{\begin{bmatrix} \mathbf{D_1}_{pp} & 0 & \dots & 0 & 0 & 0 \\ 0 & \mathbf{D_2}_{pp} & \dots & 0 & 0 & 0 \\ \vdots & \vdots & \ddots & \vdots & \vdots & \vdots \\ 0 & 0 & \dots & \mathbf{D_{N_p-1}}_{pp} & 0 & 0 \\ 0 & 0 & \dots & 0 & \mathbf{D_{N_p}}_{pp} & 0 \\ 0 & 0 & \dots & 0 & 0 & \mathbf{D}_{cc} \end{bmatrix}}_{\boldsymbol{D}} \begin{Bmatrix} \dot{\mathbf{q}}_1(t) \\ \dot{\mathbf{q}}_2(t) \\ \vdots \\ \dot{\mathbf{q}}_{N_p-1}(t) \\ \dot{\mathbf{q}}_{N_p}(t) \\ \dot{\mathbf{r}}(t) \end{Bmatrix} +$$

$$+ \underbrace{\begin{bmatrix} \mathbf{K_1}_{pp} & 0 & \dots & 0 & 0 & \mathbf{K_1}_{pc} \\ 0 & \mathbf{K_2}_{pp} & \dots & 0 & 0 & \mathbf{K_2}_{pc} \\ \vdots & \vdots & \ddots & \vdots & \vdots & \vdots \\ 0 & 0 & \dots & \mathbf{K_{N_p-1}}_{pp} & 0 & \mathbf{K_{N_p-1}}_{pc} \\ 0 & 0 & \dots & 0 & \mathbf{K_{N_p}}_{pp} & \mathbf{K_{N_p}}_{pc} \\ 0 & 0 & \dots & 0 & 0 & \mathbf{K}_{cc} \end{bmatrix}}_{\boldsymbol{K}} \begin{Bmatrix} \mathbf{q}_1(t) \\ \mathbf{q}_2(t) \\ \vdots \\ \mathbf{q}_{N_p-1}(t) \\ \mathbf{q}_{N_p}(t) \\ \mathbf{r}(t) \end{Bmatrix} = \begin{Bmatrix} \mathbf{p_1}_{tbl}(t) \\ \mathbf{p_2}_{tbl}(t) \\ \vdots \\ \mathbf{p_{N_p-1}}_{tbl}(t) \\ \mathbf{p_{N_p}}_{tbl}(t) \\ \mathbf{0} \end{Bmatrix}, \tag{14}$$

where $\mathbf{M_i}_{pp}$ and $\mathbf{M_i}_{cp}$ are mass matrices of the i^{th} plate, $\mathbf{D_i}_{pp}$ is the damping matrix of the i^{th} plate, $\mathbf{K_i}_{pp}$ and $\mathbf{K_i}_{pc}$ are stiffness matrices of the i^{th} plate. Note that, since $\mathbf{M_i}_{pp}$, $\mathbf{D_i}_{pp}$, and $\mathbf{K_i}_{pp} \in \Re^{M\times M}$, $\mathbf{M_i}_{cp} \in \Re^{N\times M}$, $\mathbf{K_i}_{pc} \in \Re^{M\times N}$, and $\mathbf{M}_{cc}$, $\mathbf{D}_{cc}$ and $\mathbf{K}_{cc} \in \Re^{N\times N}$, it results that $\boldsymbol{M}$, $\boldsymbol{D}$ and $\boldsymbol{K} \in$

$\Re^{\{(Np\times M)+N\}\times\{(Np\times M)+N\}}$. Now, writing the governing equations in the frequency domain, and similarly to eqns(9), it becomes:

$$\mathbf{Y}(\omega) = \mathbf{H}(\omega)\,\mathbf{X}(\omega), \tag{15a}$$

in which:

$$\mathbf{Y}(\omega)=\begin{Bmatrix} \mathbf{Q_1}(\omega) \\ \mathbf{Q_2}(\omega) \\ \vdots \\ \mathbf{Q_{N_p-1}}(\omega) \\ \mathbf{Q_{N_p}}(\omega) \\ \mathbf{R}(\omega) \end{Bmatrix},\ \mathbf{X}(\omega)=\begin{Bmatrix} \mathbf{P_{1}}_{tbl}(\omega) \\ \mathbf{P_{2}}_{tbl}(\omega) \\ \vdots \\ \mathbf{P_{N_p-1}}_{tbl}(\omega) \\ \mathbf{P_{N_p}}_{tbl}(\omega) \\ \mathbf{0} \end{Bmatrix},\ \mathbf{H}(\omega) = \begin{bmatrix} \mathbf{A} & \mathbf{B} \\ \mathbf{C} & \mathbf{D} \end{bmatrix}^{-1}, \tag{15b}$$

and

$$\mathbf{A} = \begin{bmatrix} \mathbf{A_1} & 0 & \dots & 0 & 0 \\ 0 & \mathbf{A_2} & \dots & 0 & 0 \\ \vdots & \vdots & \ddots & \vdots & \vdots \\ 0 & 0 & \dots & \mathbf{A_{N_p-1}} & 0 \\ 0 & 0 & \dots & 0 & \mathbf{A_{N_p}} \end{bmatrix}, \text{ with } \mathbf{A_i} = -\omega^2\mathbf{M_i}_{pp} + i\omega\,\mathbf{D_i}_{pp} + \mathbf{K_i}_{pp}\ , \tag{15c}$$

$$\mathbf{B} = \begin{bmatrix} \mathbf{B_1} & \mathbf{B_2} & \dots & \mathbf{B_{N_p-1}} & \mathbf{B_{N_p}} \end{bmatrix}^T, \text{ with } \mathbf{B_i} = \mathbf{K_i}_{pc}\ , \tag{15d}$$

$$\mathbf{C} = \begin{bmatrix} \mathbf{C_1} & \mathbf{C_2} & \dots & \mathbf{C_{N_p-1}} & \mathbf{C_{N_p}} \end{bmatrix}, \text{ with } \mathbf{C_i} = -\omega^2\,\mathbf{M_i}_{cp}\ , \tag{15e}$$

$$\mathbf{D} = -\,\omega^2\,\mathbf{M}_{cc} + i\,\omega\,\mathbf{D}_{cc} + \mathbf{K}_{cc}\ , \tag{15f}$$

where $\mathbf{A} \in \Re^{(Np\times M)\times(Np\times M)}$, $\mathbf{B} \in \Re^{(Np\times M)\times N}$, $\mathbf{C} \in \Re^{N\times(Np\times M)}$, and $\mathbf{D} \in \Re^{N\times N}$. The matrices $\mathbf{S_{WW}}(\omega)$ is and $\mathbf{S_{PP}}(\omega)$ are obtained as in eqns(10a) and (10b), $\mathbf{H_W}(\omega)$ and $\mathbf{H_P}(\omega)$ though eqns(11a) and(11b), and the matrix PSD matrix for the multi-panel single-enclosure system, $\mathbf{S_{tbl}}(\omega) \in \Re^{(Np\times M)\times(Np\times M)}$, is defined as follows

$$\mathbf{S_{tbl}}(\omega) = \begin{bmatrix} \mathbf{S_{1}}_{tbl}(\omega) & 0 & \dots & 0 & 0 \\ 0 & \mathbf{S_{2}}_{tbl}(\omega) & \dots & \vdots & \vdots \\ \vdots & \vdots & \ddots & \vdots & \vdots \\ 0 & 0 & \dots & \mathbf{S_{N_p-1}}_{tbl}(\omega) & 0 \\ 0 & 0 & \dots & 0 & \mathbf{S_{N_p}}_{tbl}(\omega) \end{bmatrix}, \tag{16}$$

with each $\mathbf{S_{i}}_{tbl}(\omega) \in \Re^{M\times M}$ representing the TBL excitation matrix for the i^{th} plate, and defined by eqn(11b). After determining these matrices the acoustic enclosure pressure PSD can be calculated from eqns(12) and (13), respectively for local and average values.

3. PREDICTED FLOW-INDUCED NOISE IN A BWB AIRCRAFT CABIN

3.1 Model verification

In the present Section, the analytical model presented in the previous Section is used to predict the interior noise inside a simpler cabin, which configuration is shown in Figure 2. The predictive results are obtained for four different cases, as following: (a) acoustic cabin coupled only with panel 1; (b) acoustic cabin coupled with panels 1 to 4; (c) acoustic cabin coupled with panels 1 to 6; and (d) acoustic cabin coupled with all 10 panels. The case (a) is the base model, from [2], and was used as a validation case in [14]. The properties of the system shown in Figure 2 are presented in Table 2.

The results for the cavity power spectrum were calculated through the acoustic cabin pressure power spectral density, S_{pp}, as follows

$$E_{pp} = \frac{L_x L_y L_z}{4\,\rho_0 c_0^2}\,\omega\,S_{pp}\,, \tag{17}$$

for frequencies up to 1000 Hz. For this frequency range, a total number of 20 plate modes ($M_x = 4$ and $M_y = 5$), and 189 acoustic modes ($N_x = 21$, $N_y = 3$ and $N_z = 3$) were necessary to achieve convergence of the spectral quantities. The results for the average E_{pp} (averaged over the enclosure volume) are shown in Figure 3, increasing the number of vibrating panels from 1 to 10. As expected, the average cavity power spectrum increases with the number of vibrating plates, and the curve maintains a similar shape since all plates have the same properties and dimensions. As shown in previous works, the peaks on the cavity power spectrum curve correspond to both plate and acoustic natural modes.

Figure 4 shows the cavity power spectrum prediction at four locations inside the enclosure. As can be seen, as the number of vibrating plates is increased from (a) 1 to (d) 10, the cavity power spectrum also increases in all four locations. Additionally, as the number of vibrating panels increase, the curves peaks and valleys become less evident. Specifically, considering point 1, as the number of plates increase the curve shape becomes gradually more similar with the curve for the average cavity power spectrum, shown in Figure 3. This way, the model is able to predict local and average values of interior noise, and for a variable number of vibrating panels. As shown in Figure 4, for a specific point in the enclosure, the number of vibrating panels significantly affects the prediction of interior noise, and this is an important factor in the cabin noise prediction and aircraft design.

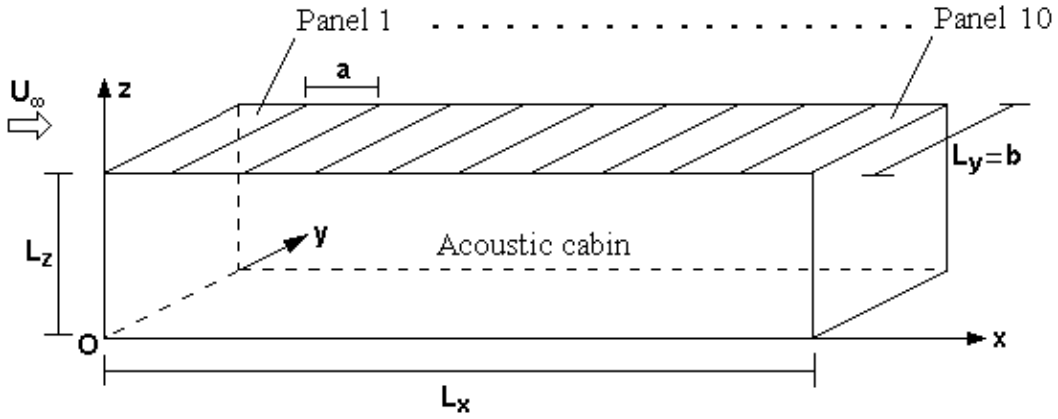

Figure 2: Configuration of a simple multi-panel wall cabin, composed by 10 panels.

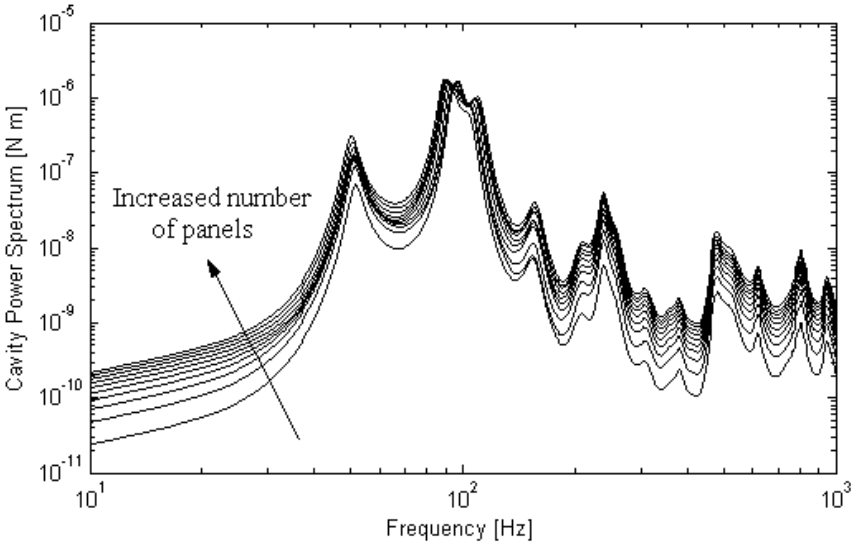

Figure 3: Cavity Power Spectrum (average over the cabin volume), by increasing the number of panels from 1 to 10.

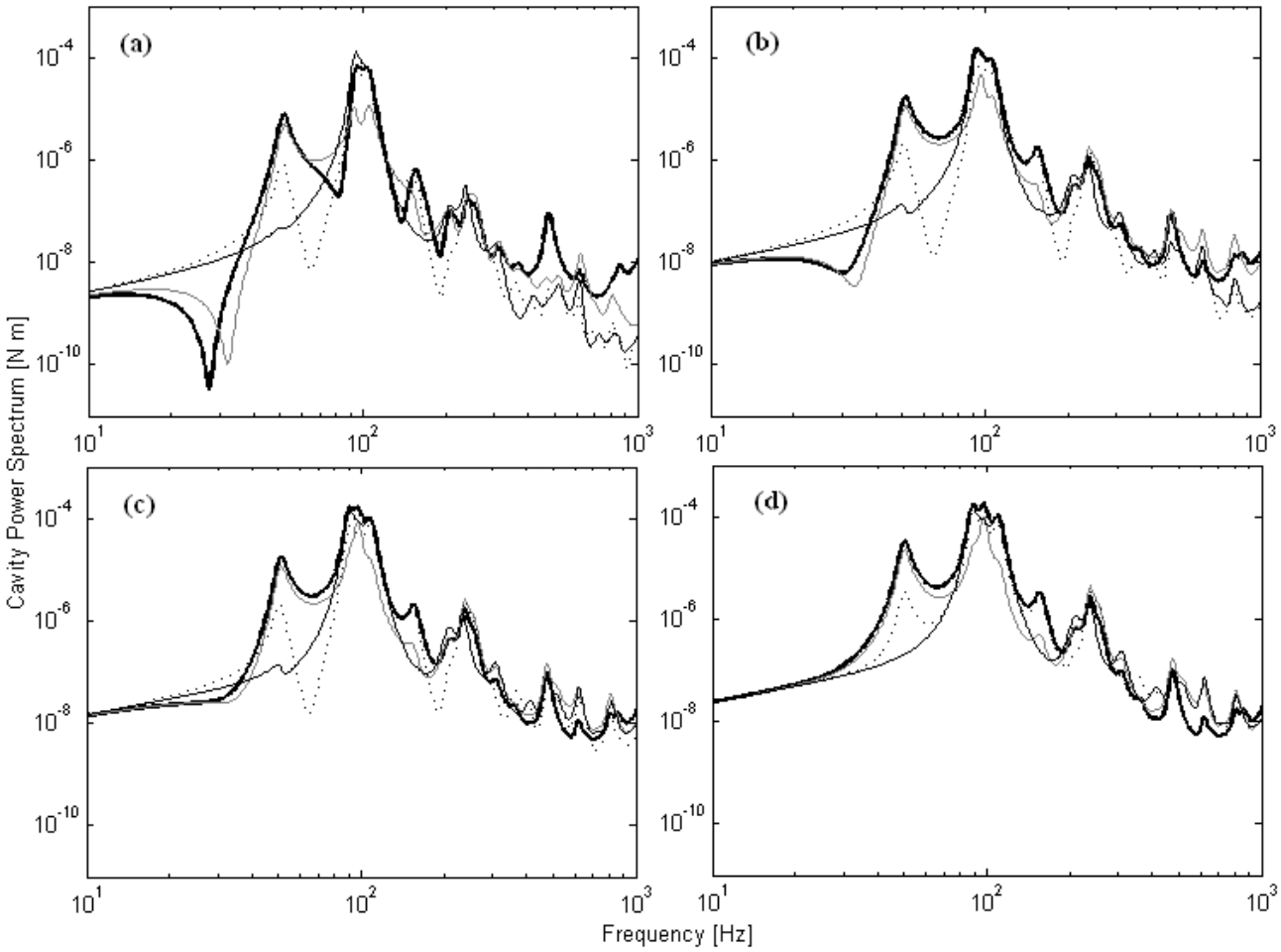

Figure 4: Cavity Power Spectrum considering (a) 1 plate, (b) 4 plates, (c) 6 plates, and (d) 10 plates, at 4 points: ——— (a/2;b/2;L_z/2), ——— (2a;b/2;L_z/2), ——— (L_x/2;b/2;L_z/2), ····· (L_x/2+a;b/2;L_z/2).

Table 2: Properties of the physical system in Figure 2.

Description	Variable	Value
External flow speed of sound	c	310 m s^{-1}
External air density	ρ	0.42 Kg m^{-3}
Free stream velocity	U_∞	0.8 c
TBL convective velocity	U_c	0.6 U_∞
Empirical parameter (x-direction)	α_x	0.1
Empirical parameter (y-direction)	α_y	0.5
Plate density	ρ_p	2800 Kg m^{-3}
Plate Elasticity Modulus	E_p	7.0×10^{10} Pa^2
Plate Poisson´s ration	ν_p	0.3
Structural damping ratio	ξ_p	0.01
Plate length	a	0.3 m
Plate width	b	0.3 m
Plate thickness	h_p	0.0018 m
Internal air speed of sound	c_0	310 m s^{-1}
Internal air density	ρ_0	0.42 Kg m^{-3}
Acoustic damping ratio	ξ_{ac}	0.05
Acoustic enclosure length	L_x	3.0 m
Acoustic enclosure width	L_y	0.3 m
Acoustic enclosure height	L_z	0.3 m

Table 3: Properties of the physical system in Figure 5.

Description	Variable	Value
Plate density	ρ_p	2800 Kg m^{-3}
Plate Elasticity Modulus	E_p	7.24×10^{10} Pa^2
Plate Poisson´s ration	ν_p	0.33
Structural damping ratio	ξ_p	0.01
Plate length	a	0.5 m
Plate width	b	0.22 m
Plate thickness	h_p	0.00102 m
Plate longitudinal tension	T_x	29300 N m^{-1}
Plate lateral tension	T_y	62100 N m^{-1}
Internal air speed of sound	c_0	340 m s^{-1}
Internal air density	ρ_0	1.2 Kg m^{-3}
Acoustic damping ratio	ξ_{ac}	0.01
Acoustic enclosure length	L_x	2.5 m
Acoustic enclosure width	L_y	2.2 m
Acoustic enclosure height	L_z	2.1 m

3.2 BWB aircraft cabin results

The cross section shape of a Blended Wing Body aircraft cabin is approximately rectangular, as illustrated in Figure 5. Figure 5(a) shows the schematic configuration of a 5 bay BWB aircraft fuselage section, with each bay being a single and separate passenger compartment. Figure 5(b) shows the configuration of a single bay, in which the upper wall is considered to be composed by 50 identical structural panels (fuselage skin panels), with 5 panel rows along the x-direction, and 10 panel rows in y-direction. In order to investigate the interior noise induced by the external fully developed TBL, it is assumed that the aircraft fuselage section, shown in Figure 5(a), is located at a

distance of 9.14 m from the aircraft nose. The characteristics of the external flow are shown in Table 1, and the properties of the physical system are given in Table 3, which are similar to those of a real aircraft. The passenger cabin compartment is assumed to be pressurized, and the results were obtained from frequencies up to 1000 Hz. In order to achieve convergence of the calculated spectral quantities up to this frequency, a total number of 44 plate modes ($M_x = 11$ and $M_y = 4$) and 2912 acoustic modes ($N_x = 16$, $N_y = 14$ and $N_z = 13$) is necessary to be considered in the analysis.

Figure 6 shows the variation of the average cabin pressure sound pressure level (averaged over the cabin volume), as a function of the frequency. The results show that, as the number of vibrating panels is increased from 1 to 20, and 20 to 50, an overall increase of the average interior SPL is also observed. As concluded for the simple case analyzed in Section 3.1, the shape of the SPL curve is maintained, as all panels have the same properties. This would not happen if the panels would have different dimensions or properties among them, which can also be obtained through the model presented in Section 2. Some of the peaks in Figure 6 correspond to the plate's natural frequencies, while others correspond to acoustic natural frequencies, showing the importance of the structural-acoustic coupling for the accurate prediction of cabin interior noise.

To assess the noise levels at specific interior locations in the cabin, the local values of SPL should be calculated. This is particularly important in the estimation of the cabin locations where the passengers will be more negatively affected by the TBL-induced noise. Figure 7 shows the results obtained for four different locations in the BWB aircraft cabin, considering three cases: 1 panel vibrating, i.e., panel (1, 1); 20 panels vibrating, i.e., from panel (1, 1) to panel (2, 10); and 50 panels vibrating, i.e., all panels in the upper wall, from (1, 1) to (5, 10). The cabin interior points under study are: $(x_1, y_1, z_1) = (a/2, b/2, 2)$, $(x_2, y_2, z_2) = (a/2, b/2, 1)$, $(x_3, y_3, z_3) = (1, 1, 2)$, and $(x_4, y_4, z_4) = (1, 1, 1)$.

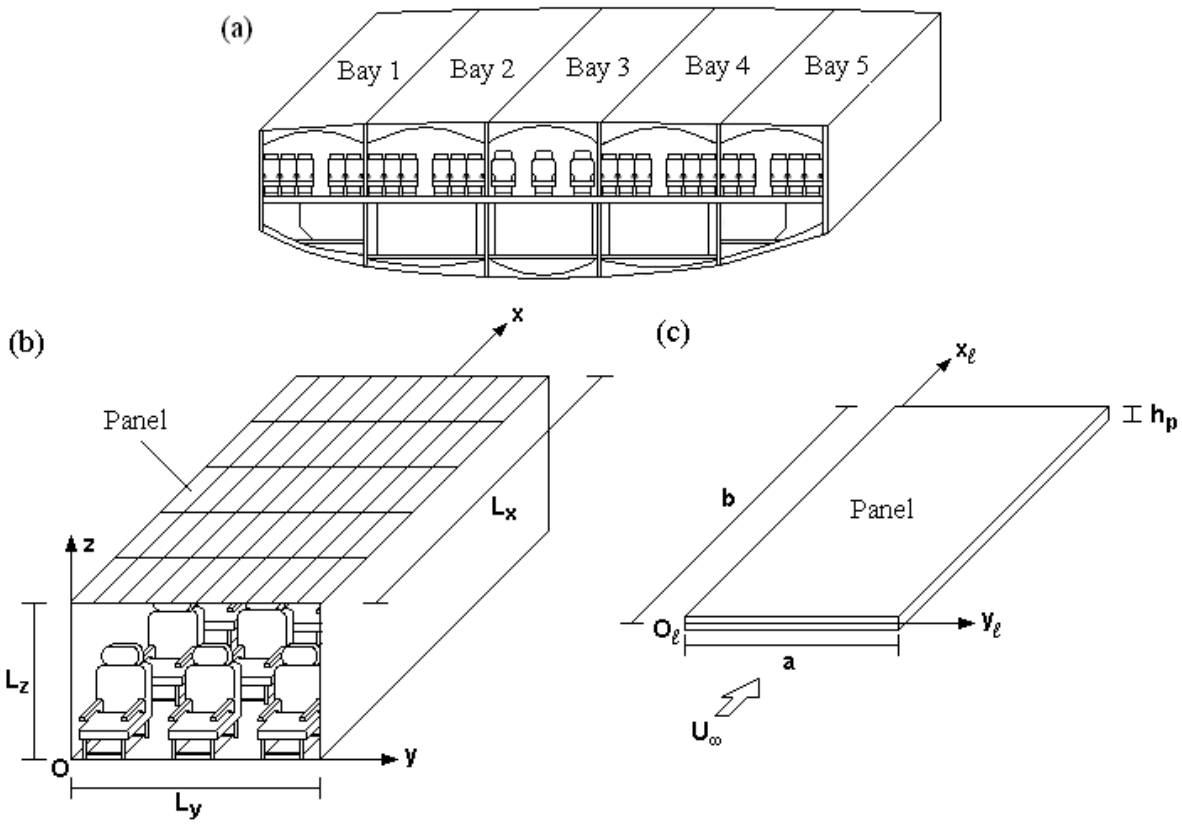

Figure 5: General BWB aircraft cabin layout: (a) 5 bay cabin cross section, (b) bay 3 schematic: multi-panel wall and box-type cabin, (c) structural panel configuration.

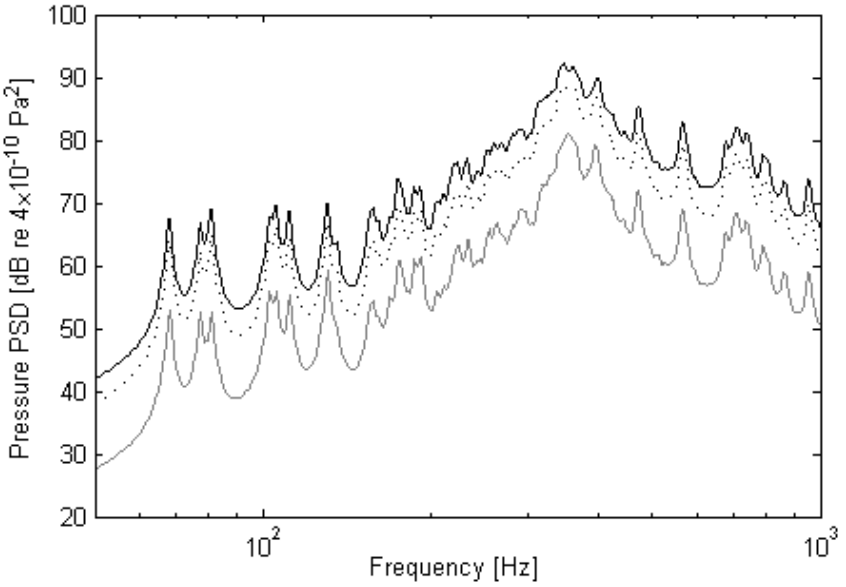

Figure 6: Average power spectral density of the cabin interior pressure (average over the cabin volume), for: —— 1 panel, ····· 20 panels, and —— 50 panels.

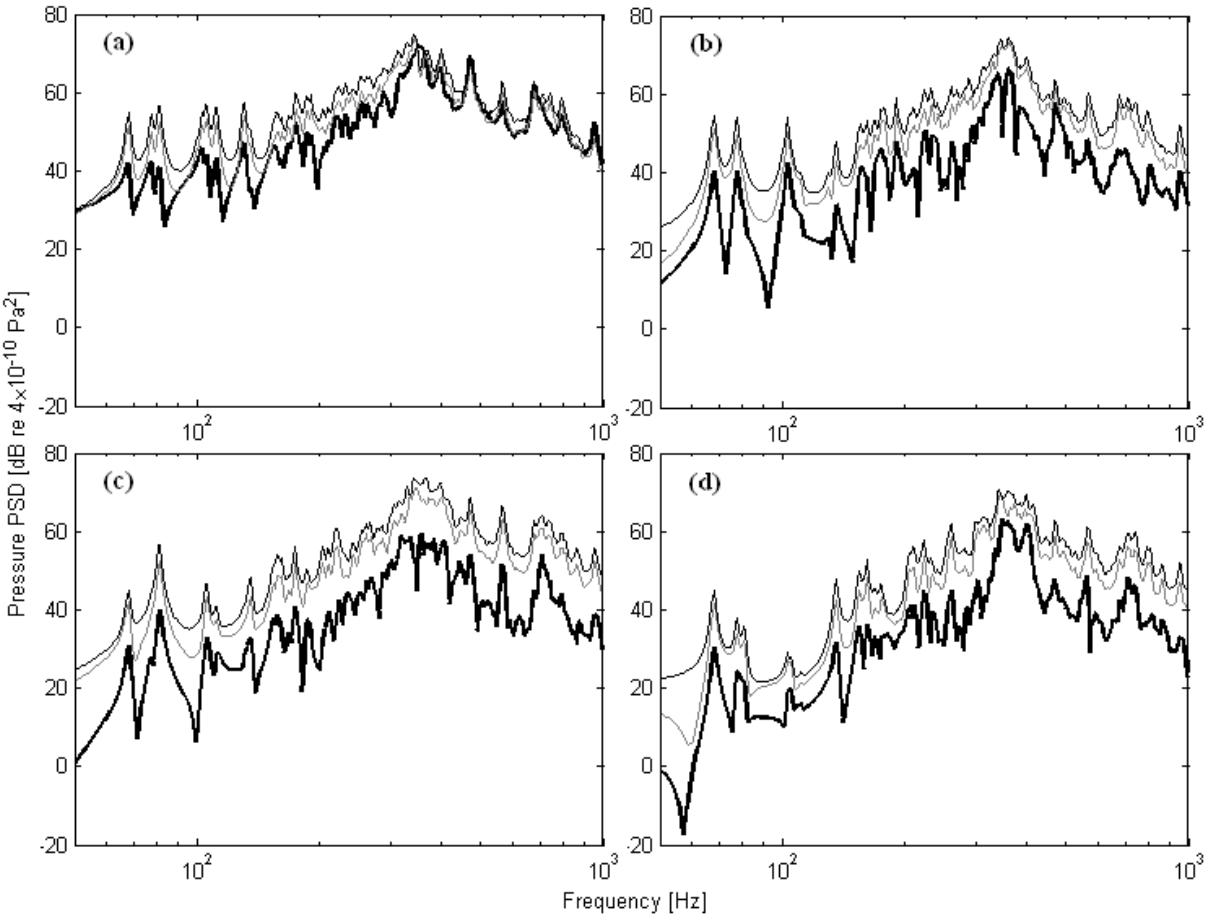

Figure 7: Power spectral density of the cabin pressure, at (a) point 1: (a/2;b/2;2), (b) point 2: (a/2;b/2;1), (c) point 3: (1;1;2), and (d) point 4: (1;1;1). Comparison among 3 cases: —— 1 panel, —— 20 panels, and —— 50 panels.

Observing the results in Figure 7, it can be concluded that considering only panel (1,1) vibrating, the results in the four locations differ significantly from one another. However, when considering the 50 panels vibrating, the SPL curves for the four locations are similar for frequencies greater than 355.45 Hz, i.e., for frequencies above the first panel´s mode. For frequencies below 355.45 Hz, the same does not occur, with curves having dissimilar shapes in the four points. In the frequency range]0; 355.45] Hz, the peaks in the SPL curve correspond to the acoustic natural modes. Even though the SPL values are smaller in this frequency range, compared with the level for the 355.45 Hz peak, some of the SPL peaks lying in this range correspond to almost 60 dB SPL in the 50 panel's configuration. This can be of particular interest, since these peaks lie in the human audible range, creating tones and directly affecting the passenger´s comfort. It is also important to verify that, depending on the location, these peaks have different amplifications, with their importance shifting from point to point. For instance, point 3 has more amplification on the 2nd peak compared with the 1st peak, the opposite is observed in point 4.

The accuracy of the predicted cabin SPL can be of crucial importance. In particular, the earlier knowledge about which locations in the cabin have more noise amplification, and at which frequencies, can be important for the implementation of noise control techniques. Motivated by this, the present model allows the user to predict the cabin interior noise, induced by the TBL, in the desired locations. Furthermore, the model can easily be used to investigate other systems, by simply changing the properties and dimensions of the panels and acoustic cabin, and also varying the number of vibrating panels. Since changing the number of vibrating panels, and their properties, can significantly affect the interior SPL, the present model can also be used as a basis for a multidisciplinary design optimization analysis, in order to find the best configuration of structural panels and acoustic cabin.

4. CONCLUSIONS

In the present work, an analytical model for the prediction of TBL-induced noise in a rectangular aircraft cabin, with multi-panel wall, is presented. Interior noise levels (average and local) were obtained for different locations in the cabin. The effect of the number of vibrating panels in the predicted SPL was analyzed. Results were obtained for a simple cabin, and for a more complex cabin, composed by 50 panels. The characteristics of the external flow, structural panel and acoustic cabin were chosen in order to represent a real aircraft cabin in cruise and stabilized flight.

The predictive results show that the cabin interior noise levels are significantly affected by the number of vibrating panels. For frequencies up to 1000 Hz, the average SPL values show an overall increase with the number of panels. Additionally, as the numbers of panels increase, the SPL curve essentially maintains the same shape, if all the vibrating panels have the same properties. Local SPL values, in specific locations inside the cabin, are also affected by the number of vibrating panels. The local SPL results show that, as the number of vibrating panels is increased, the local SPL curves and values become more similar among the several locations, for frequencies above the first panel resonance. However, for frequencies below this resonance, where the acoustic modes are dominant, the same does not happen. In that range, the SPL curves are different from point to point, which show dissimilar amplifications of the several acoustic modes.

The presented analytical model can be used to study a broad range of different systems involving a rectangular cabin coupled with several vibrating panels, excited by the TBL. The properties of the flow, acoustic cabin, and panels, as well as the number of vibrating panels, can be easily changed to represent other systems. These abilities of the model make it a solid basis for future investigations involving the implementation of noise reduction techniques and multidisciplinary design optimization analyzes.

ACKNOWLEDGEMENTS

The authors wish to thank for the financial support of the Foundation for Science and Technology, through a post-graduate scholarship program.

REFERENCES

[1] Bishop, D. E., Cruise flight noise levels in a turbojet transport airplane, Noise Control, 1961, 7(2), 37-42.
[2] Frampton, K. D., and Clark, R. L., Power flow in an aeroelastic plate backed by a reverberant cavity. Journal of the Acoustical Society of America, 1997, 102(3), 1620-1627.
[3] Maestrello, L., Measurement of noise radiated by turbulent boundary layer excited panels, Journal of Sound and Vibration, 1965, 2(2), 100-115.
[4] Bies, D. A., A review of flight and wind tunnel measurements of boundary layer pressure fluctuations and induced structural response, NASA CR-626, 1966.
[5] Davies, H. G., Sound from turbulent-boundary-layer-excited panels, Journal of the Acoustical Society of America, 1971, 49(3), 878-889.
[6] Wilby, J. F., and Gloyna, F. L., Vibration measurements of an airplane fuselage structure I. Turbulent boundary layer excitation, Journal of Sound and Vibration, 1972, 23(4), 443-466.
[7] Han, F., Bernhard, R. J., and Mongeau, L. G., Prediction of flow-induced structural vibration and sound radiation using energy flow analysis, Journal of Sound and Vibration, 1999, 227(4), 685-709.
[8] Allen, M., and Vlahopoulos, N., Noise generated from a flexible and elastically supported structure subject to turbulent boundary layer flow excitation, Finite Elements in Analysis and Design, 2001, 37, 687-712.
[9] Liu, B., Noise radiation of aircraft panels subjected to boundary layer pressure fluctuations, Journal of Sound and Vibration, 2008, 314, 693-711.
[10] Barton, C. K., and Daniels, E. F., Noise transmission through flat rectangular panels into a closed cavity, NASA TP-1321, 1978.
[11] Heatwole, C. M., Bernhard, R. J., and Francheck, M. A., Robust feedback control of flow induced structural radiation of sound, NASA Report 0278-1, 1997.
[12] Frampton, K. D., and Clark, R. L., Power flow in an aeroelastic plate backed by a reverberant cavity, Journal of the Acoustical Society of America, 1997, 102(3), 1620–1627.
[13] Smith, G. C., Clark, R. L., and Frampton, K. D., Optimal tranducer placement for active control of sound transmission through aeroelastic plates. Journal of the Intelligent Material Systems and Structures, 1998, 9, 975-987.
[14] da Rocha, J., Suleman, A., and Lau, F., Prediction of flow-induced noise in transport vehicles: development and validation of a coupled structural-acoustic analytical framework, Canadian Acoustics, 2009, 37(4), 13-29.
[15] Jackson, A. C., Balena, F. J., LaBarge, W. L., Pei, G., Pitman, W. A., and Wittlin, G., Transport composite fuselage technology - impact dynamics and acoustic transmission, NASA CR-4035, 1986.
[16] Rizzi, S. A., Rackl, R. G., Cline, J., and Andrianov, E. V., Flight test measurements from the Tu-144LL structure/cabin noise experiment, NASA TM-209858, 2000.
[17] Beier, T. H., Bhat, W. V., Rizzi, S. A., Silcox, R. J., and Simpson, M. A., High speed research program structural acoustics multi-year summary report, NASA TM-213536, 2005.
[18] Bhat, W. V., Flight test measurement of exterior turbulent boundary layer pressure fluctuations on Boeing Model 737 airplane, Journal of Sound and Vibration, 1971, 14(4), 439-457.
[19] Wilby, J. F., and Gloyna, F. L., Vibration measurements of an airplane fuselage structure II. Jet noise excitation, Journal of Sound and Vibration, 1972, 23(4), 467-486.
[20] Gibbs, G. P., Cabell, R. H., and Juang, J., Controller Complexity for Active Control of Turbulent Boundary-Layer Noise from Panels, AIAA Journal, 2004, 42(7), 1314-1320.
[21] Maury, C., Gardonio, P., and Elliot, S. J., A wavenumber approach to modeling the response of a randomly excited panel, part II: application to aircraft panels excited by a turbulent boundary layer, Journal of Sound and Vibration, 2002, 252(1), 115-139.
[22] Corcos, G. M., Resolution of pressure in turbulence, Journal of the Acoustical Society of America, 1963, 35(2), 192-199.
[23] Corcos, G. M., The structure of the turbulent pressure field in boundary-layer flows, Journal of Fluid Mechanics, 1964, 18, 353-378.

[24] Maury, C., Gardonio, P., and Elliot, S. J., Active control of the flow-induced noise transmitted through a panel, AIAA Journal, 2001, 39(10), 1860-1867.
[25] Han, F., Mongeau, L. G., and Bernhard, R. J., A model for the vibro-acoustic response of plates excited by complex flows, Journal of Sound and Vibration, 2001, 246(5), 901-926.
[26] Maury, C., Gardonio, P., and Elliot, S. J., Model for the active control of flow-induced noise transmitted through double partitions, AIAA Journal, 2002, 40(6), 1113-1121.
[27] Elliot, S. J., Maury, C., and Gardonio, P., The synthesis of spatially correlated random pressure fields, Journal of the Acoustical Society of America, 2005, 117(3), 1186-1201.
[28] Efimtsov, B. M., Characteristics of the field of turbulent wall pressure fluctuations at large Reynolds numbers, Soviet Physics Acoustics, 1982, 28(4), 289-292.
[29] Graham, W. R., A comparison of models for the wavenumber frequency spectrum of turbulent boundary layer pressures, Journal of Sound and Vibration, 1997, 206(4), 541-565.
[30] Rackl, R., and Weston, A., Modeling of turbulent boundary layer surface pressure fluctuation auto and cross spectra - verification and adjustments based on TU-144LL data, NASA CR-213938, 2005.
[31] Mukhopadhyay, V., Blended-Wing-Body (BWB) fuselage structural design for weight reduction, AIAA-2005-2349, in: 46th AIAA/ASME/ASCE/AHS/ASC Structures, Structural Dynamics and Materials Conference, Austin, Texas, 18-21 April, 2005.
[32] Wahidi, R., Chakroun, W., and Al-Fahed, S., The behavior of the skin friction coefficient of a turbulent boundary layer flow over a flat plate with differently configured transverse square grooves, Experimental Thermal and Fluid Science, 2005, 30(2), 141–152.

Appendix D

Flow-Induced Noise and Vibration in Aircraft Cylindrical Cabins: Closed-Form Analytical Model Validation

Flow-Induced Noise and Vibration in Aircraft Cylindrical Cabins: Closed-Form Analytical Model Validation

Joana da Rocha*
Ph.D. Candidate, Student Member of ASME
Department of Mechanical Engineering
University of Victoria
Victoria, British Columbia, V8W 2Y2
Canada
Email: jdarocha@uvic.ca

Afzal Suleman
Professor
Department of Mechanical Engineering
University of Victoria
Victoria, British Columbia, V8W 2Y2
Canada

Fernando Lau
Professor
Departamento de Engenharia Mecânica (Aeroespacial)
Instituto Superior Técnico
1049-001 Lisboa
Portugal

ABSTRACT

The turbulent boundary layer is a major source of interior noise in transport vehicles, mainly in aircraft during cruise flight. Furthermore, as new and quieter jet engines are being developed, the turbulent flow-induced noise will become an even more important topic for investigation. However, in order to design and develop systems to reduce the cabin interior noise, the understanding of the physical system dynamics is fundamental. In this context, the main objective of the current research is to develop closed-form analytical models for the prediction of turbulent boundary-layer-induced noise in the interior of aircraft cylindrical cabins. The mathematical model represents the structural-acoustic coupled system, consisted by the aircraft cabin section coupled with the fuselage structure. The aircraft cabin section is modeled as a cylindrical acoustic enclosure, filled with air. The fuselage structure, excited by external random excitation or by turbulent flow, is represented through two different models: (1) as a whole circular cylindrical shell with simply supported end caps, and (2) as a set of individual simply supported open circular cylindrical shells. This paper presents the results obtained from the developed analytical framework, and its validation through the successful comparison with several experimental studies. Analytical predictions are obtained for the shell structural vibration and sound pressure levels, for the frequency range up to 10,000 Hz.

Keywords: Aircraft Cabin Noise, Cylindrical Cabin, Closed-Form Analytical Model, Flow Induced Noise and Vibration, Random Vibration, Structural-Acoustic Coupling.

1 Introduction

Turbulent boundary layer (TBL) is a major source of aircraft cabin interior noise. In fact, jet powered aircraft cabin interior noise is mostly generated by the external flow excitation and engine noise. However, while during takeoff the engine is the dominant source of noise, in cruise flight the airflow sources are the major contribution for the interior noise [1]. As referred in [2], TBL excitation is regarded as the most important noise source for jet powered aircraft at cruise speed, particularly, as new quieter jet engines are being developed. For these reasons, reducing the turbulent flow induced noise in

*Address all correspondence related to ASME style format and figures to this author.

aircraft cabin is an important topic of research. Still, since the TBL is stochastic phenomenon and due to the complexity of the aircraft structure itself, this is an ongoing topic of investigation. In order to successfully design effective noise control systems, a clear understanding of the mechanisms involved in the aircraft cylindrical cabin TBL-induced noise, such as the sound transmission and radiation of the coupled structural-acoustic system, is crucial. The main goal of the present work is the development of a closed-form analytical framework for the prediction TBL-induced noise into a cylindrical cabin, and its validation against experimental studies. The closed-form framework here presented can easily be adapted for different systems, in which the user only needs to change the flow parameters, and physical system properties. Besides this, closed-form analytical expressions are also presented for the physical system consisted by several shells coupled with a cylindrical cabin, and thus adds a step forward to the traditional single-panel single-cabin analysis.

Several theoretical, numerical and experimental studies were performed to explore the vibration and radiation of sound from isolated panels (i.e., not coupled with an acoustic cabin), excited by turbulent flows, for flat panels [3–5] and for curved panels [6, 7]. Additionally, a number of studies were conducted to investigate structural-acoustic coupled systems, consisted by a single flat panel coupled with a rectangular acoustic enclosure, and excited by random noise or by turbulent flow [2, 8–10]. These studies provide a good basis, and were utilized as validation examples in the previous work for rectangular cabins performed by the authors [11], to confirm the analytical predictions obtained for the structural vibration levels and interior noise levels.

However, in order to accurately predict the interior noise levels in a cylindrical aircraft cabin, the structural model must account for the effects of aircraft panel curvature on the structural dynamics, and the acoustic model should be modeled as a cylinder. As concluded in [12], the curvature of the panels is shown to have a significant effect on the bandwidth of the noise control systems. Previous research was conducted on the structural-acoustic coupling between the vibration of a cylindrical structure and its interior. The sound transmission through a closed cylindrical shell, with simply supported end caps, to the internal acoustic cavity was numerically and experimentally investigated, for external random excitation by [13–15], and for an impinging external plane acoustic wave by [16, 17]. Additionally, several studies were performed to investigate the noise transmitted through a single curved panel into a cylindrical enclosure. In [18], a numerical study was developed for predicting the noise transmitted through a stiffened curved panel into a semicylindrical enclosure. In [6, 12, 19] the sound transmission through a typical aircraft panel into the interior of a cylindrical cabin, due to the turbulent boundary layer excitation (which is modeled as a white noise process) is investigated, as well as the development of control systems to attenuate the sound transmission. Several experimental studies were also undertaken to evaluate the performance of active noise control systems, with the objective of reducing the interior noise and vibration of aircraft cylindrical cabins, such as in [20–22] for random noise excitation, and in [23] for an incident acoustic field.

This paper presents the development and validation of an analytical framework, for the prediction TBL-induced noise into aircraft cylindrical cabins. To validate the analytical framework, several studies were considered for comparison. The acoustic enclosure is of cylindrical shape, filled with air, with simply supported end caps, and with a flexible cylindrical shell. The flexible cylindrical shell is backed by random noise or by turbulent flow. Additionally, the model was extended for the cylindrical structure consisted by several curved panels. The closed-form analytical solution of the coupled system response is obtained, and the analytical expressions are presented. As concluded in [11, 17, 24], both the structural and acoustic resonances can have a significant contribution for the interior noise in the cabin. For this reason, the dynamic response of a fully coupled vibro-acoustic system is derived in terms of the acoustic modes and structural modes. It is shown that the analytical model provides a good prediction of the reality, and that it is important to consider the full coupling between structural and acoustic systems. Analytical predictions are obtained for random and TBL excitations, both for the shell vibration and sound pressure levels.

2 Analytical Model Development

2.1 Turbulent Flow Model for Cylindrical Coordinates

As described in detail in [11, 24], the power spectral density (PSD) of the TBL wall pressure fluctuations over a flat panel, $p_{tbl}(x,y,t)$, can be defined using Corcos model [25, 26] for flow in the x-direction, as follows

$$S(x,\xi_x,\xi_y,\omega) = S_{ref}(x,\omega)e^{-\frac{\alpha_x\omega|\xi_x|}{U_c}}e^{-\frac{\alpha_y\omega|\xi_y|}{U_c}}e^{-\frac{i\omega\xi_x}{U_c}}, \tag{1}$$

in which $\xi_x = x - x'$ and $\xi_y = y - y'$ are the spatial separations in the x- and y- directions of the panel, $S_{ref}(x,\omega)$ is the reference PSD, U_c is the TBL convective speed, and α_x and α_y are empirical parameters, chosen to yield the best agreement with the reality, which denote the loss of coherence in the longitudinal and transverse directions. Recommended empirical values for aircraft boundary layers are $\alpha_x = 0.1$ and $\alpha_y = 0.77$ [27]. Now, assuming that in substitution of a flat panel, one has a shallow open circular shell. In this case, Eq.(1) may be re-written in the cylindrical coordinates systems as

$$S(x,\xi_x,\xi_\theta,\omega) = S_{ref}(x,\omega)e^{-\frac{\alpha_x\omega|\xi_x|}{U_c}}e^{-\frac{\alpha_y\omega|\xi_\theta|}{U_c}}e^{-\frac{i\omega\xi_x}{U_c}}, \tag{2}$$

where $\xi_\theta = R(\theta - \theta')$, in which R is the radius of the cylindrical cabin. Finally, using Efimtsov model [28], $S_{ref}(x,\omega)$ is defined by

$$S_{ref}(x,\omega) = \frac{\tau_w^2(x)\delta(x)}{U_\tau(x)} \frac{0.01\pi}{1+0.02\,Sh(x,\omega)^{\frac{2}{3}}}, \tag{3}$$

where $U_\tau(x)$ is the friction velocity, $\tau_w(x)$ is the mean wall shear stress, $\delta(x)$ is the boundary layer thickness, all defined as in [24, 29], and $Sh(x,\omega) = \frac{\omega\delta(x)}{U_\tau(x)}$ is the Strouhal number.

2.2 Cylindrical Shell Structural Model

For a given applied external pressure, $p_{ext}(x,\theta,t)$, the shell governing equation may be defined as follows [30]

$$\begin{aligned} w + \nu_s R\frac{\partial u}{\partial x} + \frac{\partial v}{\partial \theta} + \frac{h_s^2}{12R^2}\nabla^4 w + \frac{\rho_s(1-\nu_s^2)R^2}{E_s}\ddot{w} + \zeta_s\dot{w} \\ = \frac{(1-\nu_s^2)R^2}{E_s h_s} p_{ext}(x,\theta,t), \end{aligned} \tag{4}$$

in which ν_s is the Poisson ratio of the shell, h_s is the shell thickness, E_s is the shell Young's modulus, $\zeta_s = 2\,\omega^s_{m_x m_\theta}\xi_s$ is the structural modal damping, ξ_s is the shell damping ratio, $\omega^s_{m_x m_\theta}$ is the shell natural frequency corresponding to the (m_x, m_θ) shell mode, and $p_{ext}(x,\theta,t) = p(x,\theta,r=R,t) - p_{tbl}(x,\theta,t)$, where $p(x,\theta,r=R,t)$ is the acoustic cabin interior pressure acting on the shell. The structural displacement may be defined as follows

$$w(x,\theta,t) = \sum_{m_x=1}^{M_x}\sum_{m_\theta=1}^{M_\theta} \alpha_{m_x}(x)\beta_{m_\theta}(\theta)q_{m_x m_\theta}(t), \tag{5}$$

in which $\alpha_{m_x}(x)$ and $\beta_{m_\theta}(\theta)$ are the mode shape functions, $q_{m_x m_\theta}(t)$ is a function of time, and $M = M_x \times M_\theta$ is the total number of shell structural modes considered in the analysis.

2.2.1 Closed Circular Cylindrical Shell

Considering a circular cylindrical shells with simply supported end caps, and without axial constraint at its ends, as shown in part (a) of Fig. 1, the mode shape functions are defined by

$$\alpha_{m_x}(x) = \sqrt{\frac{2}{L_x}}\sin\left(\frac{m_x\pi x}{L_x}\right), \tag{6a}$$

$$\beta_{m_\theta}(\theta) = \sqrt{\frac{1}{\pi}}\cos\left(m_\theta\theta\right), \tag{6b}$$

where L_x is the cabin length. The shell natural frequencies, for an unpressurized cabin, are

$$\omega^s_{m_x m_\theta} = \sqrt{\frac{E_s\lambda^2}{\rho_s(1-\nu_s^2)R^2}}, \tag{7}$$

in which the dimensionless parameter λ is calculated using the procedure described in [31].

2.2.2 Cylindrical Cabin composed by a Set of Shells

Consider a circular cylindrical cabin, composed by several open cylindrical shells as the one in part (b) of Fig. 1. For the curved panel with simply supported edges, the mode shape functions are defined as

$$\alpha_{m_x}(x) = \sqrt{\frac{2}{a}}\sin\left(\frac{m_x\pi(x-x_i)}{a}\right), \tag{8a}$$

$$\beta_{m_\theta}(\theta) = \sqrt{\frac{2}{\theta_0}}\cos\left(\frac{m_\theta\pi(\theta-\theta_i)}{\theta_0}\right), \tag{8b}$$

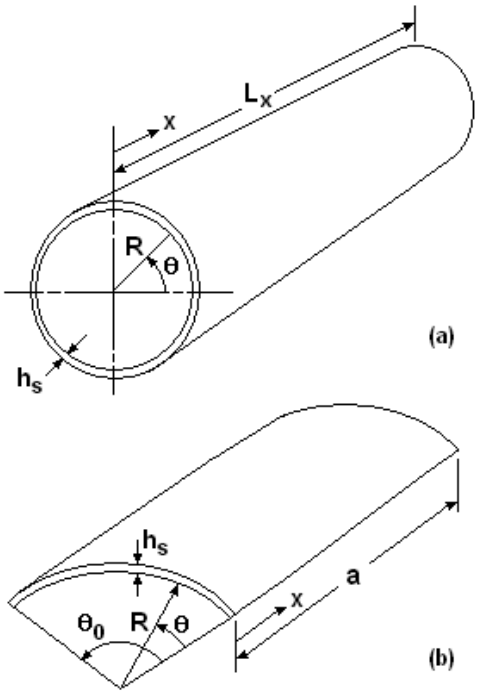

Fig. 1. Schematics of: (a) closed circular cylindrical shell; (b) open shell.

in which a is the shell length, θ_0 is its arc, x_i and θ_i are the starting coordinates of the shell in the cabin global coordinates system. For a pressurized cabin, the natural frequencies of the curved shell are

$$\omega^s_{m_x m_\theta} = \left\{ \frac{E_s h_s^2}{12\rho_s(1-\nu_s^2)} \left[\left(\frac{m_x\pi}{a}\right)^2 + \left(\frac{m_\theta\pi}{R\theta_0}\right)^2 \right]^2 + \frac{N_x}{\rho_s h_s}\left(\frac{m_x\pi}{a}\right)^2 + \frac{N_\theta}{\rho_s h_s}\left(\frac{m_\theta\pi}{R\theta_0}\right)^2 + \frac{\frac{E_s}{\rho_s R^2}\left(\frac{m_x\pi}{a}\right)^4}{\left[\left(\frac{m_x\pi}{a}\right)^2 + \left(\frac{m_\theta\pi}{R\theta_0}\right)^2\right]^2} \right\}^{1/2}, \tag{9}$$

where N_x and N_θ are the in-plane tensions in the x- and θ-directions.

2.3 Cylindrical Enclosure Acoustic Model

The governing equation of a cylindrical acoustic enclosure is the wave equation written in the Cylindrical Coordinates system, as follows

$$\nabla^2 p - \frac{1}{c_0^2}\ddot{p} - \zeta_{ac}\dot{p} = 0, \tag{10}$$

where c_0 is the speed of sound inside the enclosure, the damping term $\zeta_{ac} = 2\omega^{ac}_{n_x n_\theta n_r}\xi_{ac}$ is the acoustic modal damping, added to account for the acoustic damping in the cabin [32, 33], ξ_{ac} is the acoustic damping ratio, and $\omega^{ac}_{n_x n_\theta n_r}$ is the acoustic natural frequency corresponding to the (n_x, n_θ, n_r) acoustic mode. The pressure field inside the enclosure can be defined by

$$p(x,\theta,r,t) = \sum_{n_x=0}^{N_x}\sum_{n_\theta=0}^{N_\theta}\sum_{n_r=0}^{N_r} \psi_{n_x}(x)\phi_{n_r}(\theta)\Gamma_{n_\theta}(r) r_{n_x n_\theta n_r}(t), \tag{11}$$

in which $\psi_{n_x}(x)$, $\phi_{n_r}(\theta)$ and $\Gamma_{n_\theta}(r)$ are the mode shape functions, $r_{n_x n_\theta n_r}(t)$ are functions of time, and $N = (N_x+1)\times(N_\theta+1)\times(N_r+1)$ is the total number of acoustic modes considered. The mode shape functions are assumed to be orthogonal

between each other, and are defined as follows [31]

$$\psi_{n_x}(x) = \frac{A_{n_x}}{\sqrt{L_x}} \cos\left(\frac{n_x \pi x}{L_x}\right), \tag{12a}$$

$$\phi_{n_r}(\theta) = \frac{1}{\sqrt{\pi}} \sin\left(n_r \theta + \gamma \frac{\pi}{2}\right), \tag{12b}$$

$$\Gamma_{n_\theta}(r) = \frac{A_{n_\theta}}{R J_{n_r}(\lambda_{n_r n_\theta})} J_{n_r}\left(\lambda_{n_r n_\theta} \frac{r}{R}\right), \tag{12c}$$

where J_{n_r} are Bessel functions of the 1^{st} kind of n_r^{th} order, $\lambda_{n_r n_\theta}$ factor represents the n_r^{th} root of the equation $dJ_{n_r}(\lambda_{n_r n_\theta} r/R)/d(r/R) = 0$ at $r = R$, and A_n are chosen to satisfy normalization. The natural frequencies of a circular cylindrical cavity can be determined as following

$$\omega^{ac}_{n_x n_\theta n_r} = c_0 \sqrt{\left(\frac{\lambda_{n_r n_\theta}}{R}\right)^2 + \left(\frac{n_x \pi}{L_x}\right)^2}. \tag{13}$$

3 Coupled Structural-Acoustic Cylindrical Model

Following a mathematical procedure similar as the one described in [11,24,29], the governing equations for the coupled structural-acoustic system are obtained from the combination of the governing equations of the individual uncoupled systems, and applying of the boundary conditions, which in the present study are

$$\frac{\partial p(x,\theta,r,t)}{\partial r} = \begin{cases} -\rho_0 \ddot{w}(x,\theta,t) & \text{at r=R} \\ 0 & \text{elsewhere.} \end{cases} \tag{14}$$

Combining the equations of the individual uncoupled subsystems, the governing equations of the coupled system are defined by Eq. (18) of [11], for the closed cylindrical shell, and by Eq. (12) of [24], for the cylindrical cabin composed by a set of curved panels, but now with the system matrices and excitation defined by:

$$\mathbf{M}_{ss} = \text{diag}\left[\frac{\rho_s(1-\nu_s^2)R^2}{E_s}\right], \tag{15}$$

$$\mathbf{D}_{ss} = \text{diag}\left[\frac{\rho_s(1-\nu_s^2)R^2}{E_s} 2\,\omega^s_{m_x m_\theta} \xi_s\right], \tag{16}$$

$$\mathbf{K}_{ss} = \text{diag}\left[\frac{\rho_s(1-\nu_s^2)R^2}{E_s} (\omega^s_{m_x m_\theta})^2\right], \tag{17}$$

$$\mathbf{M}_{cc} = \text{diag}\left[\frac{1}{c_0^2}\right], \tag{18}$$

$$\mathbf{D}_{cc} = \text{diag}\left[\frac{1}{c_0^2} 2\,\omega^{ac}_{n_x n_\theta n_r} \xi_{ac}\right], \tag{19}$$

$$\mathbf{K}_{cc} = \text{diag}\left[\frac{1}{c_0^2} (\omega^{ac}_{n_x n_\theta n_r})^2\right], \tag{20}$$

$$\mathbf{M}_{cs} = \rho_0 \left[A_{n_r} \int_{x_i}^{x_f} \alpha_{m_x} \psi_{n_x} dx \int_{\theta_i}^{\theta_f} \beta_{m_\theta} \phi_{n_r} d\theta\right], \tag{21}$$

$$\mathbf{K}_{sc} = \frac{(\nu_s^2-1)R^2}{E_s h_s} \left[A_{n_r} \int_{x_i}^{x_f} \alpha_{m_x} \psi_{n_x} dx \int_{\theta_i}^{\theta_f} \beta_{m_\theta} \phi_{n_r} d\theta\right], \tag{22}$$

$$\mathbf{p}_{tbl}(t) = \frac{(\nu_s^2-1)R^2}{E_s h_s} \left[\int_{\theta_i}^{\theta_f} \int_{x_i}^{x_f} \alpha_{m_x}(x) \beta_{m_\theta}(\theta) p_{tbl}(x,\theta,t) dx d\theta\right]. \tag{23}$$

The closed-form analytical expressions obtained for matrices $\mathbf{M}_{cs}$ and $\mathbf{K}_{sc}$ are shown in Appendix A. Previous matrices are then used to compute the PSD matrix of TBL excitation, $\mathbf{S}_{TBL}(\omega)$, the PSD matrix of the coupled shells displacement, $\mathbf{S}_{WW}(\omega)$, and the PSD matrix of the coupled acoustic cabin pressure, $\mathbf{S}_{PP}(\omega)$, as in [11, 24]. Finally, through the PSD matrices, one can obtain the PSD functions of the shells displacement, S_{ww}, and of the acoustic cabin pressure, S_{pp}, as

following

$$S_{ww}(x_1,\theta_1,x_2,\theta_2,\omega) = \sum_{m_{x_1},m_{x_2}=1}^{M_x^2} \sum_{m_{\theta_1},m_{\theta_2}=1}^{M_\theta^2} \alpha_{m_{x_1}}(x_1)\alpha_{m_{x_2}}(x_2) \beta_{m_{\theta_1}}(\theta_1)\beta_{m_{\theta_2}}(\theta_2)\mathbf{S}_{WW}(\omega)_{m_1 m_2} \tag{24}$$

$$S_{pp}(x_1,\theta_1,r_1,x_2,\theta_2,r_2,\omega) = \sum_{n_{x_1},n_{x_2}=0}^{N_x^2} \sum_{n_{\theta_1},n_{\theta_2}=0}^{N_\theta^2} \sum_{n_{r_1},n_{r_2}=0}^{N_r^2} \psi_{n_{x_1}}(x_1)\psi_{n_{x_2}}(x_2)\phi_{n_{r_1}}(\theta_1)\phi_{n_{r_2}}(\theta_2)\Gamma_{n_{\theta_1}}(r_1)\Gamma_{n_{\theta_2}}(r_2)\mathbf{S}_{PP}(\omega)_{n_1 n_2} \tag{25}$$

Finally, the overall-average PSD functions, $S_{ww}(\omega)$ and $S_{pp}(\omega)$, are obtained by integration of $S_{ww}(x_1,\theta_1,x_2,\theta_2,\omega)$ over the shell area and of $S_{pp}(x_1,\theta_1,r_1,x_2,\theta_2,r_2,\omega)$ over the cabin volume. Closed-form analytical expressions obtained for functions $S_{ww}(\omega)$ and $S_{pp}(\omega)$ are shown in Appendix B.

4 Results

4.1 Validation of the Analytical Model

Two independent studies are utilized as validation cases for the analytical framework. The first validation case, [13], shows a theoretical model, based on the power balance method of analysis, for the prediction of sound transmission into a aluminum cylinder under a broad band random excitation. In [13] predictions were also compared with experimental measurements, and statistical significant differences were identified, which were related to input data deficiencies. The properties of the physical system used for the validation case 1 are shown in Table 1, and the average damping ratios for each one-third octave band are provided in [13]. Part (b) of Fig. 2 shows the noise reduction results and measurements obtained in [13], while part (a) displays the noise reduction obtained through our analytical framework. To obtain our analytical results, a total number of $M_x = 30$ and $M_\theta = 30$ shell modes, and $N_x = 12$, $N_\theta = 8$ and $N_r = 8$ acoustic modes were necessary. By comparing parts (a) and (b) of Fig. 2, it can be concluded that our analytical framework provides a good approximation to the experimental data limits.

The second validation case is the study described by [34]. This study presents a numerical formulation based on a variational approach, in order to investigate the vibroacoustic behavior of an isotropic thin cylindrical shell, with and without an internal floor partition. The numerical results are also compared with experimental results. The boundary conditions at the two ends of the cylinder are assumed to be simply supported. The properties of the physical system are shown in Table 2. Figure 3(b) displays the results from [34], showing the acoustic effect of the floor on the internal pressure filed. Figure 3(a) shows the SPL results obtained through our analytical framework, considering a random excitation applied to the shell. To obtain the analytical results, a total number of $M_x = 15$ and $M_\theta = 15$ shell modes, and $N_x = 10$, $N_\theta = 10$ and $N_r = 10$ acoustic modes were used to achieve convergence. Comparing the analytical predictions in part (a) and part (b) (solution without attached floor), it can be concluded that our analytical model provides an overall good prediction of the interior SPL. The difference between the results in parts (a) and (b) may be explained by the differences in the shape of the cylindrical acoustic cavity - i.e., while in our model a purely cylindrical acoustic enclosure is considered, in [34] the existence of an internal floor changes the shape of the acoustic enclosure, which directly affects the acoustic natural modes, and thus the interior acoustic field.

4.2 Cylindrical Cabin composed by a Set of Shells

The study by [12,19] was used as the basis for this part of the work, and is refereed as case 3. It investigates the reduction and sound transmission through a single aircraft fuselage panel, excited by the TBL, into a cylindrical acoustic enclosure. The model analyzed is of a typical aircraft panel coupled to the interior acoustics of a rigid-wall cylinder. The dimensions of the curved panel have been selected to approximate the Boeing 737 fuselage sub-panels, while the dimensions of the cylinder approximate the size of a Boeing 737 fuselage. Properties of the physical system are defined in Table 3. Results for the shell vibration and interior acoustic field are presented. Using our analytical model, predictions were calculated for three different cases, using the dimensions and properties in [12, 19] as a basis, as follows: (1) single shell, excited by random white noise, coupled with the cylindrical enclosure; (2) the same single shell, but now excited by the TBL, coupled with the same cylindrical enclosure; (3) twelve shells (of the same dimensions and properties as the previous ones, and all located along the same x-coordinate), excited by the TBL, and coupled with the same cylindrical enclosure. Figures 4 and 5 show,

Table 1. Physical system properties for the validation case 1.

Symbol	Description	Value
a	Shell length	1.1938 m
h_s	Shell thickness	0.0016 m
R	Cylinder radius	0.254 m
L_x	Acoustic enclosure length	1.2192 m
ρ_0	Internal air density	1.21 Kg m^{-3}
c_0	Internal air speed of sound	343 m s^{-1}

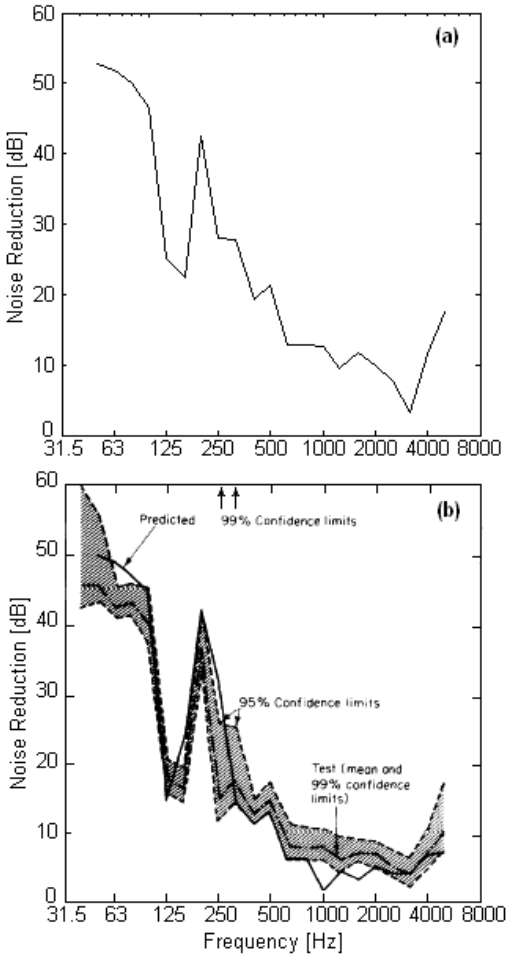

Fig. 2. Noise reduction for the validation case 1. (a) From our analytical framework. (b) From [13]: —— predictions, - - - measurements.

respectively, the results for the shell vibration levels and sound pressure levels, in which parts (a), (b) and (c) are obtained through our analytical model, and parts (d) are results from [12].

The first result is shown in Fig. 4 which depicts the shell velocity response due to the TBL and random excitations. Parts (a) and (b) show the analytical predictions for shell velocity at specific points in the surface of the shell, while part (c) shows the average shell velocity. The in vacuo shell natural mode frequencies are shown in Table 4. It can be observed, for both local and average values, that the shell response due to the TBL differs from the shell response due to the random excitation, mainly for frequencies above approximately $338Hz$, i.e., above the first shell natural mode. This result should be expected as the white random excitation has a flat power spectral density, exciting all the frequencies with the same power,

Table 2. Physical system properties for the validation case 2.

Symbol	Description	Value
a	Shell length	1.209 m
h_s	Shell thickness	0.0032 m
E_s	Shell Elasticity Modulus	2.07×10^{11} N m^2
ρ_s	Shell density	7860 Kg m^{-3}
ν_s	Shell Poisson's ratio	0.3
ξ_s	Structural damping ratio	0.01
R	Cylinder radius	0.254 m
L_x	Acoustic enclosure length	1.1684 m
ρ_0	Internal air density	1.2 Kg m^{-3}
c_0	Internal air speed of sound	343 m s^{-1}
ξ_{ac}	Acoustic damping ratio	0.01

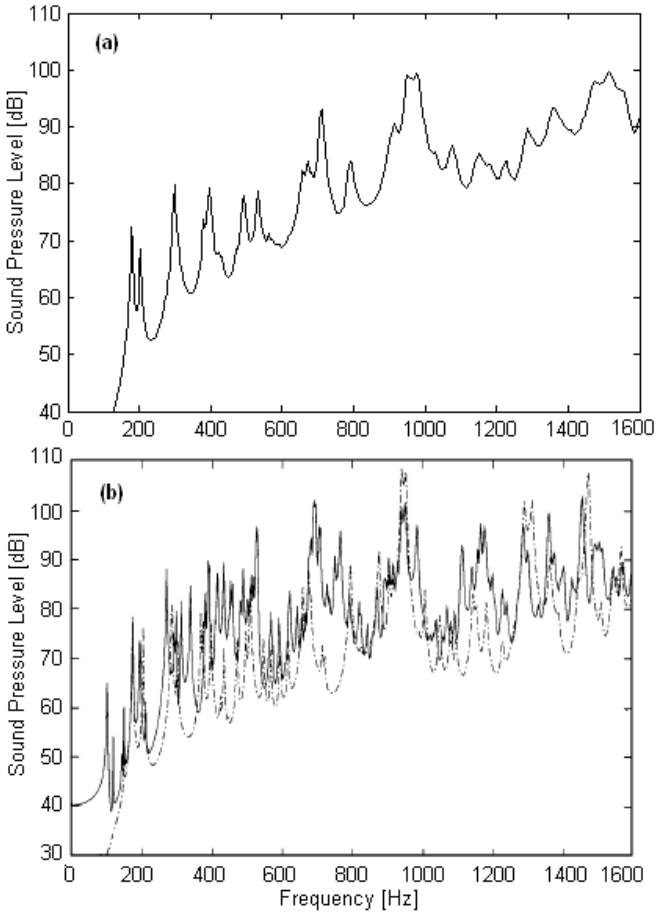

Fig. 3. SPL for the validation case 2. (a) From our analytical framework. (b) From [34]: —— with attached floor, - - - without attached floor.

Table 3. Physical system properties for the validation case 3.

Symbol	Description	Value
a	Shell length	0.508 m
θ_0	Shell arc	0.131 rad
h_s	Shell thickness	0.0018 m
E_s	Shell Elasticity Modulus	6.93×10^{10} N m^2
ρ_s	Shell density	2680 Kg m^{-3}
ν_s	Shell Poisson's ratio	0.33
ξ_s	Structural damping ratio	0.05
R	Cylinder radius	1.75 m
L_x	Acoustic enclosure length	43.18 m
ρ_0	Internal air density	1.21 Kg m^{-3}
c_0	Internal air speed of sound	343 m s^{-1}
ξ_{ac}	Acoustic damping ratio	0.05

Table 4. First 12 shell natural frequencies.

(m_x, m_θ)	Frequency, Hz
(1,1)	338
(2,1)	437
(3,1)	562
(4,1)	697
(1,2)	699
(2,2)	748
(3,2)	834
(5,1)	851
(4,2)	955
(6,1)	1032
(5,2)	1108
(1,3)	1184

while the TBL excitation power spectral density varies through the frequency spectrum, exciting the low frequencies with higher power than the high frequencies.

Comparing the solid line results in part (c) with the results in (d), it can be concluded that the curves follow the same tendency, generally decreasing with the frequency for frequencies above the first shell natural mode. The main difference between these two plots is in their respective peaks. While in the curve in part (d) only the plate modes were considered, in our analysis results, displayed in part (c), also the acoustic modes were taken into account. The effect of changing the observation point is analyzed in parts (a) and (b). It is shown that dissimilar shell vibration curves are found for different points of the shell. For instance, while at position $(x,\theta) = (0.5a, 0.5\theta_0)$ the first peaks correspond to the $(1,1)$, $(3,1)$, $(5,1)$ shell modes (i.e. it is not sensitive to modes with nodes at the center of the shell), the first peaks for the position $(x,\theta) = (0.33a, 0.5\theta_0)$

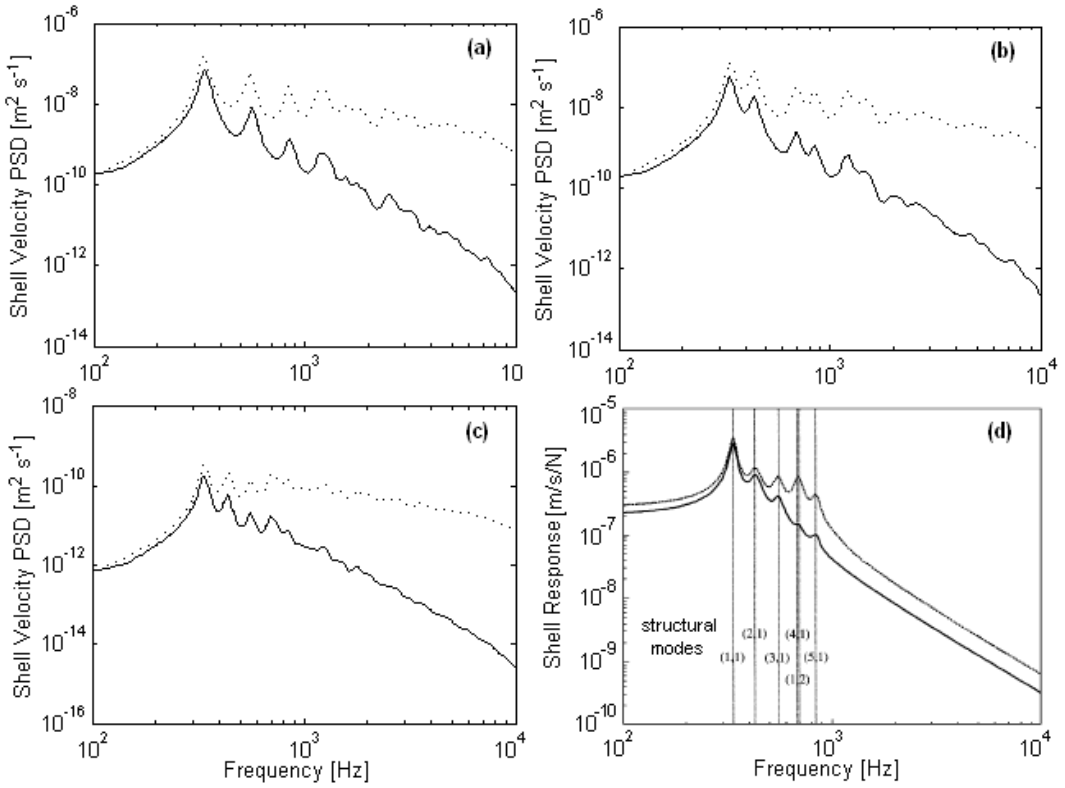

Fig. 4. Shell vibration level. From our analytical framework: (a) at $(x,\theta) = (0.5a, 0.5\theta_0)$, (b) at $(x,y) = (0.33a, 0.5\theta_0)$, and (c) average values; $\cdots$, random excitation; ——, TBL excitation. From [12]: (d).

correspond to the shell modes $(1,1)$, $(2,1)$, $(4,1)$. Furthermore, it is shown that predictions for average and local values of the shell velocity are different. These results demonstrate the significance of including the position as an important variable in the development of predictive models.

The sound pressure level analytical predictions obtained for the three different excitations are shown in parts (a) through (c) of Fig. 5. Part (c) displays average values, over the cabin volume, while parts (a) and (b) show the predictions for two specific points inside the cabin. Here, and similarly to what was observed in Fig. 4, it is shown that the random excitation is responsible for a higher amplification in the frequency range above $338Hz$, than the observed for the TBL excitation. In fact, it is observed that compared with the case of the 12 shells excited by the TBL (the bold curve), a single shell, excited by white noise, can be responsible for generating a higher SPL for frequencies above approximately $1000Hz$. Comparing the SPL from a single shell excited by the TBL, and the SPL from the 12 shells excited by the TBL, it is clear that increasing the number of shells causes an overall increase in SPL. Analyzing the results in parts (a) through (d), it is noted that SPL has the tendency to increase in the range $100-338Hz$ (below the shell first mode), and then a general decrease is observed. However, the increase in the number of shells can be responsible for changing the shape of the SPL over the frequency, as seen by the results obtained for point $(x,\theta,r) = (0.3L_x, 0.5\theta_0, 0.5R)$, in part (a). Again, the differences between plots in parts (a)/(b)/(c) and in part (d) can be attributed to the dissimilar number of acoustic modes considered in both analyzes.

As can be observed in Fig. 5, SPL curves show a much more complex prediction compared with the shell vibration curves. In fact, it is clear that peaks in the SPL curves correspond not only to structural but also to acoustic modes. Specifically, for frequencies below the first shell resonance, the observed peaks correspond to acoustic modes, showing the importance of including the acoustic field contribution in the development of the analytical model. Considering the results for position $(x,\theta,r) = (0.3L_x, 0.5\theta_0, 0)$, in part (b) of Fig. 5, the two peaks below the first shell resonance frequency correspond to frequencies $121Hz$ and $222Hz$, and to acoustic modes $(5,1,0)$ and $(8,2,0)$, respectively. In part (a), the results for point $(x,\theta,r) = (0.3L_x, 0.5\theta_0, 0.5R)$ have the peaks at frequencies $169Hz$ and $221Hz$, corresponding to acoustic modes $(8,1,1)$ and $(8,1,2)$. Note that acoustic mode shapes for modes with $n_x = 5$ and $n_x = 8$ have maximum amplitude at and near the position $x = 0.3L_x$. Depending on the location, each mode has a dissimilar amplification, with their importance shifting from point to point. Results show that not only SPL is dependent on the position, but also different from the average values shown in part (c). This leads to the conclusion that the ability of the model to predict average and local values is essential to obtain an accurate prediction of the reality.

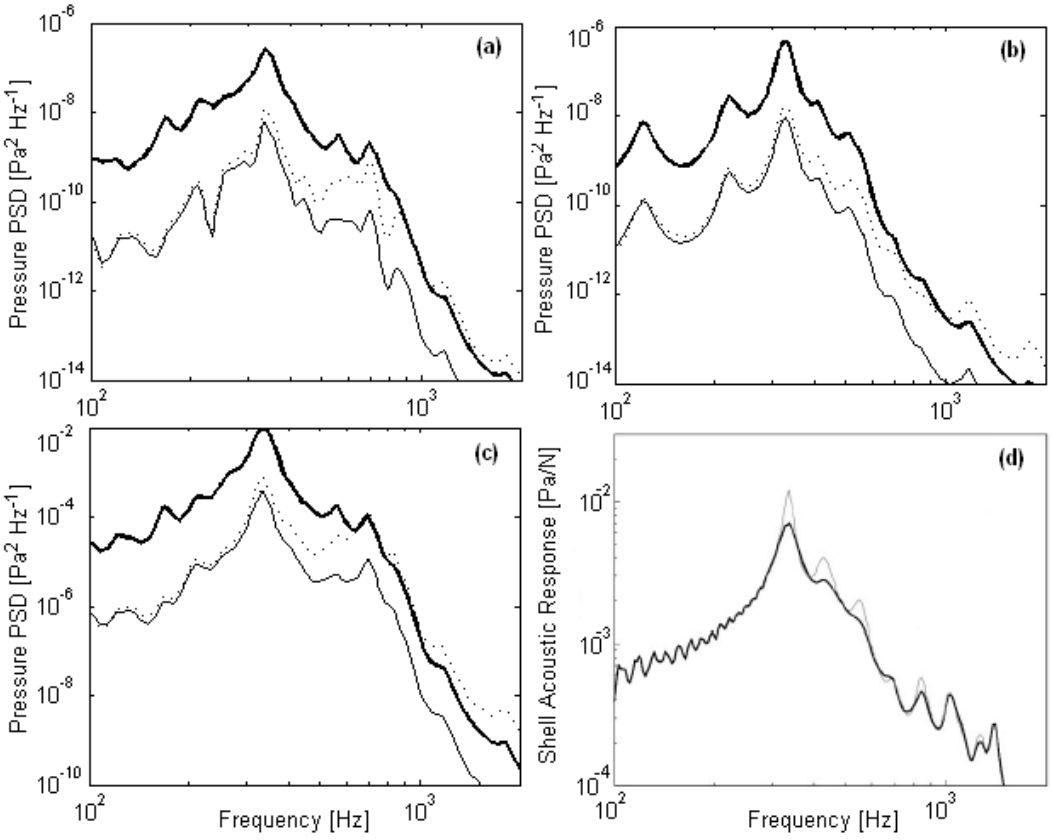

Fig. 5. Sound pressure levels. From our analytical framework: (a) at $(x,\theta,r) = (0.3L_x, 0.5\theta_0, 0.5R)$, (b) at $(x,\theta,r) = (0.3L_x, 0.5\theta_0, 0)$, and (c) average values; $\cdots$, 1 shell excited by random noise; ——, 1 shell excited by the TBL; ——, 12 shells excited by the TBL. From [12]: (d).

5 Conclusions

This study presents the development of an analytical model and gives closed-form expressions for the prediction of flow-induced noise in aircraft cylindrical cabins. The model was developed considering the full structural-acoustic coupling, and results were obtained for frequencies up to $10,000Hz$. The analytical predictions were successfully validated through the good agreement with several independent studies. The closed-form analytical expressions can be easily used for the prediction of shell structural vibration and interior sound pressure levels for a wide range of shell-cylindrical cabin type of systems, by just changing the system parameters and properties. Furthermore, the analytical framework can be used to predict vibration and noise levels for cylindrical systems with one or more vibrating shells, excited by turbulent flow or by random noise.

Analytical predictions were obtained for several different systems. It was noted that the random noise excitation is responsible for a higher amplification of shell vibration and interior noise for frequencies above the first shell natural mode, when compared with the turbulent boundary layer excitation. Additionally, the obtained results reflect the importance of including the acoustic field in the analytical model development in order to obtain an accurate prediction of the cabin sound pressure level. It is predicted that increasing the number of vibrating shell results in an overall increase of interior noise levels. However, depending on the location under consideration, increasing the number of vibrating shells may also result in a different SPL curve over the frequency spectrum, when compared with the SPL curve obtained for single shell vibration. Finally, the models show that average and local values of vibration and interior sound are dissimilar. This can be of particular interest in the design and implementation of noise control systems, where the accurate prediction of localized noise levels is crucial. This emphasizes the importance of including the effect of position change in the model used to predict the sound transmission to aircraft interiors.

Achnowledgements

The authors would like to thank to the Portuguese Foundation for Science and Technology.

References

[1] Bishop, D., 1961. "Cruise flight noise levels in a turbojet transport airplane". *Noise Control,* **7**, pp. 37–42.

[2] Frampton, K., and Clark, R., 1997. "Power flow in an aeroelastic plate backed by a reverberant cavity". *Journal of the Acoustical Society of America,* **102**(3), pp. 1620–1627.

[3] Maestrello, L., 1965. "Measurement of noise radiated by turbulent boundary layer excited panels". *Journal of Sound and Vibration,* **2**(2), pp. 100–115.

[4] Davies, H., 1971. "Sound from turbulent boundary layer excited panels". *Journal of the Acoustical Society of America,* **55**, pp. 213–219.

[5] Allen, M., and Vlahopoulos, N., 2001. "Noise generated from a flexible and elastically supported structure subject to turbulent boundary layer flow excitation". *Finite Elements in Analysis and Design,* **37**, pp. 687–712.

[6] Henry, J., and Clark, R., 1999. "A curved piezo-structure model: Implications on active structural acoustic control". *Journal of the Acoustical Society of America,* **106**(3), pp. 1400–1407.

[7] Liu, B., 2008. "Noise radiation of aircraft panels subjected to boundary layer pressure fluctuations". *Journal of Sound and Vibration,* **314**, pp. 693–711.

[8] Barton, C., and Daniels, E., 1978. Noise transmission through flat rectangular panels into a closed cavity. Tech. Rep. NASA TP-1321.

[9] Heatwole, C., Bernhard, R., and Francheck, M., 1997. Robust feedback control of flow induced structural radiation of sound. Tech. Rep. NASA 0278-1.

[10] Smith, G., Clark, R., and Frampton, K., 1998. "Optimal transducer placement for active control of sound transmission through aeroelastic plates". *Journal of the Intelligent Material Systems and Structures,* **9**, pp. 975–987.

[11] da Rocha, J., Suleman, A., and Lau, F., 2009. "Prediction of flow-induced noise in transport vehicles: development and validation of a coupled structural-acoustic analytical framework". *Canadian Acoustics,* **37**(4), pp. 13–29.

[12] Henry, J., and Clark, R., 2002. "Active control of sound transmission through a curved panel into a cylindrical enclosure". *Journal of Sound and Vibration,* **249**(2), pp. 325–349.

[13] Pope, L., Rennison, D., Willis, C., and Mayes, W., 1982. "Development and validation of preliminary analytical models for aircraft interior noise reduction". *Journal of Sound and Vibration,* **82**(4), pp. 541–575.

[14] Narayanan, S., and Shanbhag, R., 1984. "Sound transmission through layered cylindrical shells with applied damping treatment". *Journal of Sound and Vibration,* **92**(4), pp. 541–558.

[15] Vaicaitis, R., 1986. "Noise transmission into enclosures". In 4th International Modal Analysis Conference, Los Angeles, CA, February 3-6, pp. 1088–1097.

[16] Gardonio, P., Fergunson, N., and Fahy, F., 2001. "A modal expansion analysis of noise transmission through circular cylindrical shell structures with blocking masses". *Journal of Sound and Vibration,* **244**(2), pp. 259–297.

[17] Li, D., and Vipperman, S., 2005. "Mathematical model for characterizing noise transmission into finite cylindrical structures". *Journal of the Acoustical Society of America,* **117**(2), pp. 679–689.

[18] Chang, M., and Vaicaitis, R., 1982. "Noise transmission into semicylindrical enclosures through discretely stiffened curved panels". *Journal of Sound and Vibration,* **85**(1), pp. 71–83.

[19] Henry, J., and Clark, R., 2001. "Noise transmission from a curved panel into a cylindrical enclosure: Analysis of structural acoustic coupling". *Journal of the Acoustical Society of America,* **109**(4), pp. 1456–1463.

[20] Lane, S., Clark, R., and Southward, S., 2000. "Active control of low frequency modes in an aircraft fuselage using spatially weighted arrays". *Journal of Vibration and Acoustics,* **122**, pp. 227–234.

[21] Bevan, J., 2001. Piezoceramic actuator placement for actuator control of panels. Tech. Rep. NASA CR-211265.

[22] et al, K. T., 2002. "Noise and vibration reduction technology in aircraft cabins". *Advanced Composite Materials,* **13**(1), pp. 67–80.

[23] Esteve, S., and Johnson, E., 2002. "Reduction of sound transmission into a circular cylindrical shell using distributed vibration absorbers and helmholtz resonators". *Journal of the Acoustical Society of America,* **112**(6), pp. 2840–2848.

[24] da Rocha, J., Suleman, A., and Lau, F., 2010. "Turbulent flow-induced noise in the cabin of a bwb aircraft". In Proceedings of the Canadian Society for Mechanical Engineering Forum 2010, Victoria, BC, June 7-9.

[25] Corcos, G., 1964. "The structure of the turbulent pressure field in boundary layer flows". *Journal of Fluid Mechanics - Cambridge Journal Online,* **18**, pp. 353–378.

[26] Corcos, G., 1963. "Resolution of pressure in turbulence". *Journal of the Acoustical Society of America,* **35**(2), pp. 192–199.

[27] Graham, W., 1997. "A comparison of models for the wavenumber frequency spectrum of turbulent boundary layer pressures". *Journal of Sound and Vibration,* **206**(4), pp. 541–565.

[28] Efimtsov, B., 1982. "Characteristics of the field of turbulent wall pressure fluctuations at large reynolds numbers". *Soviet Physics-Acoustics,* **28**(4), pp. 289–292.

[29] da Rocha, J., Suleman, A., and Lau, F., 2010. "Turbulent boundary layer induced noise and vibration of a multi-panel walled acoustic enclosure". *Canadian Acoustics (In Press),* **38**(4).

[30] Leissa, A., 1973. *Vibration of Shells*. National Aeronautics and Space Administration, Washigton, D.C.

[31] Blevins, J., 2001. *Formulas for Natural Frequency and Mode Shape*. Krieger Publishing Company, Malabar, FL.
[32] Vaicaitis, R., Grosveld, F. W., and Mixson, J. S., 1985. "Noise transmission through aircraft panels". *Journal of Aircraft,* **22**(4), pp. 303–310.
[33] Sampath, A., and Balachandran, B., 1999. "Active control of multiple tones in an enclosure". *Journal of the Acoustical Society of America,* **106**(1), pp. 211–225.
[34] Missaoui, J., and Cheng, L., 1999. "Vibroacoustic analysis of a finite cylindrical shell with internal floor partition". *Journal of Sound and Vibration,* **226**(1), pp. 101–123.

Appendix A: Expressions for Matrices $\mathbf{M}_{cs}$ and $\mathbf{K}_{sc}$

The system matrices $\mathbf{M}_{cs}$ and $\mathbf{K}_{sc}$ are obtained, respectively, by developing expressions in Eqs.(21) and (22), resulting in the following closed-form expressions:

$$\mathbf{M}_{cs} = \rho_0 \left[A_{n_r} B_{m_x n_x} B_{m_\theta n_r} \right], \tag{26}$$

$$\mathbf{K}_{sc} = \frac{(\nu_s^2 - 1) R^2}{E_s h_s} \left[A_{n_r} B_{m_x n_x} B_{m_\theta n_r} \right], \tag{27}$$

in which, for a closed cylindrical shell with simply supported end caps, $B_{m_x n_x}$ and $B_{m_\theta n_r}$ are defined by

$$B_{m_x n_x} = \frac{\sqrt{2} A_{n_x}}{L_x} \begin{cases} 0, & m_x = n_x \\ f_1(Lx) - f_1(0), & m_x \neq n_x, \end{cases} \tag{28}$$

with

$$f_1(x) = -\frac{\cos\left[(m_x + n_x)\pi x\right]}{2(m_x + n_x)\pi} - \frac{\cos\left[(m_x - n_x)\pi x\right]}{2(m_x - n_x)\pi}, \tag{29}$$

and

$$B_{m_\theta n_r} = \begin{cases} 1, & m_\theta = n_r \\ 0, & m_\theta \neq n_r \, . \end{cases} \tag{30}$$

Considering the open cylindrical shell, $B_{m_x n_x}$ and $B_{m_\theta n_r}$ are defined by

$$B_{m_x n_x} = \sqrt{\frac{2}{a L_x}} A_{n_x} \begin{cases} 0, & \left(\frac{m_x}{a} = \frac{n_x}{L_x}\right) \\ f_2(x_f) - f_2(x_i), & \left(\frac{m_x}{a} \neq \frac{n_x}{L_x}\right) \wedge \frac{x_i}{a} \text{ odd} \wedge m_x \text{ odd} \\ f_3(x_f) - f_3(x_i), & \text{otherwise} \end{cases} \tag{31}$$

with

$$f_2(x) = \frac{\cos\left[\left(\frac{m_x}{a} + \frac{n_x}{L_x}\right)\pi x\right]}{2\left(\frac{m_x}{a} + \frac{n_x}{L_x}\right)\pi} + \frac{\cos\left[\left(\frac{m_x}{a} - \frac{n_x}{L_x}\right)\pi x\right]}{2\left(\frac{m_x}{a} - \frac{n_x}{L_x}\right)\pi}, \tag{32}$$

$$f_3(x) = -f_2(x), \tag{33}$$

and

$$B_{m_\theta n_r} = \sqrt{\frac{2}{\pi\theta_0}} \begin{cases} 0, & \left(\frac{m_\theta \pi}{\theta_0} = n_r\right) \\ f_4(\theta_f) - f_4(\theta_i), & \left(\frac{m_\theta \pi}{\theta_0} \neq n_r\right) \wedge \frac{\theta_i}{\theta_0} \text{ odd} \wedge m_\theta \text{ odd} \\ f_5(x_f) - f_5(x_i), & \text{otherwise} \end{cases} \tag{34}$$

with

$$f_4(\theta) = \frac{\cos\left[\left(\frac{m_\theta \pi}{\theta_0} + n_r\right)\theta\right]}{2\left(\frac{m_\theta \pi}{\theta_0} + n_r\right)} + \frac{\cos\left[\left(\frac{m_\theta \pi}{\theta_0} - n_r\right)\theta\right]}{2\left(\frac{m_\theta \pi}{\theta_0} - n_r\right)}, \tag{35}$$

$$f_5(\theta) = -f_4(\theta). \tag{36}$$

Appendix B: Expressions for $S_{ww}(\omega)$ and $S_{pp}(\omega)$

Functions $S_{ww}(\omega)$ and $S_{pp}(\omega)$ are obtained through the integration of $S_{ww}(x_1, \theta_1, x_2, \theta_2, \omega)$ over the shell surface and $S_{pp}(x_1, \theta_1, r_1, x_2, \theta_2, r_2, \omega)$ over the cabin volume, respectively. For a closed circular cylindrical shell with simply supported end caps, the $S_{ww}(\omega)$ closed-form analytical expression can be defined by

$$S_{ww}(\omega) = \sqrt{\frac{2}{L_x \pi}} \sum_{m_x=1}^{M_x} \sum_{m_{x'}=1}^{M_x} \sum_{m_\theta=1}^{M_\theta} \sum_{m_{\theta'}=1}^{M_\theta} C_{m_x m_{x'}} C_{m_\theta m_{\theta'}} \mathbf{S}_{WW}(\omega)_{mm'} \tag{37}$$

with

$$C_{m_x m_{x'}} = \begin{cases} \frac{L_x^2}{2}, & m_x = m_{x'} \\ \frac{L_x^2}{m_x m_{x'} \pi^2} \left[\cos(m_x \pi) - 1\right] \left[\cos(m_{x'} \pi) - 1\right], & m_x \neq m_{x'} \end{cases} \tag{38}$$

and

$$C_{m_\theta m_{\theta'}} = \begin{cases} 2\pi^2, & m_\theta = m_{\theta'} \\ 0, & m_\theta \neq m_{\theta'} \end{cases}. \tag{39}$$

Considering the cylindrical open shell, the closed-form expression for $S_{ww}(\omega)$ is

$$S_{ww}(\omega) = \frac{4}{a\theta_0} \sum_{m_x=1}^{M_x} \sum_{m_{x'}=1}^{M_x} \sum_{m_\theta=1}^{M_\theta} \sum_{m_{\theta'}=1}^{M_\theta} D_{m_x m_{x'}} D_{m_\theta m_{\theta'}} \mathbf{S}_{WW}(\omega)_{mm'} \tag{40}$$

with

$$D_{m_x m_{x'}} = \begin{cases} \frac{a^2}{2}, & m_x = m_{x'} \\ \frac{a^2}{m_x m_{x'} \pi^2} \left[\cos(m_x \pi) - 1\right] \left[\cos(m_{x'} \pi) - 1\right], & m_x \neq m_{x'} \end{cases} \tag{41}$$

and

$$D_{m_\theta m_{\theta'}} = \begin{cases} \frac{\theta_0^2}{2}, & m_\theta = m_{\theta'} \\ \frac{\theta_0^2}{m_\theta m_{\theta'} \pi^2} \left[\cos(m_\theta \pi) - 1\right] \left[\cos(m_{\theta'} \pi) - 1\right], & m_\theta \neq m_{\theta'} \end{cases} \tag{42}$$

Finally, the closed-form expression for $S_{pp}(\omega)$ may be defined by

$$S_{pp}(\omega) = \sum_{n_x=0}^{N_x}\sum_{n_{x'}=0}^{N_x}\sum_{n_\theta=0}^{N_\theta}\sum_{n_{\theta'}=0}^{N_\theta}\sum_{n_r=0}^{N_r}\sum_{n_{r'}=0}^{N_r} \frac{A_{n_x}A_{n_{x'}}A_{n_r}A_{n_{r'}}\mathbf{S}_{PP}(\omega)_{nn'}}{L_x\pi R^2 J_{n_r}(\lambda_{n_r n_\theta})J_{n_{r'}}(\lambda_{n_{r'}n_{\theta'}})} E_{n_x n_{x'}}E_{n_\theta n_{\theta'}}E_{n_r n_{r'}} \tag{43}$$

in which

$$E_{n_x n_{x'}} = \begin{cases} \frac{L_x^2}{2}, & n_x = n_{x'} \\ 0, & n_x \neq n_{x'} \end{cases} \tag{44}$$

$$E_{n_\theta n_{\theta'}} = \begin{cases} 2\pi^2, & n_\theta = n_{\theta'} \\ 0, & n_\theta \neq n_{\theta'} \end{cases} \tag{45}$$

and

$$E_{n_r n_{r'}} = 4\sum_{k=0}^{K} J_{n_r+2k+1}(\lambda_{n_r n_\theta})\sum_{k'=0}^{K'} J_{n_{r'}+2k'+1}(\lambda_{n_{r'}n_{\theta'}}) \tag{46}$$

List of Figures

List of Tables

Appendix E

On the Sensitivity of Sound Power Radiated by Aircraft Panels to Turbulent Boundary Layer Parameters

On the Sensitivity of Sound Power Radiated by Aircraft Panels to Turbulent Boundary Layer Parameters

Joana da Rocha[a,*], Dan Palumbo[b]

[a] *University of Victoria, Department of Mechanical Engineering, 3800 Finnerty Road, Victoria, BC, V8W 2Y2 Canada*
[b] *Structural Acoustics Branch, NASA Langley Research Center, 2 North Dryden Street, Hampton, VA, 23681-2199 USA*

Abstract

The objective of the present study is to investigate and quantify how sensitive the response of an aircraft panel is to the change of the turbulent flow parameters. Several empirical models exist nowadays that provide the turbulent boundary layer wall pressure cross spectrum. These wall pressure cross spectrum models are usually dependent on four parameters: the reference power spectrum, the flow convective velocity, and the coherence lengths in streamwise and spanwise directions. All the proposed models provide different predictions for the wall pressure cross spectrum. Also, real flow conditions over aircraft do not conform to the ideal behavior of the turbulent boundary layer pressure predicted by the models. In this context, the questions that this work aims to explore are "What is the impact of different wall pressure estimates in the radiated sound power?" and "What is the effect of the range of possible flow conditions on the radiated sound power?". For that objective, data from flight tests and estimates provided by the empirical models are used to predict radiated sound power, and the results are compared. A sensitivity analysis is performed and the relative contribution of each boundary layer parameter to the radiated sound power is obtained.

Keywords:
Turbulent Boundary Layer, Wall Pressure Spectral Density, Radiated Sound Power, Aircraft Panel

*Corresponding author. Tel.: +1-250-721-8923; Fax: +1-250-721-6051.
Email addresses: jdarocha@uvic.ca (Joana da Rocha), d.l.palumbo@nasa.gov (Dan Palumbo)

1. Introduction

The turbulent boundary layer (TBL) wall pressure modeling has been a subject of investigation for several years. Several empirical models have been developed to predict the TBL wall pressure spectrum, as described in [1, 2]. The models were developed to describe the TBL wall pressure fluctuations on a flat plate, and it is assumed that the TBL power spectral density (PSD) can be expressed as a stationary and homogeneous function, for zero mean pressure gradient. It is well established that the TBL cross power spectral density can be expressed as a product of a reference PSD function and a correlation function, such as described in [3 - 8]. The correlation function is usually written in a separable form in the streamwise and spanwise direction, in which streamwise and spanwise functions decay exponentially with the distance. In this work, the Corcos [3, 4] and Efimtsov [5] models were used to provide the TBL parameters and to relate with the flight tests data. The objective is to compare the experimental data with the empirical results, and establish a quantitative analysis on the produced plate radiated sound power (RSP). The experimental data for the present study were acquired in a flight test that was a cooperative work between the Gulfstream Aerospace Corporation, Boeing Commercial Airplanes and the National Aeronautics and Space Administration (NASA) [9].

The wall pressure spectrum provided by Corcos model [3, 4] is dependent on four parameters: (1) the reference power spectrum function, (2) the flow convective velocity (associated with the flow Mach number), (3) and (4) the coherence lengths in the streamwise and spanwise directions. The Corcos model assumes that coherence lengths are directly proportional to the convection velocity, and inversely proportional to the frequency and an empirical parameter. The fact that the coherence lengths are inversely proportional to frequency leads to the prediction that they tend to infinity as the frequency approaches zero. This problem is overcome by Efimtsov model [5], which considers the coherence lengths also dependent on the boundary layer thickness, δ, Strouhal number, Sh, and friction velocity, U_τ. In the comparison of models by [2], the Efimtsov model [5] is cited as a suitable candidate, being the only model derived from aircraft rather than laboratory measurements. Flight tests of Tupolev 144LL aircraft, conducted at the Flying Laboratory in Russia, NASA and Boeing [10], demonstrated that the model developed

by Efimtsov has the best agreement with the experimental data.

At cruise conditions, turbulent boundary layer pressure fluctuations on the exterior of the fuselage are a major source of noise inside jet aircraft [11, 12], and is more significant as the flight Mach number increases, as shown in [13] for subsonic Mach number. The TBL induces vibrations on the fuselage skin, and the vibrating structure radiates noise into the aircraft cabin. Early experimental tests have been conducted as an effort to characterize the radiation of sound from single panels excited by the turbulent boundary layer [14 - 18]. These studies provide knowledge about the shape of the spectrum, convection velocity and space-time correlation of the TBL pressure fluctuations on aircraft panels, as well as displacement and acceleration spectra of the vibrating panels. In [16], the aircraft panel acceleration spectra was measured for two locations on the fuselage - a forward location and a aft location -, and for three flight Mach numbers. In both locations, the measurements were performed at the center of the panels. At these measurement points, the acceleration spectra showed maximum vibration around 1000 Hz, and the phenomenon of hydrodynamic coincidence was identified to occur in the neighborhood of $1000Hz$, at Mach number 0.6. In addition, several theoretical studies have been performed for the vibration and sound radiated by panels excited by turbulent flows [19 - 24].

The present study deals with the RSP of aircraft panels subjected to TBL excitation. The structural vibration response PSD is obtained through a previously validated model developed by the author [25]. The panel is assumed to be simply supported in the all four boundaries. The RSP is calculated for measured data and the Efimtsov model, and the results are compared. A sensitivity analysis is performed to investigate the influence of TBL parameters on RSP.

2. Flight Tests Data versus Predicted Data

The flight test data presented and analyzed in this section were obtained through a cooperative effort between the Gulfstream Aerospace Corporation, Boeing Commercial Airplanes and NASA. The tests were performed in a Gulfstream G550 aircraft, which has windows that provide a good platform for a long, streamwise, array of sensors. The sensor array was located in the first window of the G550 aircraft, at a distance of $6.7m$ from the nose. Detailed information about the flight test data, test bed instrumentation, data consistency and analysis are described in [9]. The flight tests measurements

were acquired at 3 different flight conditions, as shown in Table 1, which will be referred as Cases 1, 2 and 3 throughout this paper. Measurements of the TBL wall pressure PSD, and coherence lengths in the streamwise and spanwise directions were undertaken for the 3 flight conditions. Fig. 1 shows the TBL power spectrum for the 3 flight conditions and also the predicted TBL spectrum by the Efimtsov model for the respective 3 flight conditions. Fig. 2 shows the coherence lengths from flight measurements, and those predicted through Corcos and Efimtsov models. To obtain the predicted values for the coherence lengths for Corcos model, the following equations were used [3]:

$$L_x = \frac{U_c}{\alpha_x \omega}, \tag{1}$$

and

$$L_y = \frac{U_c}{\alpha_y \omega}, \tag{2}$$

in which U_c is the TBL convective velocity, ω is the angular frequency, $\alpha_x = 0.1$ and $\alpha_y = 0.77$. The coherence lengths predicted by the Efimtsov model were defined as following [5]:

$$L_x = \delta \left[\left(\frac{a_1 Sh}{U_c/U_\tau} \right)^2 + \frac{a_2^2}{Sh^2 + (a_2/a_3)^2} \right]^{-\frac{1}{2}}, \tag{3}$$

and

$$L_y = \begin{cases} \delta \left[\left(\frac{a_4 Sh}{U_c/U_\tau} \right)^2 + \frac{a_5^2}{Sh^2 + (a_5/a_6)^2} \right]^{-\frac{1}{2}}, & \text{for } M < 0.75 \\ \delta \left[\left(\frac{a_4 Sh}{U_c/U_\tau} \right)^2 + a_7^2 \right]^{-\frac{1}{2}}, & \text{for } M > 0.9 \end{cases}, \tag{4}$$

where δ is the TBL thickness, $U_\tau = U\sqrt{C_f/2}$ is the friction velocity, C_f is the friction coefficient, $Sh = \omega\delta/U_\tau$ is the Strouhal number, M is the flight Mach number, and constants a_1-a_7 are, respectively, 0.1, 72.8, 1.54, 0.77, 548, 13.5, and 5.66. Predicted L_y values for $M = 0.8$ were obtained through interpolation. Values for δ and C_f were calculated using the following equation for turbulent boundary layers [26, 27]:

$$\delta = 0.37\, x\, Re_x^{-\frac{1}{5}} \left[1 + \left(\frac{Re_x}{6.9 \times 10^7} \right)^2 \right]^{\frac{1}{10}}, \tag{5}$$

and

$$C_f = 0.37 \, (Log_{10} \, Re_x)^{-2.584}, \tag{6}$$

in which $Re_x = Ux/\nu$ is the Reynolds number. To calculate the TBL pressure spectrum, the following Efimtsov equation was used [10]:

$$S_{ref}(\omega) = 2\,\pi\,\alpha\,U_\tau^3\,\rho^2\,\delta\,\frac{\beta}{(1+8\alpha^3 Sh^2)^{\frac{1}{3}} + \alpha\,\beta\,Re_\tau\left(\frac{Sh}{Re_\tau}\right)^{\frac{10}{3}}}, \tag{7}$$

where $\alpha = 0.01$ and

$$\beta = \left[1 + \left(\frac{Re_{\tau_0}}{Re_\tau}\right)^3\right]^{\frac{1}{3}}. \tag{8}$$

The analysis of Fig. 1 shows that predicted and measured TBL spectrum differ from one another for the 3 flight conditions. Flight data PSD levels are bigger than predicted PSD, for frequencies between approximately 200Hz and 4KHz for Case 1 and Case 2, and for frequencies between approximately 350Hz and 2KHz for Case 3. At 1KHz, measured PSD is about 3dB higher than predicted PSD for Cases 1 and 2, and 2dB higher for Case 3. Even though one expects S_{ref} to increase with Mach number, the PSD for $M = 0.8$ has an overall lower amplitude compared with $M = 0.56$ and $M = 0.7$, since data for $M = 0.8$ is measured at higher altitude. Fig. 2 illustrates that measured and predicted coherence lengths also have different values. Measured coherence lengths are higher than lengths predicted by Efimtsov model, for low frequencies. Coherence lengths exhibit a maximum for Case 3, $M = 0.8$, measured data, opposite of what is observed with the PSD. These results suggest that real conditions in the aircraft TBL do not conform with the behavior predicted by the models. The fact that predicted and measured TBL parameters do not match exactly will have an effect on the RSP. Considering this, the objective of this work is to analyze what are the effects on the aircraft panel RSP, and the range of possible condition on RSP.

3. Panel Radiated Sound Power

The total acoustic pressure field radiated by a baffled panel, at an observation point, $\mathbf{R}$=(x, y, z), can be found from the Rayleigh integral [28, 29], as

$$p(x,y,z) = -\frac{i\omega\rho_0}{2\pi}\int_0^b\int_0^a \frac{v(x_s,y_s)e^{\frac{i\omega}{c_0}|\mathbf{R}-\mathbf{r}_s|}}{|\mathbf{R}-\mathbf{r}_s|}dx_s dy_s, \tag{9}$$

in which ρ_0 and c_0 are the density and the speed of sound of the interior fluid, respectively, ω is the angular frequency, $v(x_s, y_s)$ is the panel normal surface velocity, which is a function of the position in the panel, $\mathbf{r}_s$=(x_s, y_s). As described in [29], the analytical evaluation of this integral is facilitated by assuming that the plate is simply supported, the observer point, $R = |\mathbf{R} - \mathbf{r_s}|$ is in the far field, and that R is much greater than the characteristic dimension of the plate so that $R \approx r$. For the exponential term, the observation distance is normalized about the point $r = \mathbf{r}$, $\phi = 0$, $\theta = 0$, leading to the approximation $R \approx r - x\sin\theta\cos\phi - y\sin\theta\sin\phi$. Using this approximations, the acoustic field in the far field is defined by

$$p(x, y, z) = -i\omega\rho_0 \frac{e^{\frac{i\omega r}{c_0}}}{2\pi R} \int_0^b \int_0^a v(x_s, y_s) e^{-i\left(\frac{\alpha x}{a}\right) - i\left(\frac{\beta y}{b}\right)} dx_s dy_s, \tag{10}$$

where $\alpha = \frac{\omega}{c_0} a \sin\theta\cos\phi$ and $\beta = \frac{\omega}{c_0} b \sin\theta\sin\phi$. The panel surface velocity can be described through the panel natural modes by

$$v(x_s, y_s, t) = \sum_{m_x=1}^{M_x} \sum_{m_y=1}^{M_y} \alpha_{m_x}(x_s)\, \beta_{m_y}(y_s)\, V_{m_x m_y} e^{i\omega t}, \tag{11}$$

in which $\alpha_{m_x}(x_s) = \sin(m_x \pi x_s / a)$ and $\beta_{m_y}(y_s) = \sin(m_y \pi y_s / b)$ are the spatial functions, and $M = M_x \times M_y$ is the total number of plate modes (m_x, m_y) considered. Substituting Eq. (11) into Eq. (10), and integrating over the panel surface, the acoustic pressure associated with the m^{th} panel mode is given by

$$p(x, y, z) = -iV_{m_x m_y}\omega\rho_0 \frac{e^{\frac{i\omega r}{c_0}}}{2\pi R} \frac{ab}{m_x m_y \pi^2} \left[\frac{(-1)^{m_x} e^{-i\alpha} - 1}{(\alpha/m_x\pi)^2 - 1}\right] \left[\frac{(-1)^{m_y} e^{-i\beta} - 1}{(\beta/m_y\pi)^2 - 1}\right]. \tag{12}$$

The average acoustic power radiated by a mode from one side of the panel is found from [31]

$$\Pi_{m_x m_y} = \int_0^{2\pi} \int_0^{\frac{\pi}{2}} \frac{|p(x, y, z)|^2}{\rho_0 c_0} r^2 \sin\theta d\theta d\phi. \tag{13}$$

Substituting Eq. (12) into Eq. (13), and considering the symmetry of the acoustic field, the radiated sound power associated with the m^{th} mode is

obtained by

$$\Pi_{m_x m_y} = 8\frac{\rho_0}{c_0}\left(\frac{V_{m_x m_y}\omega ab}{\pi^3 m_x m_y}\right)^2 \int_0^{\frac{\pi}{2}}\int_0^{\frac{\pi}{2}} \left\{ \frac{\begin{matrix}\cos \\ \sin\end{matrix}\left(\frac{\alpha}{2}\right)\begin{matrix}\cos \\ \sin\end{matrix}\left(\frac{\beta}{2}\right)}{\left[\left(\frac{\alpha}{m_x\pi}\right)^2-1\right]\left[\left(\frac{\beta}{m_y\pi}\right)^2-1\right]} \right\}^2 \sin\theta d\theta d\phi, \tag{14}$$

where $\cos(\alpha/2)$ and $\cos(\beta/2)$ are used, respectively, when m_x and m_y are odd integers, and $\sin(\alpha/2)$ and $\sin(\beta/2)$ are used, respectively, when m_x and m_y are even integers. The radiated sound power matrix, containing the several $\Pi_{m_x m_y}$ components, can be defined by

$$\mathbf{\Pi}(\omega) = \mathbf{V}^T\mathbf{M}(\omega)\mathbf{V}, \tag{15}$$

in which $\mathbf{V}$ is the structural modal velocity vector, and $\mathbf{M}(\omega)$ is the radiation matrix, which is evaluated numerically, and given by

$$\mathbf{M}(\omega) = 8\frac{\rho_0}{c_0}\left(\frac{\omega ab}{\pi^3 m_x m_y}\right)^2 \int_0^{\frac{\pi}{2}}\int_0^{\frac{\pi}{2}} \left\{ \frac{\begin{matrix}\cos \\ \sin\end{matrix}\left(\frac{\alpha}{2}\right)\begin{matrix}\cos \\ \sin\end{matrix}\left(\frac{\beta}{2}\right)}{\left[\left(\frac{\alpha}{m_x\pi}\right)^2-1\right]\left[\left(\frac{\beta}{m_y\pi}\right)^2-1\right]} \right\}^2 \sin\theta d\theta d\phi, \tag{16}$$

Eq. (15) can also be written as function of the panel surface velocity power spectrum, $\mathbf{S}_{VV}$, as follows

$$\mathbf{\Pi}(\omega) = \mathbf{S}_{VV}\mathbf{M}(\omega), \tag{17}$$

in which $\mathbf{S}_{VV} = \omega^2\mathbf{S}_{WW}$, where $\mathbf{S}_{WW}$ is the panel displacement power spectrum. In the present study, the panel radiated sound power was obtained using Eq. (17), and the displacement power spectrum of the turbulent flow excited panel, $\mathbf{S}_{WW}$, was calculated using the previously validated analytical model described in [25].

4. Sensitivity Analysis

To better understand the sensitivity of the RSP to turbulent flow parameters, the radiated sound power is predicted for turbulent flow excitation from flight measurements, representing the observed PSD levels, and from the empirical models, representing the expected PSD levels, for the three

flight conditions described in Section 2. The following four flow parameters are analyzed in the RSP sensitivity study: (1) TBL power spectrum, S_{ref}, (2) convective velocity, U_c, or Mach number, M, (3) and (4) coherence lengths in the streamwise, L_x, and spanwise, L_y, directions. The numerical study was obtained assuming appropriate parameters for a typical aircraft panel [22, 23]. These values are given in Table 2, and Table 3 shows the first 16 panel natural frequencies. A total number of $M_x = 19$ and $M_y = 14$ panel modes were used to achieve convergence of the results up to $5KHz$. As in [22, 23], the quantities were calculated based on the panel displacement level predicted for the point $(x, y) = (0.3a; 0.2b)$. The predicted RSP is in good agreement with the results shown in [22]. Additionally, the average RSP, calculated based on the average panel displacement level, was also analyzed. Throughout this study, the quantities calculated for these two situations will be referred as local and average values of RSP, respectively. Fig. 3 shows the predicted RSP for Case 1 conditions, obtained for measured data and for predicted values from the Efimtsov model. It is observed that, mainly for low frequencies, the RSP for measured data have higher values than the RSP for the predicted values from Efimtsov model. In the following section a more detailed discussion is performed for the comparison of the RSP from TBL measured and predicted data.

4.1. RSP levels from measured and predicted data

The objective of this Section is to compare and analyze the predicted RSP results obtained through the measured flight data and predicted data from Efimtsov model. The TBL data obtained in the flight measurements and the predicted TBL data from the Efimtsov model were previously presented in Figs. 1 and 2. Figs. 4 and 5 show the relation between RSP obtained from flight and predicted data, for flight conditions Case 1, Case 2 and Case 3, respectively, for point and average values.

For the low frequency range, it can be shown that the frequency range where the PSD raises above the predictions corresponds to longer measured coherence lengths than predicted. For all Mach numbers, when measured L_x and L_y are greater than predicted the L_x and L_y, higher RSP levels are observed. For Cases 1 and 2, measured S_{ref}, L_x and L_y are greater than predicted values, and the same is observed for RSP. Considering Case 3 results, at frequencies below $350Hz$, measured S_{ref} is lower than predicted S_{ref}, while measured coherence lengths are bigger than the measured coherence lengths. With this in mind, and looking at part (c) of Fig. 4, one can observe that

RSP obtained from measured data is still higher than RSP obtained from predicted data for the frequency range below $350Hz$. This suggests that, for the low frequency range, coherence lengths have a more significant effect on RSP level than S_{ref}. However, one should also take into account that the difference between measured and predicted coherence length can be as great as about 500% for L_x, and about 600% for L_y, while the maximum difference for S_{ref} is about 55%. For higher frequencies, measured and predicted coherence lengths have similar values and, for Case 3, measured S_{ref} is lower than predicted S_{ref}. Looking at Case 3 results, in part (c) of Fig. 4, the negative values of the RSP at higher frequencies are related with the fact that the measured power spectrum is lower than the predicted one. However, to have a better understanding on how the each parameter affects RSP, an uncertainty and sensitivity analyses are necessary. That is the objective of the following sections.

4.2. RSP Sensitivity to TBL Power Spectrum

By maintaining constant Mach number and coherence lengths, and varying the TBL power spectrum, one observes the effect of S_{ref} on the panel RSP. The flight measurements for Case 1, $M = 0.56$, conditions are used as the reference. Keeping the L_x, L_y, and $M = 0.56$ as constant, the S_{ref} is increased by $1dB$ and $5dB$. The results are plotted in Fig. 6. It can be seen that increasing the TBL power spectrum has a direct effect on the RSP without regard to hydrodynamic coincidence and modal interaction, i.e., an increase of xdB in S_{ref} yields an increase of xdB in RSP, over the entire frequency spectrum. A similar conclusion is drawn for the Cases 2 and 3 flight conditions. So, as a sensitivity measure to TBL spectrum variation, the radiated sound power can be defined as follows, for each frequency ω:

$$RSP(\omega, S_{ref} + x\,[dB]) = RSP(\omega, S_{ref}\,[dB]) + x,\ [dB]\,. \tag{18}$$

4.3. RSP Sensitivity to Streamwise Coherence Length

Holding Mach number, S_{ref}, and L_y constants, we can evaluate the effect of variable L_x on the RSP. Changing L_x while maintaining constant the other TBL parameters should reflect the hydrodynamic coincidence influence in the RSP for each Mach number condition. The hydrodynamic coincidence frequency provides an upper limit above which no structural modes can be efficiently excited by the turbulent pressure field, and it is defined as the frequency at which hydrodynamic wavenumber, $k_c = \omega/U_c$,

matches the plate bending wavenumber, $k_b = (m_p\omega^2/D_p)^{1/4}$, and is obtained by $\omega_c = U_c^2(m_p/D_p)^{1/2}$, in which m_p is the panel mass per unit area and $D_p = (E_p h_p^3)/(12(1-\nu_p^2))$ is the plate bending stiffness. For the flight conditions and panel properties considered in the present study, the hydrodynamic coincidence frequencies are $1521.05Hz$, $2220.53Hz$, and $2794.53Hz$, respectively, for Cases 1, 2 and 3. Figs. 7, 8 and 9 show the RSP results for L_x variation.

Fig. 7 plots the results for Case 1 conditions, considering $L_y = 0.02m$, and varying L_x between $0.05m$ and $0.5m$, with predicted point RSP in part (a) and predicted average RSP in part (b). It is shown that the RSP variation along the frequency spectrum has a different behavior below or above the hydrodynamic frequency, $1521.05Hz$. As expected, in the absence of hydrodynamic coincidence, i.e., for frequencies above $1521.05Hz$, smaller L_x values will produce higher RSP levels. Below this frequency, the hydrodynamic coincidence phenomenon has an important effect on RSP, with longer L_x producing higher RSP in the regions where the hydrodynamic coincidence occur. This is easier to observe in Figs. 8 and 9, which plot the RSP for the several cases, relative to the baseline RSP (obtained for $L_x = 0.05m$ and $Ly = 0.02m$). In these figures, one can observe that as the Mach number is increased, from Case 1 to Case 3, a progression of the hydrodynamic coincidence effects for higher frequencies is observed, up to approximately $1521.05Hz$ for Case 1, $2220.53Hz$ for Case 2, and $2794.53Hz$ for Case 3, respectively, i.e., up to the respective hydrodynamic coincidence frequencies. Where hydrodynamic frequency occurs, a longer L_x is responsible for higher values of RSP. This is well visible, for instance, in parts (b) and (c) of Fig. 8.

In order to find how sensitive RSP is to the change in L_x, the results in previous figures were analyzed. For the frequency range above the hydrodynamic frequency, and for each Mach number, the difference between the RSP for a specific L_x and the RSP for the baseline $L_x = 0.05m$ was taken for each L_x, and averaged over that frequency range. Following this approach, and as shown in Fig. 10, parts (a) and (c), one obtains the following relationship between RSP and L_x, for each Mach number:

$$RSP(M, L_x) - RSP(M, L_x = 0.05m) = f_1(M)ln(L_x) + f_2(M),\ [dB] \quad (19)$$

in which $f_1(M)$ and $f_2(M)$ are functions of Mach number, shown in parts (b) and (d) of Fig. 10. Results in parts (a) and (b) of Fig. 10 correspond to

the predicted point RSP, while parts (c) and (d) correspond to the average RSP. Following this analysis, the following equations are found for RSP as function of L_x, respectively, for point and average RSP:

$$RSP(M, L_x) = (2.5438M - 4.7437)\, ln(L_x) + \\ +8.33M - 14.64 + RSP(M, L_x = 0.05m),\ [dB] \tag{20}$$

and

$$RSP(M, L_x) = (1.8975M - 5.0166)\, ln(L_x) + \\ +5.6014M - 14.966 + RSP(M, L_x = 0.05m),\ [dB] \tag{21}$$

in which $RSP(M, L_x = 0.05m)$ is equal to $-117.45dB$, $-117.59dB$, and $-124.43dB$, respectively, for Cases 1, 2 and 3, in Eq. (20), and equal to $-161.15dB$, $-162.90dB$, and $-170.78dB$ in Eq. (21).

4.4. RSP Sensitivity to Spanwise Coherence Length

Similarly to L_x, this section explores the RSP sensitivity to the change of L_y. Fig. 11 shows the results for Case 1 conditions, considering a constant $L_x = 0.2m$, and varying L_y between $0.005m$ and $0.05m$. Fig. 12 plots the results for Case 1 conditions, considering a constant $L_x = 0.2m$, for L_y between $0.01m$ and $0.05m$, with relation to the baseline RSP obtained with $L_y = 0.005m$. In the two figures, parts (a) display the predicted point RSP, and parts (b) the predicted average RSP. As expected, changing L_y is not related with hydrodynamic coincidence phenomenon. The RSP results obtained for Cases 2 and 3 conditions are very similar to the results for Case 1, leading to conclude that the change in Mach number has a minor effect on the RSP results for different L_y values. For the values of L_y analyzed, it is shown that increased L_y produces a general increase in RSP level over all the frequency spectrum.

To find the sensitive of RSP to the change in L_y, a similar approach as performed for L_x analysis was undertaken. In this case, the difference between the RSP for a specific L_y and the RSP for the baseline $L_y = 0.005m$ was taken for each L_y, and averaged over the frequency spectrum. As shown is Fig. 13, the relationship between RSP and L_y was found to be, respectively, for point and average RSP:

$$RSP(L_y) = 3.6654ln(L_y) + 19.855 + RSP(L_y = 0.005m),\ [dB] \tag{22}$$

and

$$RSP(L_y) = 2.7106ln(L_y) + 15.336 + RSP(L_y = 0.005m),\ [dB] \qquad (23)$$

with $RSP(L_y = 0.005m) = -103.74dB$ in Eq. (22), and $-142.503dB$ in Eq. (23).

4.5. RSP Sensitivity to Mach Number

By holding L_x, L_y, and S_{ref} constant one can establish the Mach number effect on RSP. It is expected that changes in the Mach number will also affect the hydrodynamic coincidence conditions, and this should be reflected in RSP predictions. Figs. 14 and 15 plot the predicted RSP for $S_{ref} = 0.1Pa^2Hz^{-1}$, $L_x = 0.2m$, and $L_y = 0.02m$, and show the effect of changing Mach number. Parts (a) display results for point RSP, and parts (b) for average RSP. The effect of hydrodynamic coincidence is visible both for Case 2 and Case 3, for point and average RSP. Hydrodynamic coincidence for Case 2 should occur below $2220.53Hz$, and for Case 3 below $2794.53Hz$. It is up to these frequencies, respectively for each Mach number, that one observes a rise in RSP, followed by a drop in RSP for higher frequencies. The RSP increases with frequency up to hydrodynamic coincidence, and this his why, in Fig. 15, the RSP for Cases 2 and 3 have a higher increase above the Case 1 coincidence frequency. Also, an increase in the Mach number results in higher RSP levels for frequencies above the hydrodynamic coincidence frequency.

To find the RSP sensitivity to M a similar analysis was performed as in previous Sections. The difference between the RSP for a specific M and the RSP for the baseline, Case 1, was taken and averaged over the frequency spectrum above the hydrodynamic coincidence frequency. The following relationships were found, respectively, for point RSP and average RSP:

$$RSP(M) = 32.4005ln(M) + 16.1408 + RSP(M = 0.56),\ [dB] \qquad (24)$$

and

$$RSP(M) = 20.5493ln(M) + 10.1722 + RSP(M = 0.56),\ [dB] \qquad (25)$$

where $RSP(M = 0.56) = -135.67dB$ in Eq. (24), and $-180.53dB$ in Eq. (25).

4.6. Uncertainty and Sensitivity

In this section the objective is to discuss and evaluate the sensitivity of each one of the functions previously determined, to specific perturbations in the independent variables, i.e., variation in S_{ref}, L_x, L_y and M. For that, the derivatives of the RSP functions with respect to the each independent variable were calculated. The derivative with respect to S_{ref} is equal to unity, for the point and average values, as follows:

$$\frac{dRSP(S_{ref})}{dS_{ref}} = 1\,. \tag{26}$$

For point RSP, the derivatives with respect to coherence lengths and Mach number are, respectively:

$$\frac{dRSP(M, L_x)}{dL_x} = \frac{1}{L_x}\left(2.5438M - 4.7437\right)\,, \tag{27}$$

$$\frac{dRSP(L_y)}{dL_y} = \frac{3.6654}{L_y}\,, \tag{28}$$

$$\frac{dRSP(M)}{dM} = \frac{32.4005}{M}\,, \tag{29}$$

and for average values of RSP, the derivatives are, respectively:

$$\frac{dRSP(M, L_x)}{dL_x} = \frac{1}{L_x}\left(1.8975M - 5.0166\right)\,, \tag{30}$$

$$\frac{dRSP(L_y)}{dL_y} = \frac{2.7106}{L_y}\,, \tag{31}$$

$$\frac{dRSP(M)}{dM} = \frac{20.5493}{M}\,. \tag{32}$$

The total uncertainty in RSP, ϵ_{RSP}, can be calculated in terms of the uncertainties of the individual variables, i.e.,

$$\epsilon_{RSP} = \epsilon_{S_{ref}}\left|\frac{dRSP}{dS_{ref}}\right| + \epsilon_{L_x}\left|\frac{dRSP}{dL_x}\right| + \epsilon_{L_y}\left|\frac{dRSP}{dL_y}\right| + \epsilon_M\left|\frac{dRSP}{dM}\right|\,, \tag{33}$$

in which the respective derivatives were previously calculated for point and average values of RSP. For specific values of individual uncertainties, and of independent variables, it is possible to calculate ϵ_{RSP}. Finally, considering

those values, the sensitivities of the RSP to changes in each of the four variables are obtained as following:

$$S_{S_{ref}} = \frac{\epsilon_{S_{ref}}}{\epsilon_{RSP}} \frac{dRSP}{dS_{ref}}\,, \tag{34}$$

$$S_{L_x} = \frac{\epsilon_{L_x}}{\epsilon_{RSP}} \frac{dRSP}{dL_x}\,, \tag{35}$$

$$S_{L_y} = \frac{\epsilon_{L_y}}{\epsilon_{RSP}} \frac{dRSP}{dL_y}\,, \tag{36}$$

$$S_M = \frac{\epsilon_M}{\epsilon_{RSP}} \frac{dRSP}{dM}\,. \tag{37}$$

Recalling that the sensitivity functions were obtained for frequencies above the respective hydrodynamic frequency, this analysis is only valid for that range of frequencies. Table 4 shows the results for the sensitivity analysis for flight conditions in Case 1. The uncertainties for the S_{ref}, L_x and L_y parameters were calculated based on the difference between measured and predicted values of each parameter. For the Mach number, a constant uncertainty of 1% was used. For this range of frequencies, it is shown that higher values of M, S_{ref} and L_y produce higher values of RSP, while higher values of L_x have the opposite effect on RSP. Additionally, Fig. 16 shows the ratios S_{x_i}/ϵ_{x_i} for the four TBL parameters, giving the information on how much a 1% change in each parameter x_i affects the change of S_{x_i}. It is concluded that the Mach number is the parameter that most affects the RSP, both for point and average values of RSP. For instance, at $4000Hz$, a 1% variation in M will affect the point RSP in 41% and the average RSP in 32%. S_{ref} is the next more significant parameter affecting the RSP variation. The change in coherence lengths, L_x and L_y, have similar effect on the point RSP, while for average RSP the variation in L_x is more significant than the variation in L_y. So, when predicting TBL parameters through empirical models, it is important to have a low uncertainty in the TBL parameters, first in the Mach number, then in the S_{ref}, and last in the coherence lenghts.

5. Conclusions

Several empirical models exist to provide the TBL wall pressure cross spectrum. These models provide different predictions for the wall pressure cross spectrum. Furthermore, it is known that real flow conditions over

aircraft do not conform to the ideal behavior, predicted by the empirical models, for the TBL wall pressure PSD. The accuracy of the empirical models is important in the prediction of aircraft cabin interior noise. Considering this, the aim of the present work was to investigate how sensitive is the sound radiated by aircraft panels to the change of TBL conditions.

Data from flight measurements were compared with the data provided by the Efimtsov model. The RSP was obtained both for flight measurements data and for data predicted by the empirical model. The RSP for both conditions was then compared, to investigate the the effect of different flow conditions on the RSP. From this comparison, it is shown that, for the low frequency range, the RSP obtained for the predicted data is higher that the RSP obtained for the measured data. In the high frequency range the RSP for both conditions are similar. It is observed that the frequency range where the PSD raises above the predictions is due to the longer measured coherence lengths than predicted coherence lengths. Also, it is observed that, for the low frequency range, the change in coherence lengths has a more significant effect on RSP level than S_{ref}. However, this is due to the higher difference between measured and predicted values of coherence lengths, compared with the difference between the measured and predicted values of S_{ref}. For that reason, a sensitivity analysis is needed for a clearer understanding on how each parameter influences RSP.

A sensitivity analysis was performed, in which the variation of RSP due to the change of the TBL parameters was obtained. Four TBL parameters were analyzed: (1) the TBL reference PSD, S_{ref}, (2) the flow Mach number, M, (3) the streamwise coherence length, L_x, and (4) the spanwise coherence length, L_y. To accomplish that, the influence of the change of each TBL parameter on the variation of the RSP was individually investigated. Specifically, mathematical functions were calculated which describe the RSP as function of each individual parameter. For the TBL reference PSD parameter, it is shown that increasing S_{ref} has a direct effect on the RSP without regard to hydrodynamic coincidence phenomenon and modal interaction, i.e., an increase of xdB in S_{ref} yields an increase of xdB in RSP. For the change in L_x parameter, a different behavior was observed for RSP variation for frequencies below or above the hydrodynamic frequency. In the absence of hydrodynamic coincidence, i.e., for frequencies above the coincidence frequency, smaller L_x values produce higher RSP levels. Below this frequency, in the regions where the hydrodynamic coincidence occur, longer L_x produce higher RSP levels. Considering the coherence length in the span-

wise direction, it is found that higher values of L_y produce an increase in RSP. Considering the Mach number parameter, the increase in M will also increase the hydrodynamic coincidence frequency, and this is reflected in the RSP predictions. An increase in the Mach number results in higher RSP levels for frequencies above the hydrodynamic coincidence frequency.

Finally, a sensitivity analysis based on the parameters uncertainty was undertaken. The uncertainties for the four parameters analyzed represent the difference between measured and predicted values for each parameter. For the frequency range analyzed, it is shown that higher values of M, S_{ref} and L_y produce higher values of RSP, while higher values of L_x are responsible for producing lower RSP. Also, it is concluded that M is the parameter that most affects the RSP, followed by S_{ref}, and then by L_x and L_y. These findings lead to an important conclusion: when predicting the TBL parameter using the empirical models, it is important to have an accurate prediction first of the Mach number, and of the S_{ref}, followed by the coherence lengths. An uncertainty of 1% in the M parameter (or in the convective velocity) is responsible by a 41% difference in RSP at $4000Hz$, while 1% uncertainty in S_{ref} causes a 9% difference in RSP at $4000Hz$. Thus, a better understanding of the TBL wall pressure in the aicraft sidewall is necessary to have more reliable RSP predictions, and to tighten uncertainty in RSP predictions.

6. Acknowledgments

The authors are grateful for the financial support of the Foundation for Science and Technology (FCT), and to the Amelia Earhart Program from ZONTA International Foundation.

References

[1] M. K. Bull, Wall-pressure fluctuations beneath turbulent boundary layers: some reflections on forty years of research. *Journal of Sound and Vibration* (1996), 190(3), pp. 299-315.

[2] W. R. Graham, A comparison of models for the wavenumber frequency spectrum of turbulent boundary layer pressures. *Journal of Sound and Vibration* (1997), 206(4), pp. 541-565.

[3] G. Corcos, The structure of the turbulent pressure field in boundary layer flows. *Journal of Fluid Mechanics - Cambridge Journal Online* (1964), 18, pp. 353-378.

[4] G. Corcos, Resolution of pressure in turbulence. *Journal of the Acoustical Society of America* (1963), 35(2), pp. 192-199.

[5] B. M. Efimtsov, Characteristics of the field of turbulent wall pressure fluctuations at large Reynolds numbers. *Soviet Physics-Acoustics* (1982), 28 (4), pp. 289-292.

[6] D. M. Chase, Modelling the wavevector-frequency spectrum of turbulent boundary layer wall-pressure. *Journal of Sound and Vibration* (1980), 70, pp. 29-67.

[7] D. M. Chase, The character of the turbulent wall pressure spectrum at subconvective wavenumbers and a suggested comprehensive model. *Journal of Sound and Vibration* (1987), 112, pp. 125-147.

[8] A. V. Smol'yakov and V. M. Tkachenko, Model of a field of pseudonic turbulent wall pressures and experimental data. *Soviet Physics-Acoustics* (1991), 37 (6), pp. 627-631.

[9] D. Palumbo, Determining Correlation and Coherence Lengths in the Wall Pressure of the Turbulent Boundary Layer, *NASA Report* (2010).

[10] R. Rackl and A. Weston, Modeling of turbulent boundary layer surface pressure fluctuation auto and cross spectra - verification and adjustments based on TU-144LL data, *NASA CR-213938* (2005).

[11] D. E. Bishop, Cruise flight noise levels in a turbojet transport airplane. *Noise Control* (1961), 7, pp. 37-42.

[12] W. V. Bhat and J. F. Wilby, Interior noise radiated by an airplane fuselage subjected to turbulent boundary layer excitation and evaluation of noise reduction treatments. *Journal of Sound and Vibration* (1971), 18 (4) , pp. 449-464.

[13] W. V. Bhat, Flight test measurement of measurement of exterior turbulent boundary layer pressure fluctuations on Boeing Model 737 airplane. *Journal of Sound and Vibration* (1971), 14 (4) , pp. 439-457.

[14] L. Maestrello, Measurement of noise radiated by turbulent boundary layer excited panels. *Journal of Sound and Vibration* (1965), 2(2), pp. 100-115.

[15] L. Maestrello, Radiation from and panel response to a supersonic turbulent boundary layer. *Journal of Sound and Vibration* (1969), 10(2), pp. 261-295.

[16] J. F. Wilby and F. L. Gloyna, Vibration measurements of an airplane fuselage structure I. Turbulent boundary layer excitation. *Journal of Sound and Vibration* (1972), 23, pp. 443 - 466.

[17] J. F. Wilby and F. L. Gloyna, Vibration measurements of an airplane fuselage structure II. Jet noise excitation. *Journal of Sound and Vibration* (1972), 23 (4), pp. 467-486.

[18] J. F. Wilby, Aircraft interior noise. *Journal of Sound and Vibration* (1996), 190 (3), pp. 545-564.

[19] W. A. Strawderman, Turbulent-flow-excited vibration of a simply supported, rectangular flat plate. *The Journal of the Acoustical Society of America* (1969), 45(1), pp. 177-192.

[20] H. G. Davies, Sound from turbulent-boundary-layer-excited panels. *The Journal of the Acoustical Society of America* (1971), 49(3), pp. 878-889.

[21] R. L. Clark and K. D. Frampton, Aeroelastic structural acoustic coupling: implications on the control of turbulent boundary-layer noise transmission. *Journal of the Acoustical Society of America* (1997), 102(3), pp. 1639-1647.

[22] C. Maury, P. Gardonio and S. J. Elliot, Active control of the flow-induced noise transmitted through a panel. *AIAA Journal* (2001), 39(10), pp. 1860-1867.

[23] C. Maury, P. Gardonio and S. J. Elliot, A wavenumber approach to the modeling the response of a random excited panel, Part II: application to aircraft panels excited by a turbulent boundary layer. *Journal of Sound and Vibration* (2002), 252(1), pp. 115-139.

[24] B. Liu, Noise radiation of aircraft panels subjected to boundary layer pressure fluctuations. *Journal of Sound and Vibration* (2002), 314, pp. 693-711.

[25] J. da Rocha, A. Suleman and F. Lau, Prediction of flow-induced noise in transport vehicles: development and validation of a coupled structural-acoustic analytical framework, *Canadian Acoustics* (2009), 37 (4), pp. 13-29.

[26] D. A. Bies, A review of flight and wind tunnel measurements of boundary layer pressure fluctuations and induced structural response, *NASA CR-626* (1966).

[27] R. Wahidi, W. Chakroun, and S. Al-Fahed. The behavior of the skin friction coefficient of a turbulent boundary layer flow over a flat plate with differently configured transverse square grooves. *Experimental Thermal and Fluid Science* (2005), 30, pp. 141152.

[28] J. Rayleigh, *Theory of Sound*, MacMillan, London, 1896.

[29] B. Bingham, M. Atalla, and N. Hagood, Comparison of structural-acoustic control designs on an active composite panel. *Journal of Sound and Vibration* (2001), 244(5), pp. 761-778.

[30] W. Baumann, W. Saunders, and H. Robertshaw, Active supression of acoustic radiation from impulsive excited structures. *Journal of the Acoustical Society of America* (1991), 90(6), pp. 3202-3208.

[31] C. Wallace, Radiation Resistance of a Rectangular Panel. *The Journal of the Acoustical Society of America* (1972), 51(3), pp. 946-952.

List of Figures

List of Tables

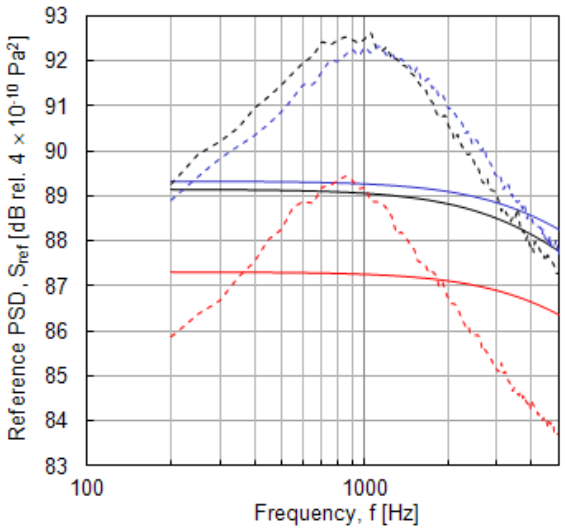

Figure 1: TBL wall pressure spectrum for: Case 1 in black, Case 2 in blue, and Case 3 in red. Dashed lines: data from flight tests. Continuous lines: predicted using Efimtsov model, by Eq. (7).

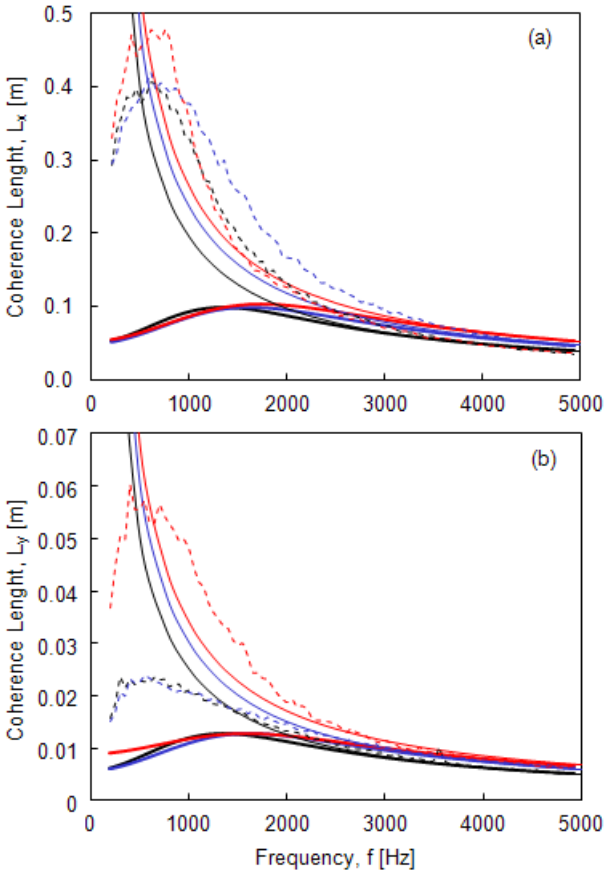

Figure 2: TBL coherence lengths, in (a) streamwise and (b) spanwise directions: Case 1 in black, Case 2 in blue, and Case 3 in red. Dashed lines: data from flight tests. Continuous bold lines: predicted using Efimtsov model, by Eqs. (3) and (4). Continuous regular lines: predicted through Corcos model, by Eqs. (1) and (2).

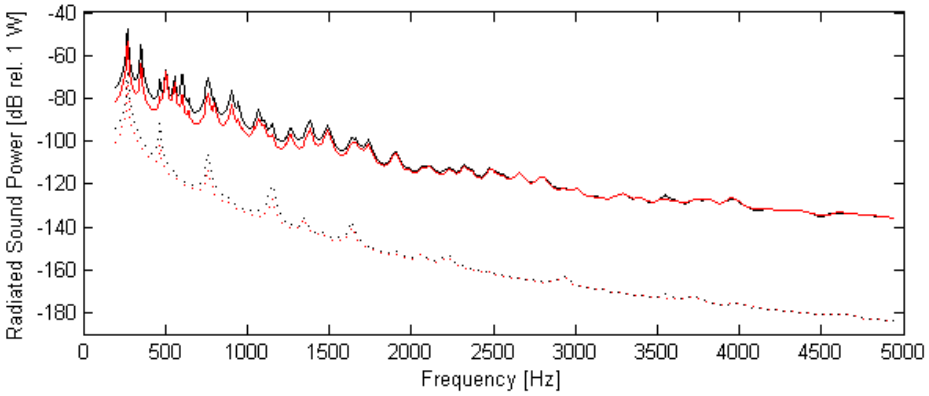

Figure 3: Predicted RSP for Case 1 conditions: back, from TBL measured data; red, from Efimtsov model predicted values. Continuous lines for point RSP, and dashed lines for average RSP.

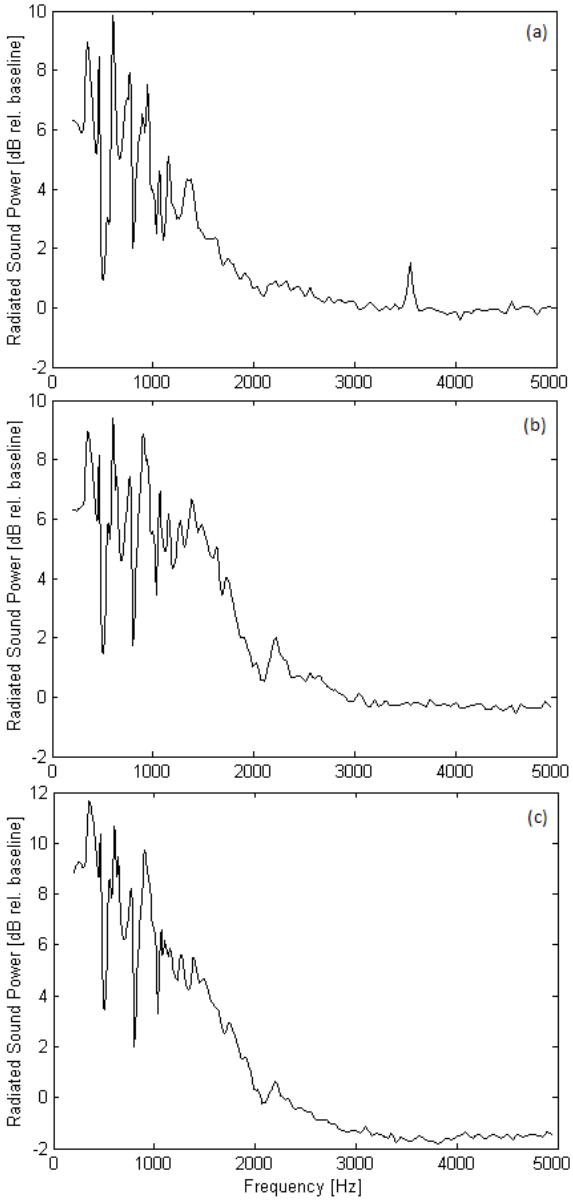

Figure 4: Point RSP for flight data with relation to RSP for Efimtsov model data, for the following conditions: (a) Case 1, (b) Case 2, and (c) Case 3.

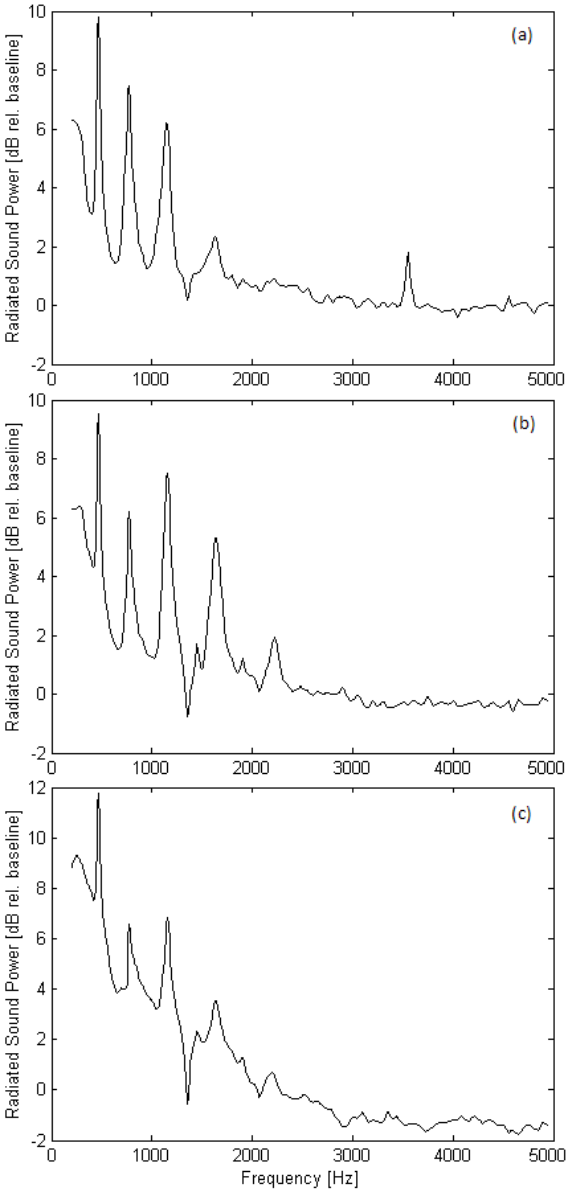

Figure 5: Average RSP for flight data with relation to average RSP for Efimtsov model data, for the following conditions: (a) Case 1, (b) Case 2, and (c) Case 3.

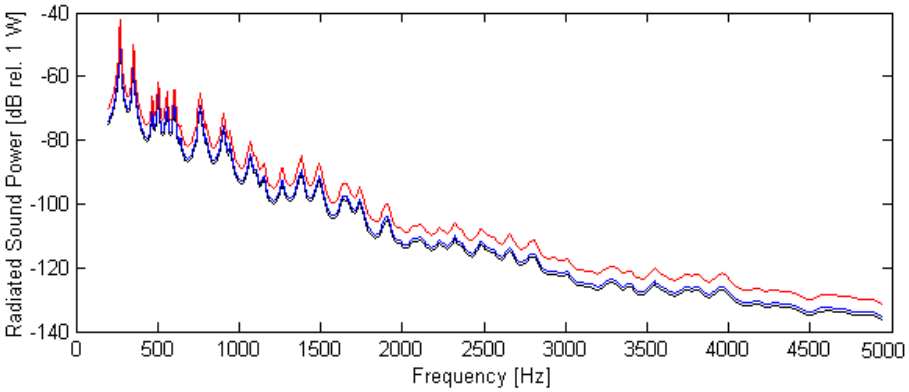

Figure 6: Predicted point RSP for Case 1 flight conditions, considering the following flow excitations: measured S_{ref} in black, measured S_{ref} plus $1dB$ in blue, and measured S_{ref} plus $5dB$ in red.

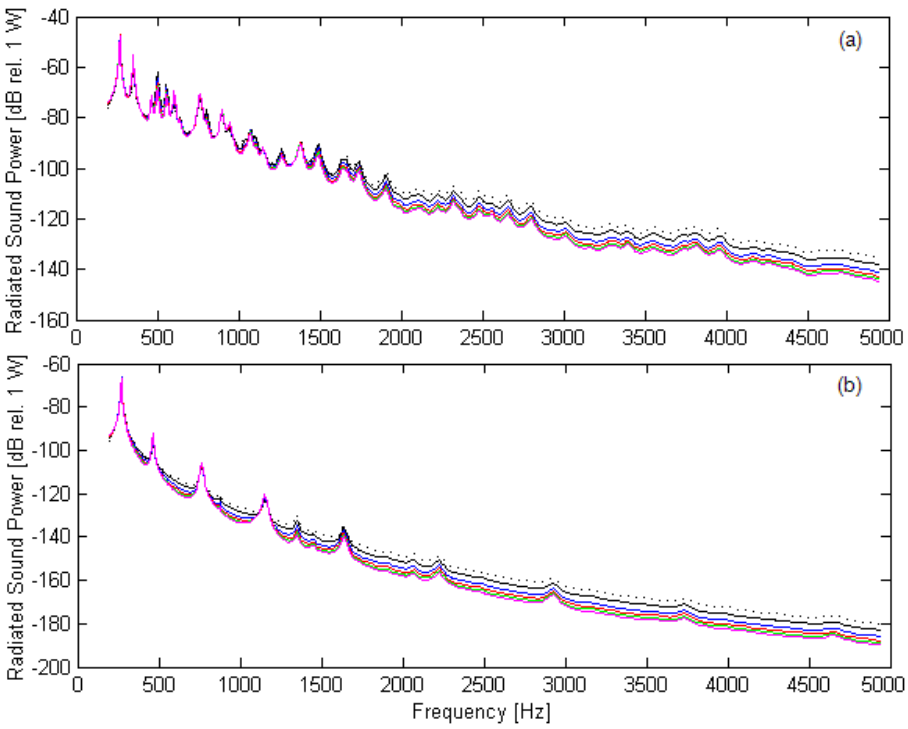

Figure 7: Predicted RSP for Case 1 conditions, measured S_{ref}, considering L_y constant and equal to $0.02m$, for the following L_x values: dashed line, $0.05m$; black, $0.1m$; blue, $0.2m$; red, $0.3m$; green, $0.4m$; purple, $0.5m$. (a) Point RSP. (b) Average RSP.

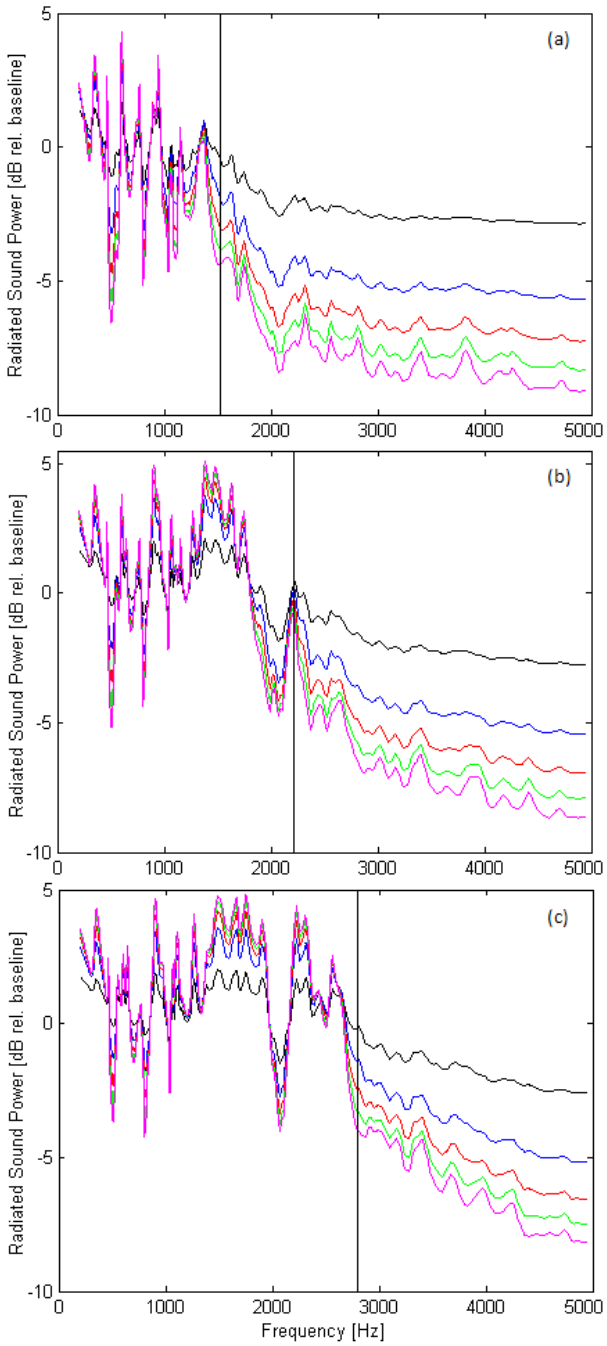

Figure 8: Predicted point RSP, considering L_y constant equal to $0.02m$, for the following measured S_{ref}: (a) Case 1, (b) Case 2, (c) Case 3. Values of L_x: black, $0.1m$; blue, $0.2m$; red, $0.3m$; green, $0.4m$; purple, $0.5m$. Baseline is RSP for $L_y = 0.02m$ and $L_x = 0.05m$.

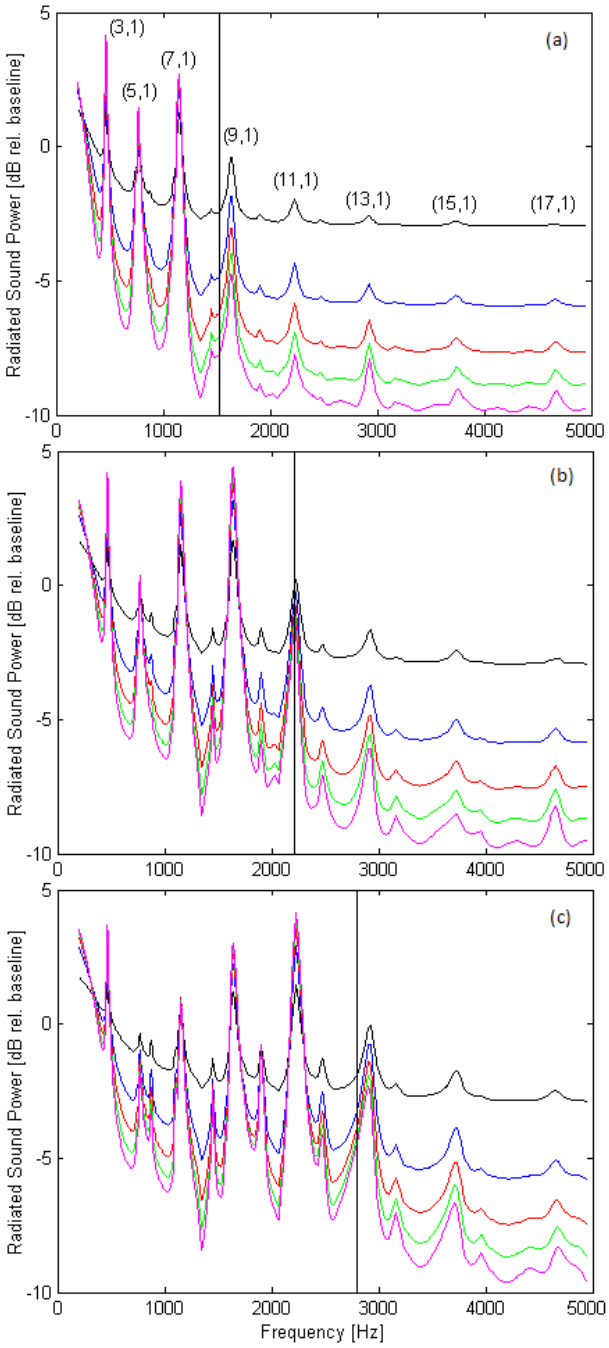

Figure 9: Predicted average RSP, considering L_y constant equal to $0.02m$, for the following measured S_{ref}: (a) Case 1, (b) Case 2, (c) Case 3. Values of L_x: black, $0.1m$; blue, $0.2m$; red, $0.3m$; green, $0.4m$; purple, $0.5m$. Baseline is RSP for $L_y = 0.02m$ and $L_x = 0.05m$.

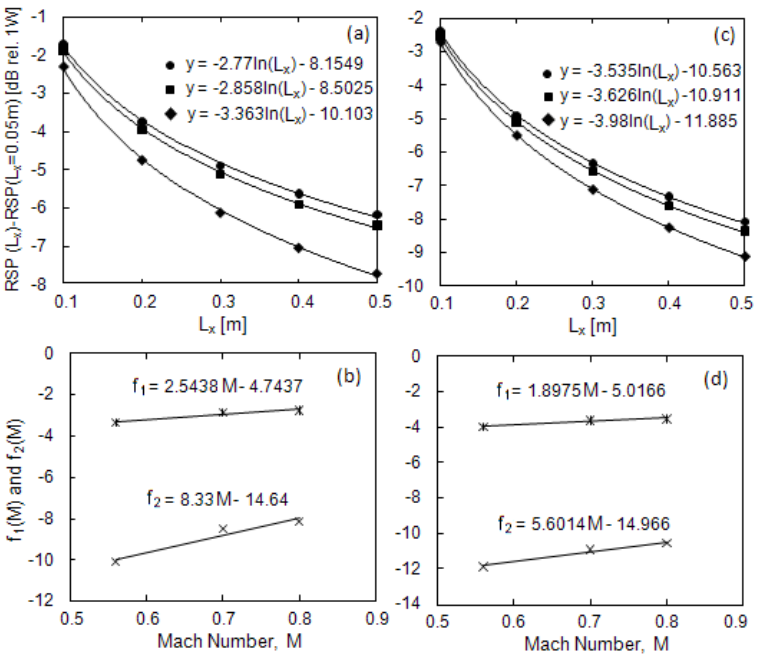

Figure 10: Functions for RSP sensitivity to L_x: (a) and (b) for point RSP, (c) and (d) for average RSP. (a) and (c): $\diamond$, Case 1; $\square$, Case 2; $\circ$, Case 3.

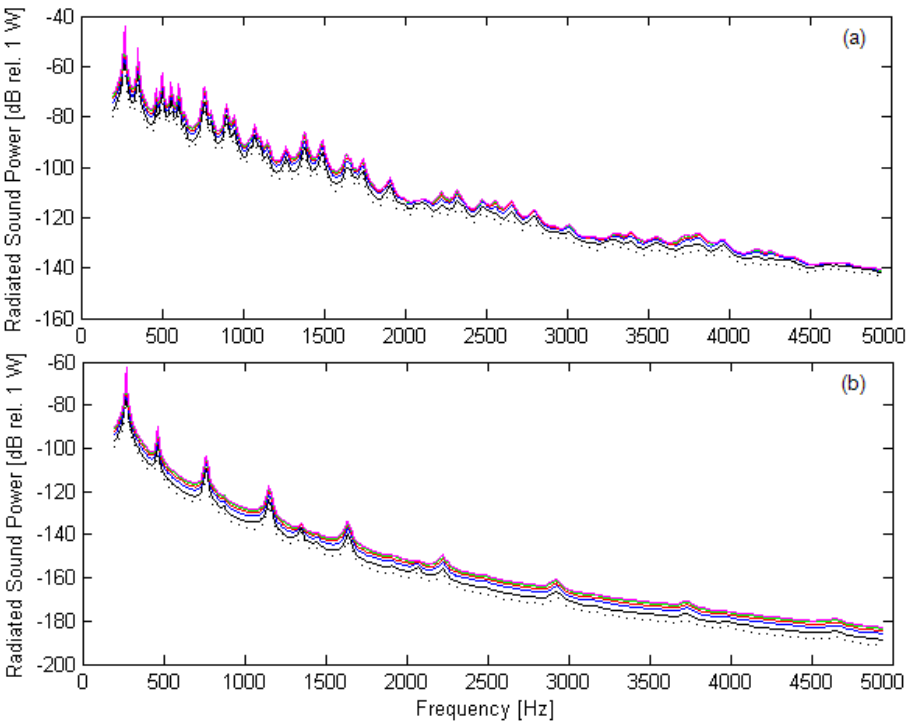

Figure 11: Predicted RSP for Case 1, measured S_{ref}, considering L_x constant equal to $0.2m$, for the following L_y values: dashed line, $0.005m$; black, $0.01m$; blue, $0.02m$; red, $0.03m$; green, $0.04m$; purple, $0.05m$. (a) Point RSP. (b) Average RSP.

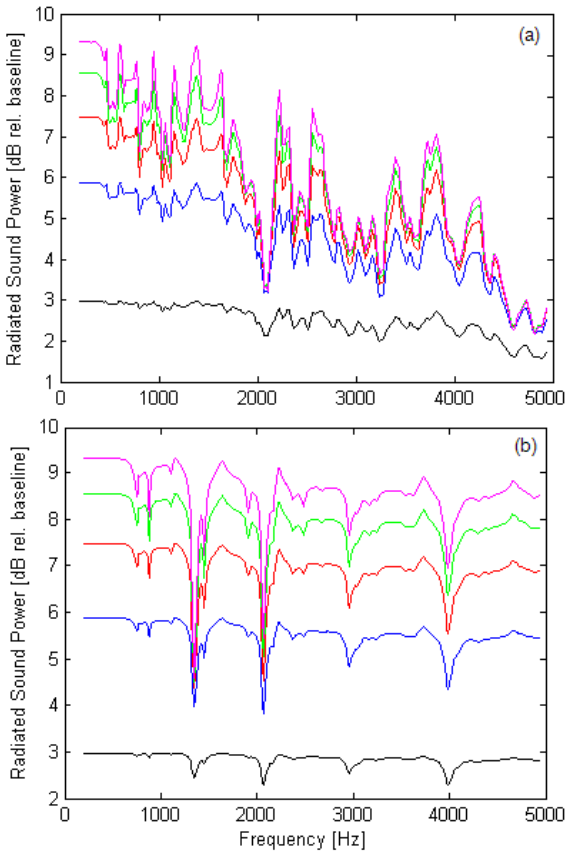

Figure 12: Predicted RSP for Case 1, measured S_{ref}, considering L_x constant equal to $0.2m$, for the following L_y values: black, $0.01m$; blue, $0.02m$; red, $0.03m$; green, $0.04m$; purple, $0.05m$. Baseline is RSP for $L_x = 0.2m$ and $L_y = 0.005m$. (a) Point RSP. (b) Average RSP.

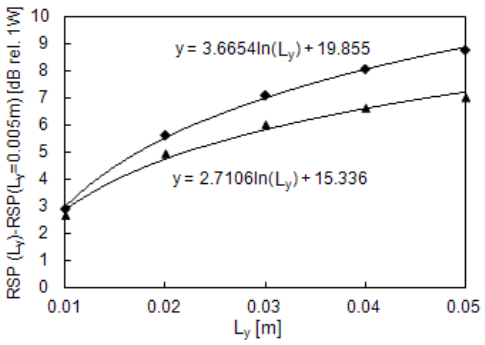

Figure 13: Functions for RSP sensitivity to L_y: $\triangle$, for point RSP ; $\diamond$, for average RSP.

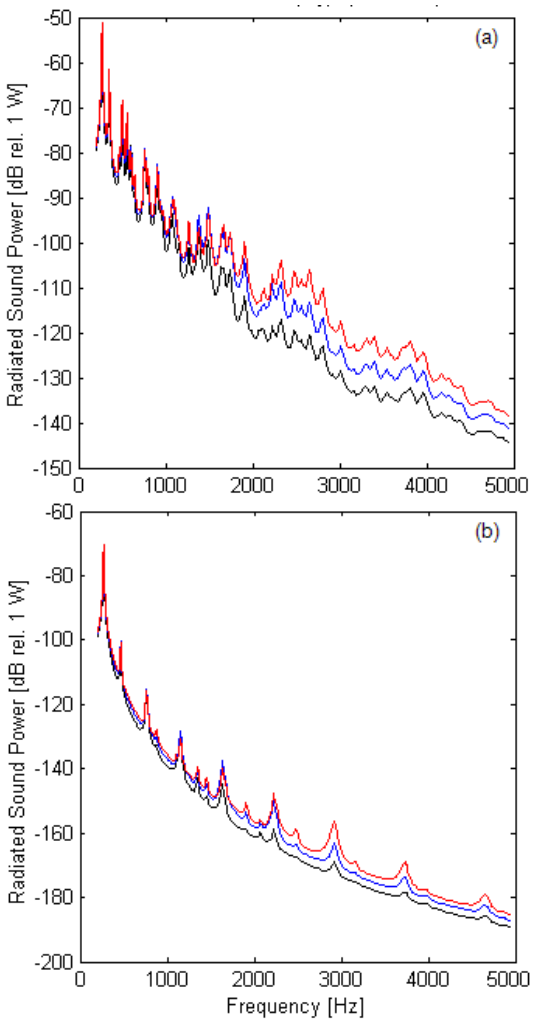

Figure 14: Predicted RSP considering $L_x = 0.2m$, $L_y = 0.02m$, $S_{ref} = 0.1Pa^2Hz^{-1}$, air conditions for Case 1, for the following Mach numbers: black, $M = 0.56$; blue, $M = 0.7$; red, $M = 0.8$. (a) Point RSP. (b) Average RSP.

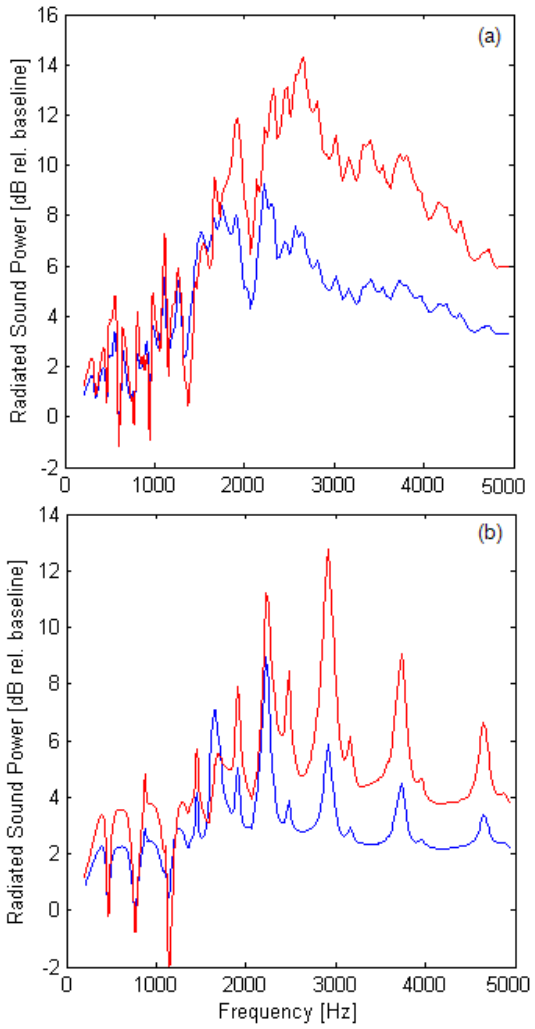

Figure 15: Predicted RSP considering $L_x = 0.2m$, $L_y = 0.02m$, $S_{ref} = 0.1Pa^2Hz^{-1}$, air conditions for Case 1, for the following Mach numbers: blue, $M = 0.7$; red, $M = 0.8$. Baseline of results is RSP for $M = 0.56$. (a) Point RSP. (b) Average RSP.

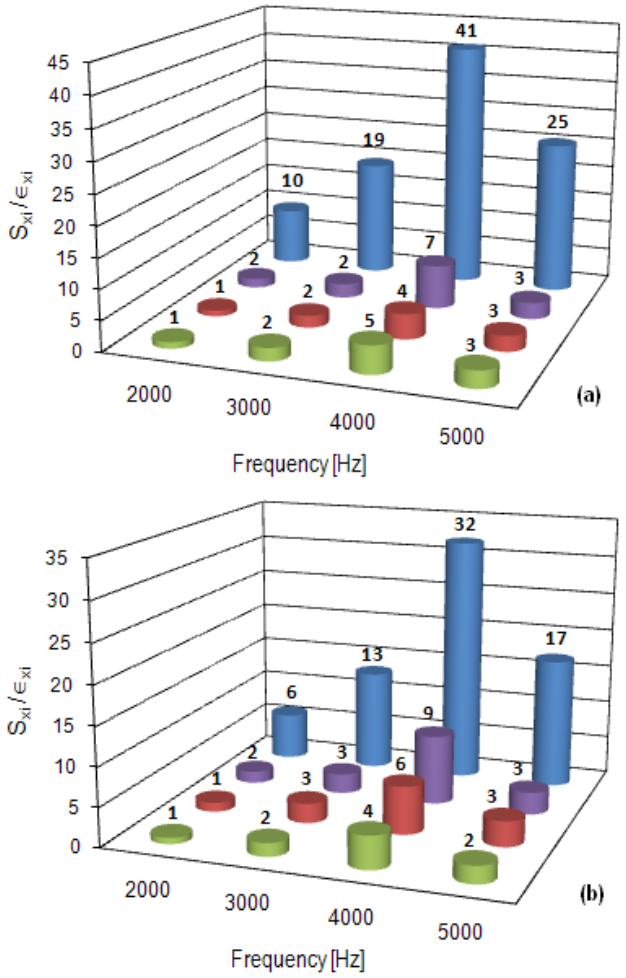

Figure 16: Ratios S_{x_i}/ϵ_{x_i} for the frequencies shown in Table 4, for the four TBL parameters: blue, M; purple, S_{ref}; red, L_x; green, L_y. (a) For point RSP data, and (b) for average RSP data.

Table 1: Flight Tests Conditions and Flow Parameters.

Variable	Description, Units	Case 1	Case 2	Case 3
M	Mach number	0.56	0.7	0.8
h	Altitude, m	7315	9754	13106
c	Speed of sound, ms^{-1}	311	301	295
U	Flow speed, ms^{-1}	174.15	210.42	236.06
ρ	Density, $Kg\ m^{-3}$	0.5692	0.4262	0.2622
ν	Kinematic viscosity, m^2s^{-1}	2.7242×10^{-5}	3.4401×10^{-5}	5.422×10^{-5}
T	Temperature, K	240.66	224.85	216.65
Re_x	Reynolds number	4.2832×10^{7}	4.0982×10^{7}	2.917×10^{7}
C_f	Friction coefficient	1.9387×10^{-3}	1.9513×10^{-3}	2.0526×10^{-3}
U_τ	Friction velocity, $m\ s^{-1}$	5.18	6.3	7.29
δ	TBL thickness, m	0.075	0.077	0.082
f_c	Coincidence frequency, Hz	1521.05	2220.53	2794.53

Table 2: Physical properties of the aircraft panel.

Variable	Description, Units	Value
a	Panel length, m	0.414
b	Panel width, m	0.314
h_p	Panel thickness, m	0.001
E_p	Panel Elasticity modulus, Pa	7.24×10^{10}
ν	Panel Poisson ratio	0.33
ρ	Panel density, $Kg\ m^{-3}$	2800
ξ_p	Panel damping ratio	0.01
N_x	Panel longitudinal Tension, $N\ m^{-1}$	29300
N_y	Panel lateral Tension, $N\ m^{-1}$	62100
c_0	Internal fluid speed of sound, $m\ s^{-1}$	340
ρ_0	Internal fluid density, $Kg\ m^{-3}$	1.42

Table 3: First 16 panel natural frequencies.

m_x	m_y	Frequency, Hz
1	1	270.2
2	1	352.1
3	1	465.8
1	2	503.0
2	2	557.1
4	1	603.6
3	2	643.4
4	2	759.1
1	3	760.0
5	1	763.6
2	3	803.5
3	3	875.7
5	2	902.2
6	1	946.0
4	3	976.6
1	4	1041.0

Table 4: Sensitivity analysis results.

f = 2000 Hz:						
Parameter, $x_i[units]$	Measured Value	Uncertainty, ϵ_{x_i}	Point $\frac{dRSP}{dx_i}$	Average $\frac{dRSP}{dx_i}$	Point Sensitivity, S_{x_i}	Average Sensitivity, S_{x_i}
M	0.56	0.0056 (1.0 %)	57.86	36.70	9.5 %	6.1 %
$L_x[m]$	0.13	0.043 (33.1 %)	-25.53	-30.42	-32.3 %	-38.8 %
$L_y[m]$	0.013	0.0017 (13.1 %)	281.95	208.51	14.1 %	10.5 %
$S_{ref}[dB]$	90.5	1.5 (1.7 %)	1	1	44.1 %	44.6 %
$[Pa^2Hz^{-1}]$	0.45	0.13 (28.9 %)				
f = 3000 Hz:						
Parameter, $x_i[units]$	Measured Value	Uncertainty, ϵ_{x_i}	Point $\frac{dRSP}{dx_i}$	Average $\frac{dRSP}{dx_i}$	Point Sensitivity, S_{x_i}	Average Sensitivity, S_{x_i}
M	0.56	0.0056 (1.0 %)	57.86	36.70	19.2 %	13.2 %
$L_x[m]$	0.074	0.011 (14.9 %)	-44.85	-30.42	-53.4 %	-37.6 %
$L_y[m]$	0.0091	0.0082 (9.9 %)	402.79	297.87	21.6 %	17.2 %
$S_{ref}[dB]$	89	0.5 (0.6 %)	1	1	29.8 %	32.0 %
$[Pa^2Hz^{-1}]$	0.32	0.04 (12.5 %)				
f = 4000 Hz:						
Parameter, $x_i[units]$	Measured Value	Uncertainty, ϵ_{x_i}	Point $\frac{dRSP}{dx_i}$	Average $\frac{dRSP}{dx_i}$	Point Sensitivity, S_{x_i}	Average Sensitivity, S_{x_i}
M	0.56	0.0056 (1.0 %)	57.86	36.70	41.0 %	32.0 %
$L_x[m]$	0.049	0.001 (2.0 %)	-67.74	-80.69	-8.6 %	-12.6 %
$L_y[m]$	0.0065	0.0003 (4.6 %)	563.91	417.02	21.4 %	19.5 %
$S_{ref}[dB]$	87.9	-0.2 (-0.3 %)	1	1	-29.0 %	-35.9 %
$[Pa^2Hz^{-1}]$	0.25	-0.01 (-4.0 %)				
f = 5000 Hz:						
Parameter, $x_i[units]$	Measured Value	Uncertainty, ϵ_{x_i}	Point $\frac{dRSP}{dx_i}$	Average $\frac{dRSP}{dx_i}$	Point Sensitivity, S_{x_i}	Average Sensitivity, S_{x_i}
M	0.56	0.0056 (1.0 %)	57.86	36.70	25.4 %	17.0 %
$L_x[m]$	0.035	-0.004 (-11.4 %)	-94.83	-112.97	29.8 %	37.4 %
$L_y[m]$	0.0052	0.0001 (1.9 %)	704.88	521.27	5.5 %	4.3 %
$S_{ref}[dB]$	87.3	-0.5 (-0.6 %)	1	1	-39.3 %	-41.3 %
$[Pa^2Hz^{-1}]$	0.21	-0.03 (-14.3 %)				